AD

Report 2006

THE EFFECT OF ANGULAR DISTRIBUTION OF COMPTON ELECTRONS ON HIGH-ALTITUDE EMP SOURCE CURRENTS

by

William T. Wyatt, Jr.

April 1971

U. S. ARMY MOBILITY EQUIPMENT RESEARCH AND DEVELOPMENT CENTER
FORT BELVOIR, VIRGINIA

146

UNCLASSIFIED
Security Classification

DOCUMENT CONTROL DATA - R & D

(Security classification of title, body of abstract and indexing annotation must be entered when the overall report is classified)

1. ORIGINATING ACTIVITY (Corporate author)	2a. REPORT SECURITY CLASSIFICATION
U. S. Army Mobility Equipment Research and Development Center Fort Belvoir, Virginia	Unclassified
	2b. GROUP

3. REPORT TITLE

THE EFFECT OF ANGULAR DISTRIBUTION OF COMPTON ELECTRONS ON HIGH-ALTITUDE EMP SOURCE CURRENTS

4. DESCRIPTIVE NOTES (Type of report and inclusive dates)
Technical Report

5. AUTHOR(S) (First name, middle initial, last name)
William T. Wyatt, Jr.

6. REPORT DATE	7a. TOTAL NO. OF PAGES	7b. NO. OF REFS
April 1971	146	

8a. CONTRACT OR GRANT NO.	9a. ORIGINATOR'S REPORT NUMBER(S)
b. PROJECT NO. DASA EA091	2006
c.	9b. OTHER REPORT NO(S) (Any other numbers that may be assigned this report)
d.	

10. DISTRIBUTION STATEMENT
Approved for public release; distribution unlimited.

11. SUPPLEMENTARY NOTES	12. SPONSORING MILITARY ACTIVITY
	USAMERDC Fort Belvoir, Virginia

13. ABSTRACT

High-altitude EMP source currents and ionization resulting from Compton scattering of gamma rays were evaluated on the basis of the forward-scattering approximation and approximations to the actual angular distribution of the Compton electrons. Large differences were noted between results of the most accurate approximation and the forward-scattering approximation for the case of relativistic Compton electrons, especially at late times. Accuracy at late times required a more accurate approximation than at early times. A special forward-scattering approximation was tested which should allow accurate evaluation of peak fields below the source region.

DD FORM 1 NOV 68 1473 REPLACES DD FORM 1473, 1 JAN 64, WHICH IS OBSOLETE FOR ARMY USE.

UNCLASSIFIED
Security Classification

14. KEY WORDS	LINK A		LINK B		LINK C	
	ROLE	WT	ROLE	WT	ROLE	WT
EMP Compton scattering Numerical integration						

1- 3-4- -32,391—Ft Belvoir

U. S. ARMY MOBILITY EQUIPMENT
RESEARCH AND DEVELOPMENT CENTER
FORT BELVOIR, VIRGINIA

Report 2006

THE EFFECT OF ANGULAR DISTRIBUTION OF COMPTON ELECTRONS ON HIGH-ALTITUDE EMP SOURCE CURRENTS

DASA NWER subtask EA 091

April 1971

Distributed by

The Commanding Officer
U. S. Army Mobility Equipment Research and Development Center

Prepared by

William T. Wyatt, Jr.
Physics Division
Electromagnetic Effects Laboratory

SUMMARY

High-altitude EMP source currents and ionization resulting from Compton scattering of gamma rays were evaluated on the basis of the forward-scattering approximation and approximations to the actual angular distribution of the Compton electrons. Large differences were noted between results of the most accurate approximation and the forward-scattering approximation for the case of relativistic Compton electrons, especially at late times. Accuracy at late times required a more accurate approximation than at early times. A special forward-scattering approximation was tested which should allow accurate evaluation of peak fields below the source region.

CONTENTS

BLANK PAGE

THE EFFECT OF ANGULAR DISTRIBUTION OF COMPTON ELECTRONS ON HIGH-ALTITUDE EMP SOURCE CURRENTS

I. INTRODUCTION

1. Subject. The evaluation of the strength and time dependence of the electromagnetic pulse (EMP) from a high-altitude nuclear burst requires that Maxwell's equations be solved for the case of time- and space-dependent source currents and air conductivity for the regions of interest. This includes the region from the surface to an altitude of several hundred kilometers. The principal mechanism, which will be treated in this report, of generation of these source currents is the Compton interaction of air molecules which bomb-produced, high-energy photons including gamma rays and x-rays. The methods and results of this study have some application to pair-production and photoelectric processes as well. (The extensive number of graphs in this report were included to facilitate further analysis which might be performed by the reader.)

II. METHOD OF CALCULATION

2. Physical Assumption. The bomb-produced photons are assumed here to be prompt, unscattered, monochromatic photons propagating radially from the burst with a flux amplitude time dependence of the form

$$f(t) = \frac{A\, e^{at}}{1 + B\, e^{bt}}$$

which is an exponentially rising and exponentially decaying function of time, t, using the following arbitrary and hypothetical values: $a = 2 \times 10^{8}$ sec^{-1}; $b = 3 \times 10^{8}$ sec^{-1}; and $B = e^{-15}$. A is arbitrary here and would be a function of the bomb yield. Thus, the y-axis amplitude values throughout this report are arbitrary. The function, f(t), reaches a maximum at about 5.23×10^{-8} sec.

The Compton electrons generated by Compton collision of the source photons with air molecules orbit in helical paths along the geomagnetic field lines and suffer kinetic-energy losses through ion pair formation during repeated collisions with air molecules. The Compton interaction is governed by the Klein-Nishina differential-scattering cross-section equations. The Compton electrons are assumed to undergo a smooth degradation in kinetic energy due to collisions with air molecules until they come to rest according to the range-energy relationship:

$$R = 0.368\ E^n\ g/cm^2, \qquad n = 1.26 - 0.064 \ln E,$$

where E is in Mev.

The "average range," which is not used here, is about two-thirds of this range. The actual slowing-down process is random and not smooth, but the assumption of smoothness is adequate for the purposes of this report. The Compton electron trajectory in the geomagnetic field is calculated by numerically solving the following equations of motion of a charged particle in a uniform, constant magnetic field with zero electric field using MKS units:

$$\frac{dE}{dt} = -v\frac{dE}{dx}$$

$$\gamma = E/m_o c^2$$

$$v = c\sqrt{\gamma(\gamma+2)} \;/\; (\gamma+1)$$

$$\frac{d\alpha}{dt} = -\frac{q}{m_o}\frac{B \sin D}{(\gamma+1)}$$

$$v_r = (\cos D \cos F + \sin D \sin F \cos \alpha)\, v$$

$$v_\phi = v \sin F \sin \alpha$$

$$v_\theta = (-\cos F \sin D + \sin F \cos D \cos \alpha)\, v$$

$$\frac{dT}{dt} = 1 - v_r c$$

where E is the Compton electron energy and $\frac{dE}{dx}$ is given by the derivative of the range-energy relationship with respect to range and

where:

v = speed of the Compton electron

m = rest mass of electron

c = speed of light

α = angle of turning of Compton electron in the geomagnetic field at time, t

q = electron charge

B = magnitude of the geomagnetic field

D = angle between the radius vector from the burst and the geomagnetic field vector

F = angle between the Compton electron initial velocity vector and the geomagnetic field vector at time, t = 0

v_r = radial component of the Compton electron velocity at time, t

v_ϕ = phi component (in polar coordinates defined by $\hat{\phi} = \hat{r} \times \vec{B} / (|B| \sin D)$ and $\hat{r} \times \hat{\theta} = \hat{\phi}$) of the Compton electron velocity at time, t

v_θ = theta component of the Compton electron velocity at time, t

T = retarded time or lag time of the Compton electron relative to the expanding photons from the burst.

The effect of the EMP on the Compton electron trajectory is not evaluated. When the kinetic energy of the Compton electron falls to zero, it is assumed to have stopped completely. The number of positive ions is assumed to equal the number of free electrons so that there are no negative ions.

3. **Computer Code.** The source currents were calculated using the NEPHI-70, high-altitude EMP computer code (developed at MERDC in June and July 1970) in conjunction with a CDC 6400 computer. The computer code calculated the currents for each altitude evaluated as follows:

a. The angular distribution of the Compton electrons was approximated by N times M individual electrons each having a unique initial direction, V (ϕ_i, θ_j), in spherical coordinates where i runs from 1 to N and j runs from 1 to M and where the radius vector from the burst is parallel to $\phi = 0$ and the nonradial (or transverse) component of the geomagnetic field is in the direction $\theta = 0$. The angle θ is measured clockwise as seen when looking along the line of sight from the burst to the observer. The NM electrons were given equal weights. The values of the ϕ_i were obtained in the following way:

The range of ϕ from 0^o to 90^o was divided into N parts: (A_o, A_1); $(A_1, A_2), \ldots (A_{N-1}, A_N)$ where $A_o = 0^o$, $A_N = 90^o$, and

$$\frac{1}{N} = \int_{A_{i-1}}^{A_i} P(\phi, \theta_j)\, d\phi.$$

The function $P(\phi, \theta_j)$ is the Klein-Nishina differential-scattering amplitude normalized so that

$$1 = \int_{0^o}^{90^o} P(\phi, \theta_j)\, d\phi.$$

The ϕ_i were then moment-centered in (A_{i-1}, A_i) by

$$\phi_i = N \int_{A_{i-1}}^{A_i} \phi\, P(\phi, \theta_j)\, d\phi.$$

The initial kinetic energy assigned to the (ϕ_i, θ_j) electron was likewise the moment-centered recoil energy for (A_{i-1}, A_i). The M θ_j were assigned values of (360j - 180)/M degrees. (This process of approximating the angular distribution of the Compton electrons is equivalent to assigning abscissas and equal weights for a subsequent two-dimensional quadrature on ϕ and θ. Other quadratures, such as Gaussian quadratures, are feasible on ϕ and will be investigated in the future as a possible means of reducing computer running time for future calculations. The equal-interval quadrature on θ is equivalent to evaluating the integral of an M-point trigonometric fit to the θ dependence of the source currents and is probably optimal since the θ dependence of the source currents is periodic.)

b. The NM source electrons thus defined were individually tracked along their helical trajectories, and the velocity components and energy-loss rate (due to formation of ion pairs) were stored at each step along the helix as a function of the source time, t. The trajectory was followed by evaluating the source electron speed, energy-loss rate, and turning frequency, $\frac{d\alpha}{dt}$, and then finding the new α after a source time step DT. DT was taken to be the minimum of the two quantities $E_o/(50\,\frac{dE}{dt})$ and 20 ns (where E_o was the initial energy of the source electron). The kinetic energy was

then decremented by DT (dE/dt) for each time step, DT. The trajectory was considered terminated when the kinetic energy became zero, or negative.

c. The velocity components and energy-loss rate were then convolved with the gamma source function, f(t), described in Paragraph 2. The source function was set to zero for all times such that its amplitude was less than 0.0001 of its peak amplitude. A sixteen-point Gaussian quadrature was then performed on the non-zero integrand of the convolution integral for each time, t, desired:

$$J(t) = \int_0^t x(t')\, f(t-t')\, dt'.$$

All currents were assumed to be zero at times, t, less than zero.

For the cases where the Compton scattering distribution is assumed to be all forward (i.e., forward-scattering approximation), a fudge factor, Q, is applied to the currents but not to the ion pair density. Q is taken to be the cosine of the average scattering angle, also, for the usual "1 x 1" (see Paragraph 4, below, for explanation of the notation) forward-scattering approximation. Two special forward-scattering approximations were also studied. One, denoted as the 1 x 1A approximation, used $\frac{dT}{dt} = 1 - (v_r/c)$ (average cos ϕ) and Q = average cos ϕ. The other, denoted as the 1 x 1B approximation, used $\frac{dT}{dt} = 1 - \frac{1}{2}(v_r/c)$ and $Q = \frac{1}{2} + \frac{1}{2}$ (average cos ϕ).

d. The resultant convolved current and ion pair density (equal to electron number density) values were stored on magnetic tape for later retrieval and plotting by the MERDC data retrieval and plotting code, BUDDHA.

4. Parameters. There were several parameters that were varied to obtain the results presented here. Results were calculated for all combinations of three gamma ray energies (1.5, 0.5, and 0.1 Mev), four altitudes above the USA (80, 60, 40, and 20 km), and two angles between the line of sight and the geomagnetic field (77.8° and 19.3°). These three parameters are termed "primary" parameters here. For each combination of primary parameters, some secondary parameters were varied. The secondary parameters were nine orders of approximation to the angular distribution of the Compton electrons (ranging from a 4-point to a 256-point approximation), three types of forward-scattering approximations (i.e., scattering angle is zero), and two gamma flux amplitude time history functions (including f(t), described in Paragraph 2, and a delta function time history).

The results are portrayed in 126 figures. Tables I through IV, Appendix A, describe the parameter values used to generate the data found in each figure (Figs. 1 through 126, Appendix B). The notation "4x8" means the angular distribution was approximated by a 4 times 8 point distribution with N=4 and M=8.

The amount of computer time consumed in the calculations was proportional to N times M so that the 16 x 16 results took 256 times more computer time than the 1x1 results.

III. DISCUSSION

5. **Results.** In the following discussion, it is assumed that the more detailed approximations tend to yield more accurate answers (all figures are located in Appendix B).

Figures 1 through 8 portray the currents and ion (electron) density for early time (zero to 100 ns) for ten angular distribution approximations, for the case of one altitude (80 km), one gamma ray energy (1.5 Mev), and two line-of-sight geomagnetic field angles (77.8^{o} and 19.3^{o}). The time histories differ strongly as a function of the angular distribution up to the 4 x 4 arrangement. For N greater than 4, the currents and ion densities do not differ appreciably. Thus, accurate time histories may be obtained for the first 100 ns with a 16-electron (N=4, M=4) approximation.

Figures 9 through 24 portray the currents and ion (electron) density for late time (zero to 4 microsec) for the same parameters. The 4 x 4 approximation maintains fair accuracy out to about 0.5 microsec but loses accuracy badly thereafter. In fact, it appears that the more electrons in the approximation, the later in time are accurate currents and ion densities obtained. The converse argues that any finite approximation to the angular distribution will fail to give accurate currents and ion densities after a certain time, and the less detailed approximations fail earlier. The 6 x 8 approximation holds well out to 1.5 microsec, but only the 12 x 16 approximation weathers the difficult 2-microsec region with good accuracy; the latter also holds well out to about 3 microsec.

It is evident that the ion density is less sensitive to the angular distribution approximation than are the current components.

It is also evident that, for 1.5-Mev gammas and 80-km altitude, there is a drastic difference between the currents obtained from the 1 x 1 forward-scattering model and the 16 x 16 angular-distribution model for times after 1 microsec. This would lead to very different EMP fields calculated from them.

Figures 25 through 42 portray the currents and ion (electron) density for late time (zero to 4 microsec), for five angular distribution approximations, for the case of one altitude (80 km), two line of sight–geomagnetic field angles (77.8° and 19.3°), and three gamma ray energies (1.5, 0.5, and 0.1 Mev). As observed earlier, the time histories differ sharply for different approximations in the 1.5-Mev gamma case; it appears that the current time histories differ less sharply for 0.5-Mev gammas and differ little for 0.1-Mev gammas. The ion density description using forward scattering does not improve so much with decreasing gamma energy, and the 1 x 1 approximation result is high by about 40% at 4 microsec for 0.1-Mev gammas.

This result suggests that the effect of the angular distribution of the Compton electrons is primarily a relativistic effect–greater for gamma energies above 0.5 Mev and less for gamma energies below 0.5 Mev.

Figures 43 through 66 portray the currents and ion (electron) density for early time (zero to 100 ns), for four angular distribution approximations (including the three forward-scattering approximations 1 x 1, 1 x 1A, and 1 x 1B, and the 16 x 16 angular-distribution approximation). These are for the case of two altitudes (80 and 20 km), two line of sight – geomagnetic field angles (77.8° and 19.3°), and three gamma ray energies (1.5, 0.5, and 0.1 Mev). Since the phi component and radial component dominate the theta component of the EMP electric fields and since the high-altitude burst fields measured on the surface are governed by the phi current and electron density (essentially equal to the ion density) at the lower edge of the source region (about 15- to 25-km altitude) for large yield bursts, it is of interest to compare the radial and phi currents and ion density for the 16 x 16, 1 x 1, 1 x 1A, and 1 x 1B approximations with particular importance laid on the 20-km altitude results.

It is seen by examining Figures 43 through 66 that the 16 x 16 approximation results are closely followed by the 1 x 1B approximation results for 1.5-Mev gammas, particularly at 20-km altitude, up to a time of about 60 ns. For 0.5-Mev gammas, the 1 x 1B results are close to the 16 x 16 results for the first 60 ns except for the phi current at 20-km altitude where the 16 x 16 results are not followed closely by any of the forward-scattering approximations. For 0.1-Mev gammas, the 16 x 16 results are followed best by the 1 x 1 results at 80-km altitude and by the 1 x 1A results at 20-km altitude.

Since the burst gamma output is "hardened up" to several Mev average energy at the lower source region, it appears that the 1 x 1B approximation would suffice to obtain accurate radial and phi currents and electron densities at all altitudes for the first 60 ns for bursts producing gammas of energy 0.5 Mev and greater. This period of time extends past the gamma flux peak in time and also past the time of peak EMP total electric field for altitudes less than roughly 50-km altitude. Thus, for low-altitude field mapping

of peak fields, the 1 x 1B forward-scattering approximation appears to be an acceptable alternative to the more detailed and time consuming angular-distribution approximations.

Figures 67 through 102 portray the currents and ion (electron) density for late time (zero to 4 microsec), for the 1 x 1 forward-scattering and 16 x 16 angular-scattering approximations, for the case of three altitudes (80, 60, and 40 km), two line of sight – geomagnetic field angles (77.8° and 19.3°), and three gamma ray energies (1.5, 0.5, and 0.1 Mev). These results illustrate the fact that relativistic Compton electrons generate source currents that have different time histories than indicated by the forward-scattering model especially at higher altitudes. On the other hand, EMP at higher altitudes (greater than 80 km, roughly) is dominated by X-rays instead of gamma rays so that the 1 x 1 forward-scattering approximation may be used safely to calculate EMP in the "X-ray source region" into the microsecond time region if the ion density is multiplied by a time-dependent correction factor. Comparison of Figures 79 and 97 suggests the correction factor will be a slight function of the angle between the line of sight and the geomagnetic field. Comparison of Figures 79 and 81 suggests the correction factor may depend on the source electron lifetime and, hence, the altitude.

Figures 103 through 126 portray the currents and ion (electron) density for late time (zero to 4 microsec), for a delta function gamma flux time dependence and the f(t) gamma flux time dependence described earlier and used throughout the previous figures. These are for the case of a 16 x 16 angular-distribution approximation, one altitude (80 km), three gamma ray energies (1.5, 0.5, and 0.1 Mev), and two line of sight – geomagnetic field angles (77.8° and 19.3°). In each case, the results for the two gamma source functions agree very well for times after about 150 ns. This means that it is not necessary to convolve the gamma source function with the source electron trajectory elements to obtain accurate source currents and ion density for times at least of the order of 100 ns after the gamma flux peak. A simple (and fast) folding with a delta function gamma source function will usually suffice. For times closer to the gamma-flux peak, however, the full convolution must still be performed to obtain accurate answers.

The exceptionally sharp peak in the currents occurring at very early time is probably spurious because the NEPHI 70 computer code was not built to fold a delta function and had to be fooled rather badly to do it.

IV. CONCLUSIONS

6. **Conclusions.** For high-altitude EMP source current and ionization amplitudes and time histories, calculated results based on the assumption of forward Compton

scattering differ markedly from calculated results based on approximations to the actual angular distribution of the Compton scattering.

For times earlier than about 500 ns after the gamma-flux peak, the currents and ionization can be accurately evaluated by using only 16 electrons in the angular-distribution approximation (the 4 x 4 model) for all altitudes and gamma energies studied. For 1.5-Mev gammas, a modification of the forward-scattering assumption (the 1 x 1B model) accurately evaluates the currents and ionization up to about 10 ns after the gamma-flux peak and may thus be useful for peak field calculations.

For 1.5-Mev gammas, the following statements appear true: For times later than about 500 ns after the gamma flux peak, the angular-distribution approximation requires more and more electrons than 16; accuracy to 1.5 microseconds requires at least 48 electrons (the 6 x 8 model); and accuracy to 3.0 microseconds requires at least 192 electrons (the 12 x 16 model) for an arbitrary angle between the line of sight and the geomagnetic field.

For 0.5-Mev gammas, the accuracy is maintained to slightly later times than for 1.5-Mev gammas for the same scattering approximations. For 0.1-Mev, the forward-scattering approximation (1 x 1 model) yields fair accuracy for the currents out to the latest time considered here, 4 microseconds, and the 4 x 4 approximation gives good accuracy. A time-dependent correction factor may be applied to the 1 x 1 ionization results for 0.1 Mev to improve accuracy. Thus, nonrelativistic Compton electrons can be treated with the forward-scattering model at higher altitudes (more than 60 km). These electrons are not effective in generating EMP at lower altitudes.

It appears that a delta function gamma flux time dependence may be assumed without significantly affecting accuracy when calculating source currents and ionization at times later than about 100 ns after the gamma flux peak.

APPENDIX A

TABLES

Table I. Parameter Values for Figures

SET A = 1X1, 1X4, 2X4, 2X8, 4X4, 4X8, 6X8, 8X8, 12X16, 16X16
SET B = 1X1, 1X4, 2X4, 2X8, 4X4, 16X16
SET C = 1X1, 4X8, 6X8, 8X8, 12X16, 16X16
SET D = 1X1, 1X4, 4X4, 8X8, 16X16
SET E = 1X1, 1X1A, 1X1B, 16X16

FIGURE NUMBER	VARIABLE PLOTTED	MAXIMUM TIME (NS)	ALTITUDE (KM)	GAMMA ENERGY (MEV)	ANGLE BETWEEN B AND R (DEGREES)	COMPTON SCATTERING APPROXIMATION	SOURCE FUNCTION
1	J_r	100	80	1.5	77.8	SET A	F(T)
2	J_r	100	80	1.5	19.3	SET A	F(T)
3	J_ϕ	100	80	1.5	77.8	SET A	F(T)
4	J_ϕ	100	80	1.5	19.3	SET A	F(T)
5	J_θ	100	80	1.5	77.8	SET A	F(T)
6	J_θ	100	80	1.5	19.3	SET A	F(T)
7	N	100	80	1.5	77.8	SET A	F(T)
8	N	100	80	1.5	19.3	SET A	F(T)
9	J_r	4000	80	1.5	77.8	SET B	F(T)
10	J_r	4000	80	1.5	77.8	SET C	F(T)
11	J_r	4000	80	1.5	19.3	SET B	F(T)
12	J_r	4000	80	1.5	19.3	SET C	F(T)
13	J_ϕ	4000	80	1.5	77.8	SET B	F(T)
14	J_ϕ	4000	80	1.5	77.8	SET C	F(T)
15	J_ϕ	4000	80	1.5	19.3	SET B	F(T)
16	J_ϕ	4000	80	1.5	19.3	SET C	F(T)
17	J_θ	4000	80	1.5	77.8	SET B	F(T)
18	J_θ	4000	80	1.5	77.8	SET C	F(T)
19	J_θ	4000	80	1.5	19.3	SET B	F(T)
20	J_θ	4000	80	1.5	19.3	SET C	F(T)
21	N	4000	80	1.5	77.8	SET B	F(T)
22	N	4000	80	1.5	77.8	SET C	F(T)
23	N	4000	80	1.5	19.3	SET B	F(T)
24	N	4000	80	1.5	19.3	SET C	F(T)
25	J_ϕ	4000	80	1.5	77.8	SET D	F(T)
26	J_ϕ	4000	80	0.5	77.8	SET D	F(T)
27	J_ϕ	4000	80	0.1	77.8	SET D	F(T)
28	J_ϕ	4000	80	1.5	19.3	SET D	F(T)
29	J_ϕ	4000	80	0.5	19.3	SET D	F(T)
30	J_ϕ	4000	80	0.1	19.3	SET D	F(T)
31	J_r	4000	80	1.5	77.8	SET D	F(T)
32	J_r	4000	80	0.5	77.8	SET D	F(T)

Table II. Parameter Values for Figures (cont'd)

SET A = 1X1, 1X4, 2X4, 2X8, 4X4, 4X8, 6X8, 8X8, 12X16, 16X16
SET B = 1X1, 1X4, 2X4, 2X8, 4X4, 16X16
SET C = 1X1, 4X8, 6X8, 8X8, 12X16, 16X16
SET D = 1X1, 1X4, 4X4, 8X8, 16X16
SET E = 1X1, 1X1A, 1X1B, 16X16

FIGURE NUMBER	VARIABLE PLOTTED	MAXIMUM TIME (NS)	ALTITUDE (KM)	GAMMA ENERGY (MEV)	ANGLE BETWEEN B AND R (DEGREES)	COMPTON SCATTERING APPROXIMATION	SOURCE FUNCTION
33	J_r	4000	80	0.1	77.8	SET D	F(T)
34	J_r	4000	80	1.5	19.3	SET D	F(T)
35	J_r	4000	80	0.5	19.3	SET D	F(T)
36	J_r	4000	80	0.1	19.3	SET D	F(T)
37	N	4000	80	1.5	77.8	SET D	F(T)
38	N	4000	80	0.5	77.8	SET D	F(T)
39	N	4000	80	0.1	77.8	SET D	F(T)
40	N	4000	80	1.5	19.3	SET D	F(T)
41	N	4000	80	0.5	19.3	SET D	F(T)
42	N	4000	80	0.1	19.3	SET D	F(T)
43	J_ϕ & N	100	80	1.5	77.8	SET E	F(T)
44	J_r & J_θ	100	80	1.5	77.8	SET E	F(T)
45	J_ϕ & N	100	20	1.5	77.8	SET E	F(T)
46	J_r & J_θ	100	20	1.5	77.8	SET E	F(T)
47	J_ϕ & N	100	80	0.5	77.8	SET E	F(T)
48	J_r & J_θ	100	80	0.5	77.8	SET E	F(T)
49	J_ϕ & N	100	20	0.5	77.8	SET E	F(T)
50	J_r & J_θ	100	20	0.5	77.8	SET E	F(T)
51	J_ϕ & N	100	80	0.1	77.8	SET E	F(T)
52	J_r & J_θ	100	80	0.1	77.8	SET E	F(T)
53	J_ϕ & N	100	20	0.1	77.8	SET E	F(T)
54	J_r & J_θ	100	20	0.1	77.8	SET E	F(T)
55	J_ϕ & N	100	80	1.5	19.3	SET E	F(T)
56	J_r & J_θ	100	80	1.5	19.3	SET E	F(T)
57	J_ϕ & N	100	20	1.5	19.3	SET E	F(T)
58	J_r & J_θ	100	20	1.5	19.3	SET E	F(T)
59	J_ϕ & N	100	80	0.5	19.3	SET E	F(T)
60	J_r & J_θ	100	80	0.5	19.3	SET E	F(T)
61	J_ϕ & N	100	20	0.5	19.3	SET E	F(T)
62	J_r & J_θ	100	20	0.5	19.3	SET E	F(T)
63	J_ϕ & N	100	80	0.1	19.3	SET E	F(T)
64	J_r & J_θ	100	80	0.1	19.3	SET E	F(T)

Table III. Parameter Values for Figures (cont'd)

SET A = 1X1, 1X4, 2X4, 2X8, 4X4, 4X8, 6X8, 8X8, 12X16, 16X16
SET B = 1X1, 1X4, 2X4, 2X8, 4X4, 16X16
SET C = 1X1, 4X8, 6X8, 8X8, 12X16, 16X16
SET D = 1X1, 1X4, 4X4, 8X8, 16X16
SET E = 1X1, 1X1A, 1X1B, 16X16

FIGURE NUMBER	VARIABLE PLOTTED	MAXIMUM TIME (NS)	ALTITUDE (KM)	GAMMA ENERGY (MEV)	ANGLE BETWEEN B AND R (DEGREES)	COMPTON SCATTERING APPROXIMATION	SOURCE FUNCTION
65	J_ϕ € N	100	20	0.1	19.3	SET E	F(T)
66	J_r € J_θ	100	20	0.1	19.3	SET E	F(T)
67	J_ϕ € N	4000	80	1.5	77.8	1X1 € 16X16	F(T)
68	J_r € J_θ	4000	80	1.5	77.8	1X1 € 16X16	F(T)
69	J_ϕ € N	4000	60	1.5	77.8	1X1 € 16X16	F(T)
70	J_r € J_θ	4000	60	1.5	77.8	1X1 € 16X16	F(T)
71	J_ϕ € N	4000	40	1.5	77.8	1X1 € 16X16	F(T)
72	J_r € J_θ	4000	40	1.5	77.8	1X1 € 16X16	F(T)
73	J_ϕ € N	4000	80	0.5	77.8	1X1 € 16X16	F(T)
74	J_r € J_θ	4000	80	0.5	77.8	1X1 € 16X16	F(T)
75	J_ϕ € N	4000	60	0.5	77.8	1X1 € 16X16	F(T)
76	J_r € J_θ	4000	60	0.5	77.8	1X1 € 16X16	F(T)
77	J_ϕ € N	4000	40	0.5	77.8	1X1 € 16X16	F(T)
78	J_r € J_θ	4000	40	0.5	77.8	1X1 € 16X16	F(T)
79	J_ϕ € N	4000	80	0.1	77.8	1X1 € 16X16	F(T)
80	J_r € J_θ	4000	80	0.1	77.8	1X1 € 16X16	F(T)
81	J_ϕ € N	4000	60	0.1	77.8	1X1 € 16X16	F(T)
82	J_r € J_θ	4000	60	0.1	77.8	1X1 € 16X16	F(T)
83	J_ϕ € N	4000	40	0.1	77.8	1X1 € 16X16	F(T)
84	J_r € J_θ	4000	40	0.1	77.8	1X1 € 16X16	F(T)
85	J_ϕ € N	4000	80	1.5	19.3	1X1 € 16X16	F(T)
86	J_r € J_θ	4000	80	1.5	19.3	1X1 € 16X16	F(T)
87	J_ϕ € N	4000	60	1.5	19.3	1X1 € 16X16	F(T)
88	J_r € J_θ	4000	60	1.5	19.3	1X1 € 16X16	F(T)
89	J_ϕ € N	4000	40	1.5	19.3	1X1 € 16X16	F(T)
90	J_r € J_θ	4000	40	1.5	19.3	1X1 € 16X16	F(T)
91	J_ϕ € N	4000	80	0.5	19.3	1X1 € 16X16	F(T)
92	J_r € J_θ	4000	80	0.5	19.3	1X1 € 16X16	F(T)
93	J_ϕ € N	4000	60	0.5	19.3	1X1 € 16X16	F(T)
94	J_r € J_θ	4000	60	0.5	19.3	1X1 € 16X16	F(T)
95	J_ϕ € N	4000	40	0.5	19.3	1X1 € 16X16	F(T)
96	J_r € J_θ	4000	40	0.5	19.3	1X1 € 16X16	F(T)

Table IV. Parameter Values for Figures (cont'd)

SET A = 1X1, 1X4, 2X4, 2X8, 4X4, 4X8, 6X8, 8X8, 12X16, 16X16
SET B = 1X1, 1X4, 2X4, 2X8, 4X4, 16X16
SET C = 1X1, 4X8, 6X8, 8X8, 12X16, 16X16
SET D = 1X1, 1X4, 4X4, 8X8, 16X16
SET E = 1X1, 1X1A, 1X1B, 16X16

FIGURE NUMBER	VARIABLE PLOTTED	MAXIMUM TIME (NS)	ALTITUDE (KM)	GAMMA ENERGY (MEV)	ANGLE BETWEEN B AND R (DEGREES)	COMPTON SCATTERING APPROXIMATION	SOURCE FUNCTION
97	J_ϕ & N	4000	80	0.1	19.3	1X1 & 16X16	F(T)
98	J_r & J_θ	4000	80	0.1	19.3	1X1 & 16X16	F(T)
99	J_ϕ & N	4000	60	0.1	19.3	1X1 & 16X16	F(T)
100	J_r & J_θ	4000	60	0.1	19.3	1X1 & 16X16	F(T)
101	J_ϕ & N	4000	40	0.1	19.3	1X1 & 16X16	F(T)
102	J_r & J_θ	4000	40	0.1	19.3	1X1 & 16X16	F(T)
103	J_r	4000	80	1.5	77.8	16X16	F(T) & G(T)
104	J_ϕ	4000	80	1.5	77.8	16X16	F(T) & G(T)
105	J_θ	4000	80	1.5	77.8	16X16	F(T) & G(T)
106	N	4000	80	1.5	77.8	16X16	F(T) & G(T)
107	J_r	4000	80	0.5	77.8	16X16	F(T) & G(T)
108	J_ϕ	4000	80	0.5	77.8	16X16	F(T) & G(T)
109	J_θ	4000	80	0.5	77.8	16X16	F(T) & G(T)
110	N	4000	80	0.5	77.8	16X16	F(T) & G(T)
111	J_r	4000	80	0.1	77.8	16X16	F(T) & G(T)
112	J_ϕ	4000	80	0.1	77.8	16X16	F(T) & G(T)
113	J_θ	4000	80	0.1	77.8	16X16	F(T) & G(T)
114	N	4000	80	0.1	77.8	16X16	F(T) & G(T)
115	J_r	4000	80	1.5	19.3	16X16	F(T) & G(T)
116	J_ϕ	4000	80	1.5	19.3	16X16	F(T) & G(T)
117	J_θ	4000	80	1.5	19.3	16X16	F(T) & G(T)
118	N	4000	80	1.5	19.3	16X16	F(T) & G(T)
119	J_r	4000	80	0.5	19.3	16X16	F(T) & G(T)
120	J_ϕ	4000	80	0.5	19.3	16X16	F(T) & G(T)
121	J_θ	4000	80	0.5	19.3	16X16	F(T) & G(T)
122	N	4000	80	0.5	19.3	16X16	F(T) & G(T)
123	J_r	4000	80	0.1	19.3	16X16	F(T) & G(T)
124	J_ϕ	4000	80	0.1	19.3	16X16	F(T) & G(T)
125	J_θ	4000	80	0.1	19.3	16X16	F(T) & G(T)
126	N	4000	80	0.1	19.3	16X16	F(T) & G(T)

APPENDIX B

ILLUSTRATIONS

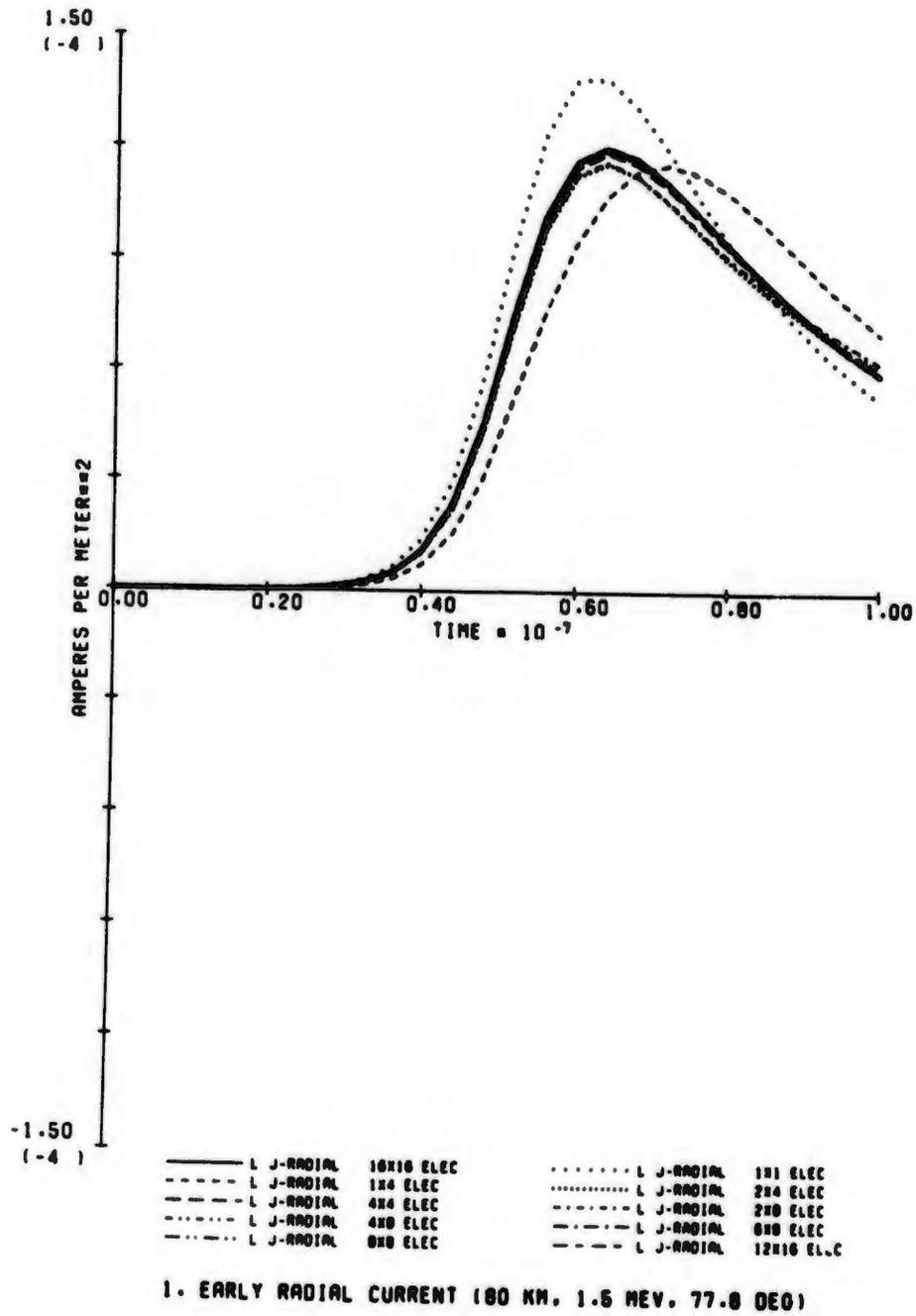

Fig. 1. Calculated Results for Parameter Set 1.

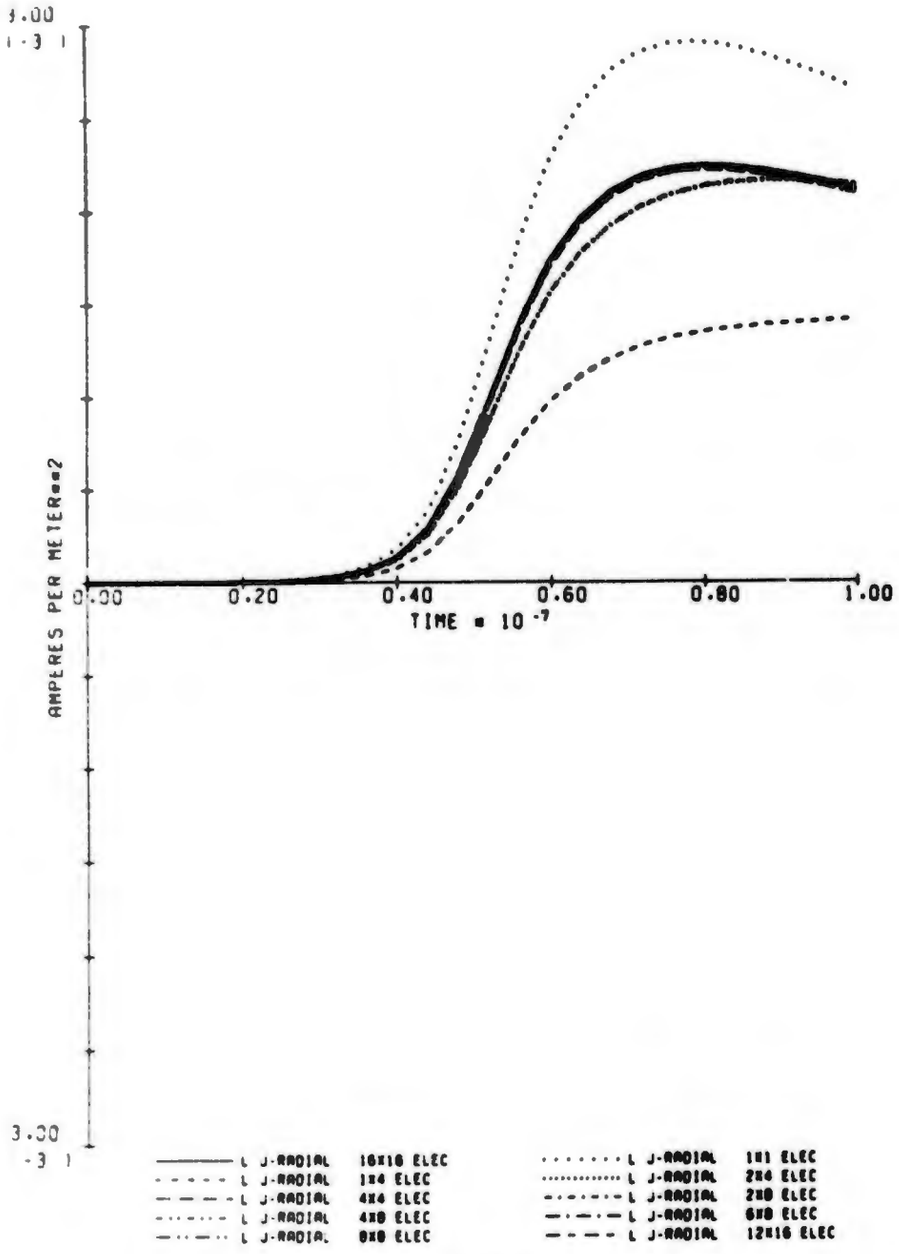

Fig. 2. Calculated Results for Parameter Set 2.

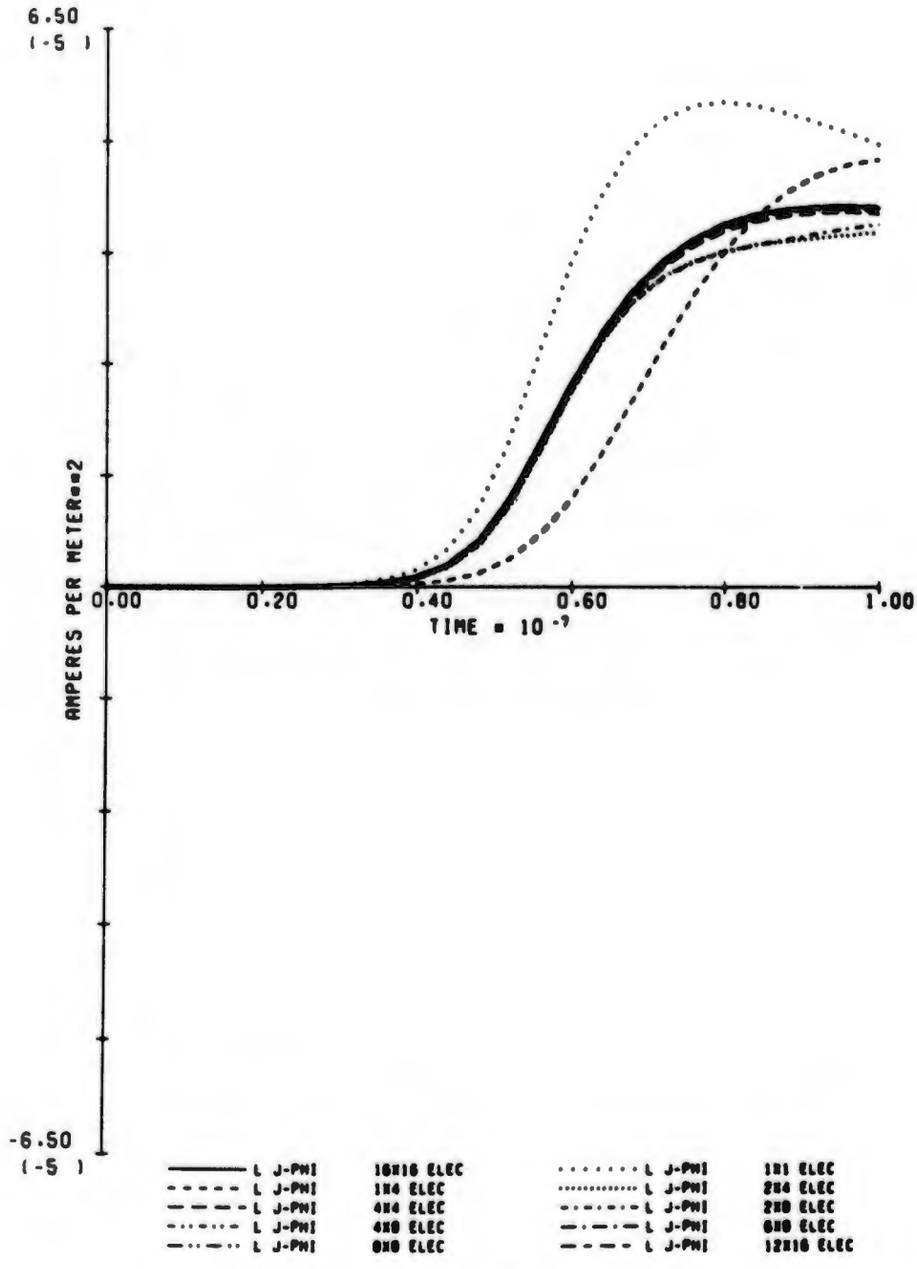

Fig. 3. Calculated Results for Parameter Set 3.

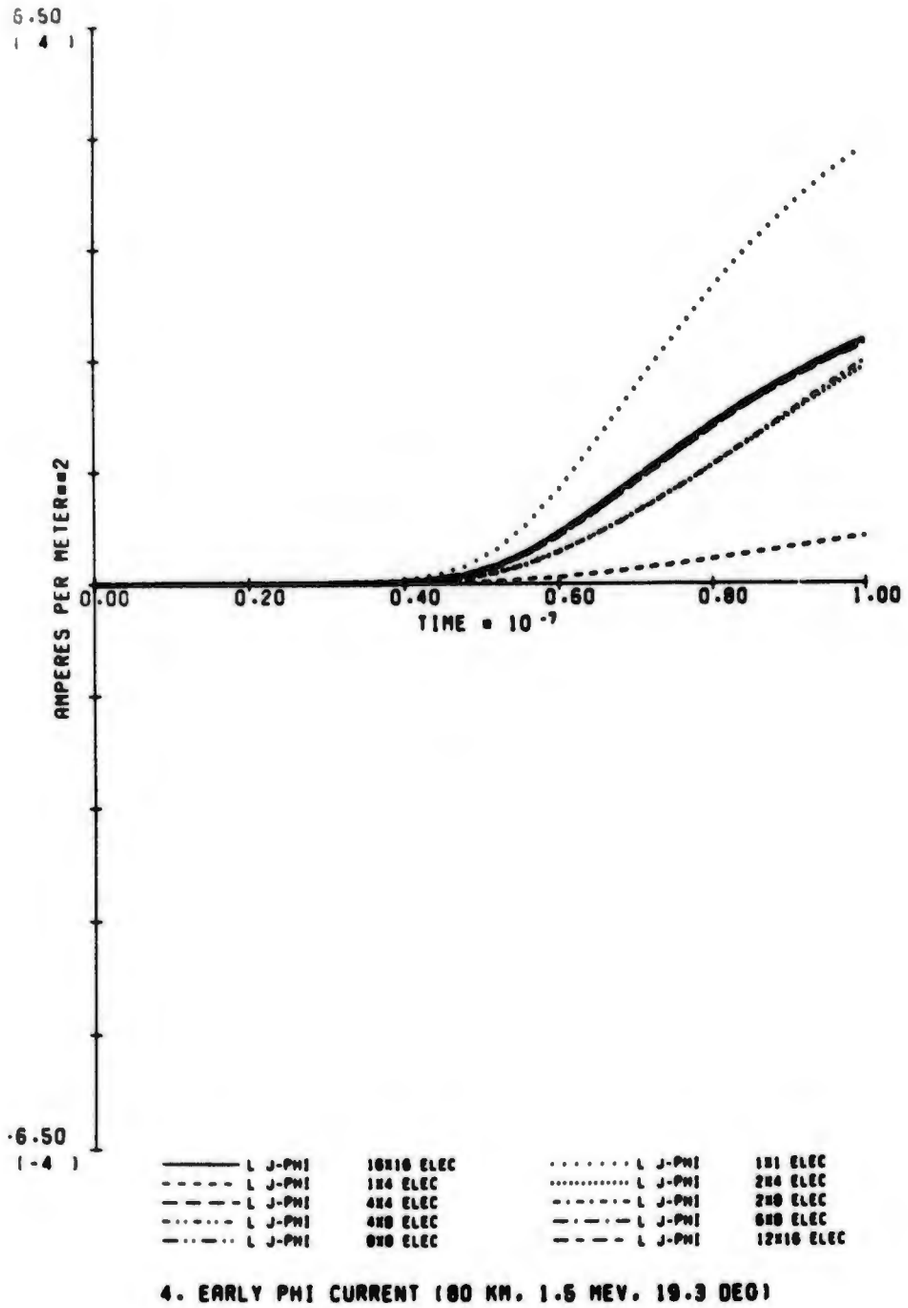

Fig. 4. Calculated Results for Parameter Set 4.

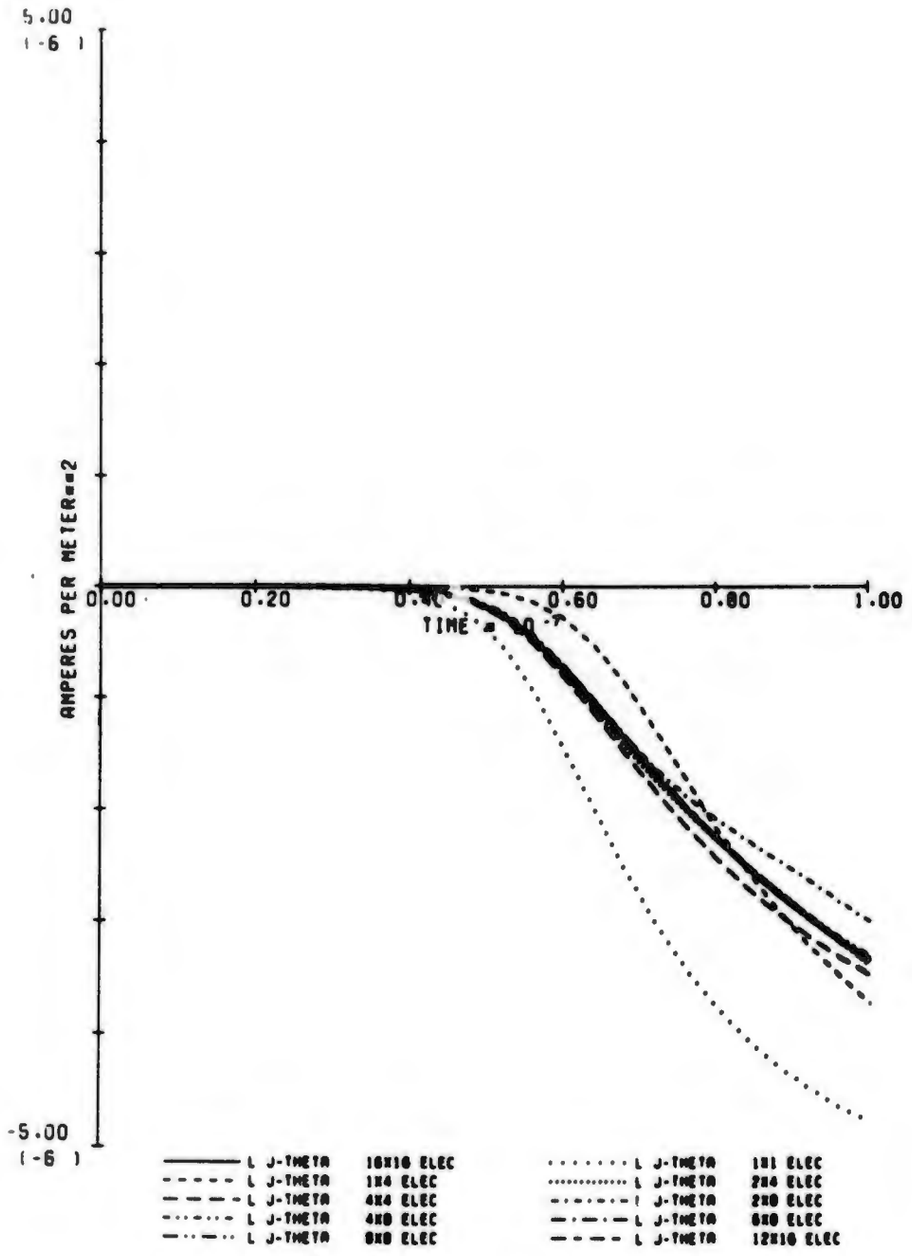

Fig. 5. Calculated Results for Parameter Set 5.

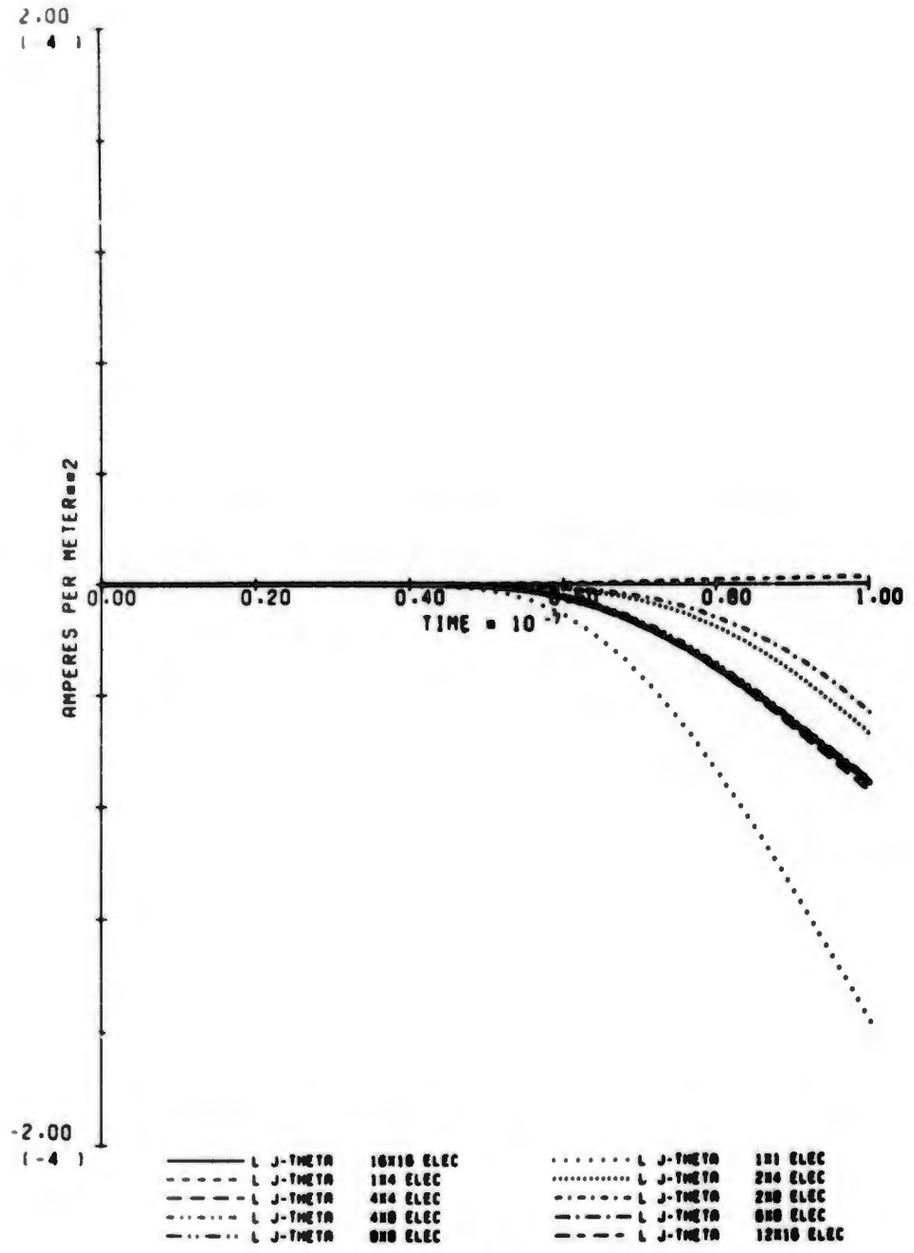

Fig. 6. Calculated Results for Parameter Set 6.

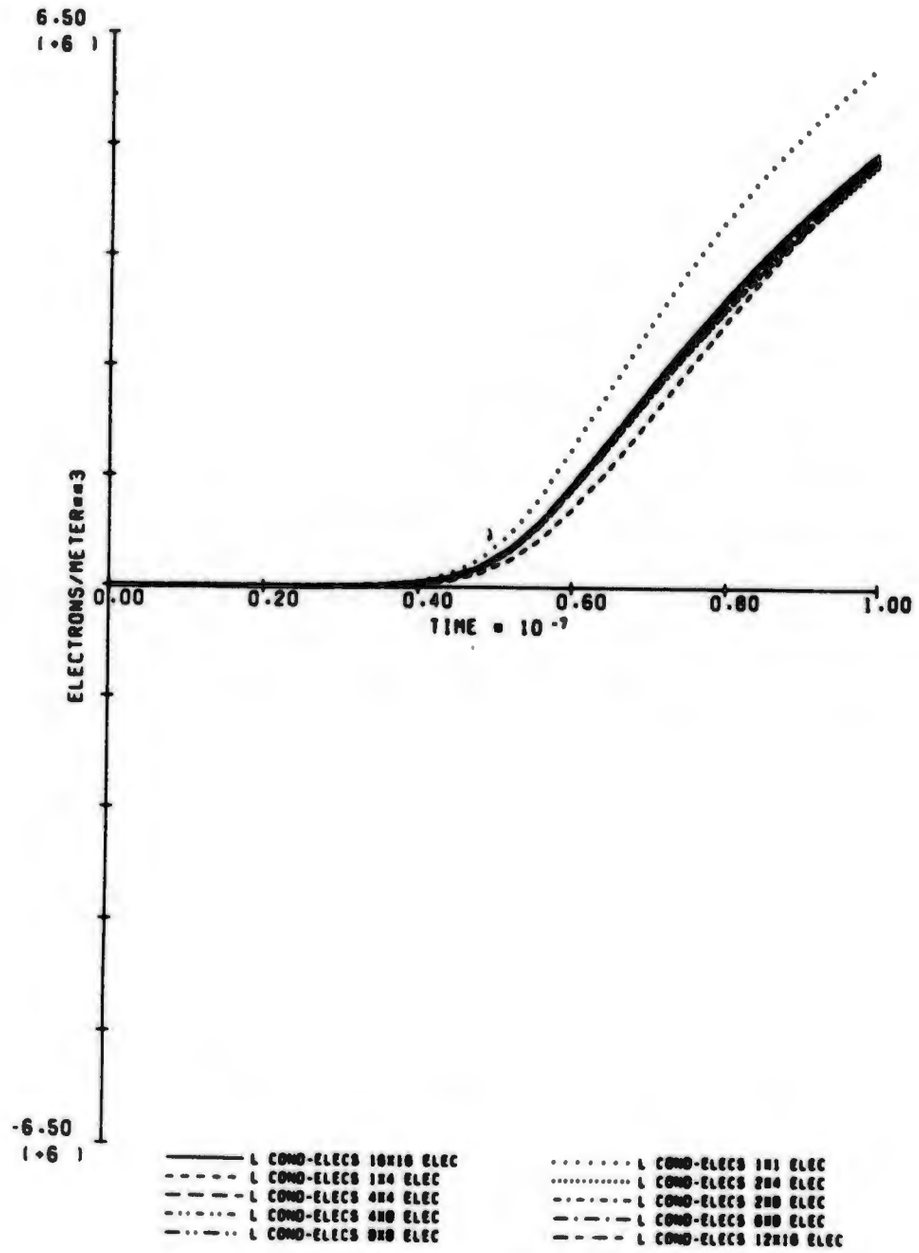

Fig. 7. Calculated Results for Parameter Set 7.

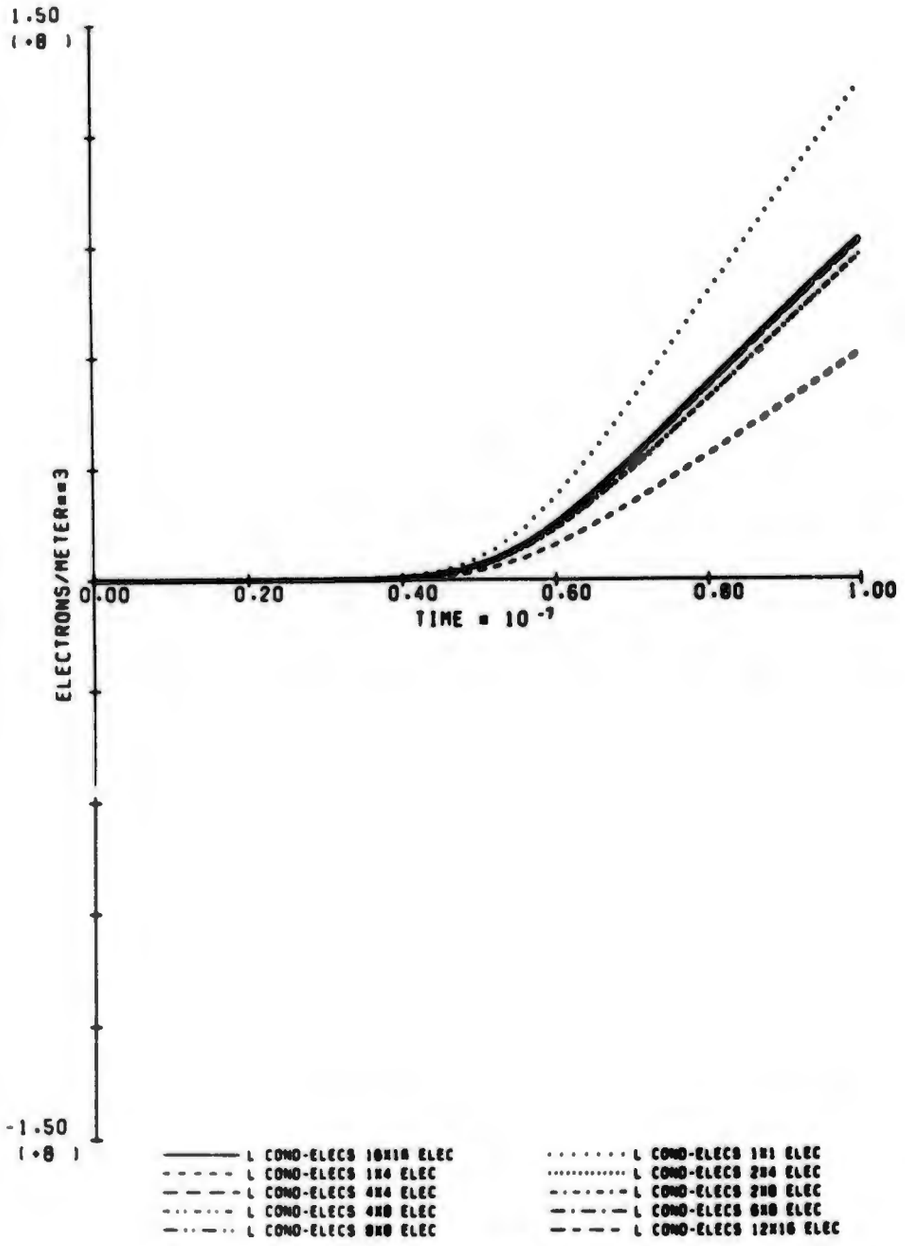

Fig. 8. Calculated Results for Parameter Set 8.

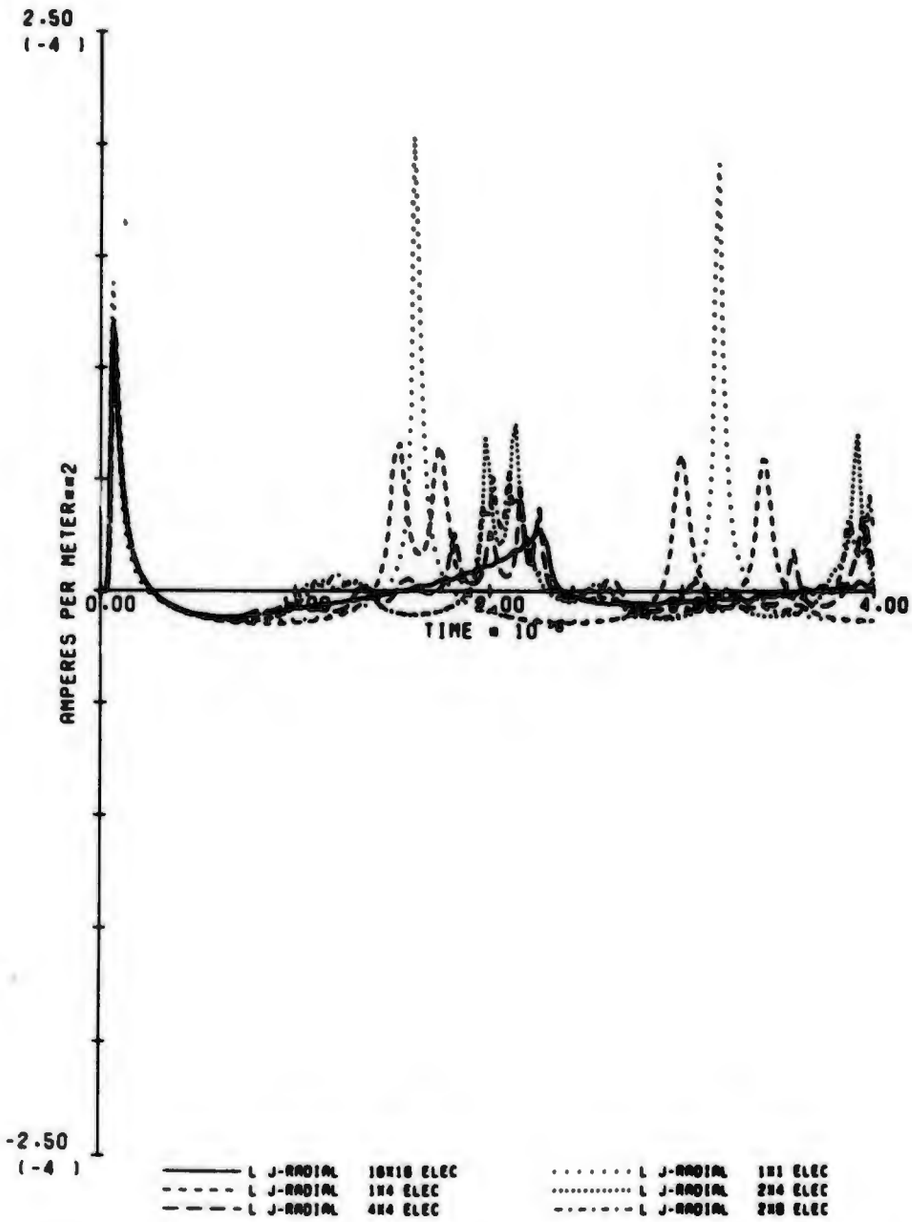

Fig. 9. Calculated Results for Parameter Set 9.

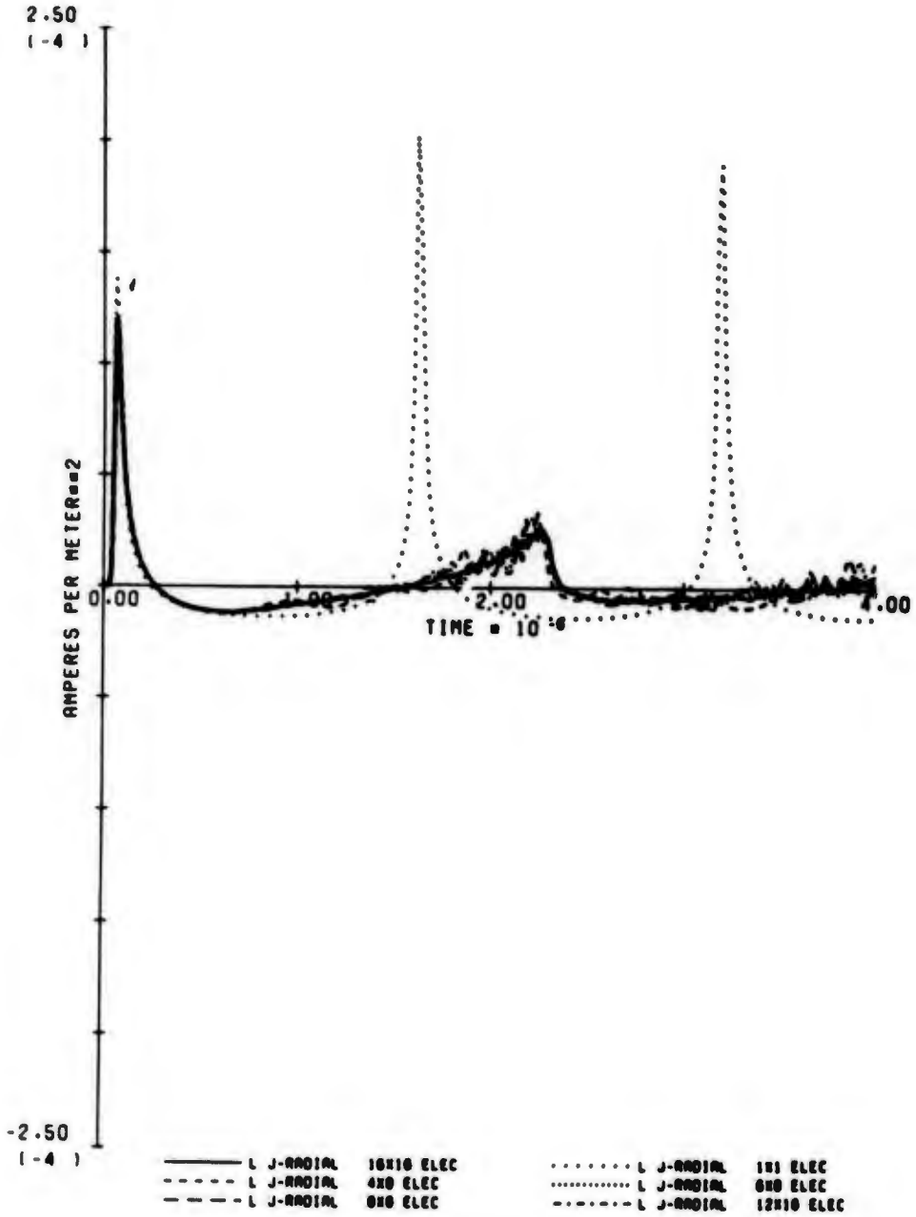

Fig. 10. Calculated Results for Parameter Set 10.

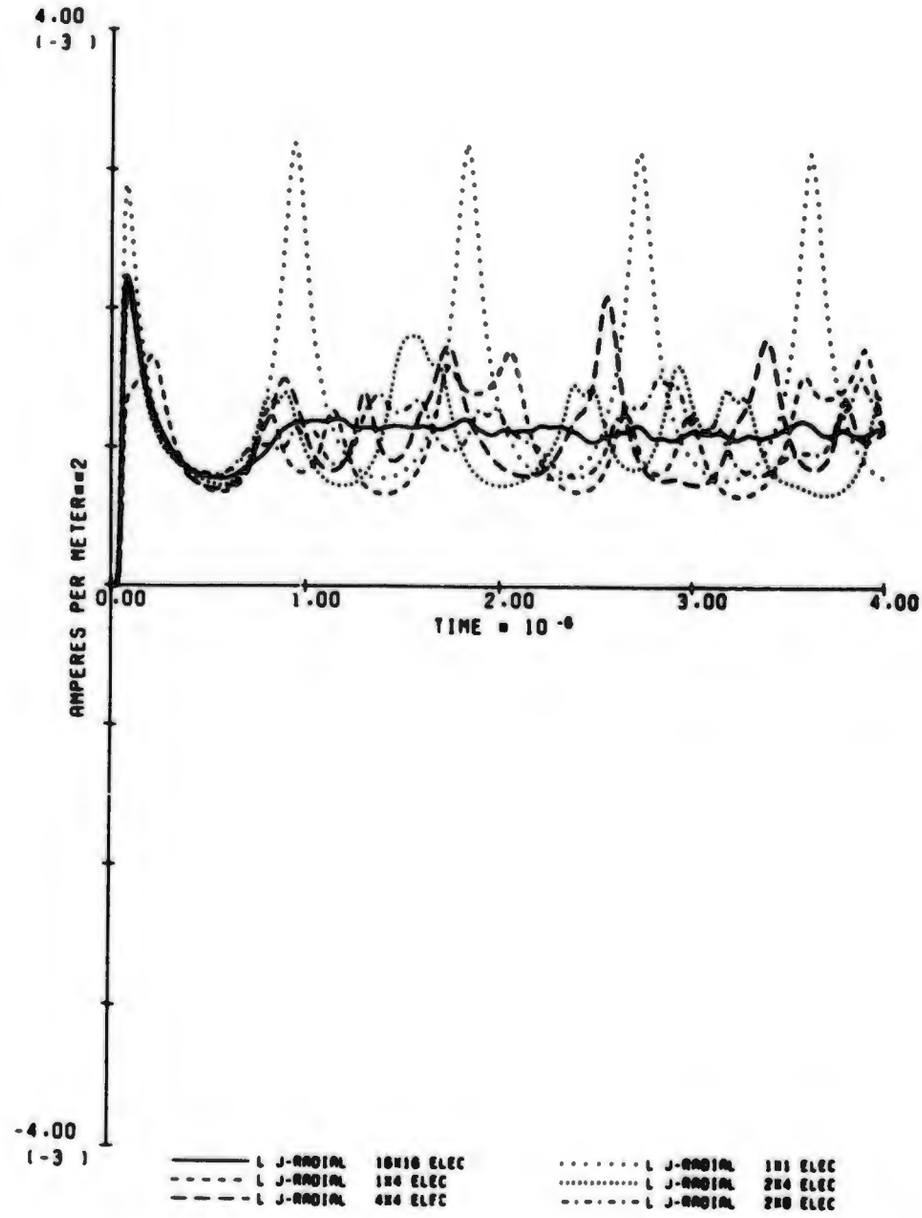

Fig. 11. Calculated Results for Parameter Set 11.

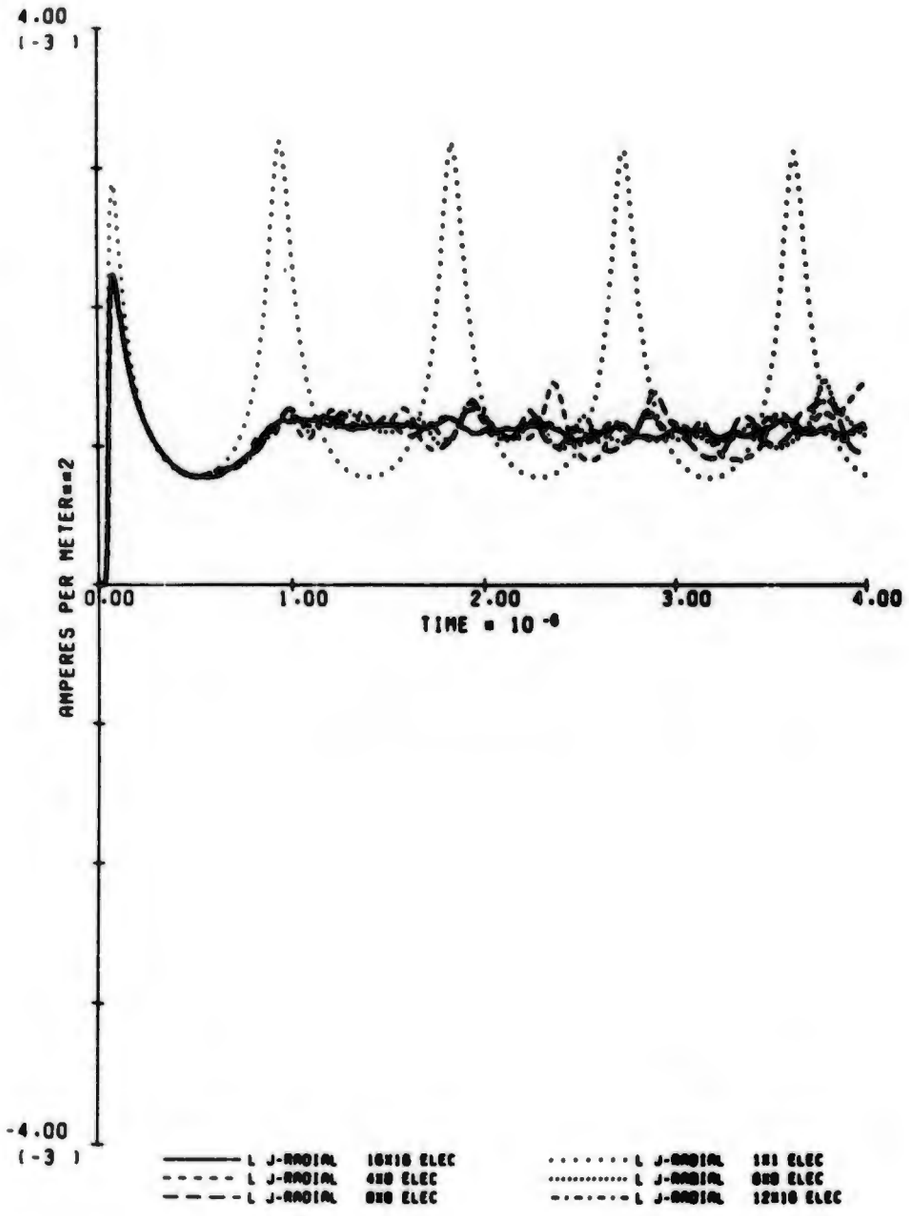

12. LATE RADIAL CURRENT (80 KM, 1.5 MEV, 19.3 DEG)

Fig. 12. Calculated Results for Parameter Set 12.

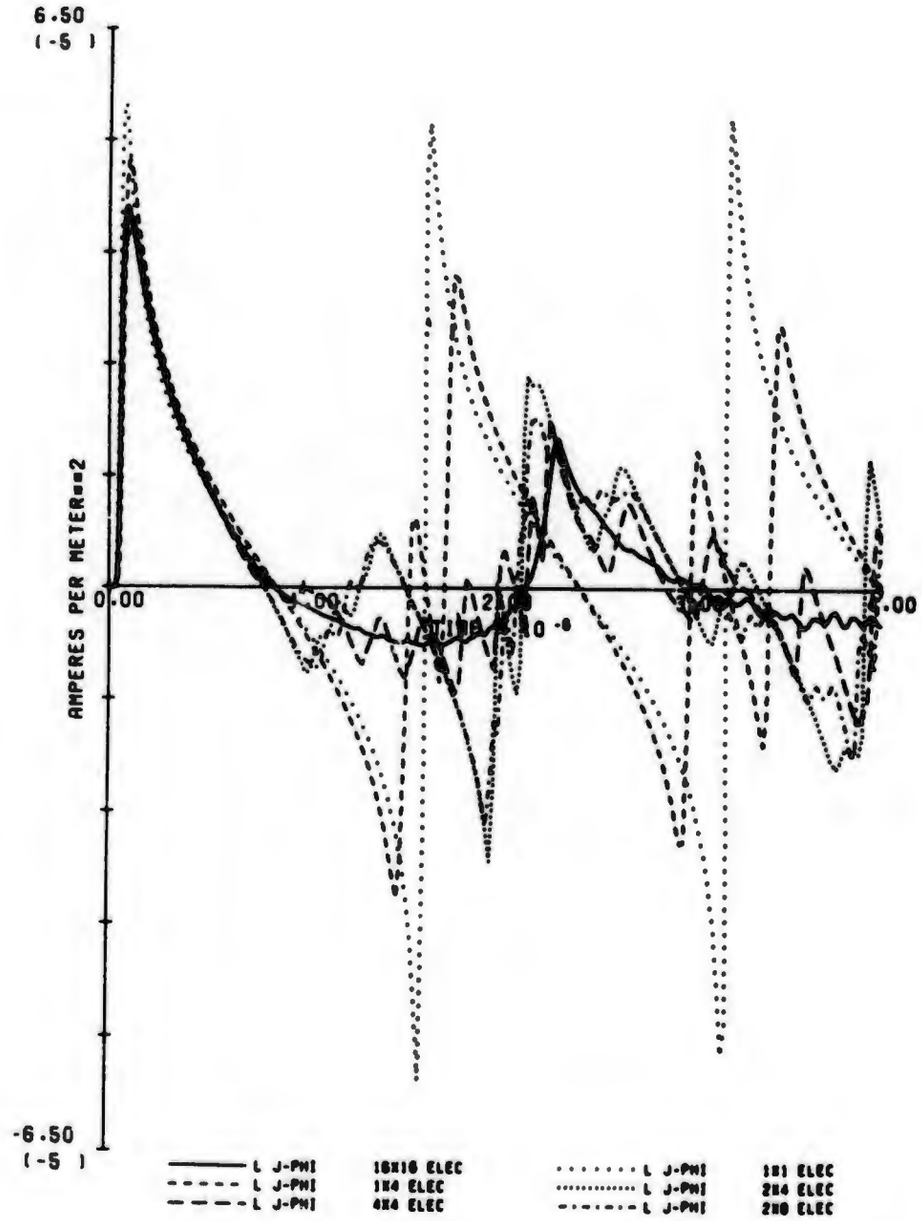

Fig. 13. Calculated Results for Parameter Set 13.

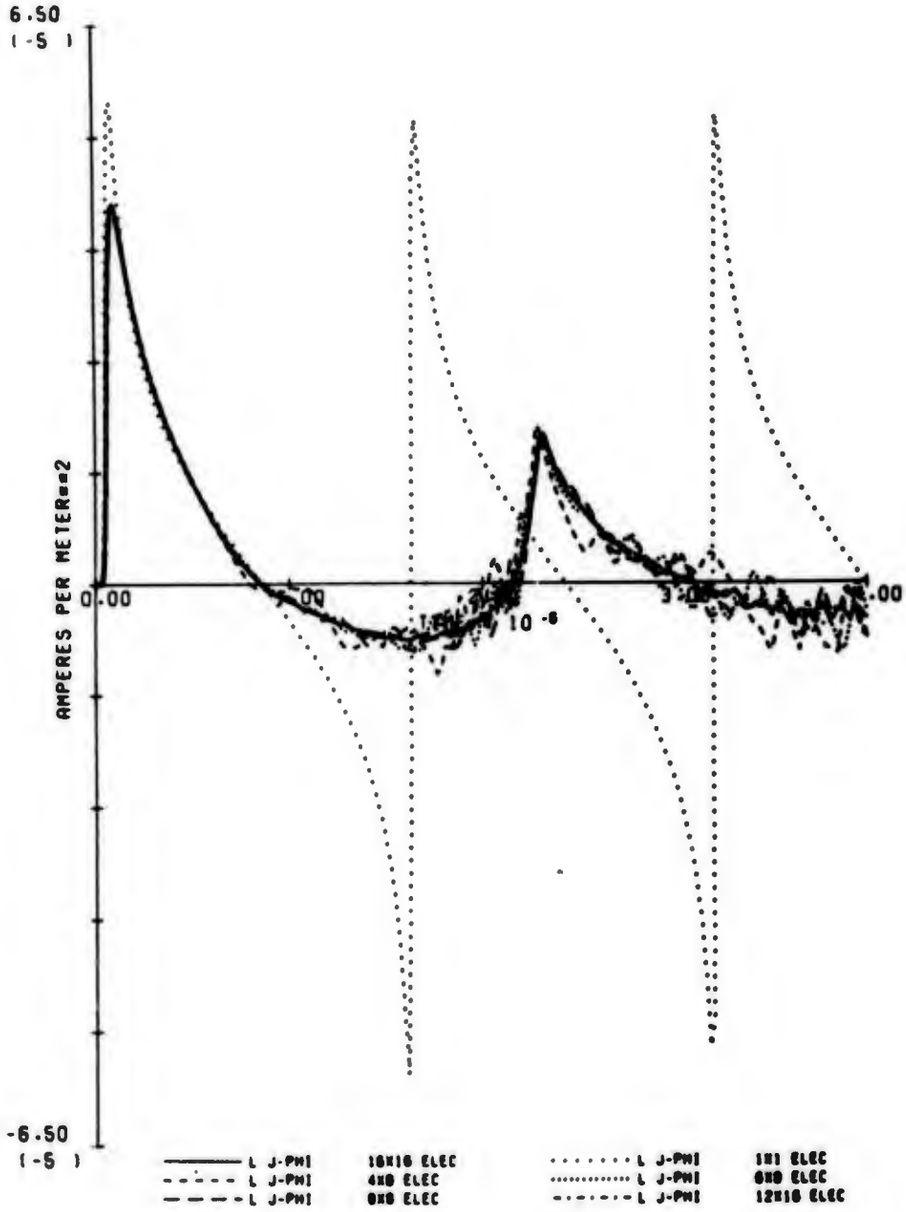

Fig. 14. Calculated Results for Parameter Set 14.

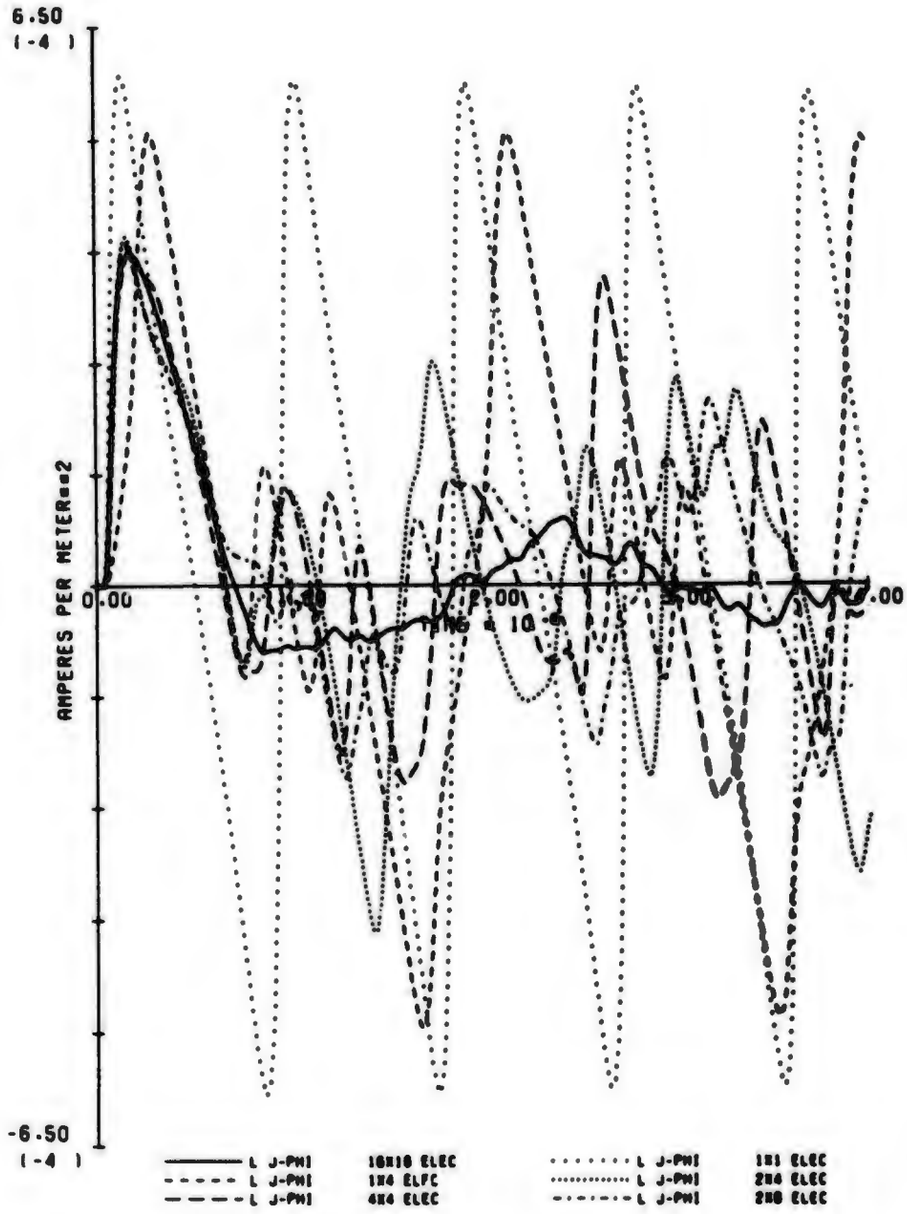

Fig. 15. Calculated Results for Parameter Set 15.

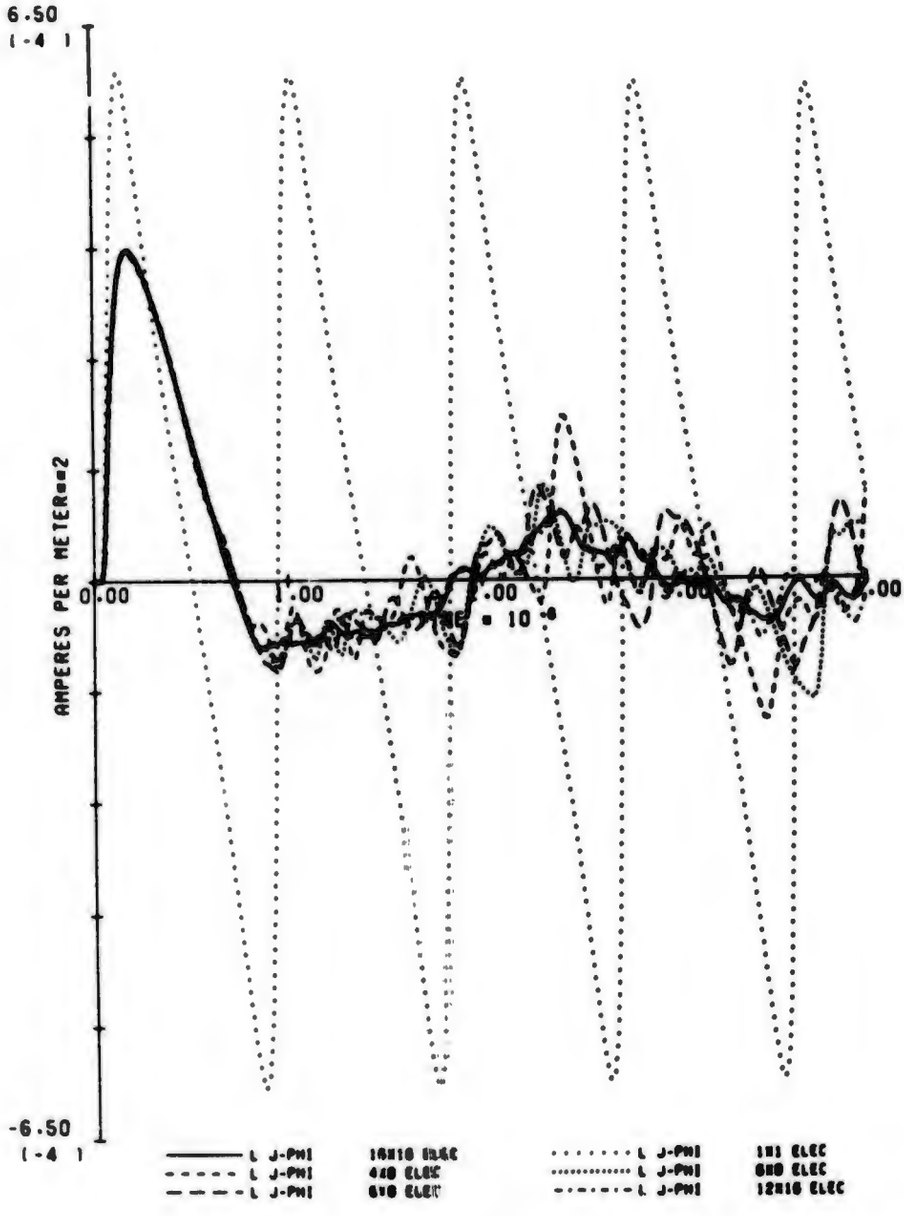

16 LATE PHI CURRENT KM. 1.5 MEV. 19.9 DEG

Fig. 16. Calculated Results for Parameter Set 16.

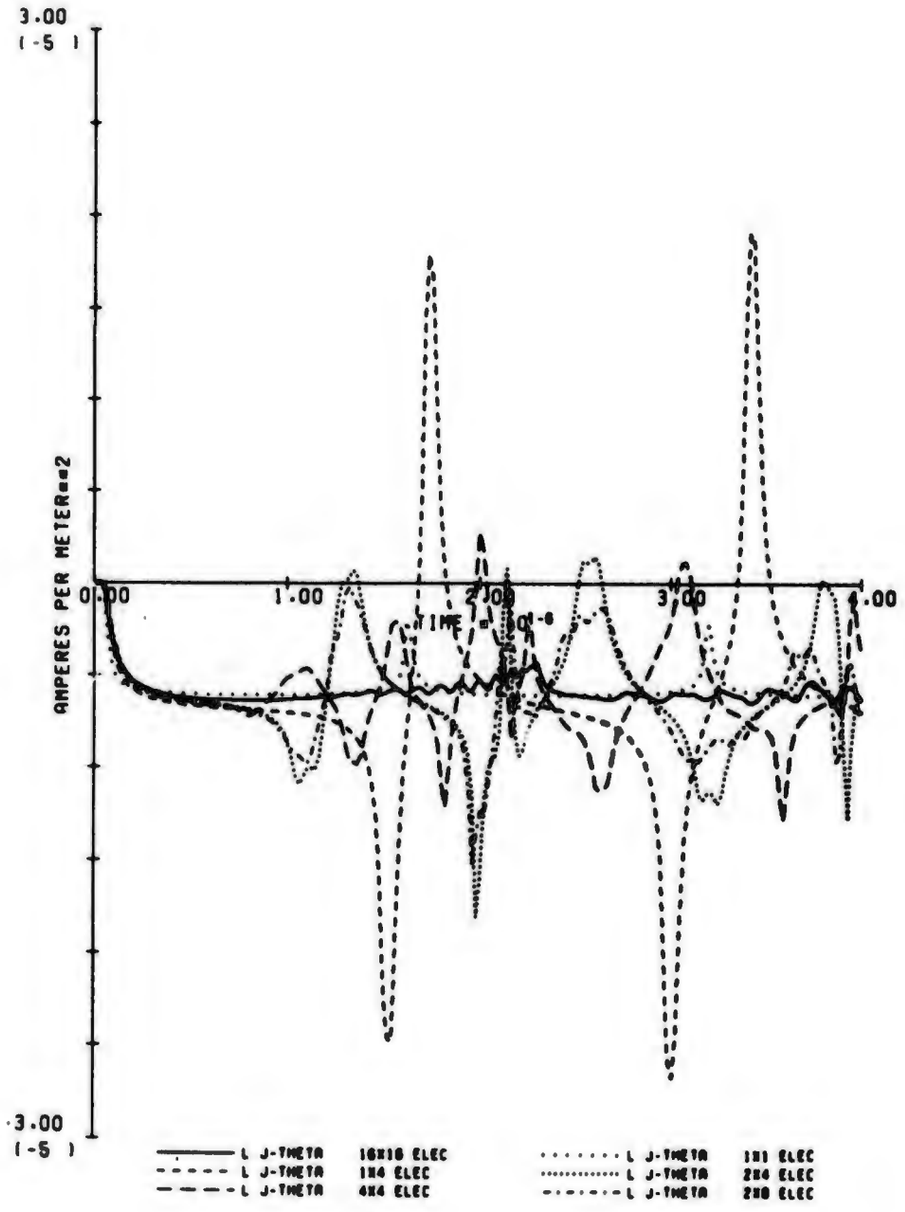

Fig. 17. Calculated Results for Parameter Set 17.

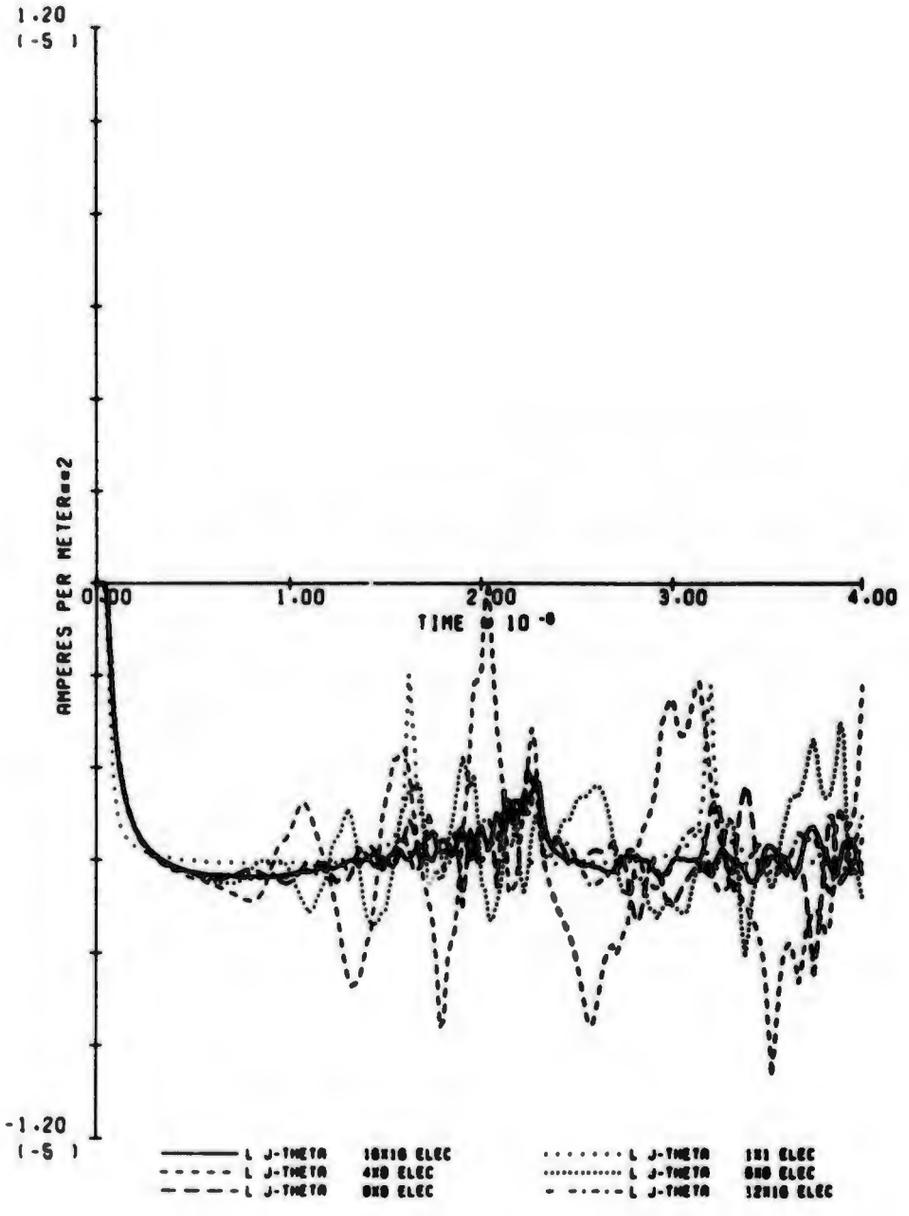

Fig. 18. Calculated Results for Parameter Set 18.

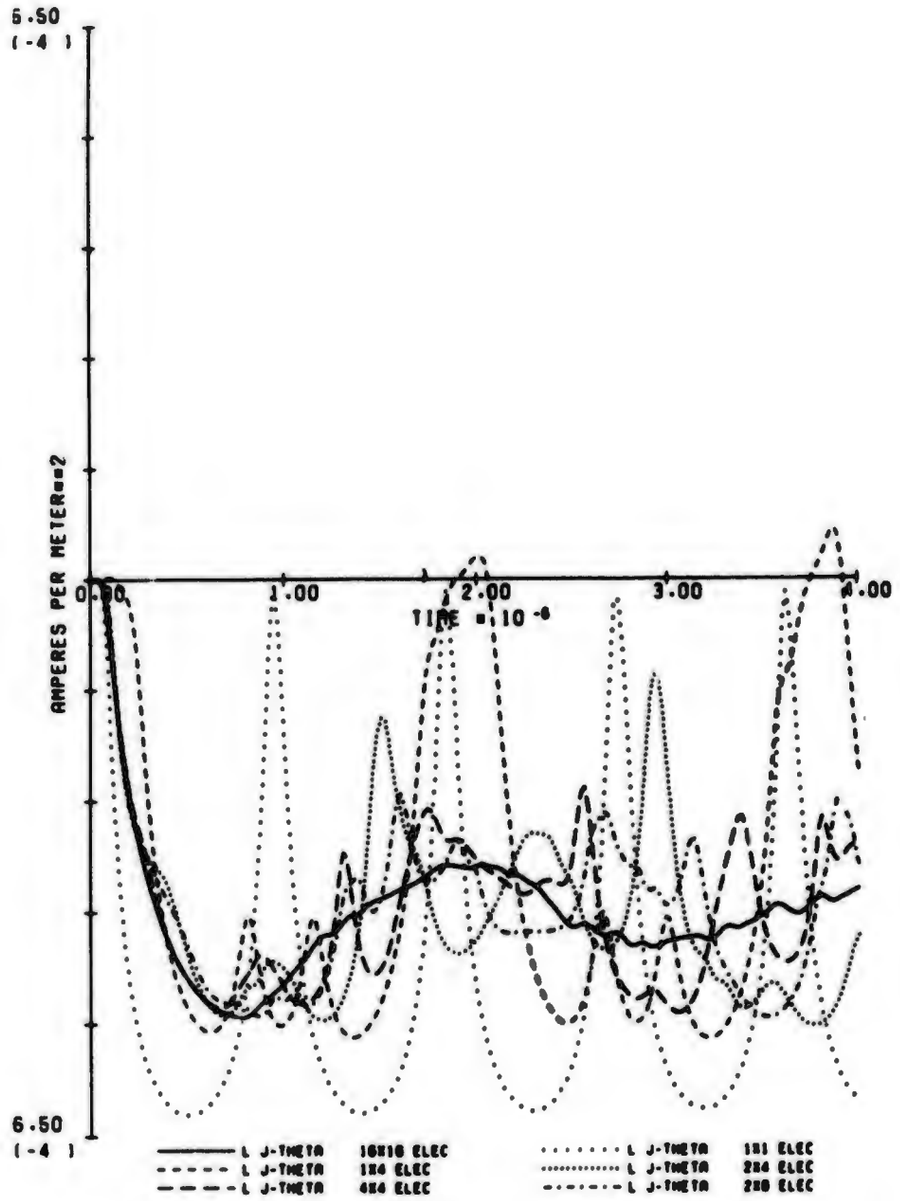

Fig. 19. Calculated Results for Parameter Set 19.

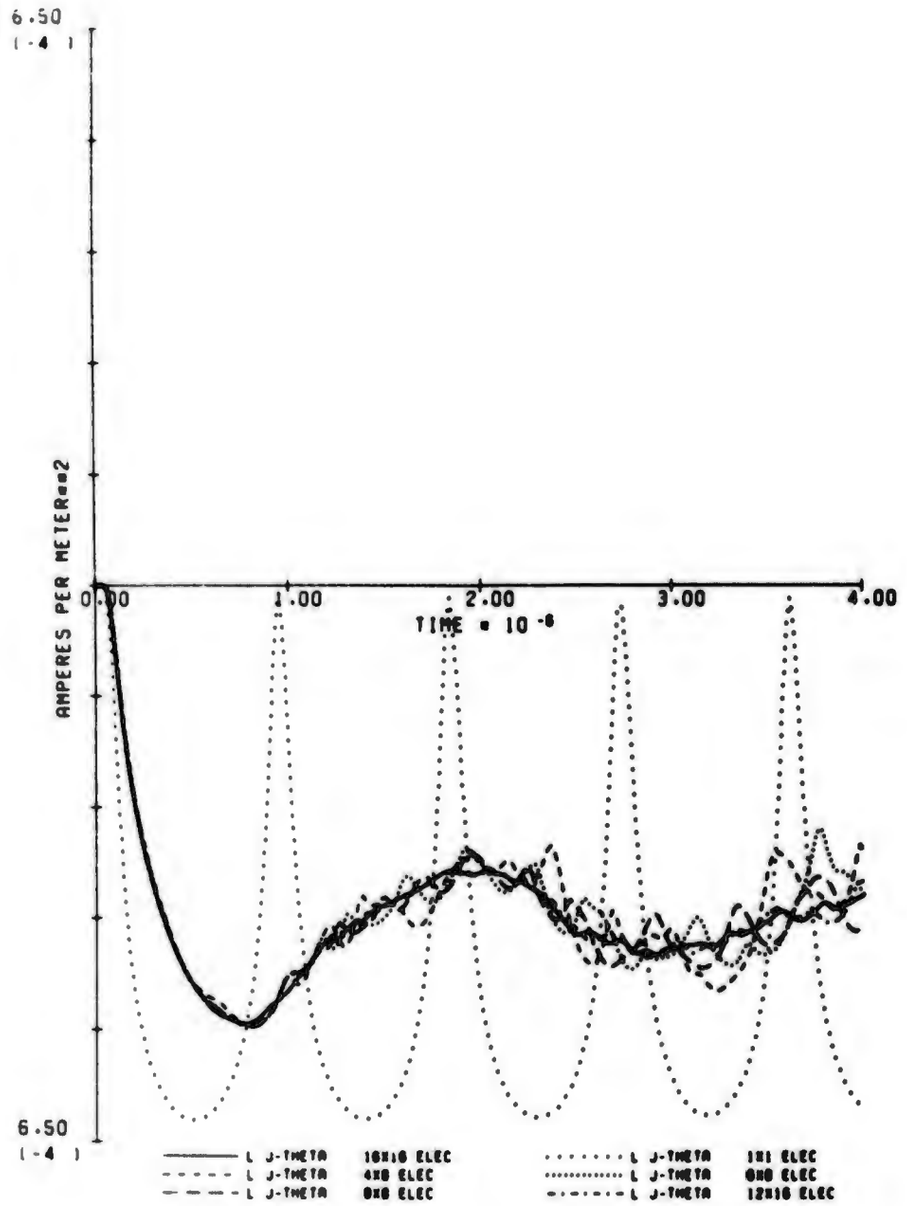

Fig. 20. Calculated Results for Parameter Set 20.

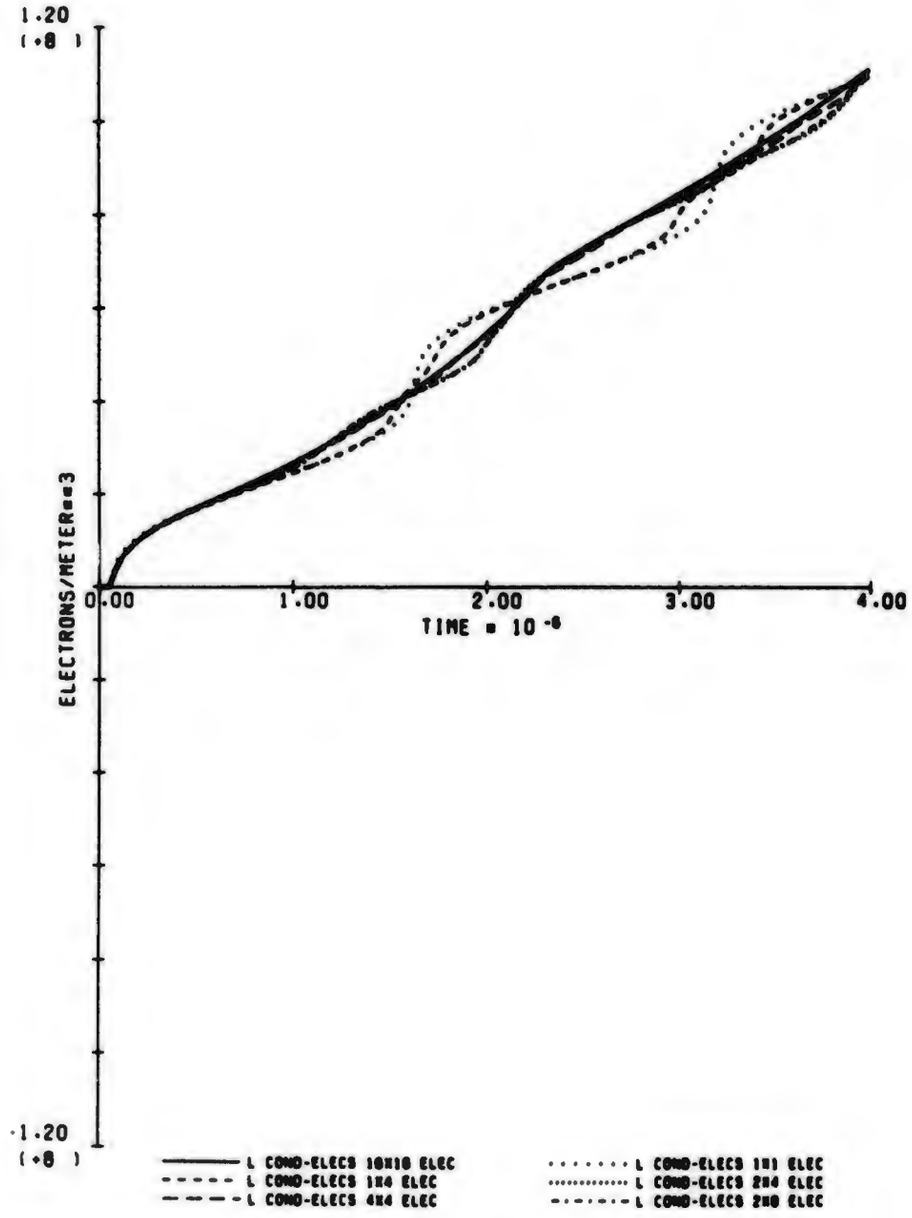

Fig. 21. Calculated Results for Parameter Set 21.

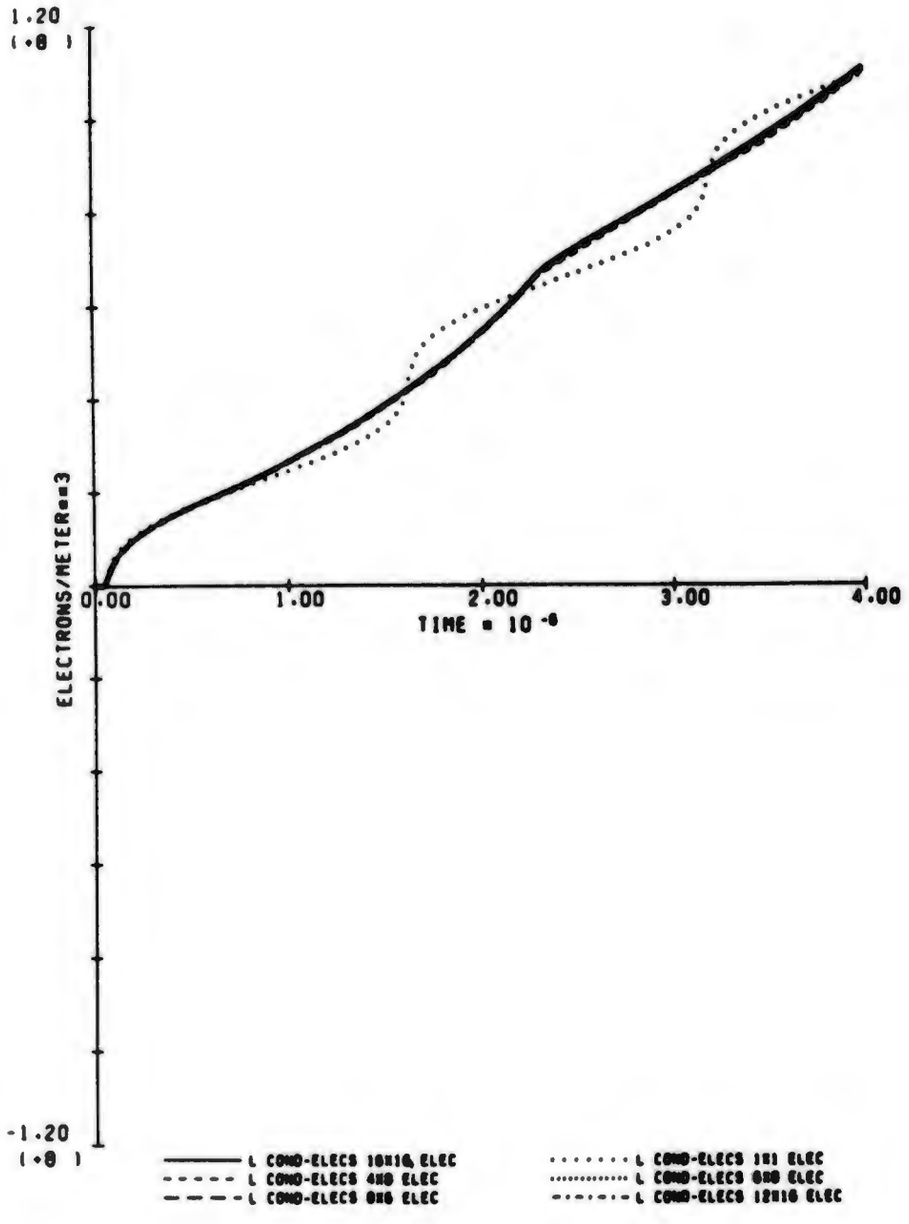

Fig. 22. Calculated Results for Parameter Set 22.

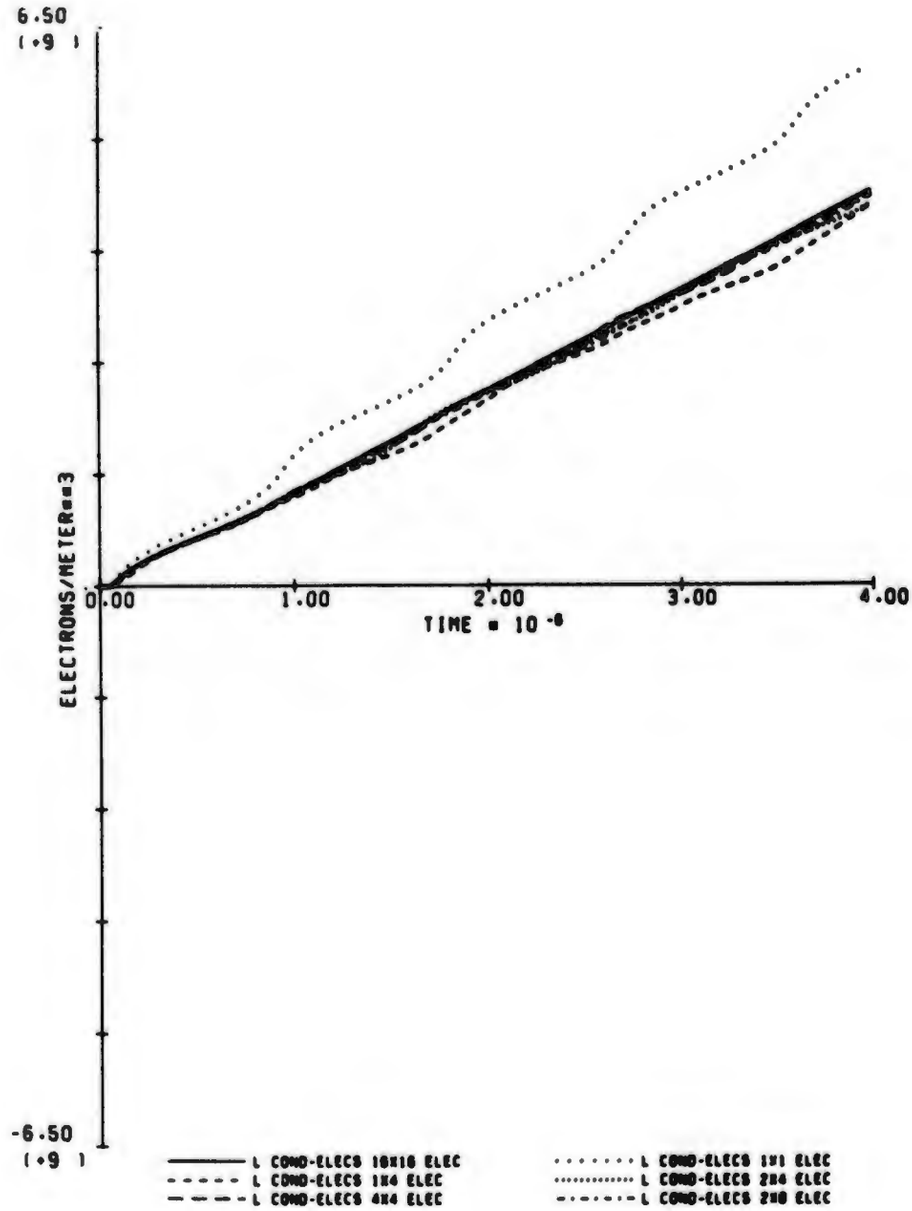

Fig. 23. Calculated Results for Parameter Set 23.

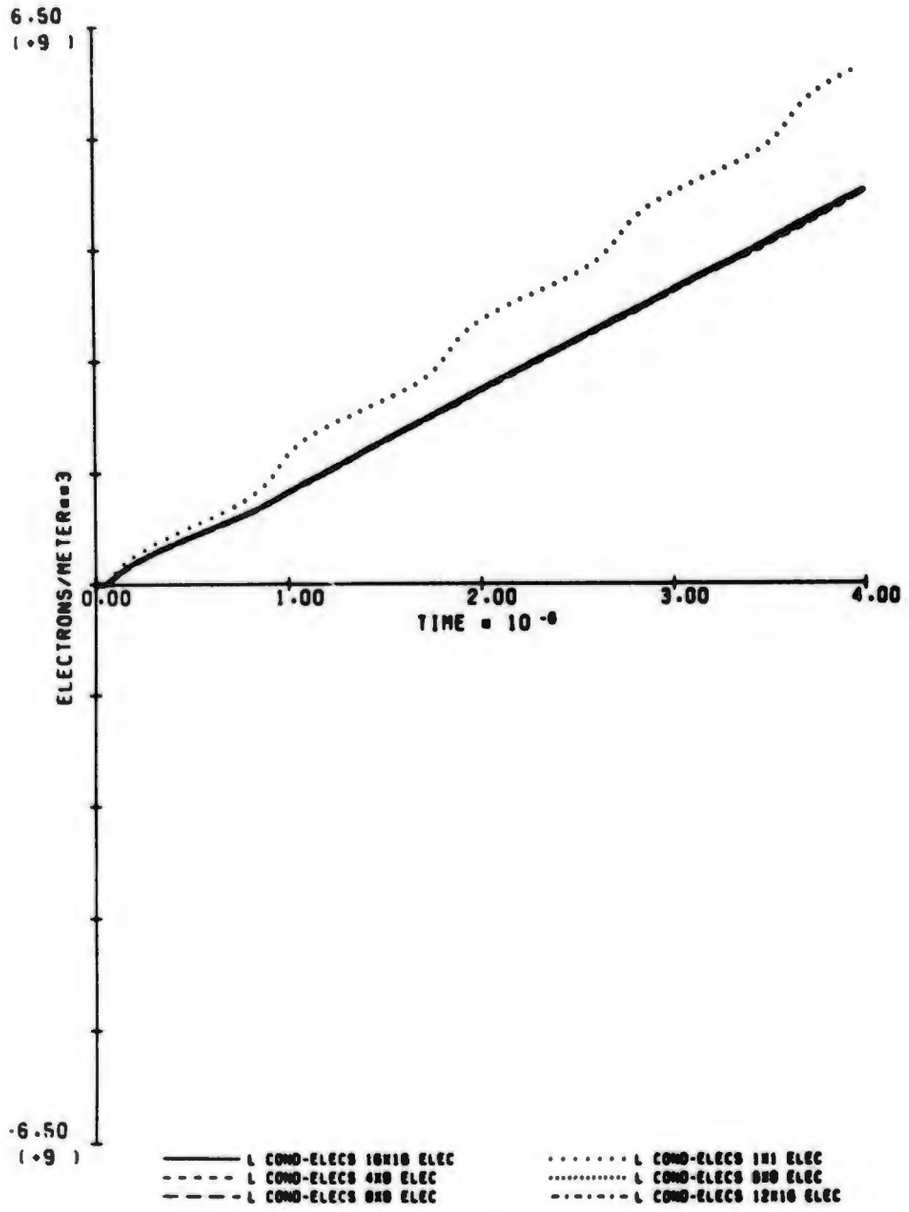

Fig. 24. Calculated Results for Parameter Set 24.

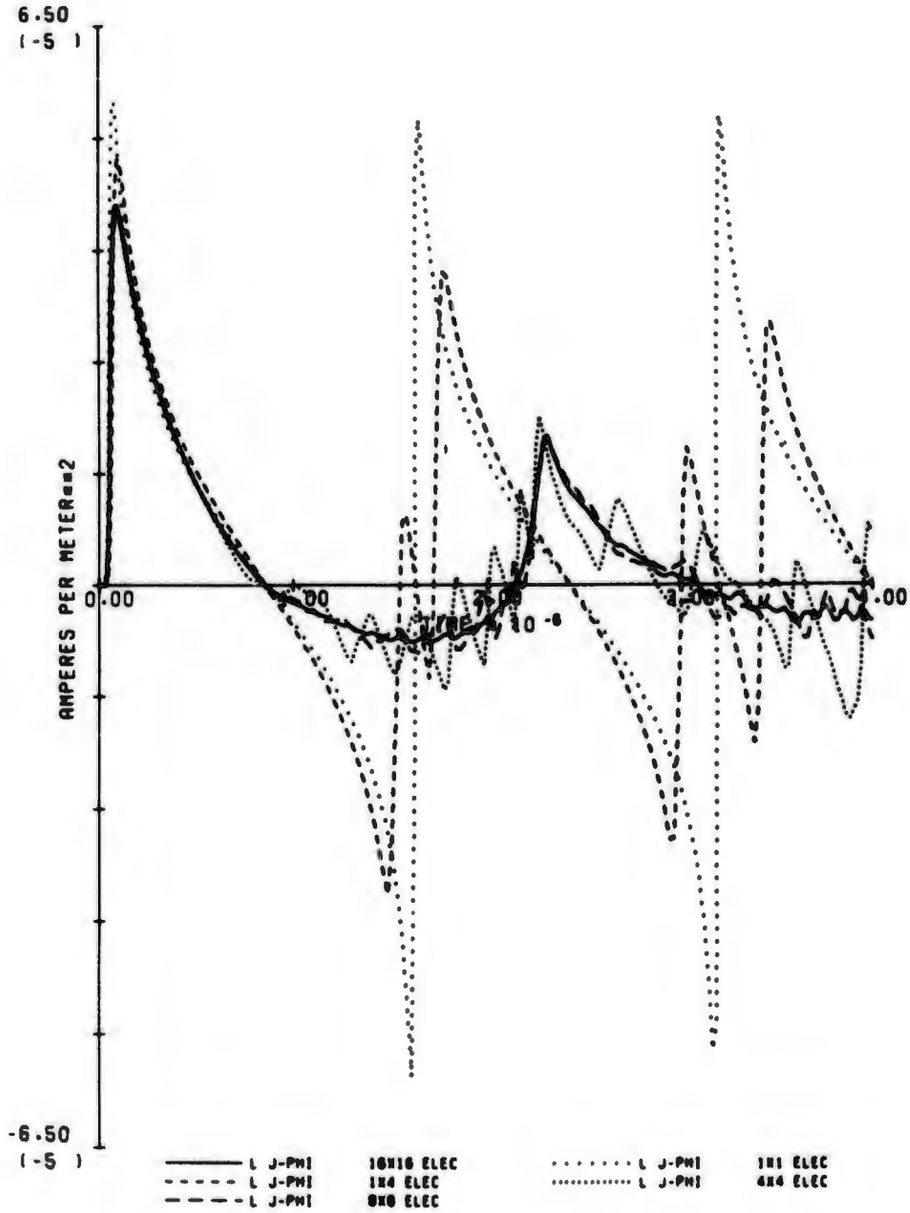

25. J-PHI FOR 1.5 MEV GAMMAS (80 KM, 77.8 DEG)

Fig. 25. Calculated Results for Parameter Set 25.

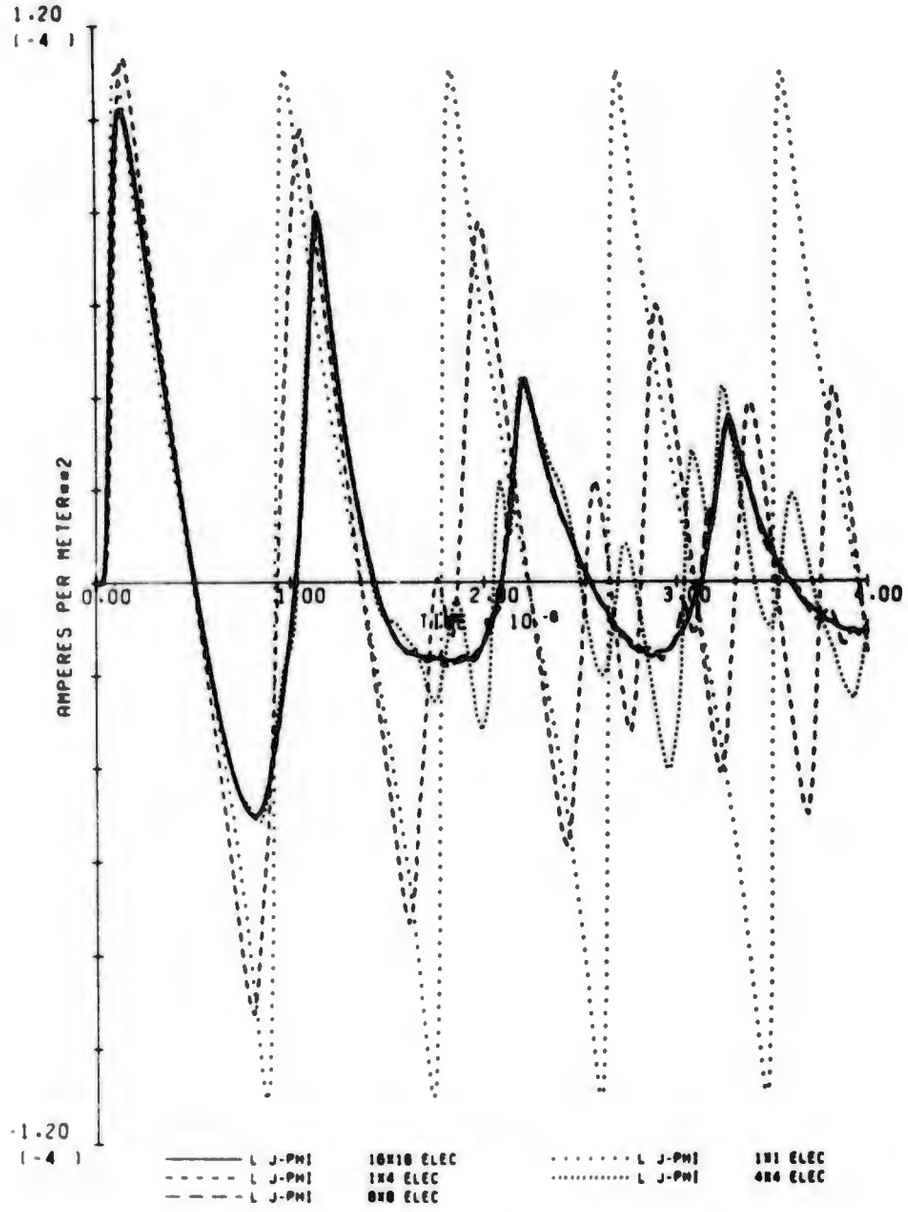

26. J-PHI FOR 0.5 MEV GAMMAS (80 KM. 77.8 DEG)

Fig. 26. Calculated Results for Parameter Set 26.

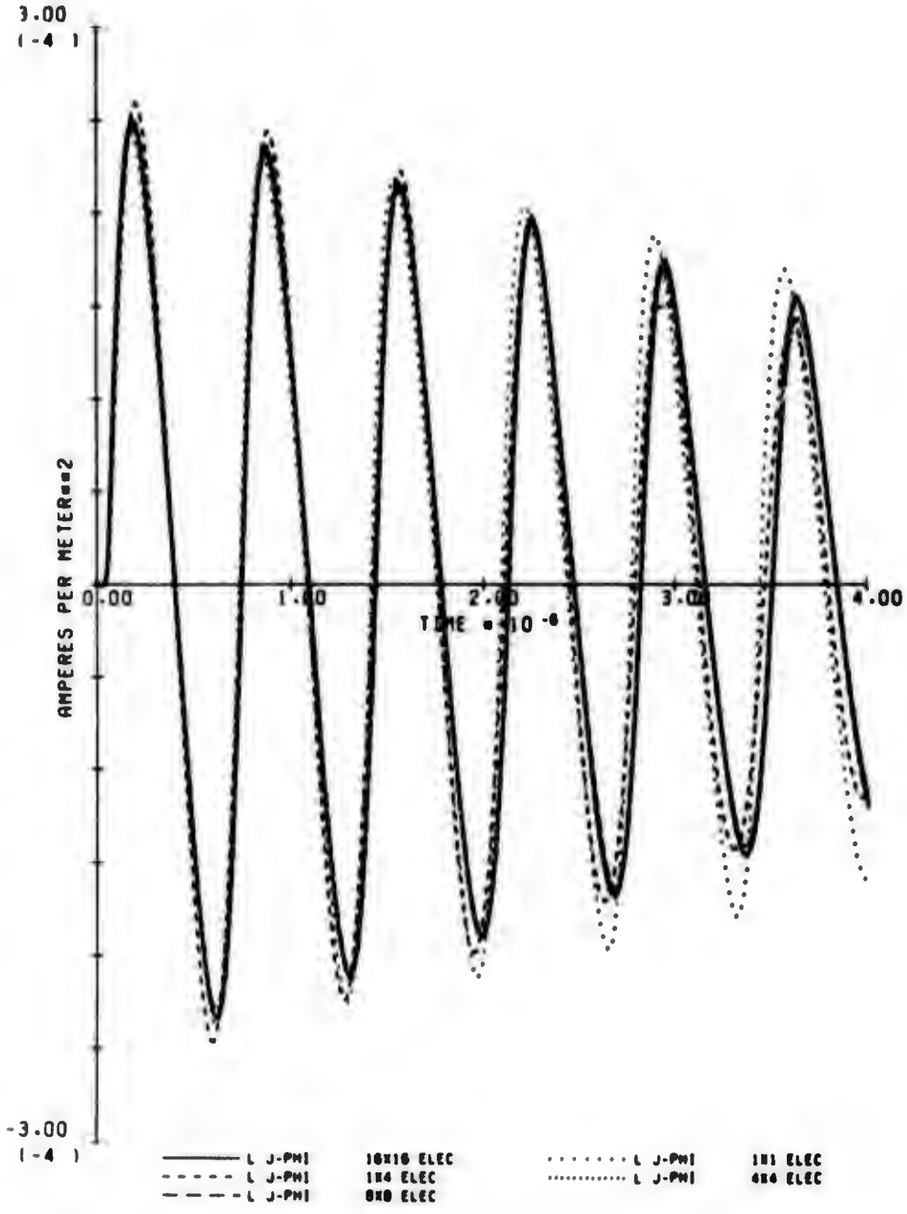

27. J-PHI FOR 0.1 MEV GAMMAS (80 KM, 77.8 DEG)

Fig. 27. Calculated Results for Parameter Set 27.

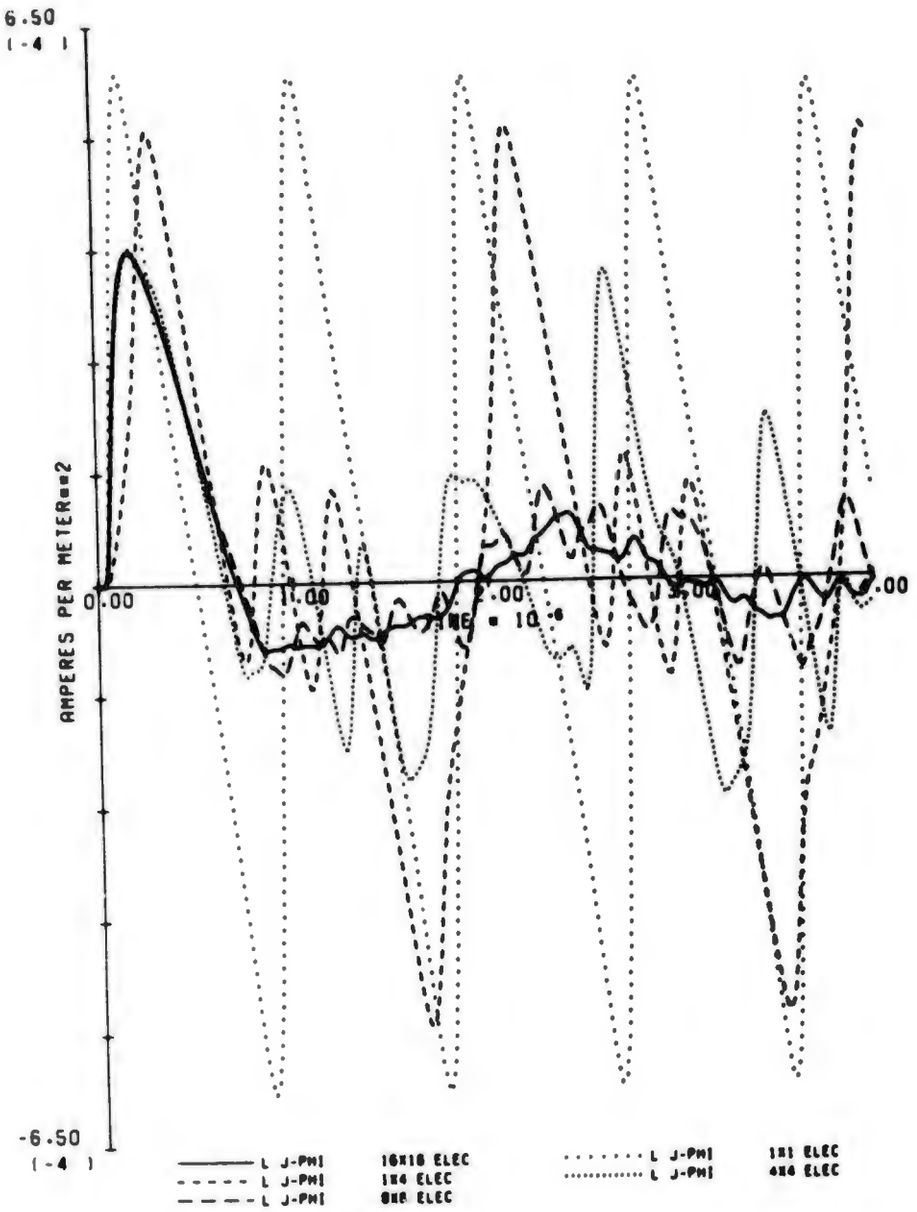

Fig. 28. Calculated Results for Parameter Set 28.

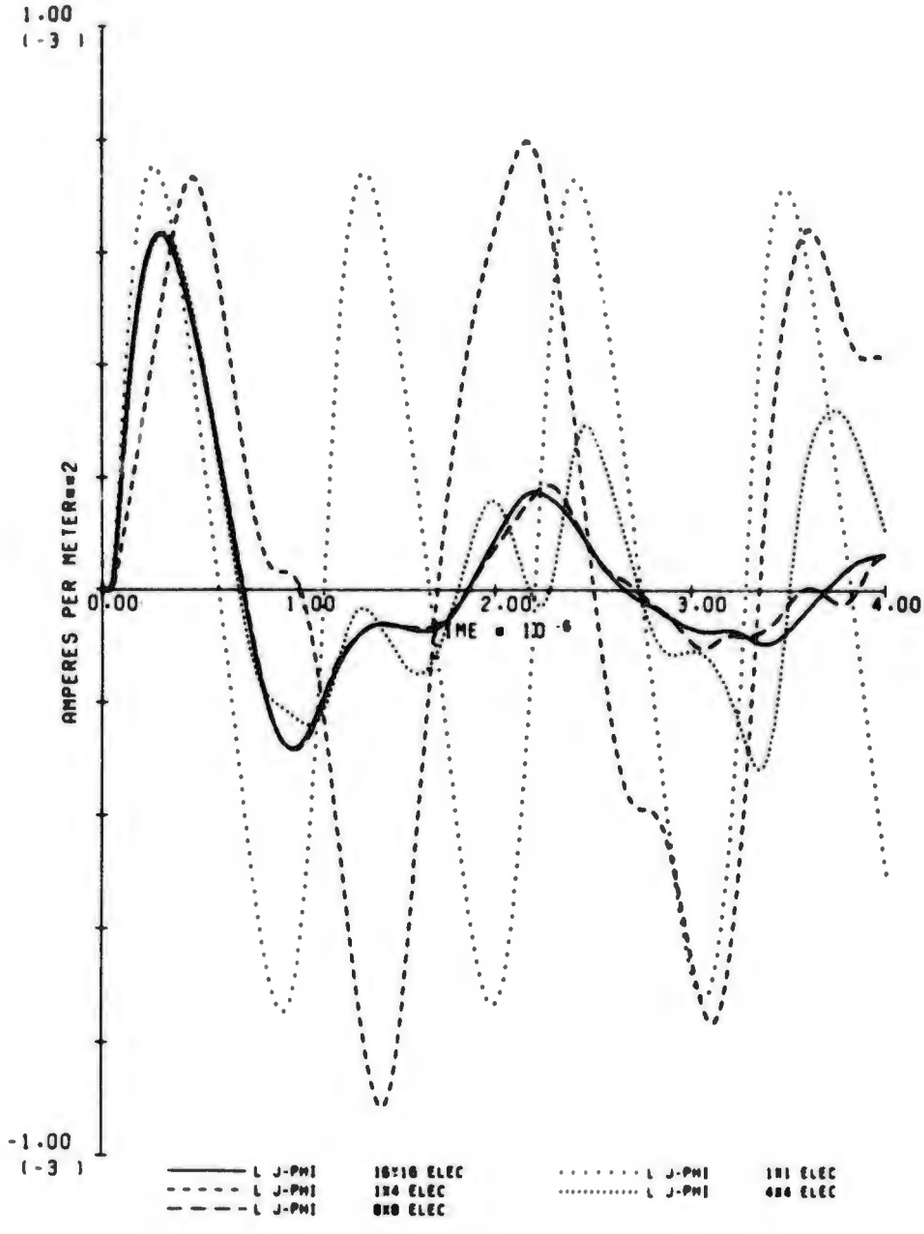

Fig. 29. Calculated Results for Parameter Set 29.

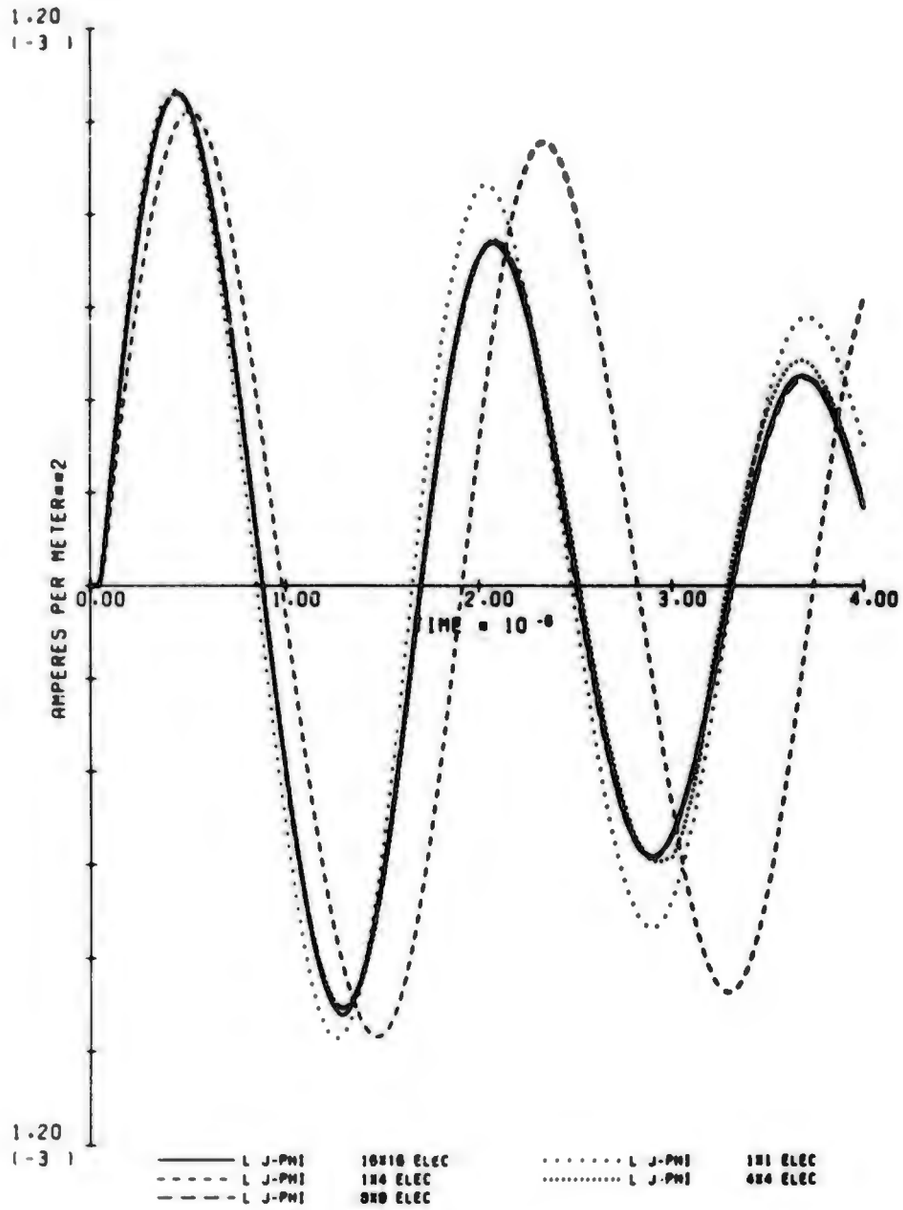

Fig. 30. Calculated Results for Parameter Set 30.

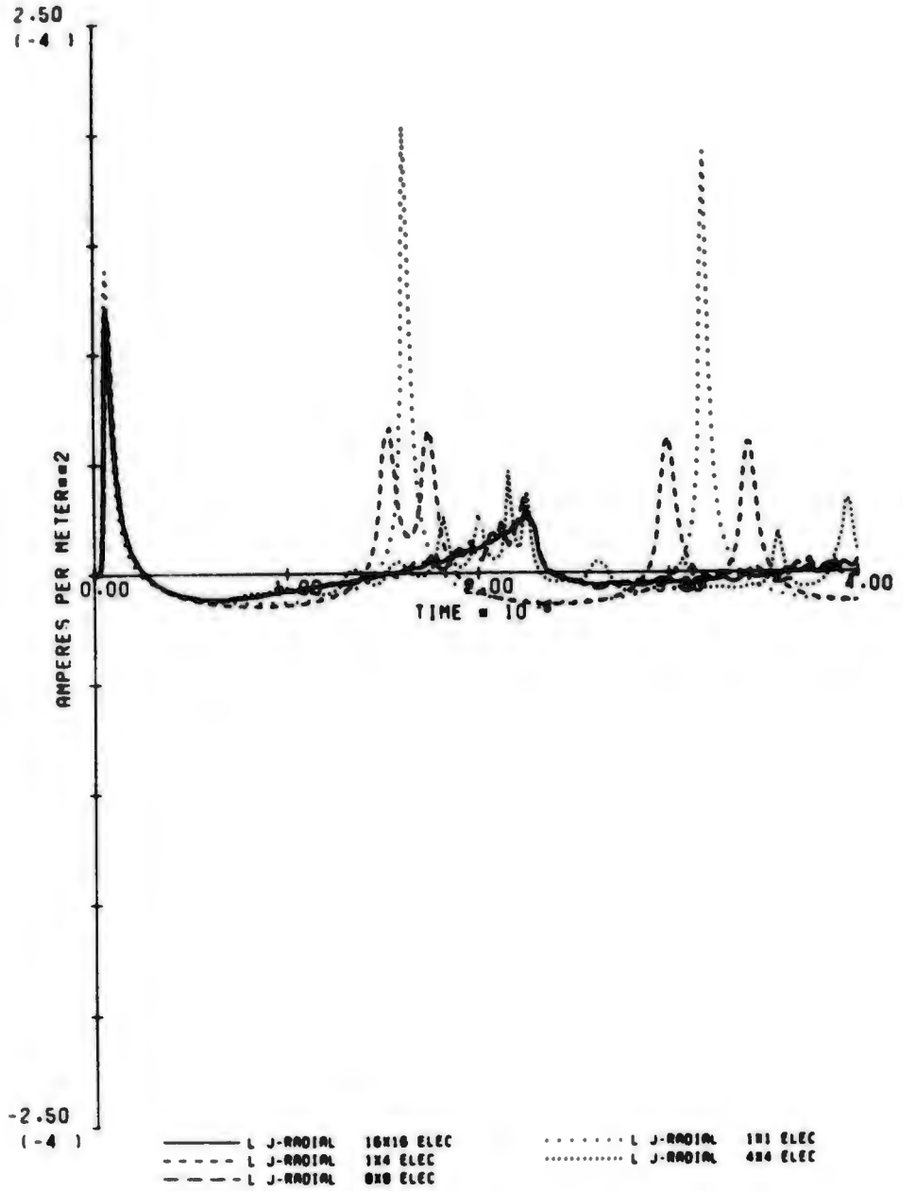

Fig. 31. Calculated Results for Parameter Set 31.

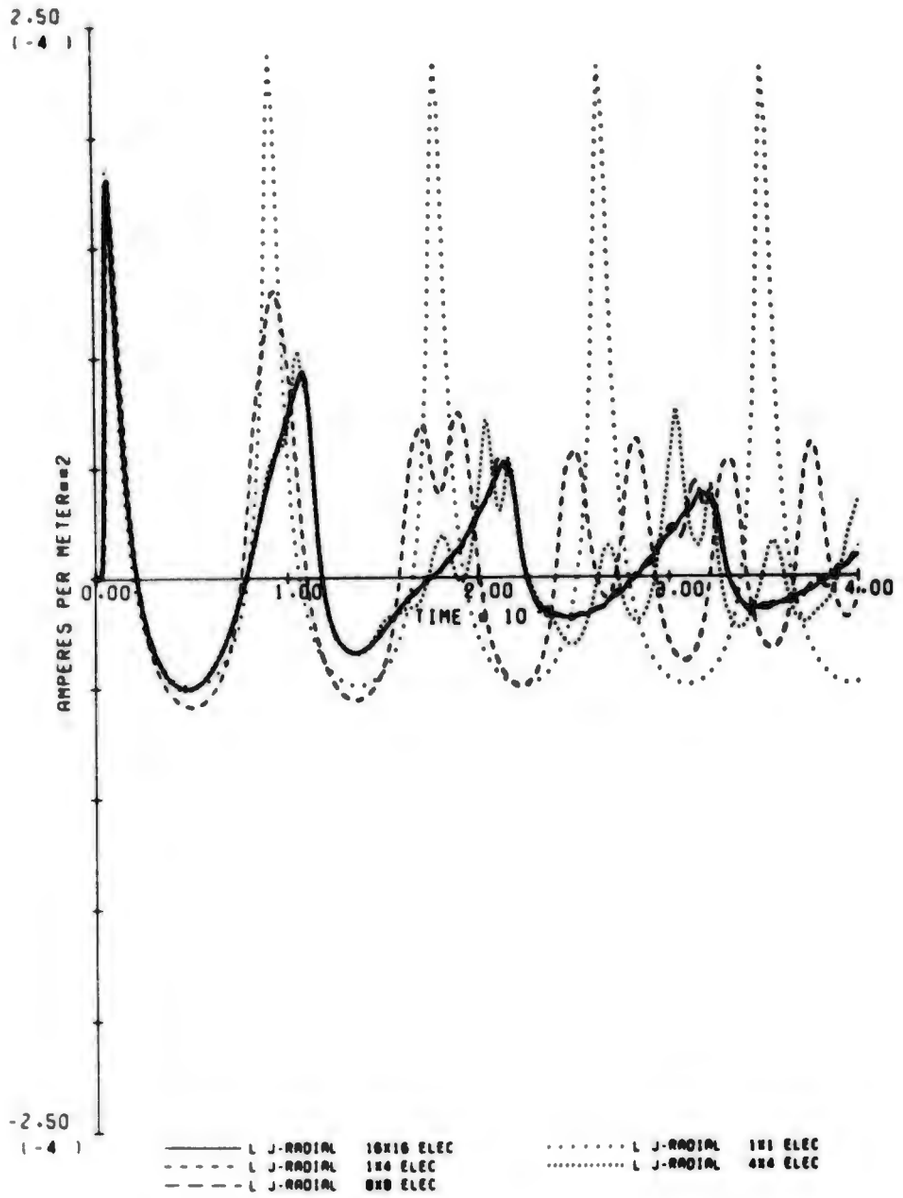

32. J-RADIAL FOR 0.5 MEV GAMMAS (80 KM. 77.8 DEG)

Fig. 32. Calculated Results for Parameter Set 32.

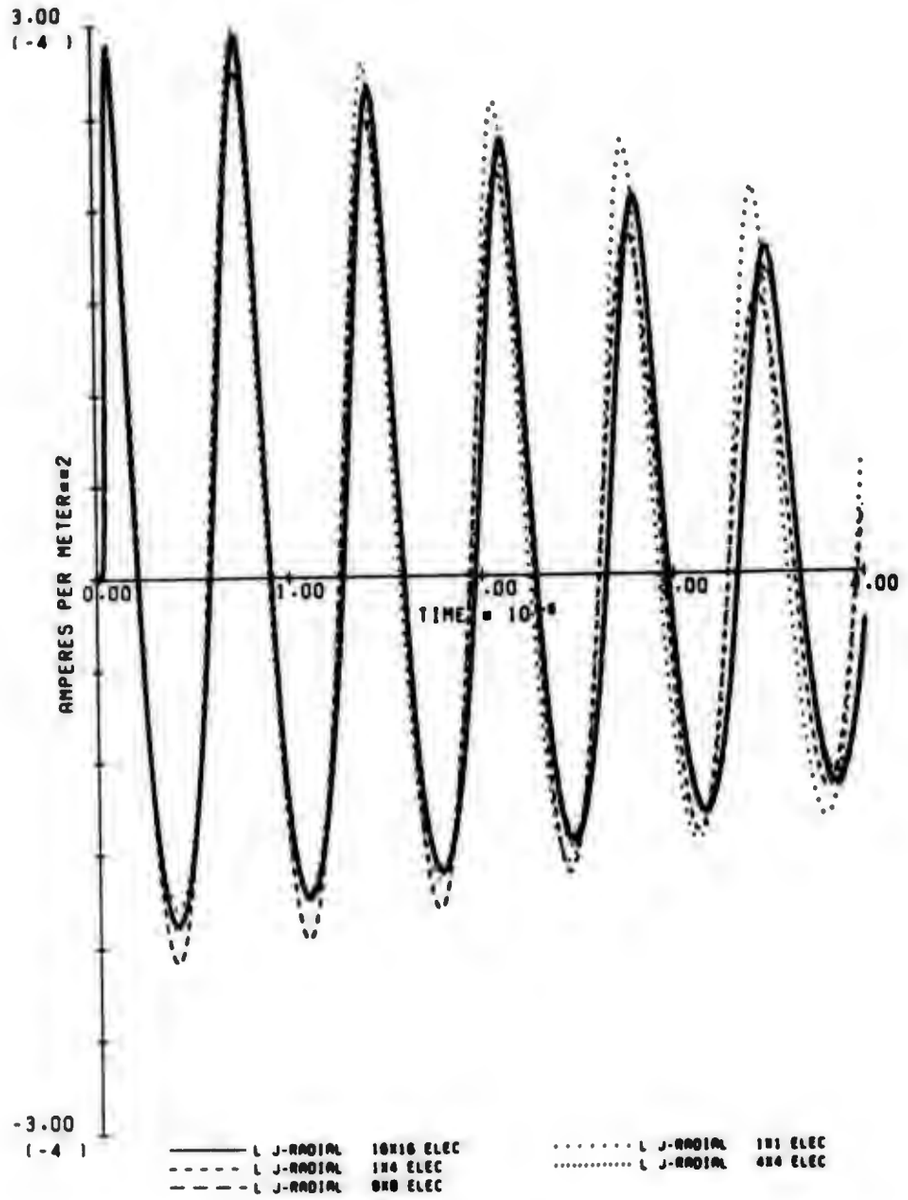

33. J-RADIAL FOR 0.1 MEV GAMMAS (80 KM, 77.8 DEG)

Fig. 33. Calculated Results for Parameter Set 33.

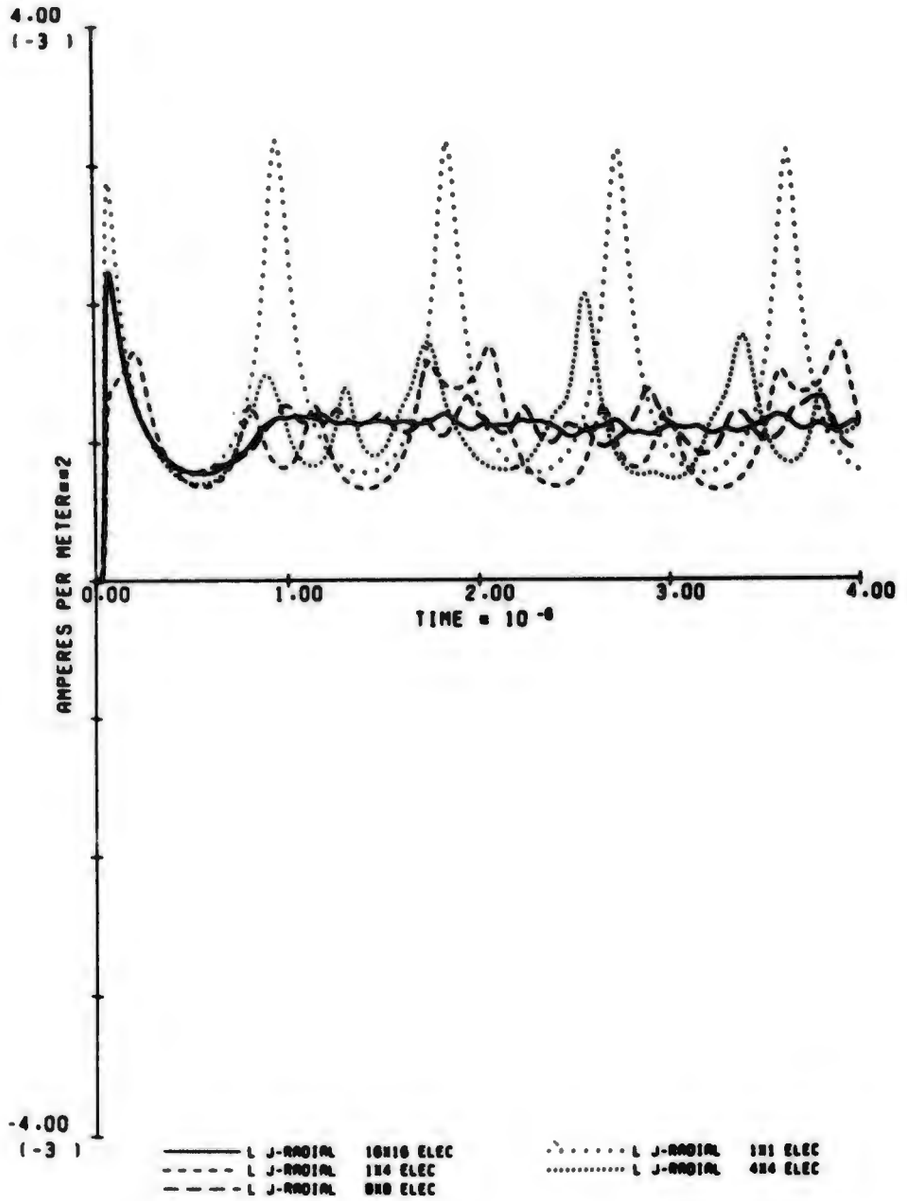

Fig. 34. Calculated Results for Parameter Set 34.

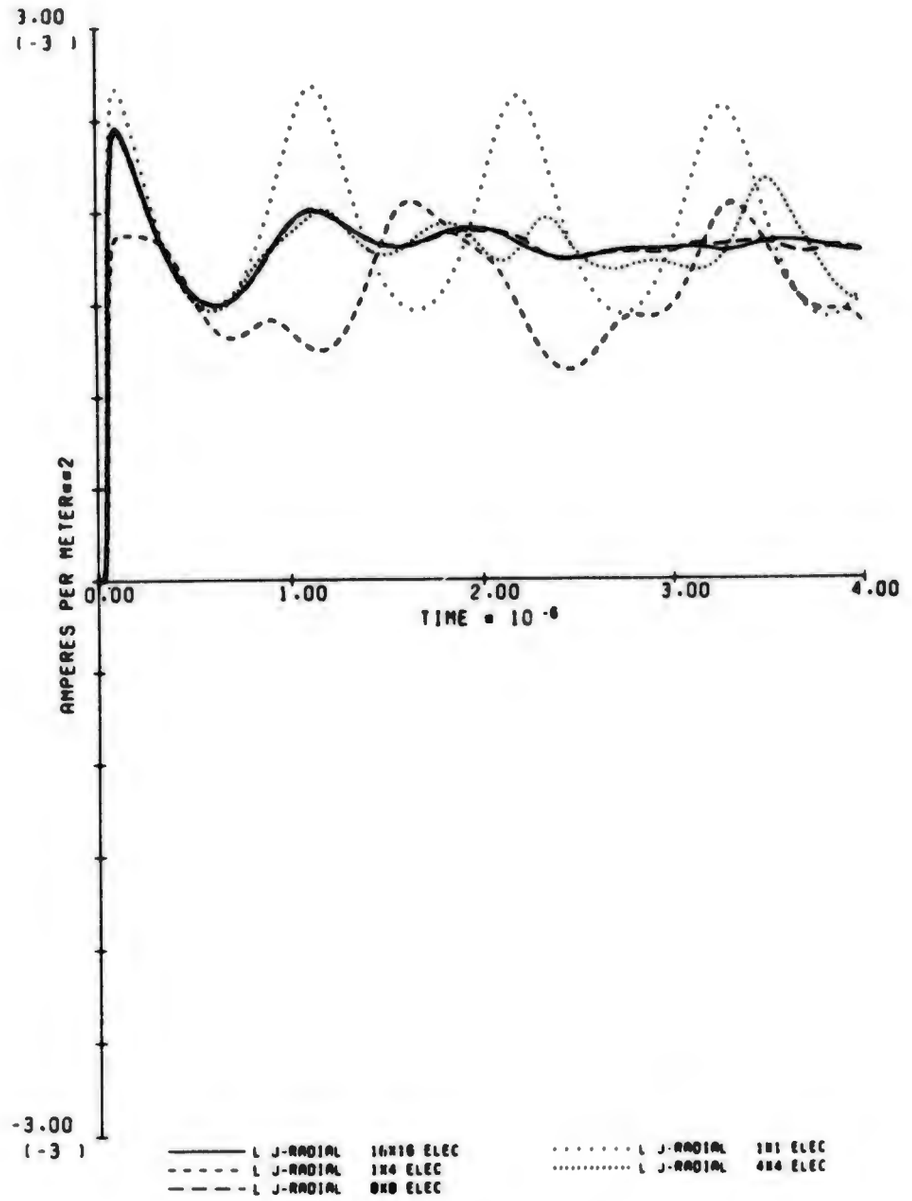

Fig. 35. Calculated Results for Parameter Set 35.

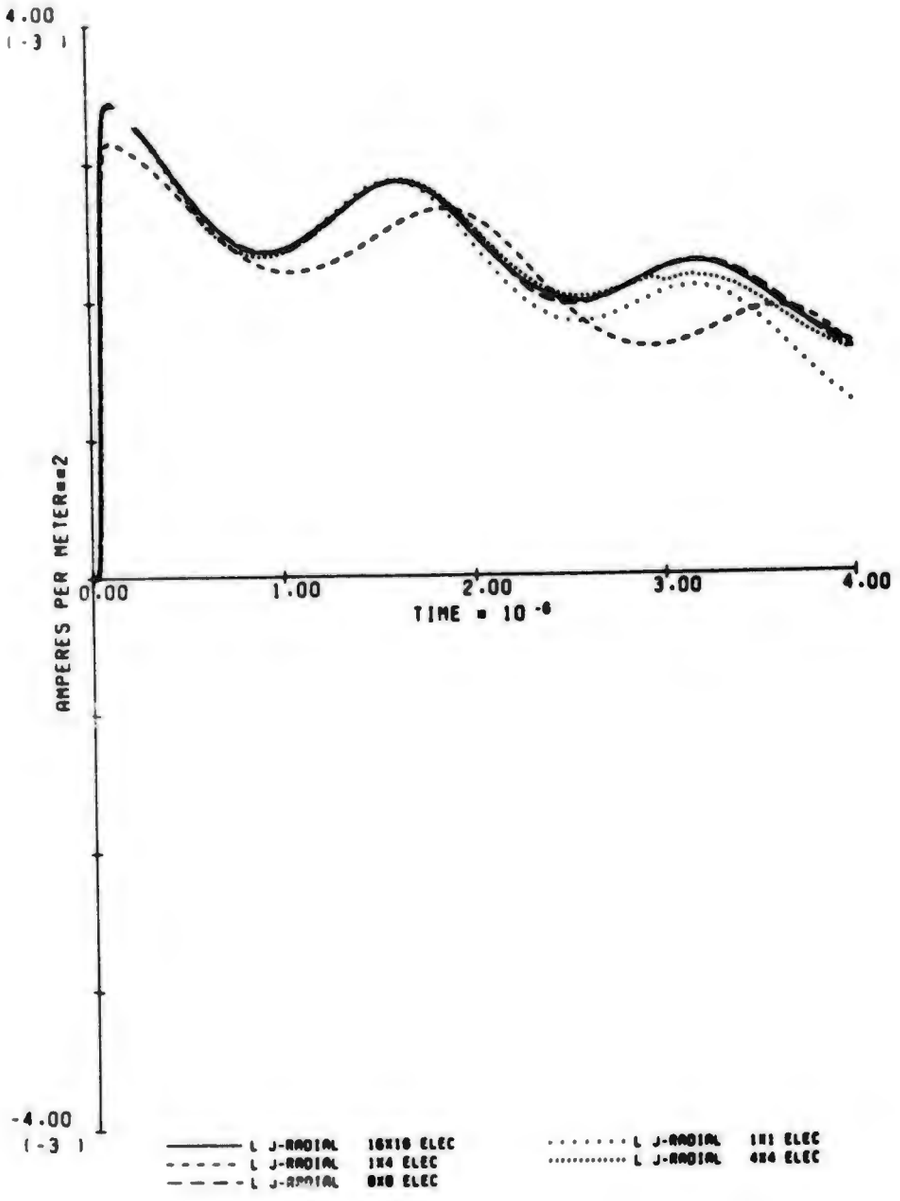

Fig. 36. Calculated Results for Parameter Set 36.

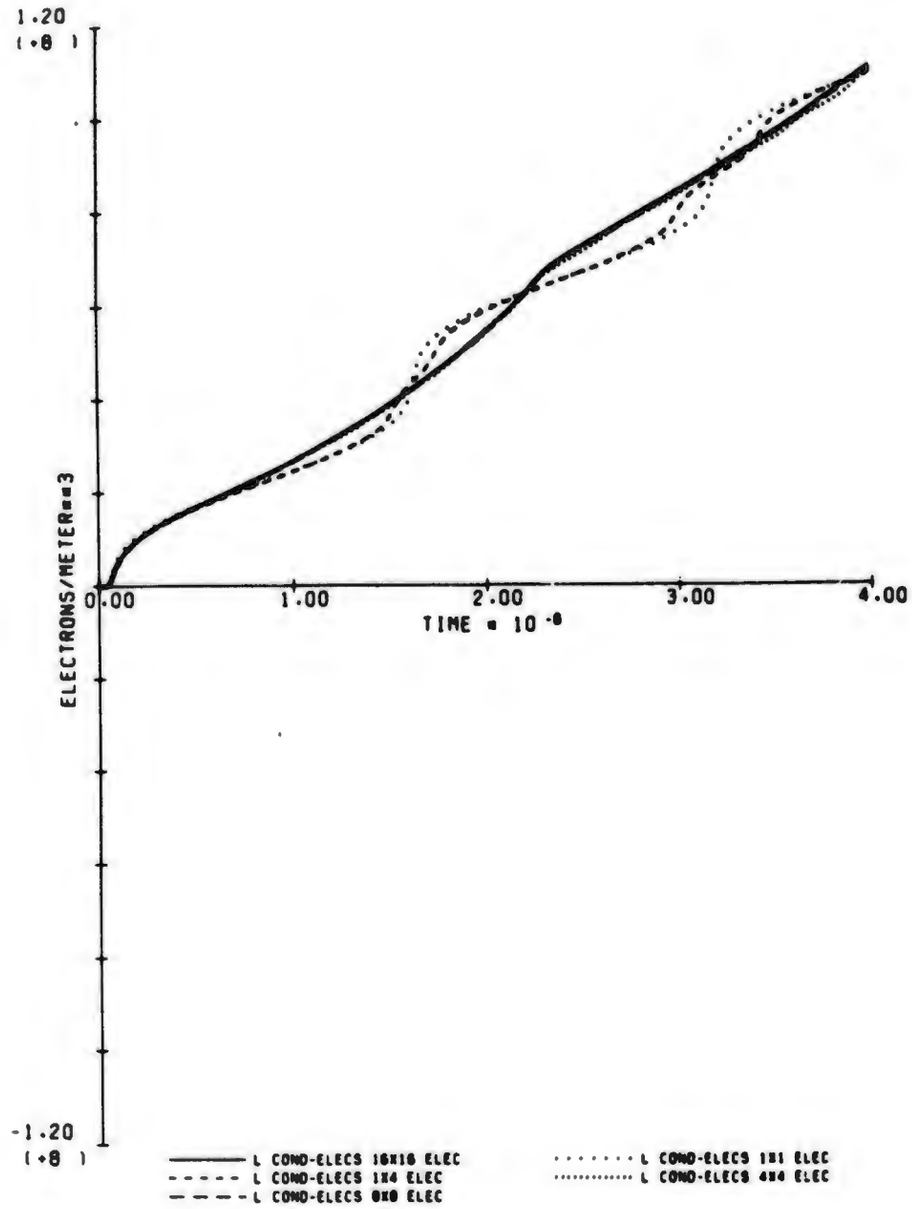

Fig. 37. Calculated Results for Parameter Set 37.

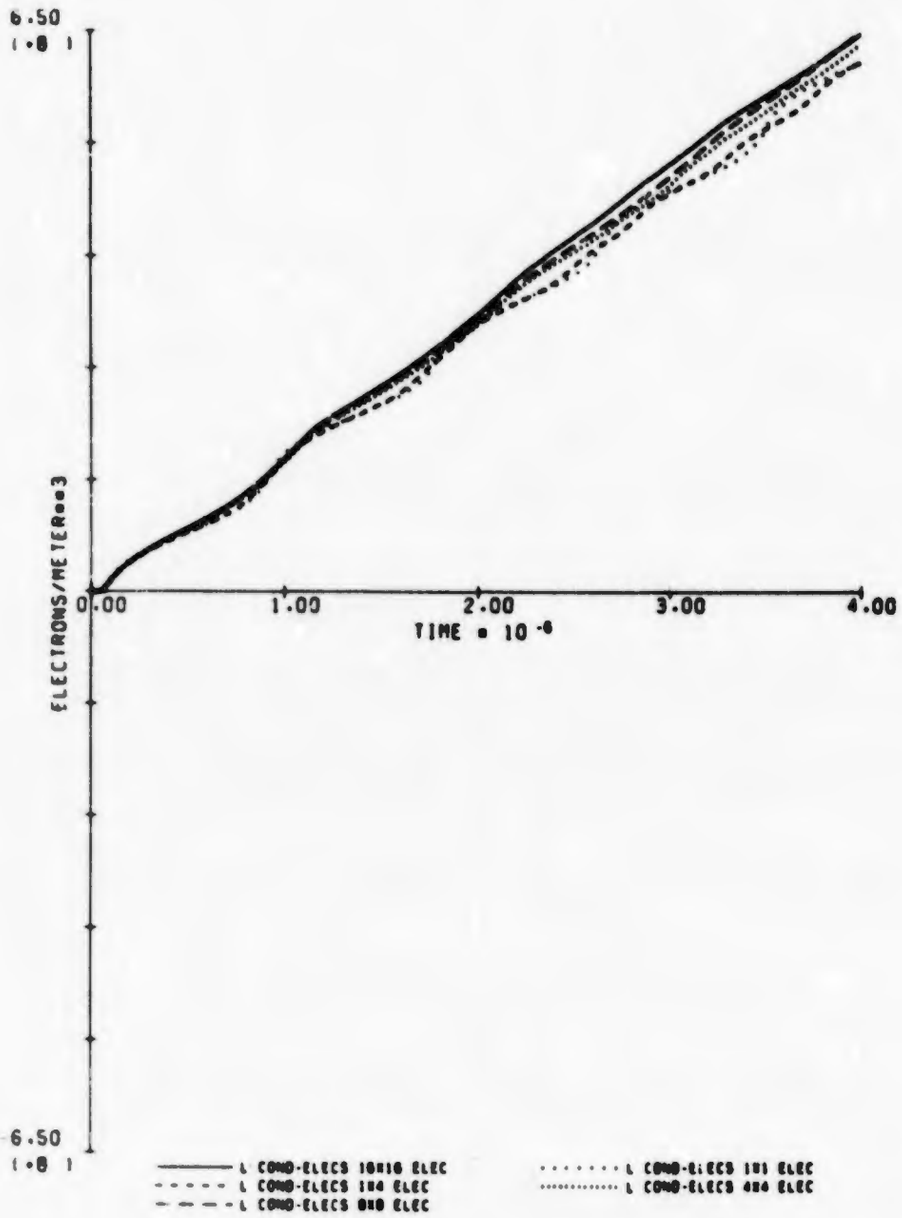

Fig. 38. Calculated Results for Parameter Set 38.

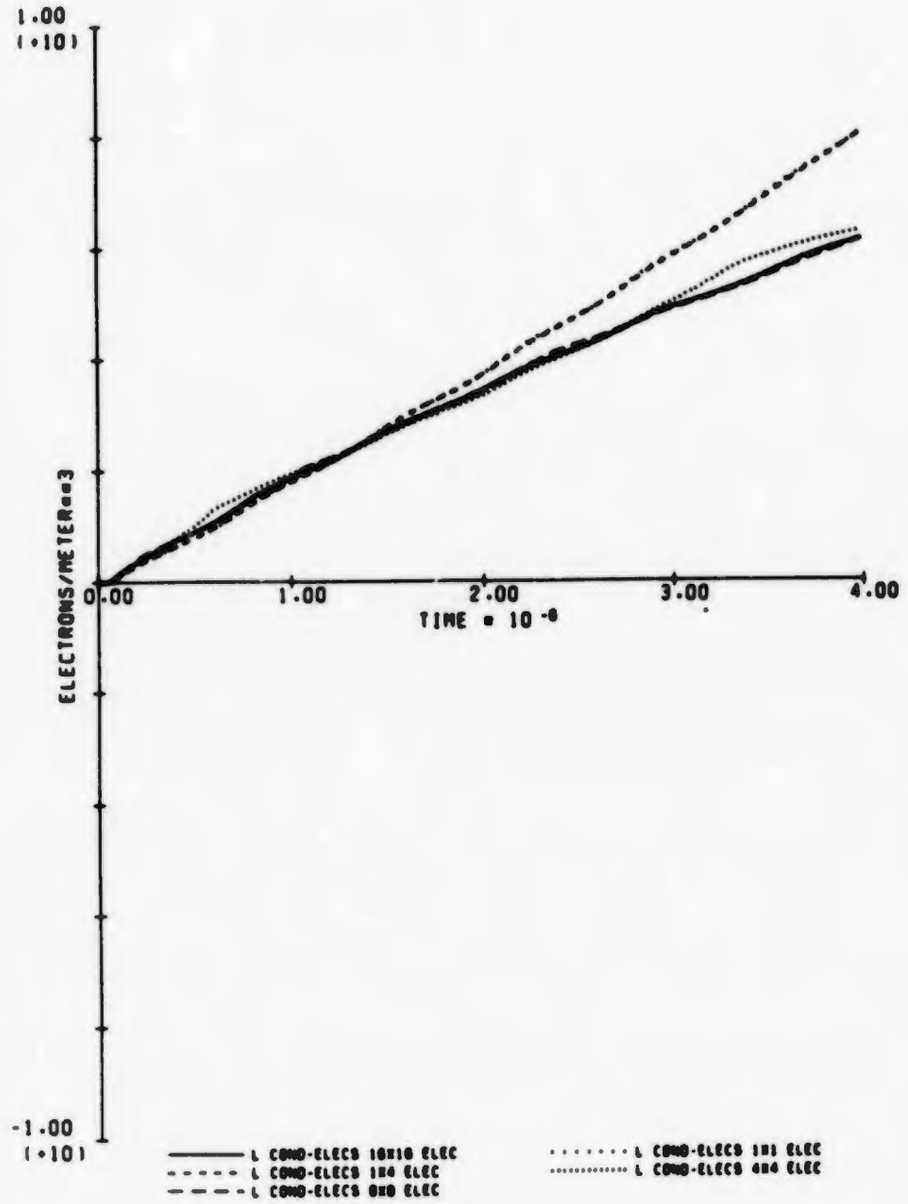

Fig. 39. Calculated Results for Parameter Set 39.

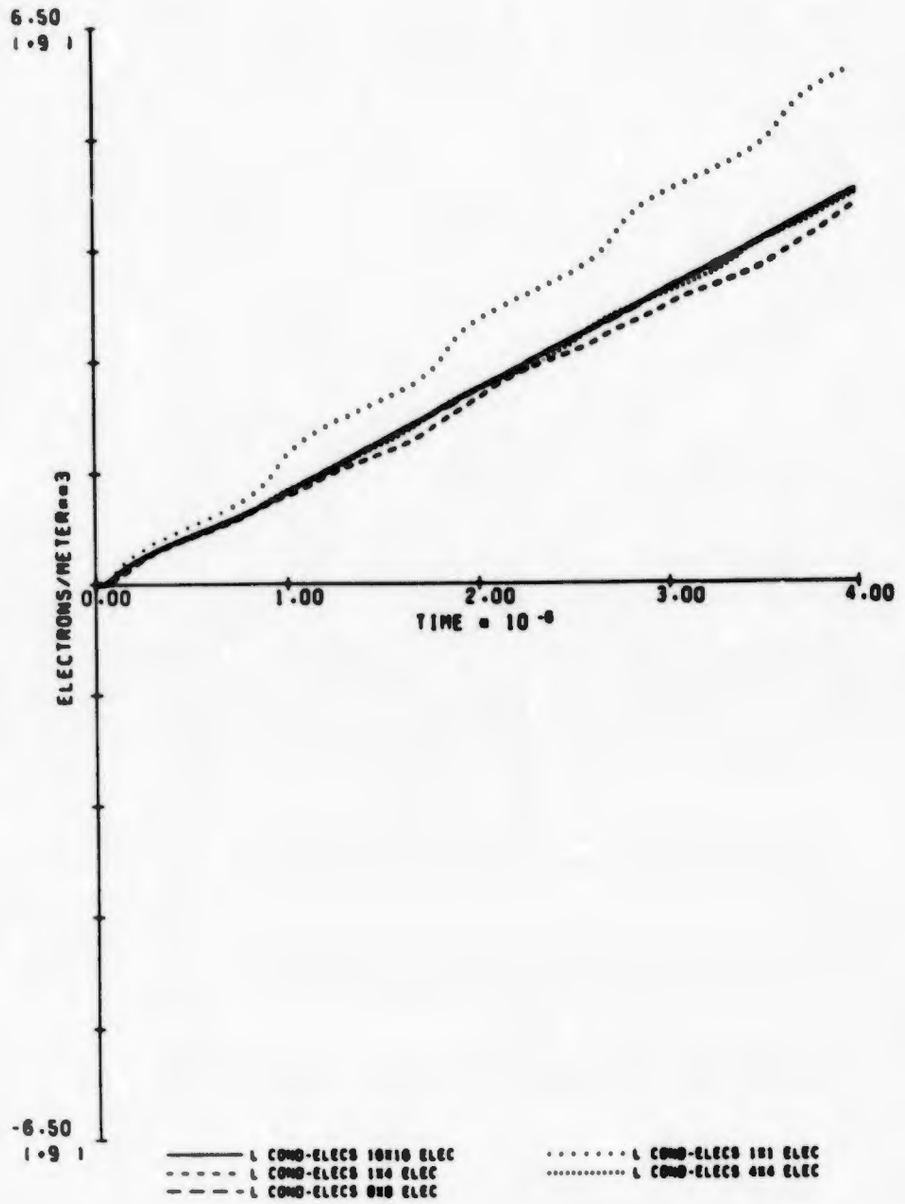

Fig. 40. Calculated Results for Parameter Set 40.

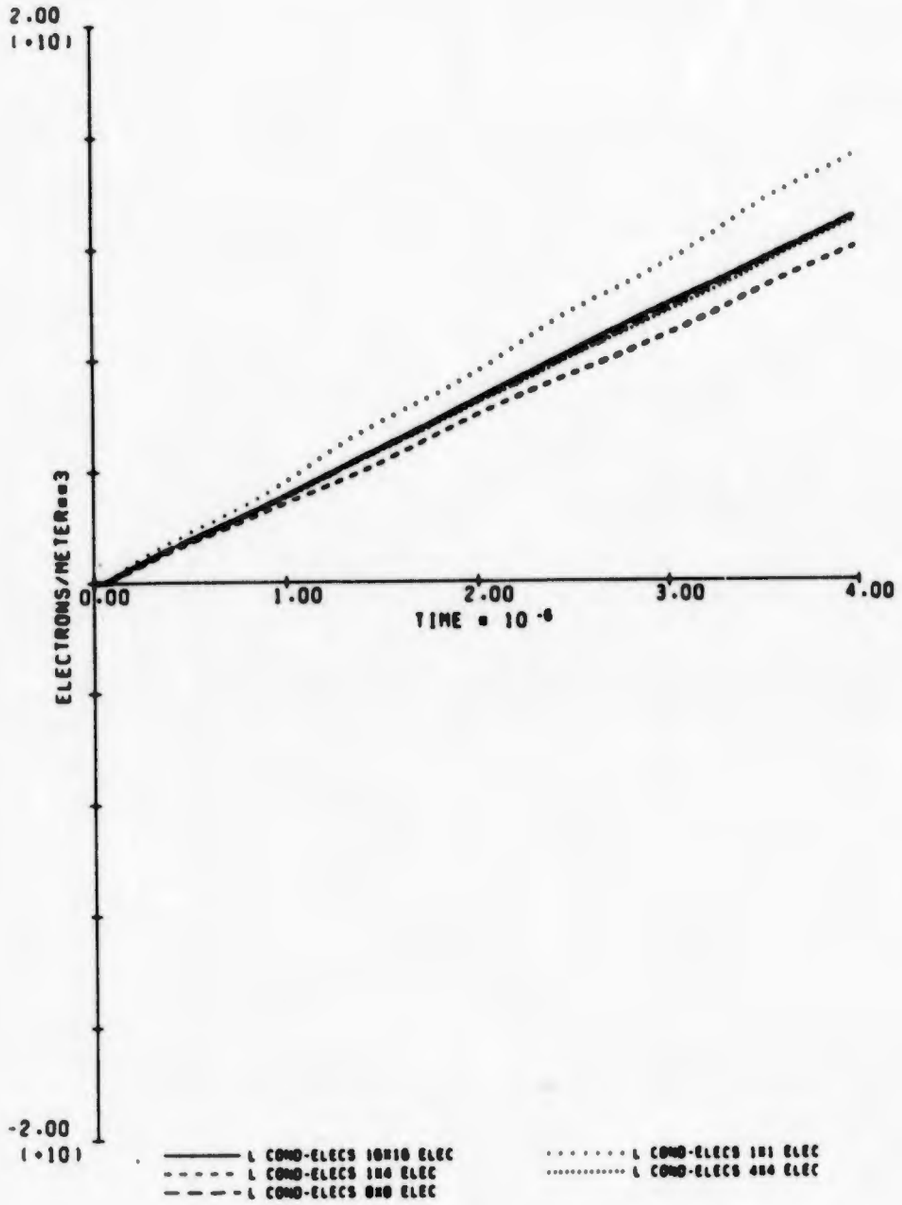

Fig. 41. Calculated Results for Parameter Set 41.

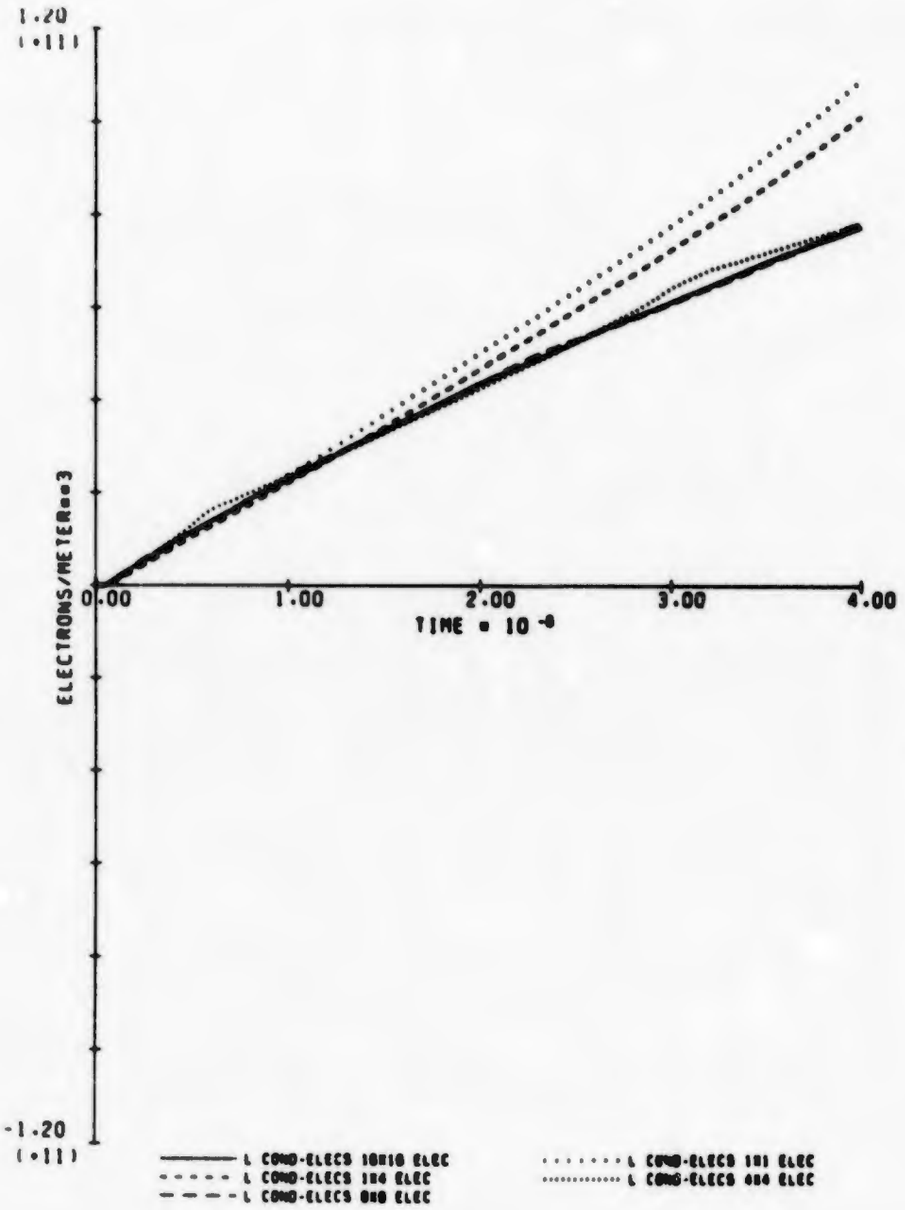

Fig. 42. Calculated Results for Parameter Set 42.

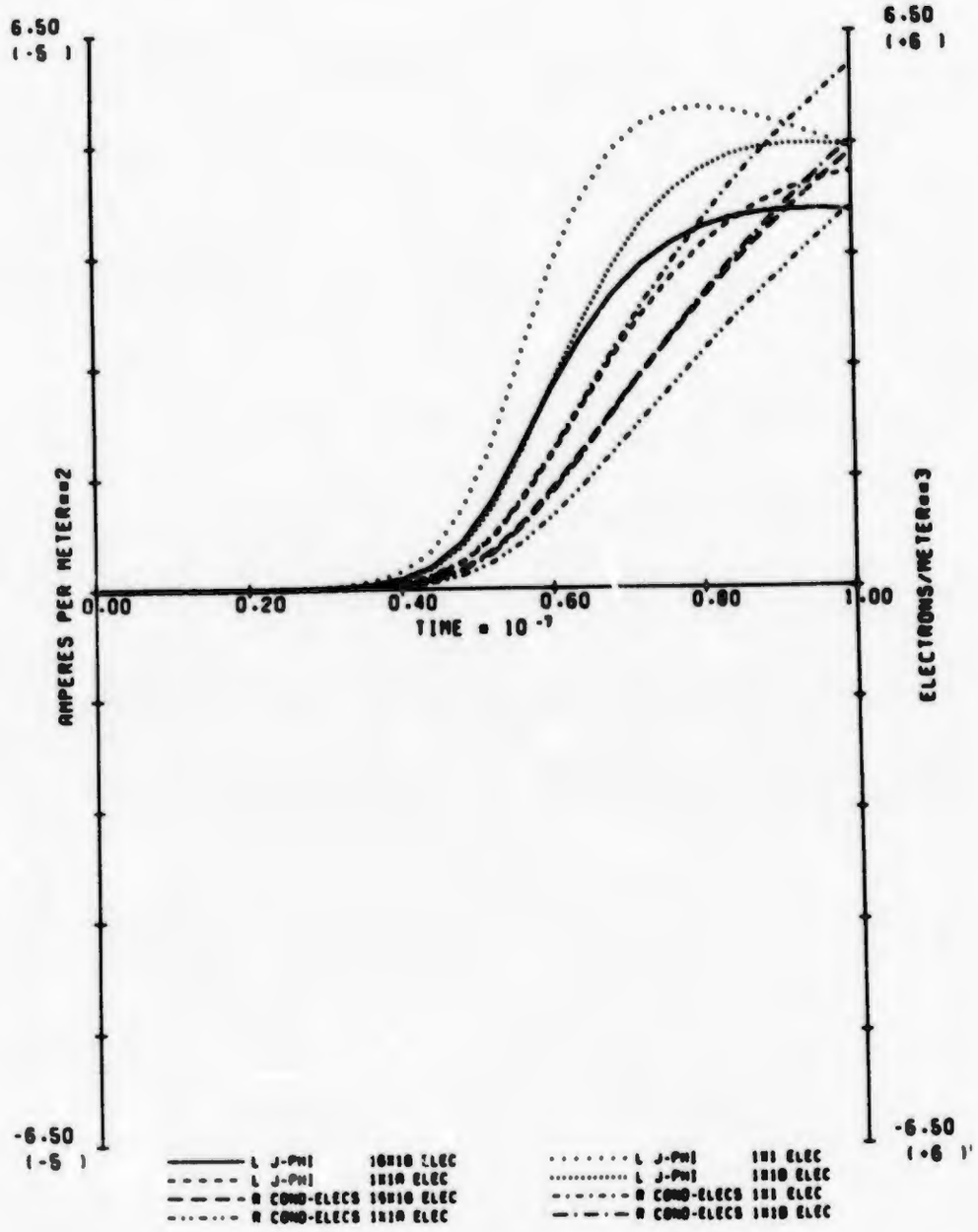

Fig. 43. Calculated Results for Parameter Set 43.

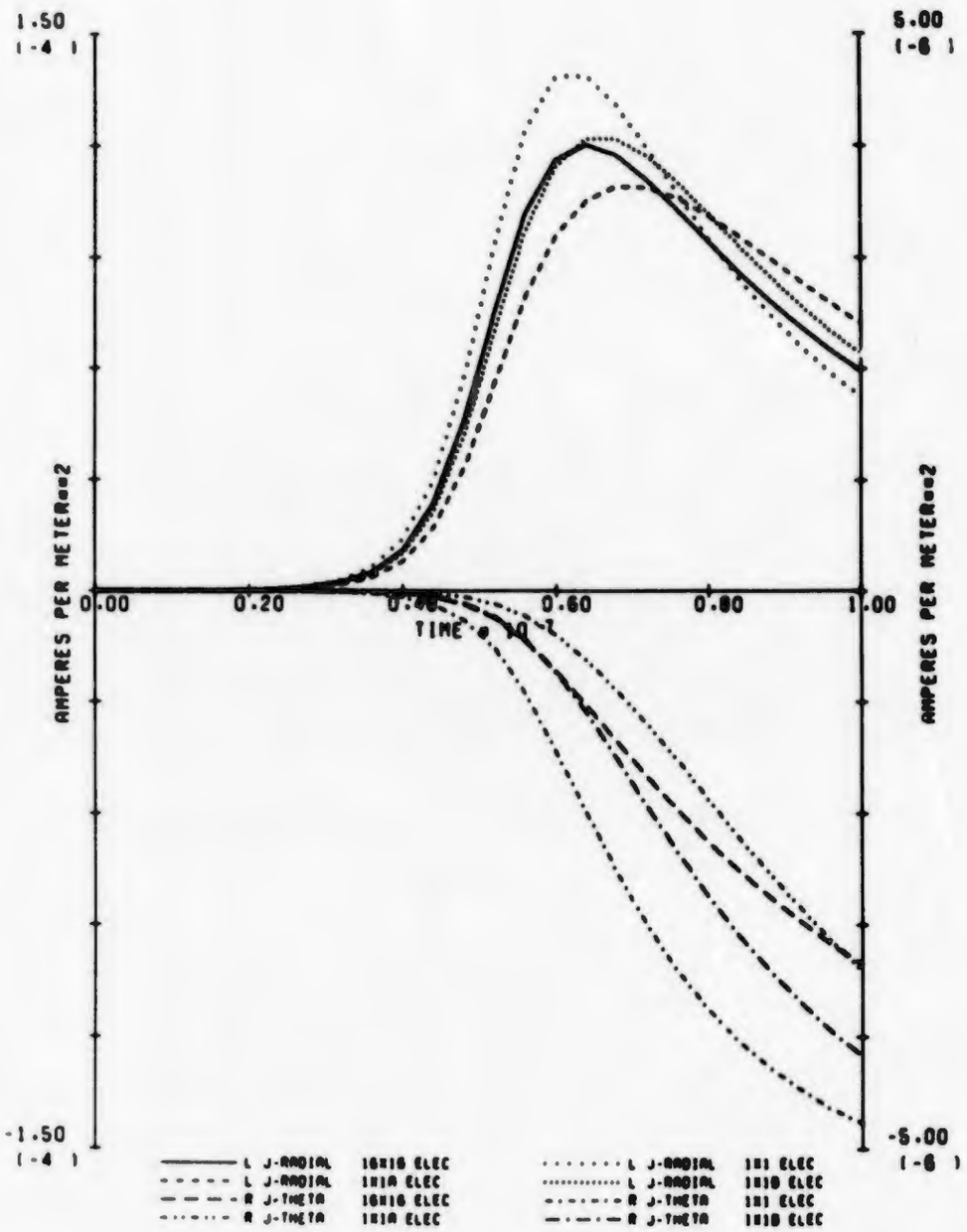

Fig. 44. Calculated Results for Parameter Set 44.

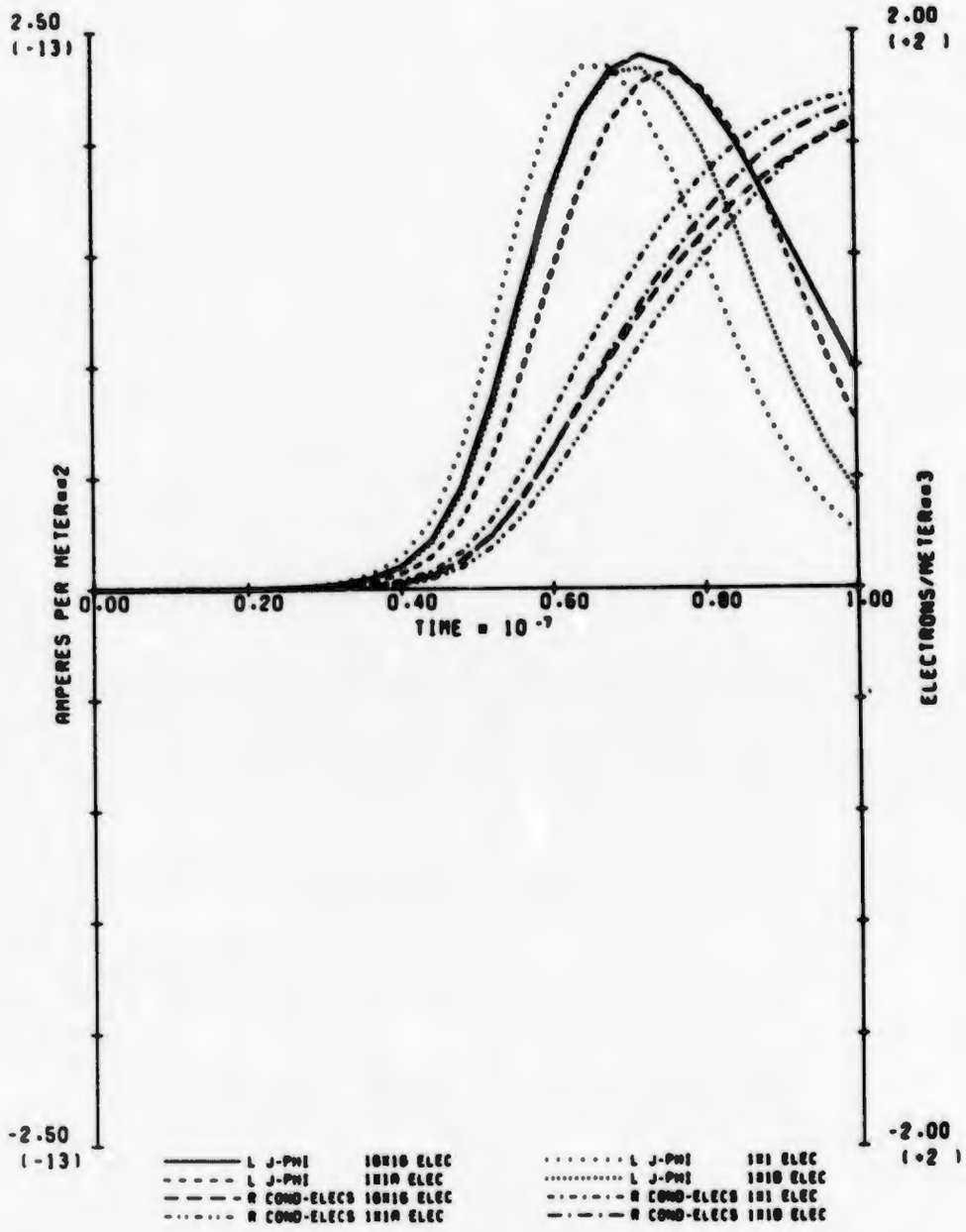

Fig. 45. Calculated Results for Parameter Set 45.

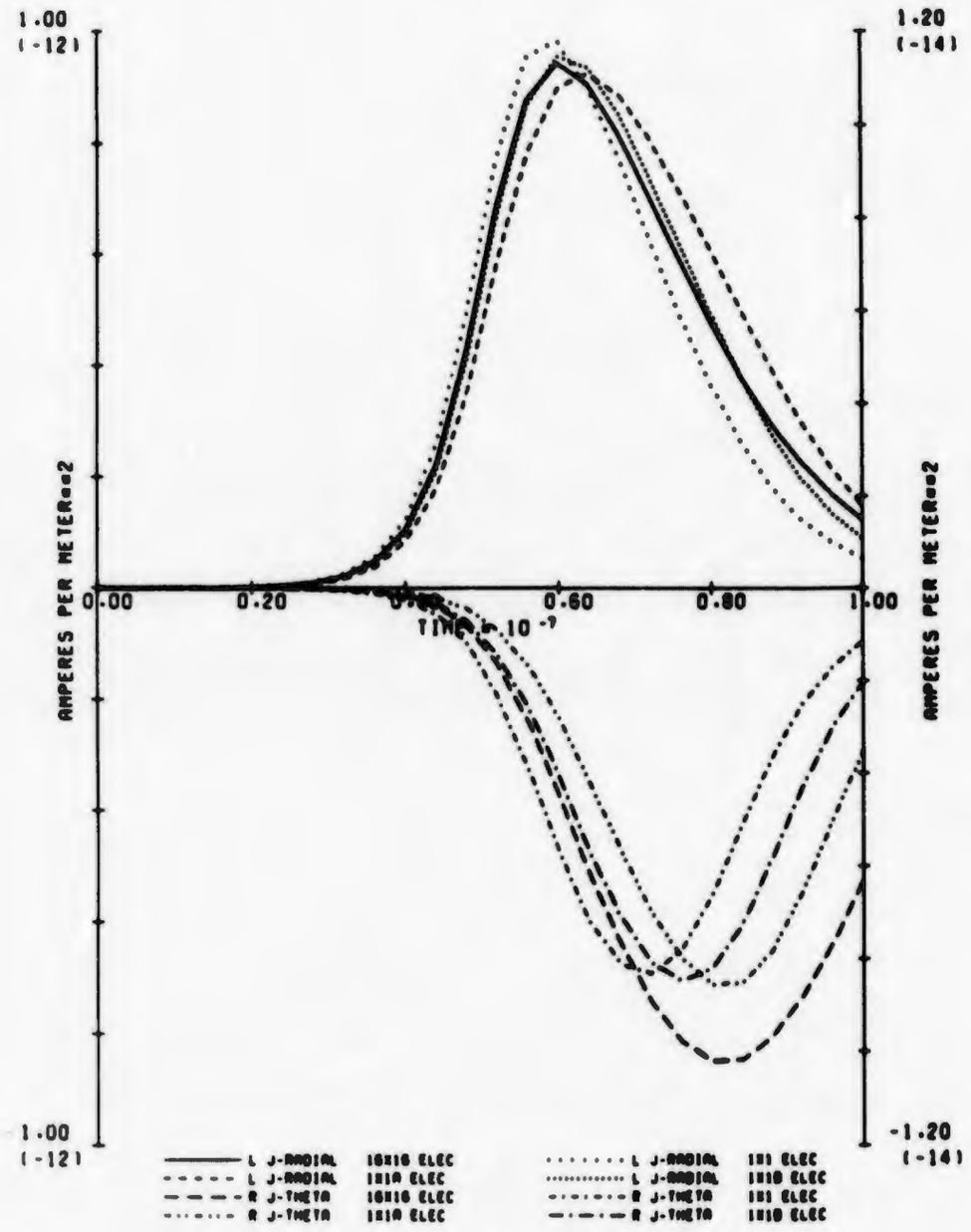

Fig. 46. Calculated Results for Parameter Set 46.

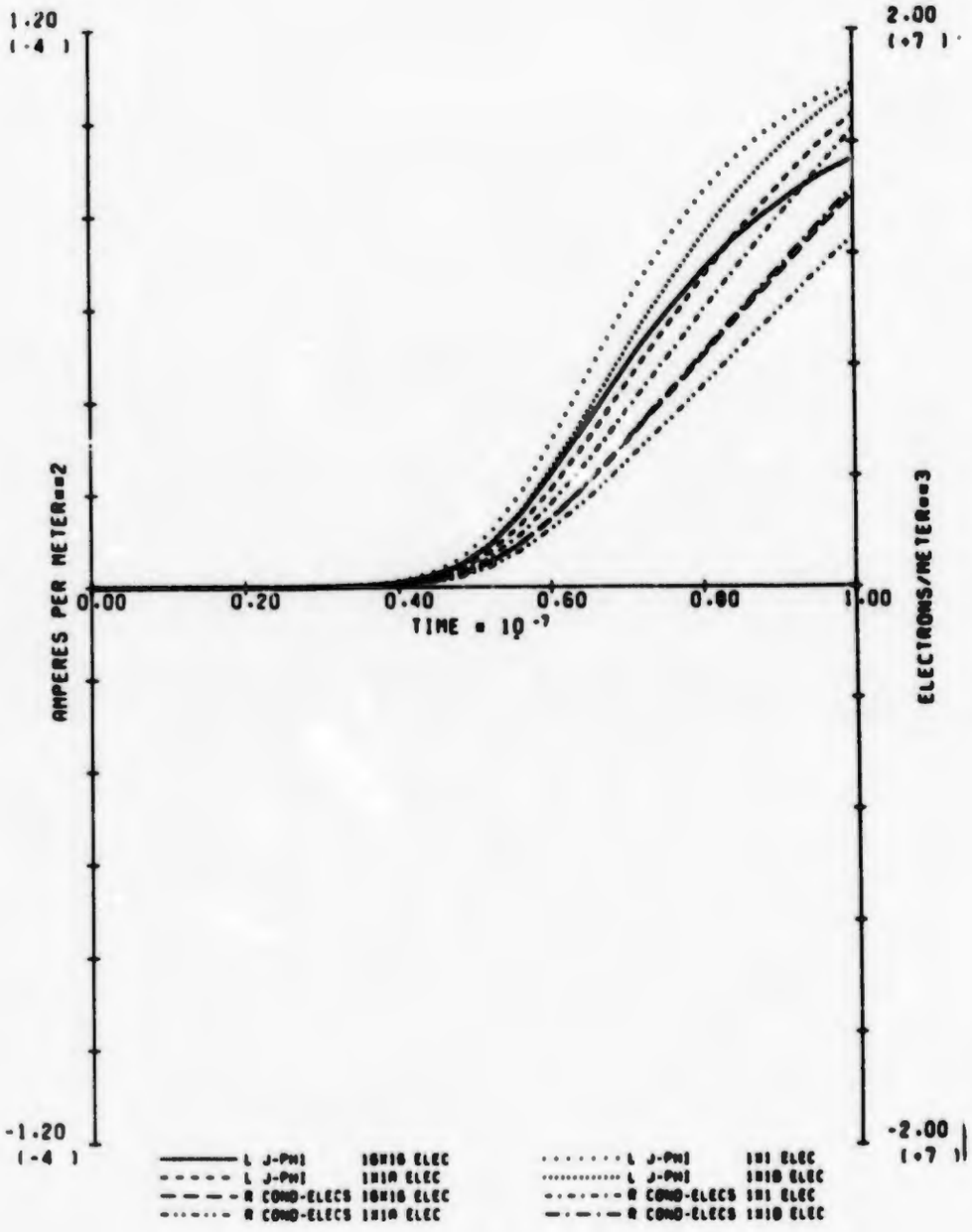

Fig. 47. Calculated Results for Parameter Set 47.

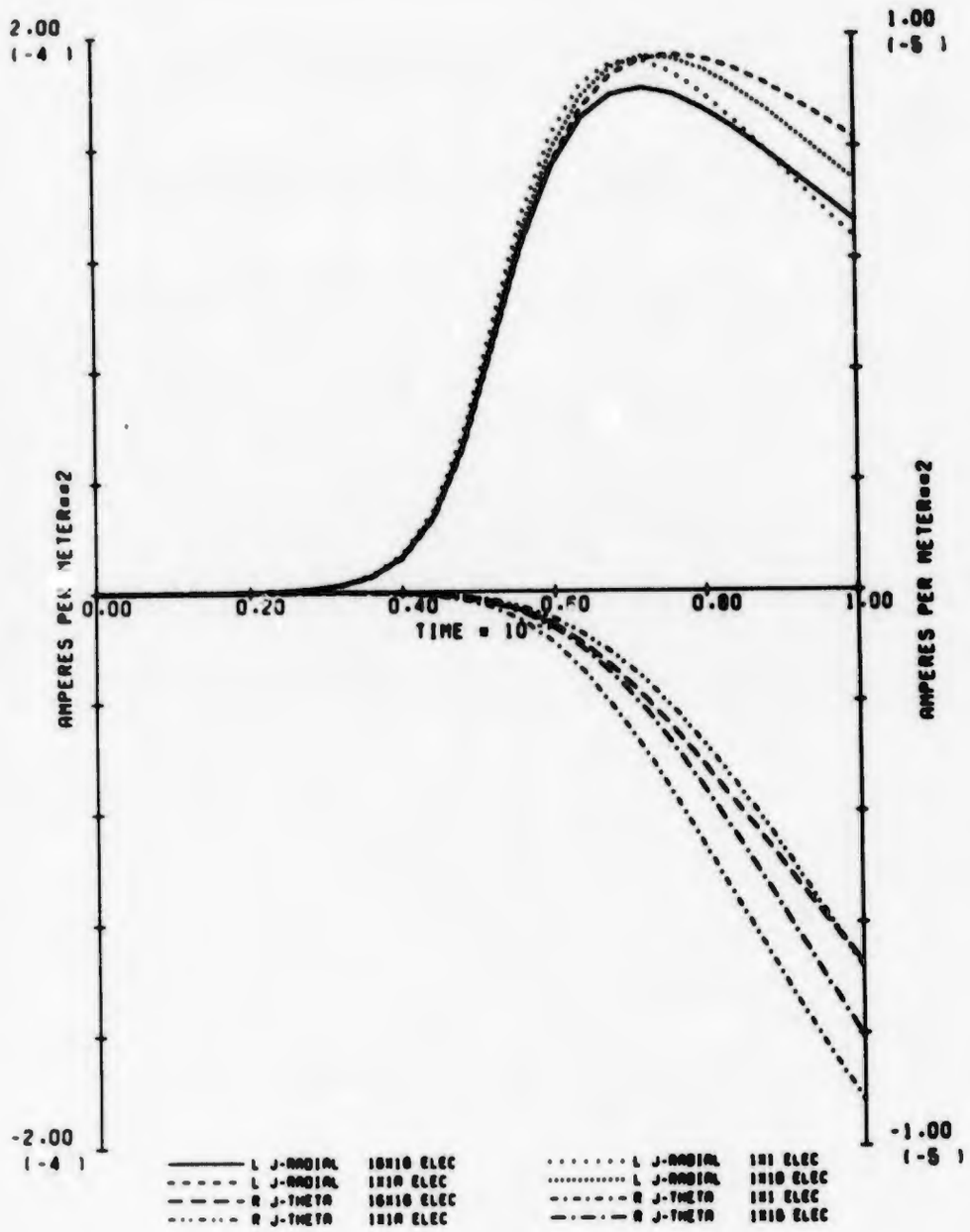

Fig. 48. Calculated Results for Parameter Set 48.

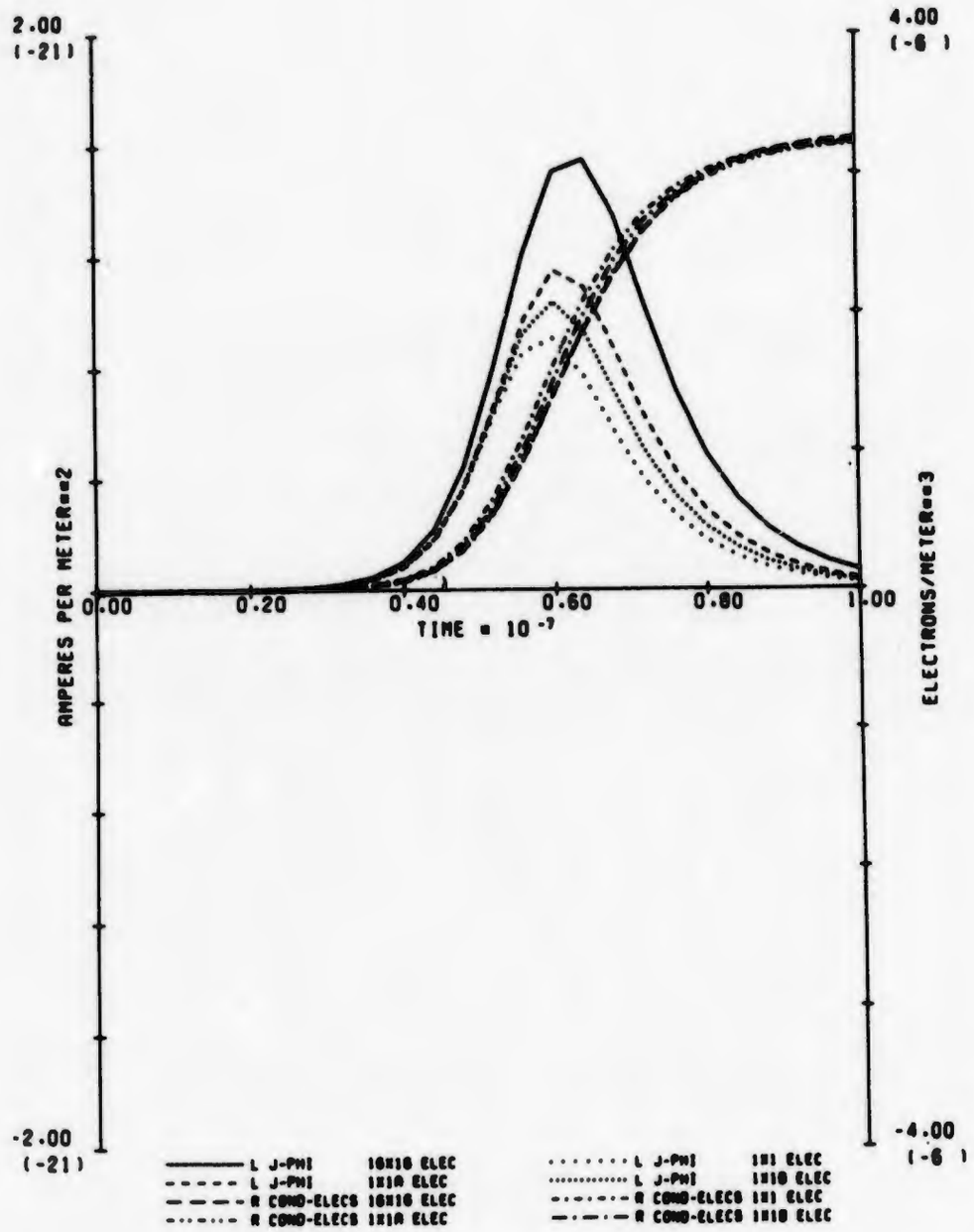

Fig. 49. Calculated Results for Parameter Set 49.

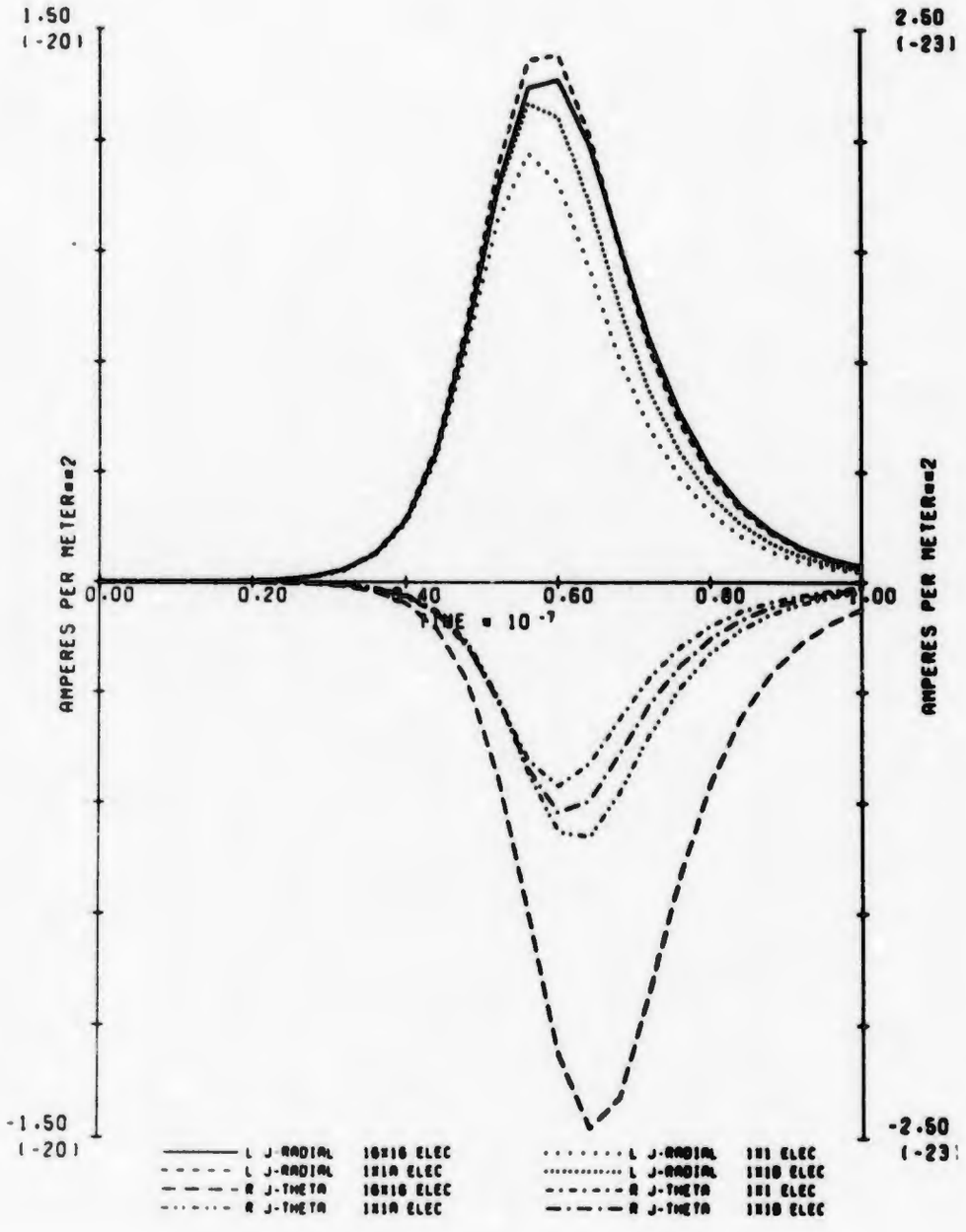

Fig. 50. Calculated Results for Parameter Set 50.

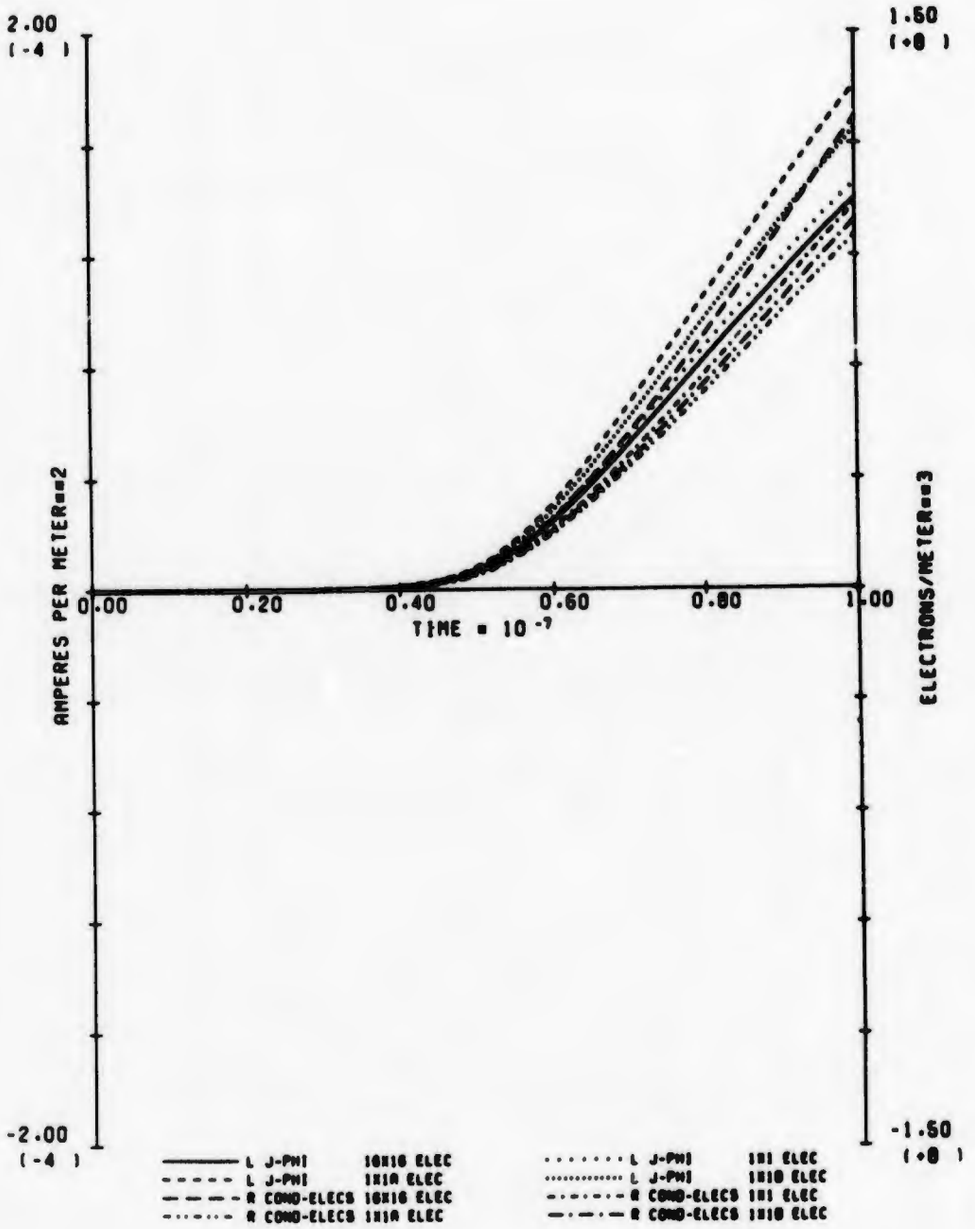

Fig. 51. Calculated Results for Parameter Set 51.

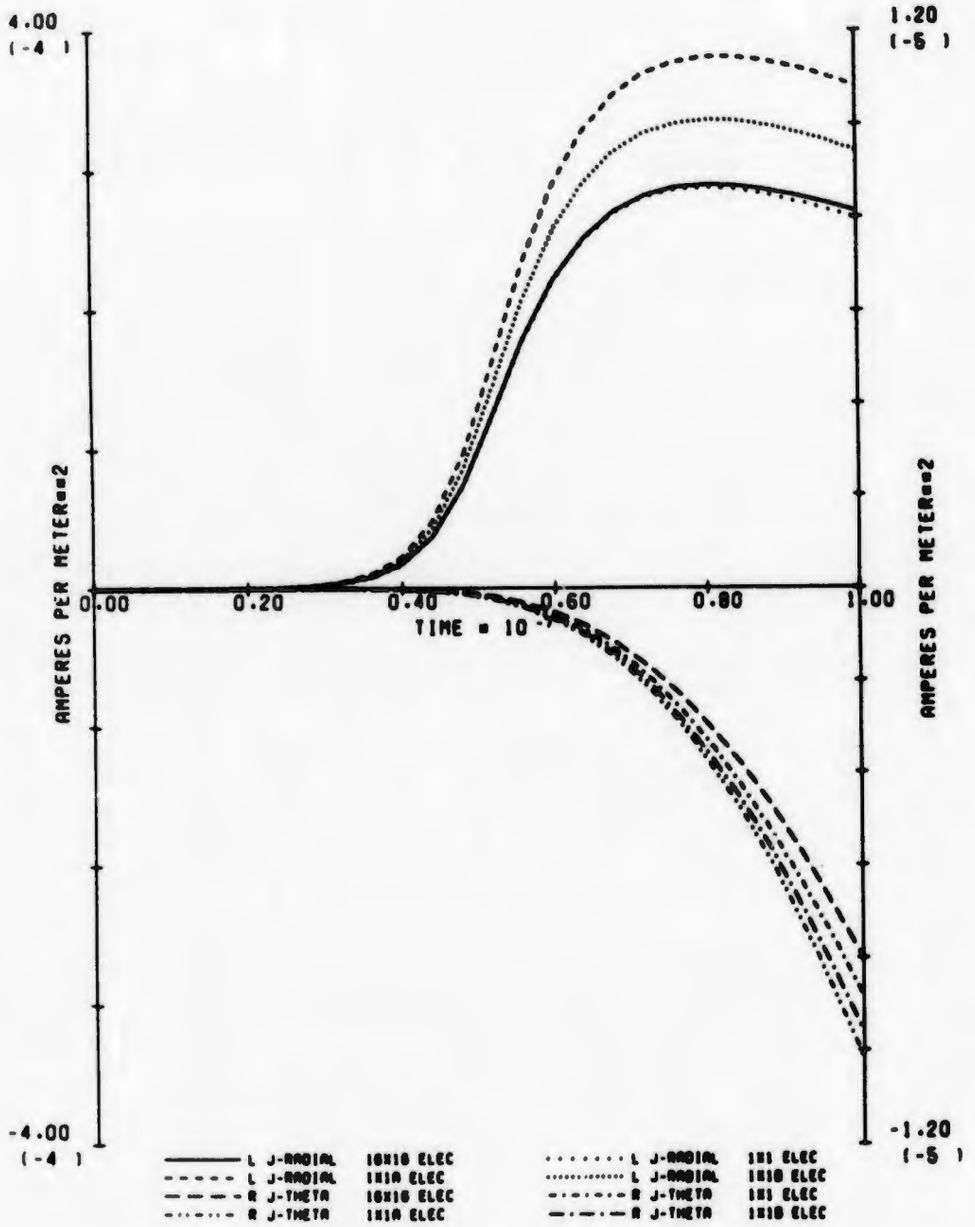

Fig. 52. Calculated Results for Parameter Set 52.

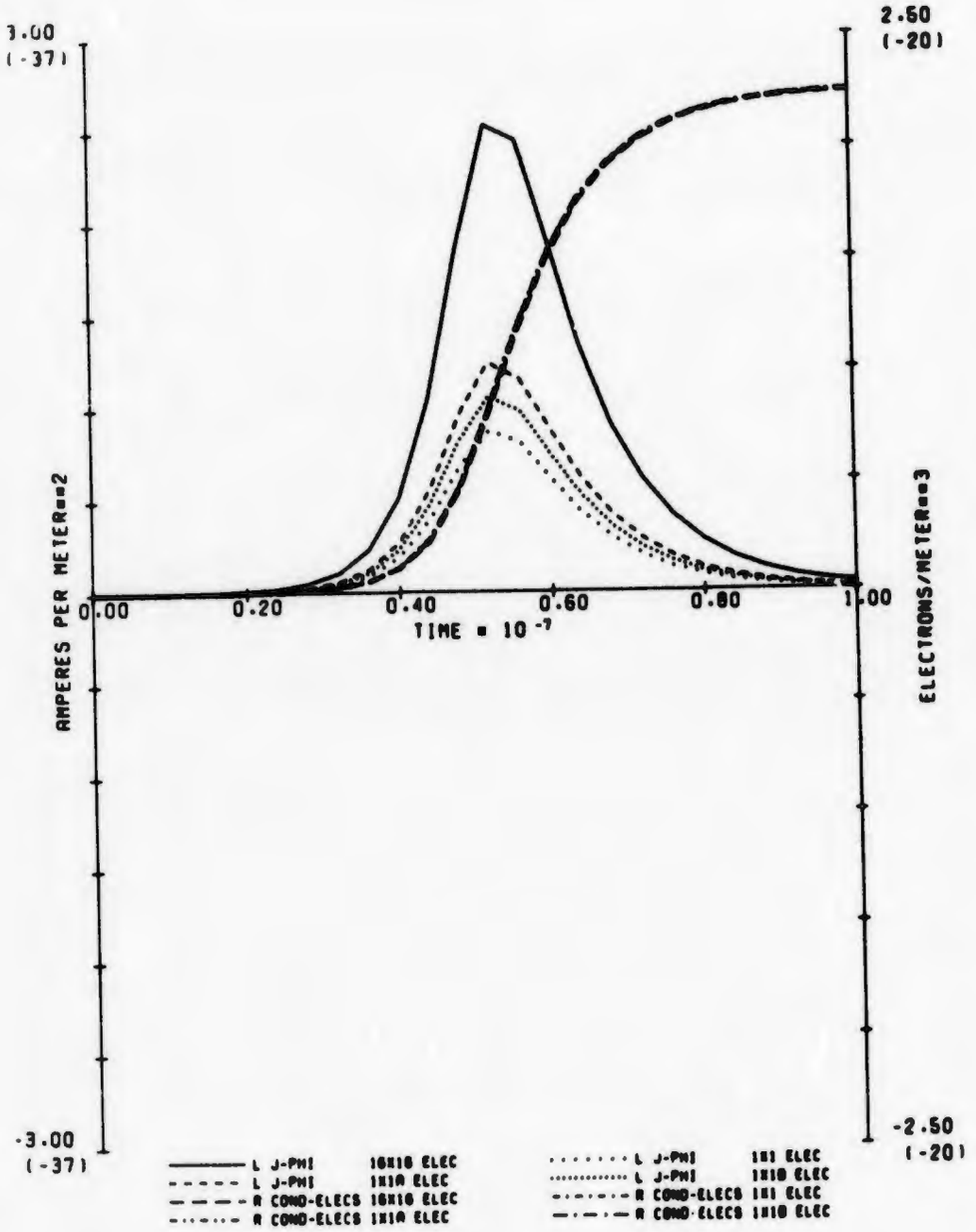

Fig. 53. Calculated Results for Parameter Set 53.

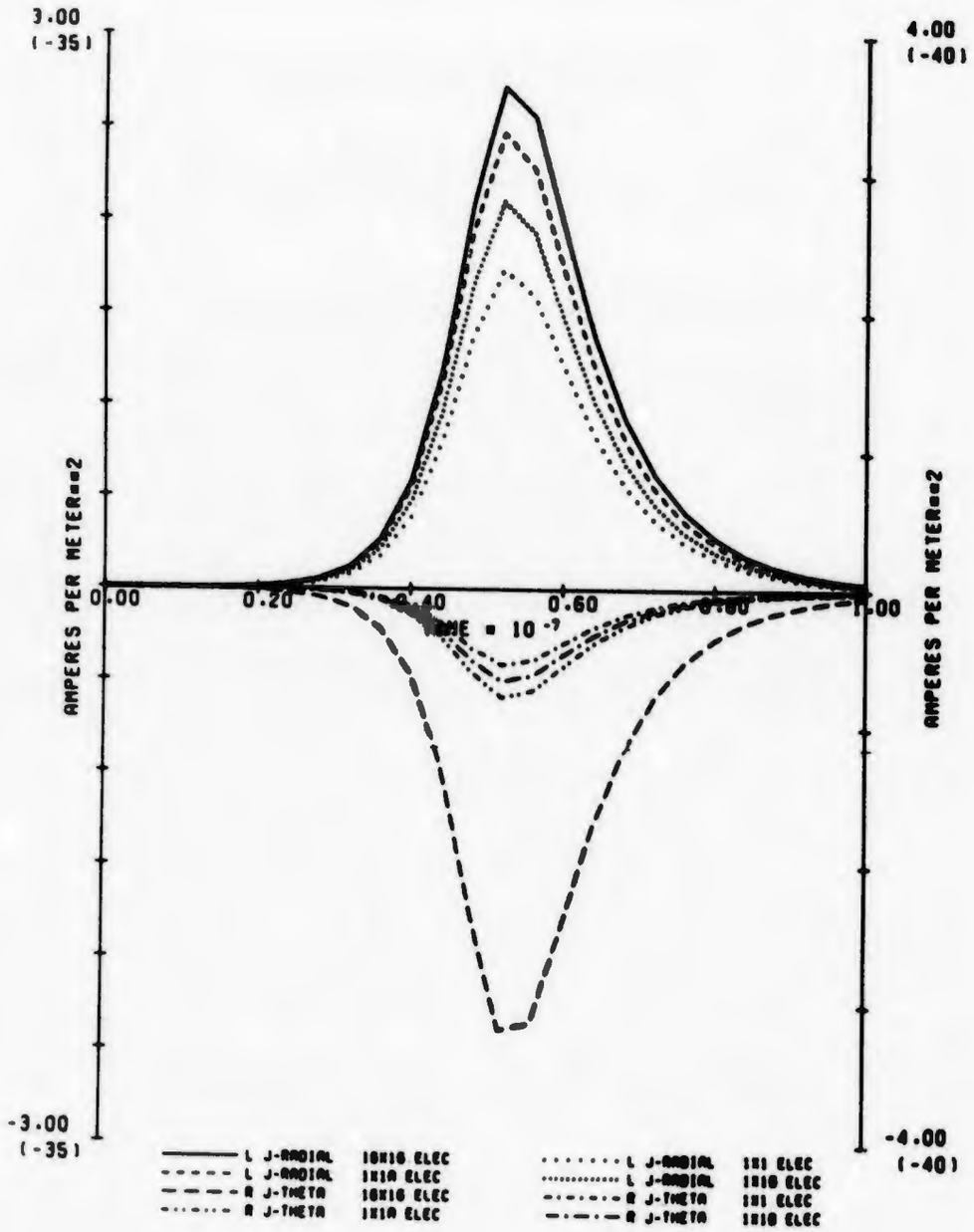

Fig. 54. Calculated Results for Parameter Set 54.

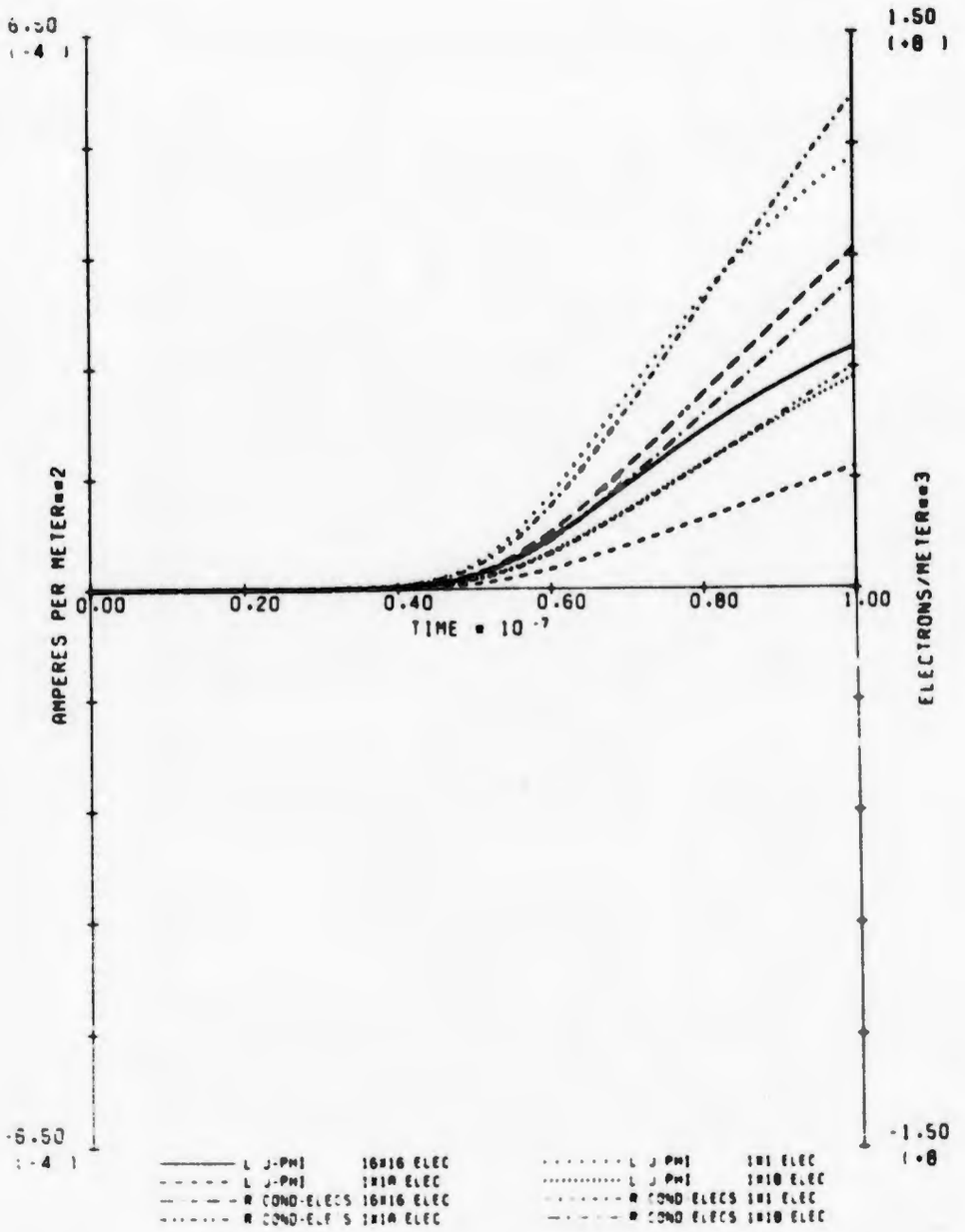

Fig. 55. Calculated Results for Parameter Set 55.

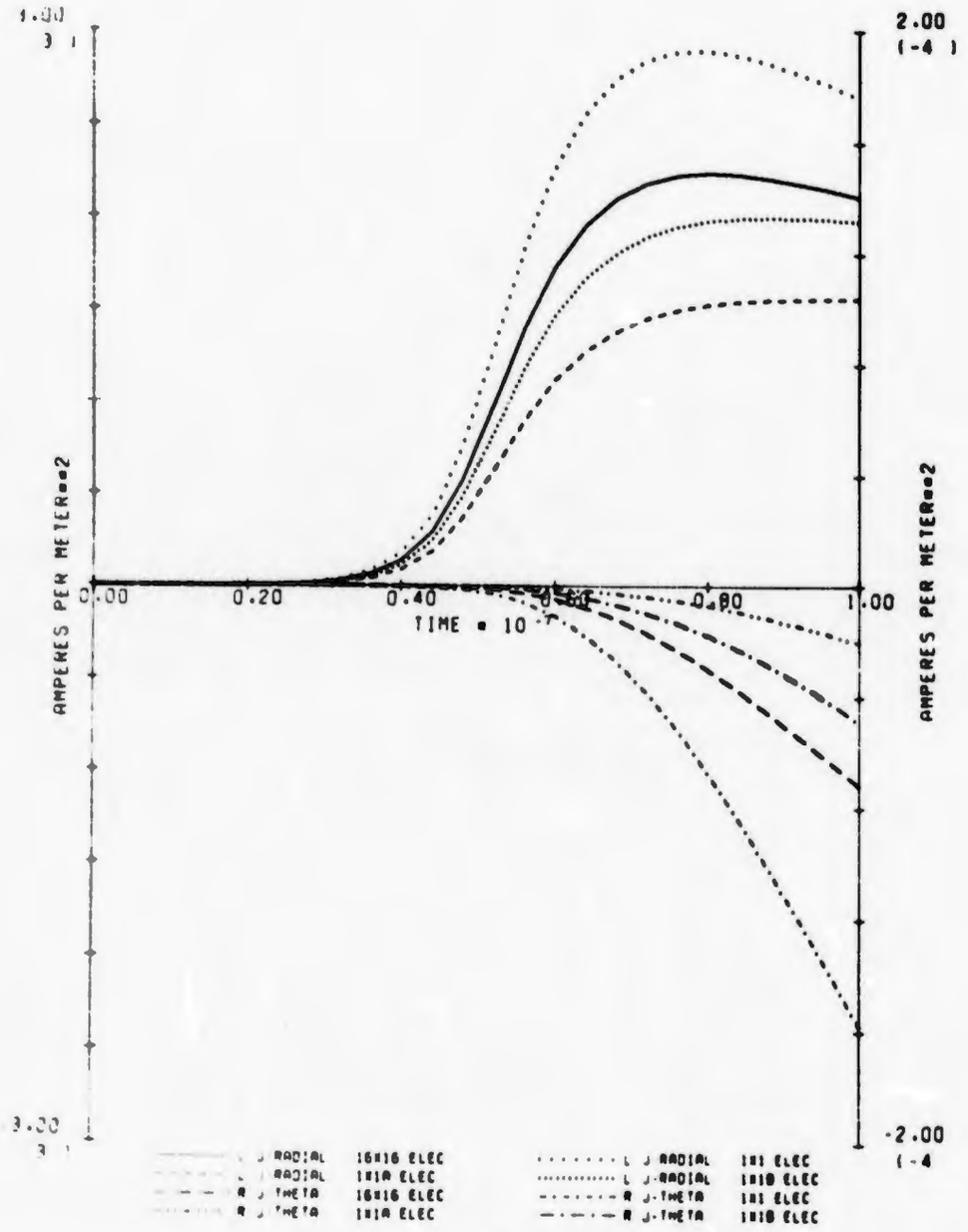

Fig. 56. Calculated Results for Parameter Set 56.

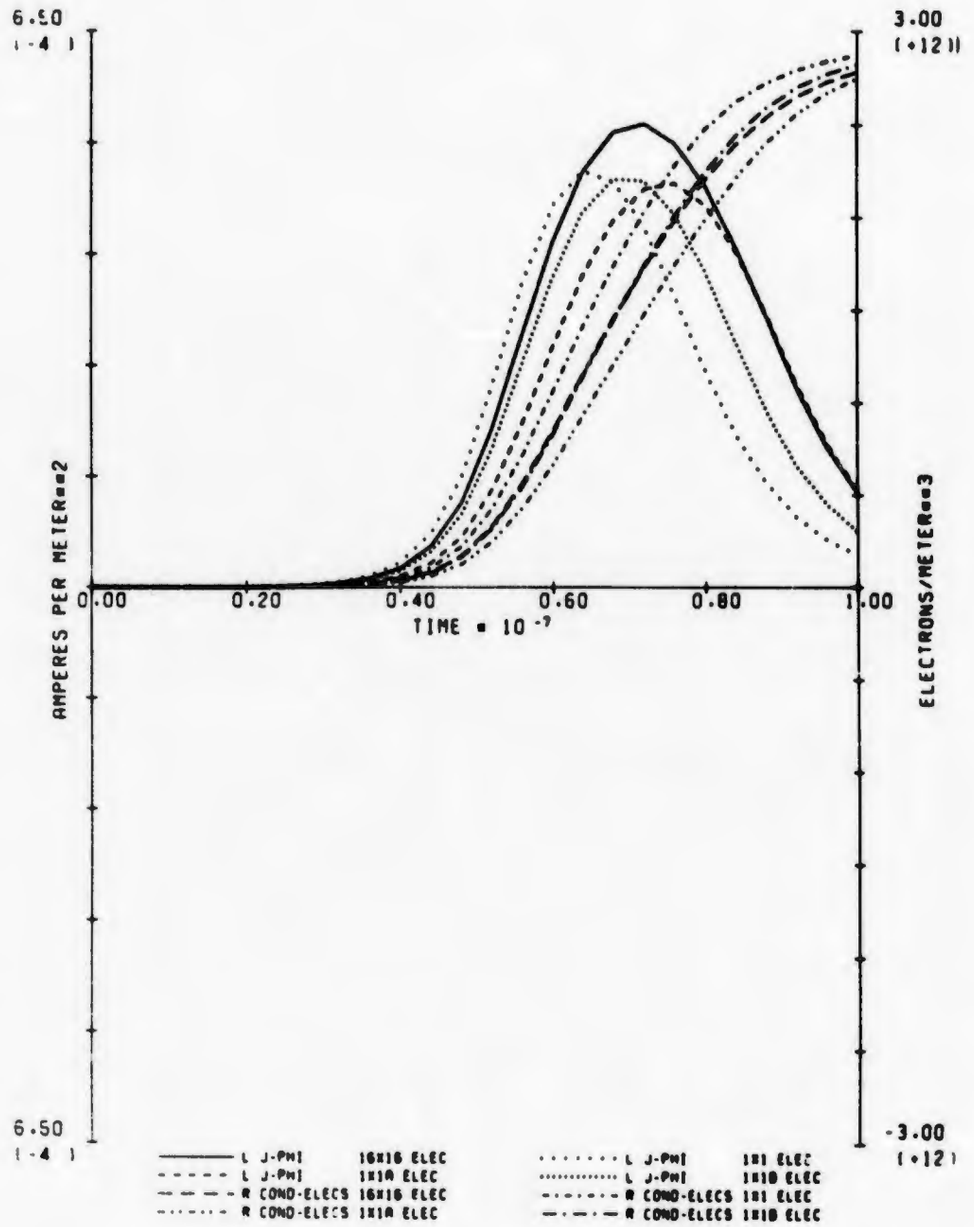

Fig. 57. Calculated Results for Parameter Set 57.

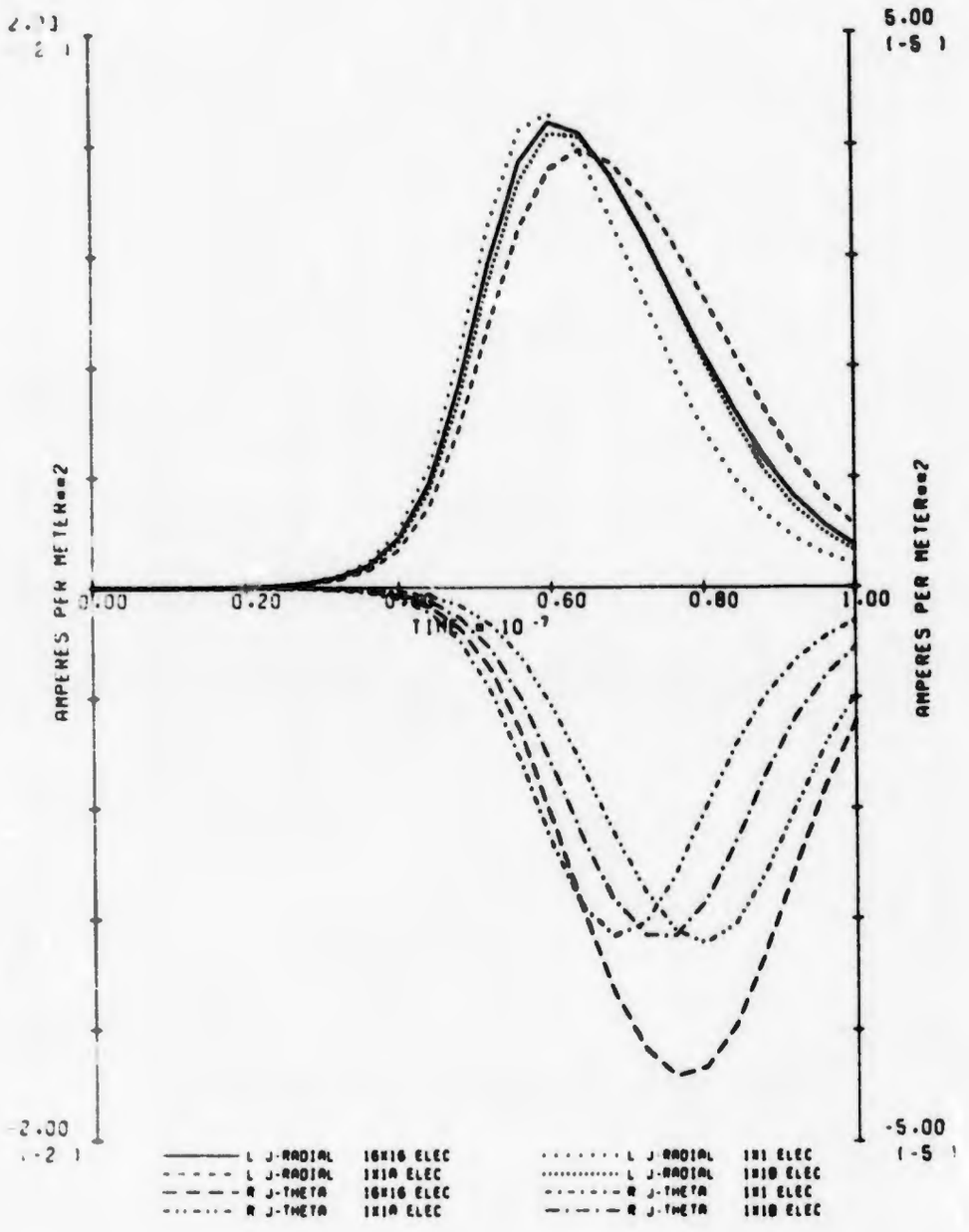

Fig. 58. Calculated Results for Parameter Set 58.

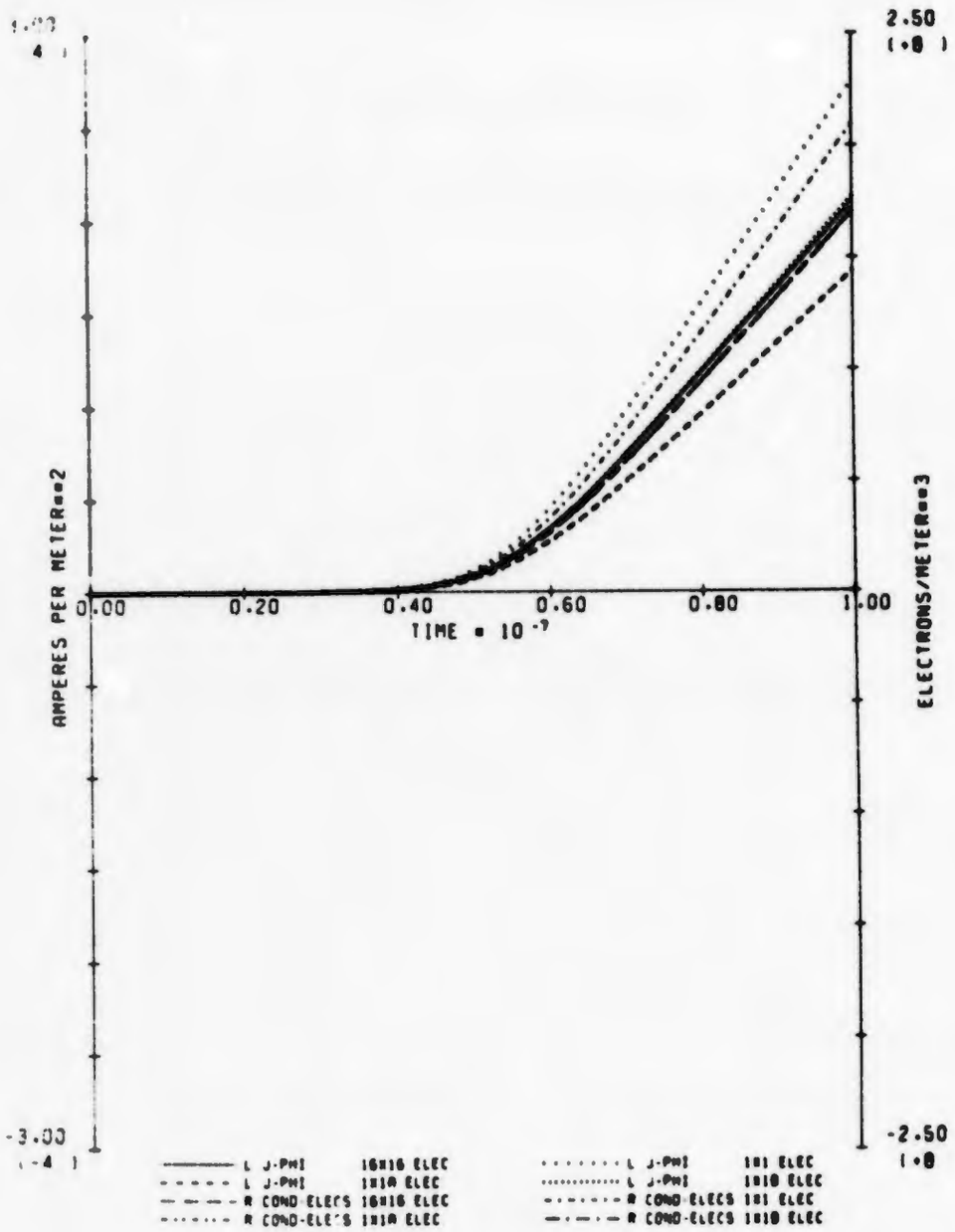

Fig. 59. Calculated Results for Parameter Set 59.

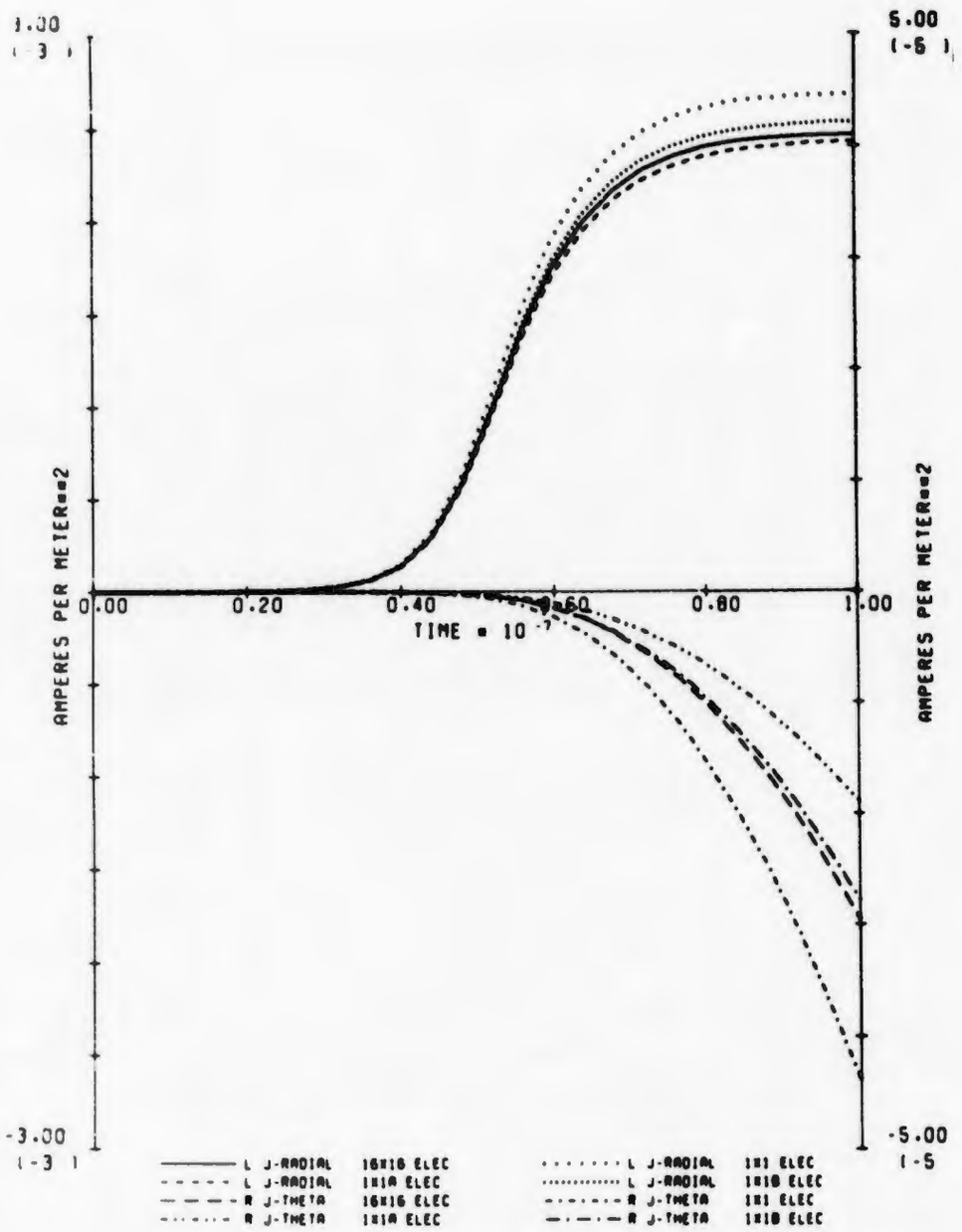

Fig. 60. Calculated Results for Parameter Set 60.

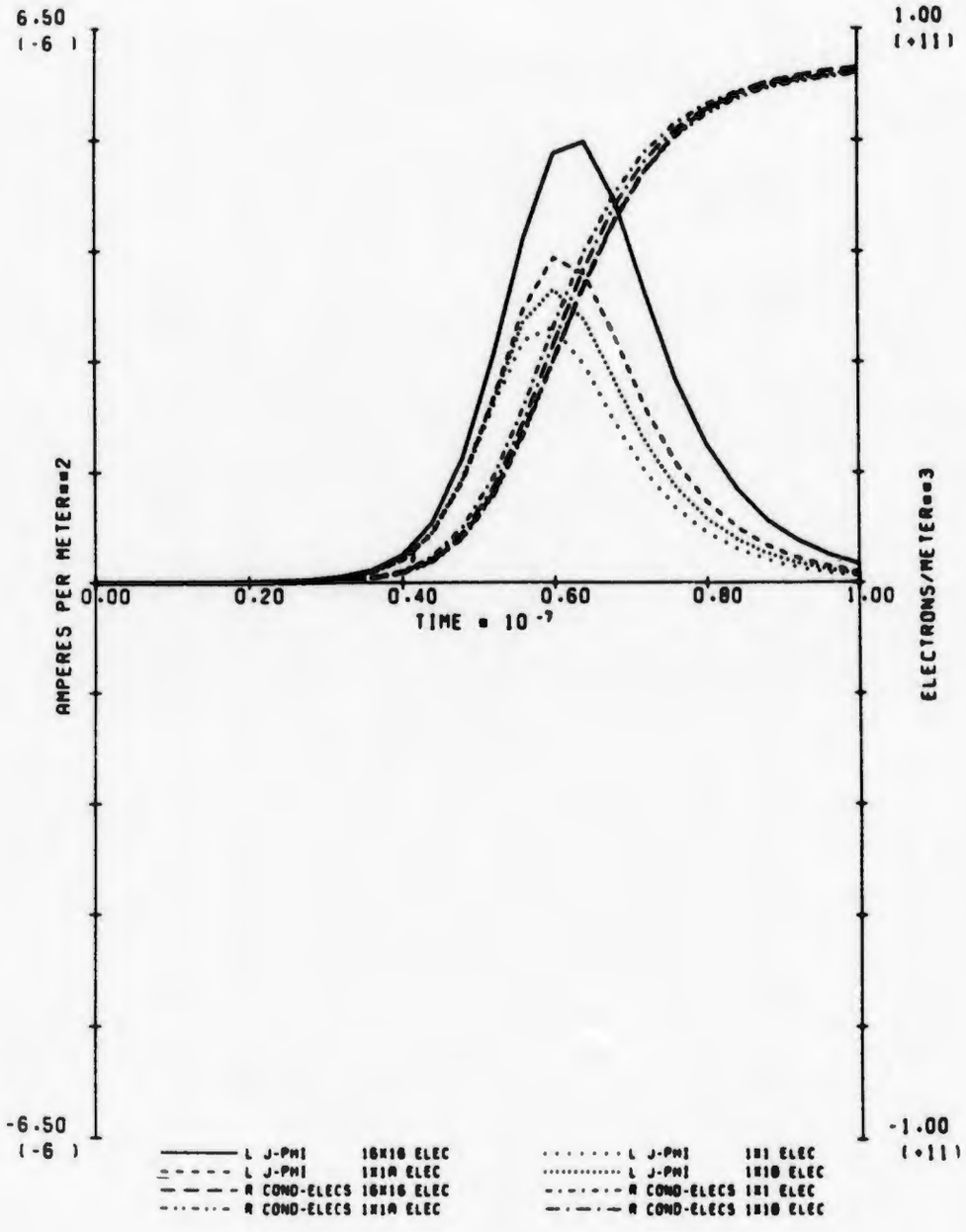

Fig. 61. Calculated Results for Parameter Set 61.

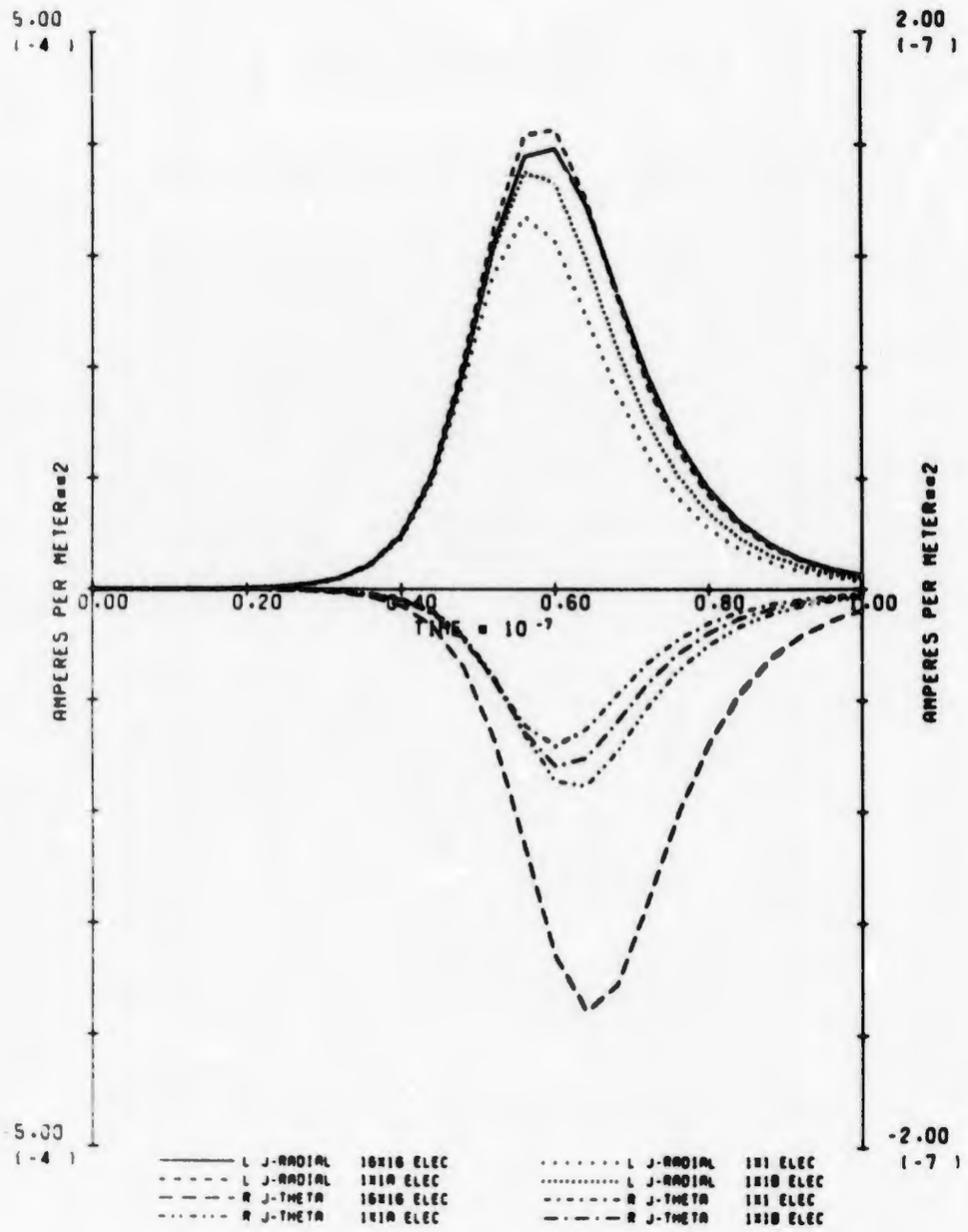

Fig. 62. Calculated Results for Parameter Set 62.

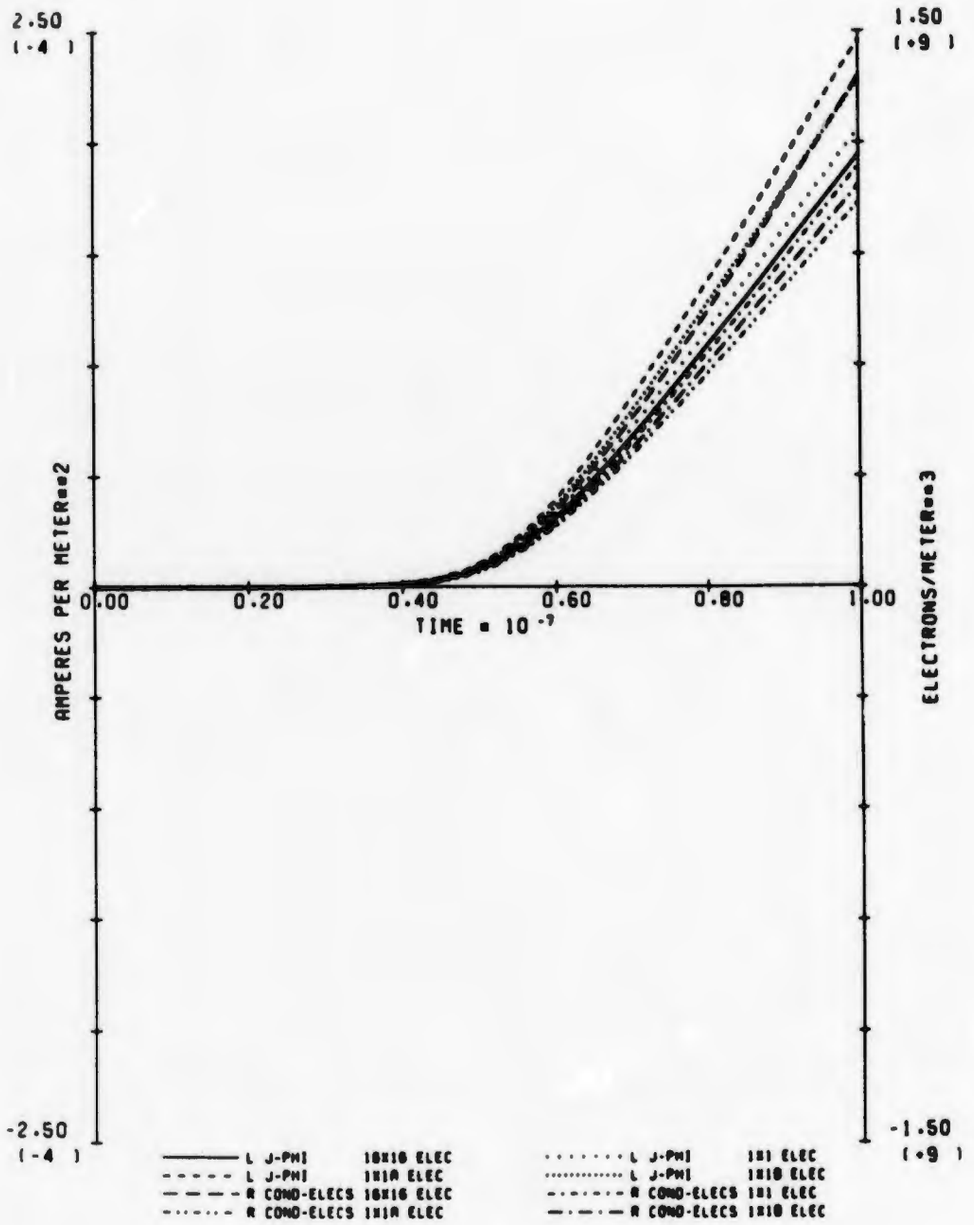

Fig. 63. Calculated Results for Parameter Set 63.

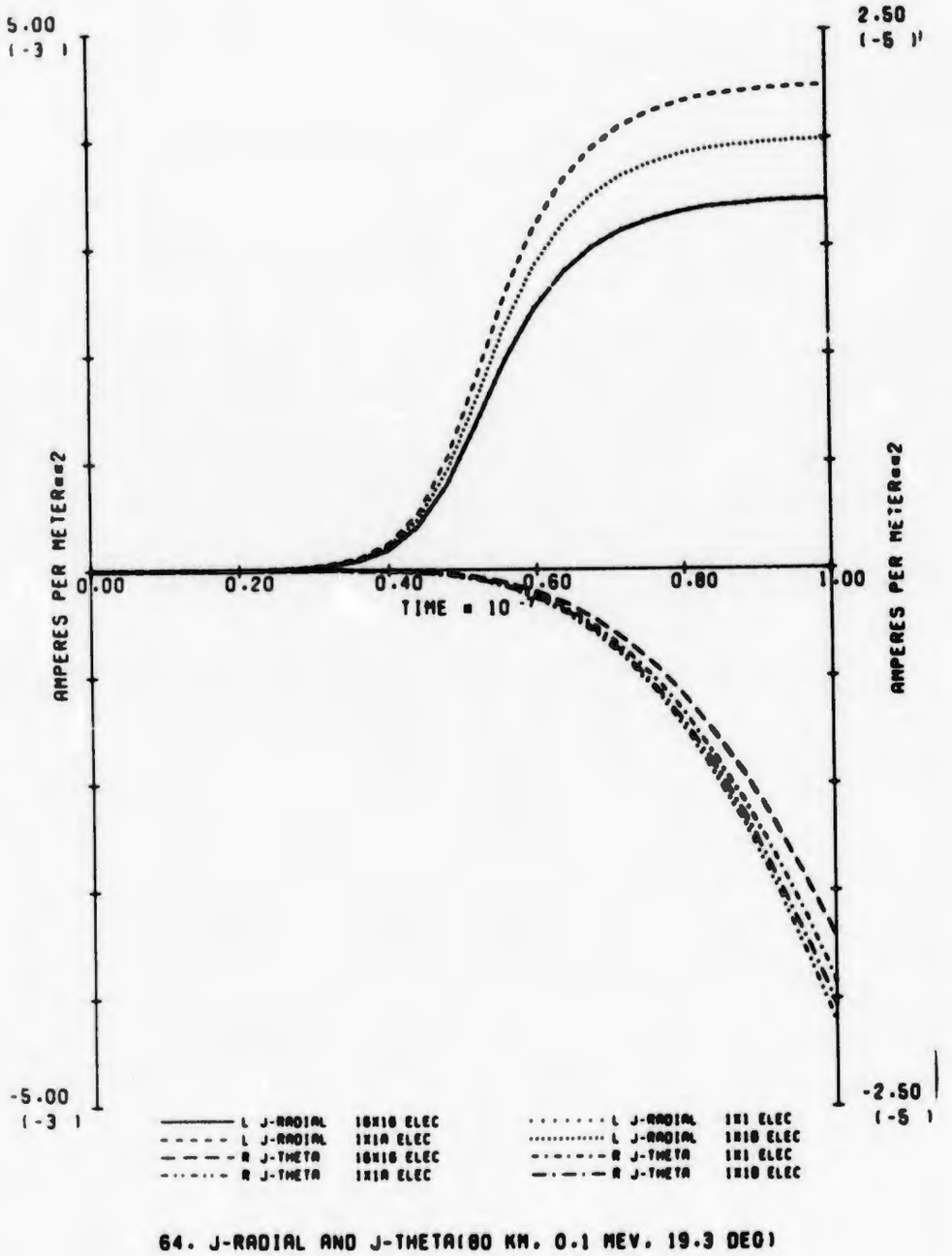

Fig. 64. Calculated Results for Parameter Set 64.

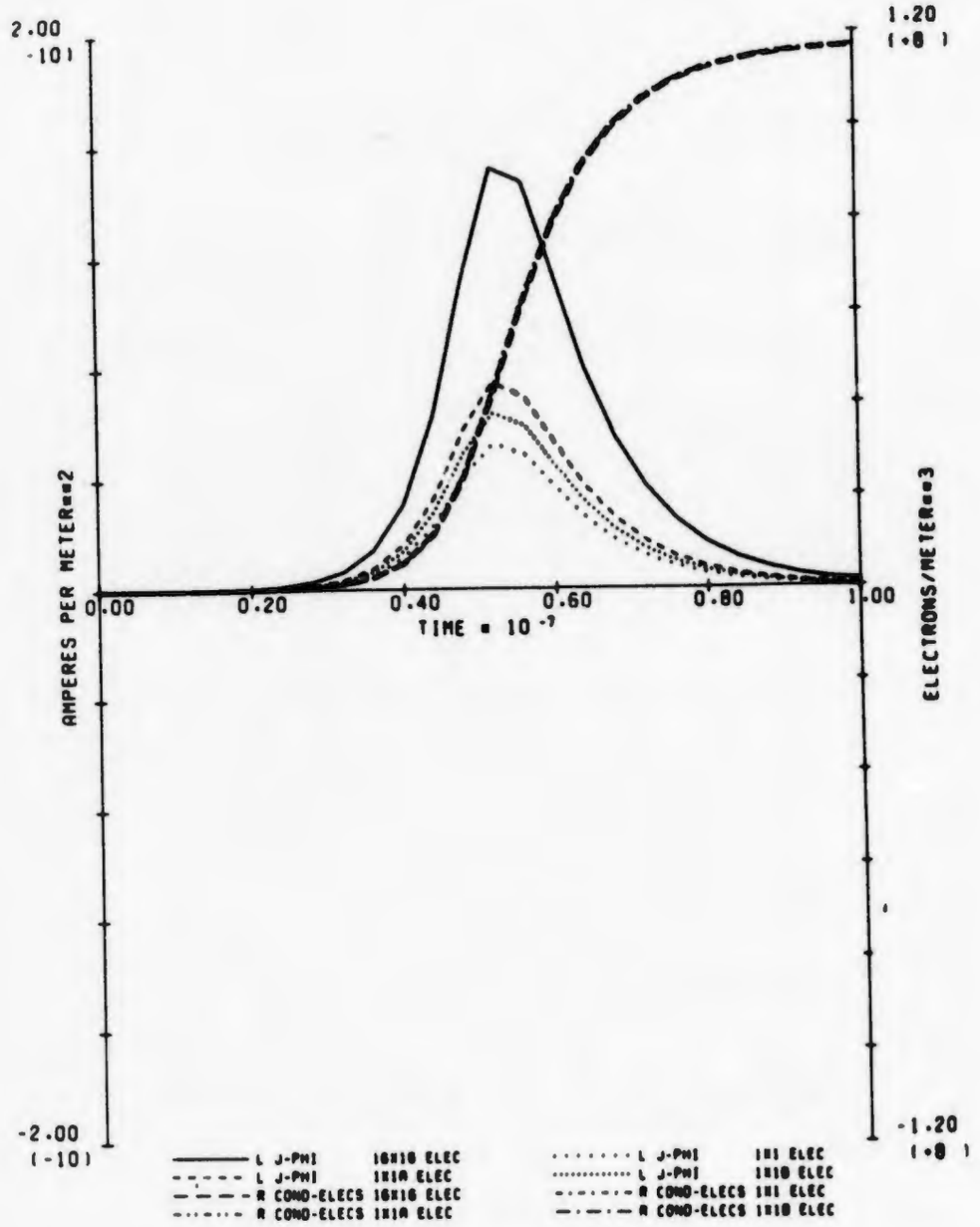

Fig. 65. Calculated Results for Parameter Set 65.

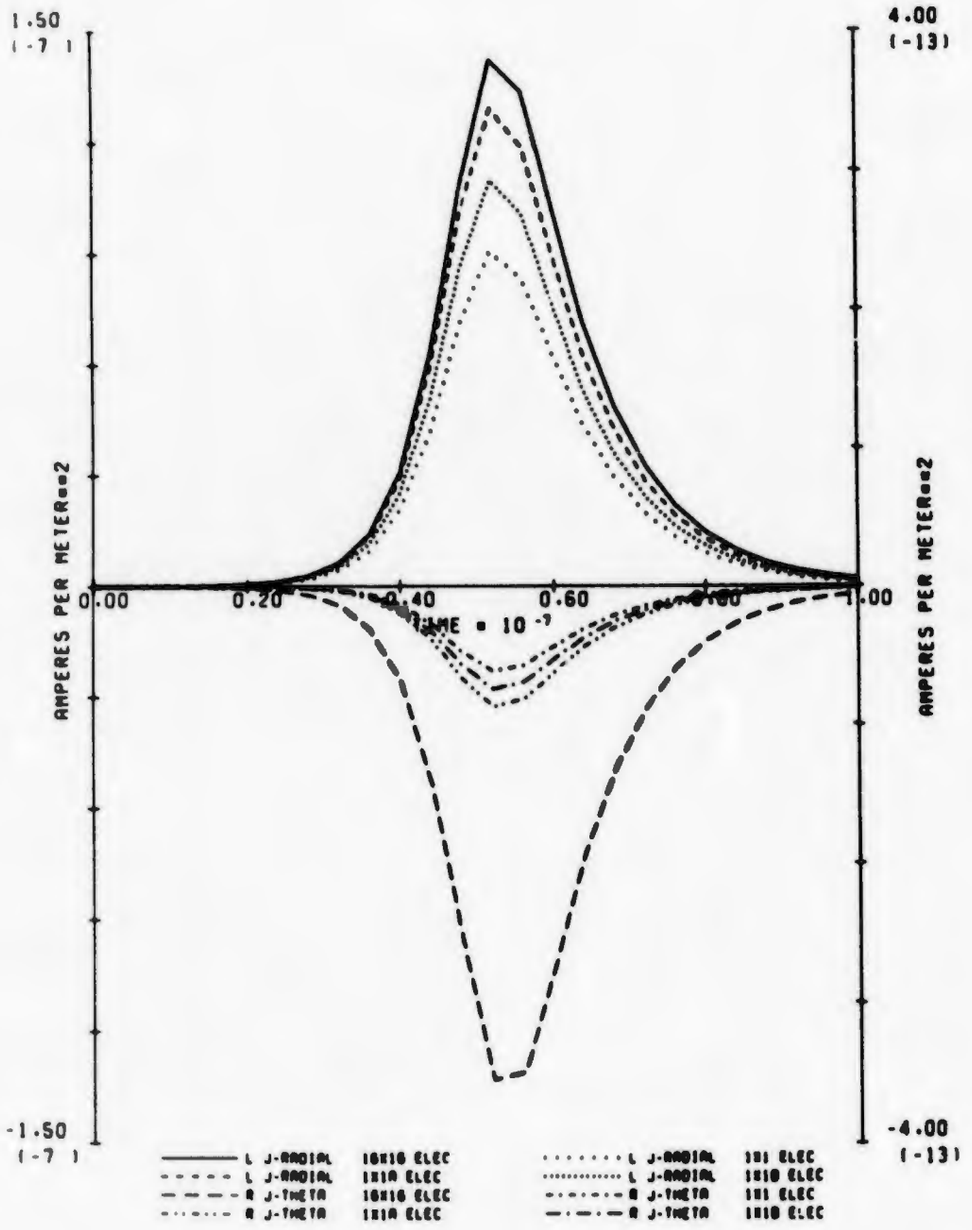

Fig. 66. Calculated Results for Parameter Set 66.

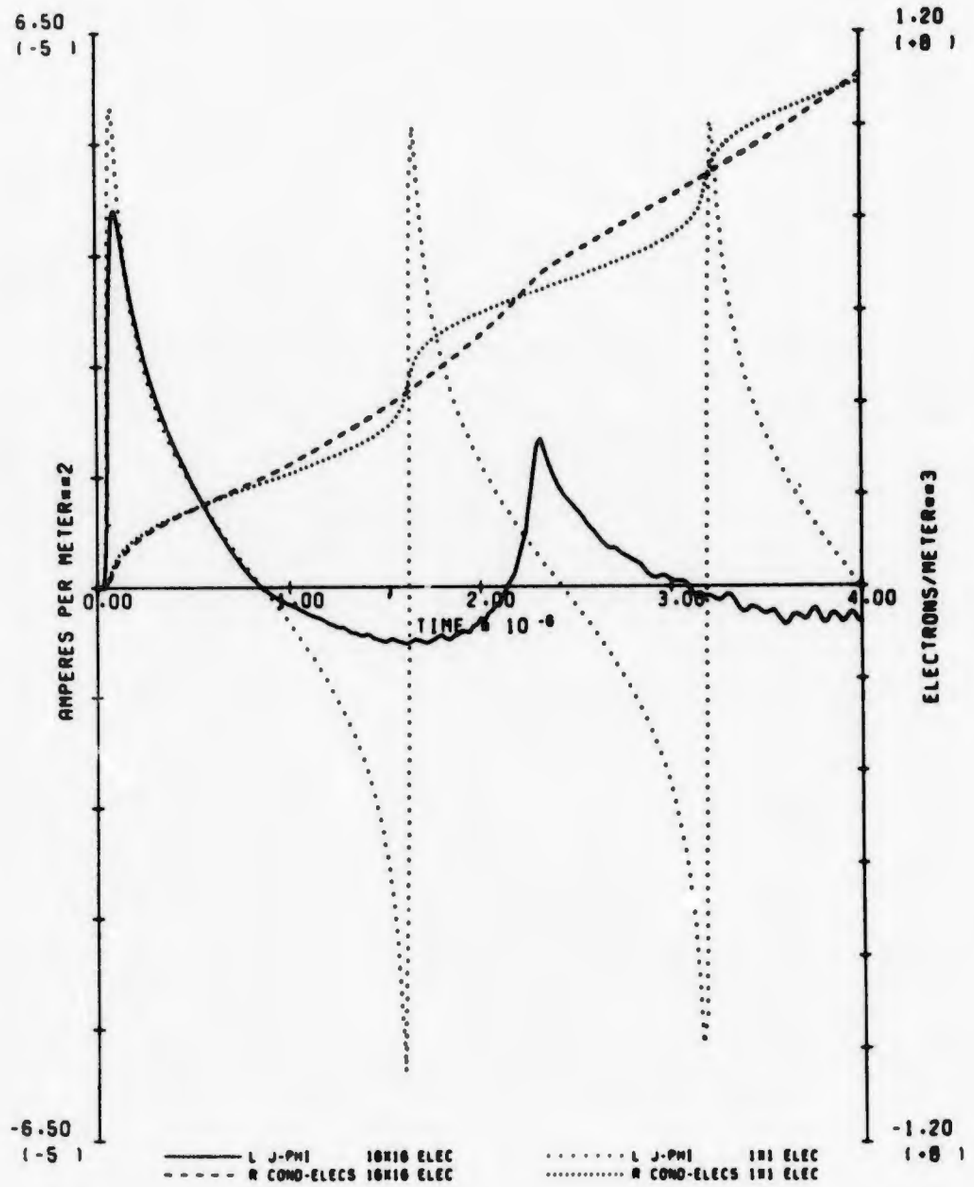

Fig. 67. Calculated Results for Parameter Set 67.

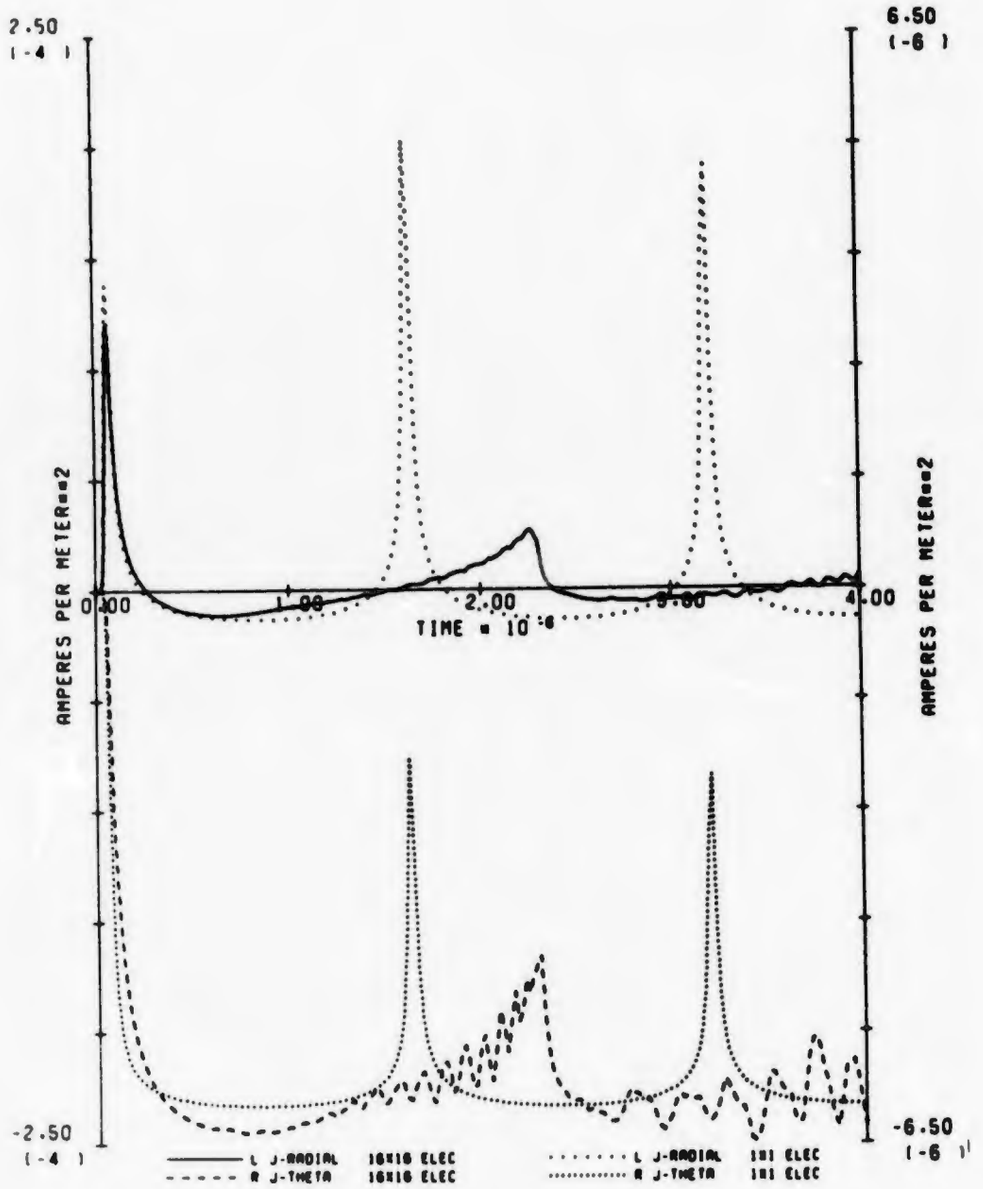

Fig. 68. Calculated Results for Parameter Set 68.

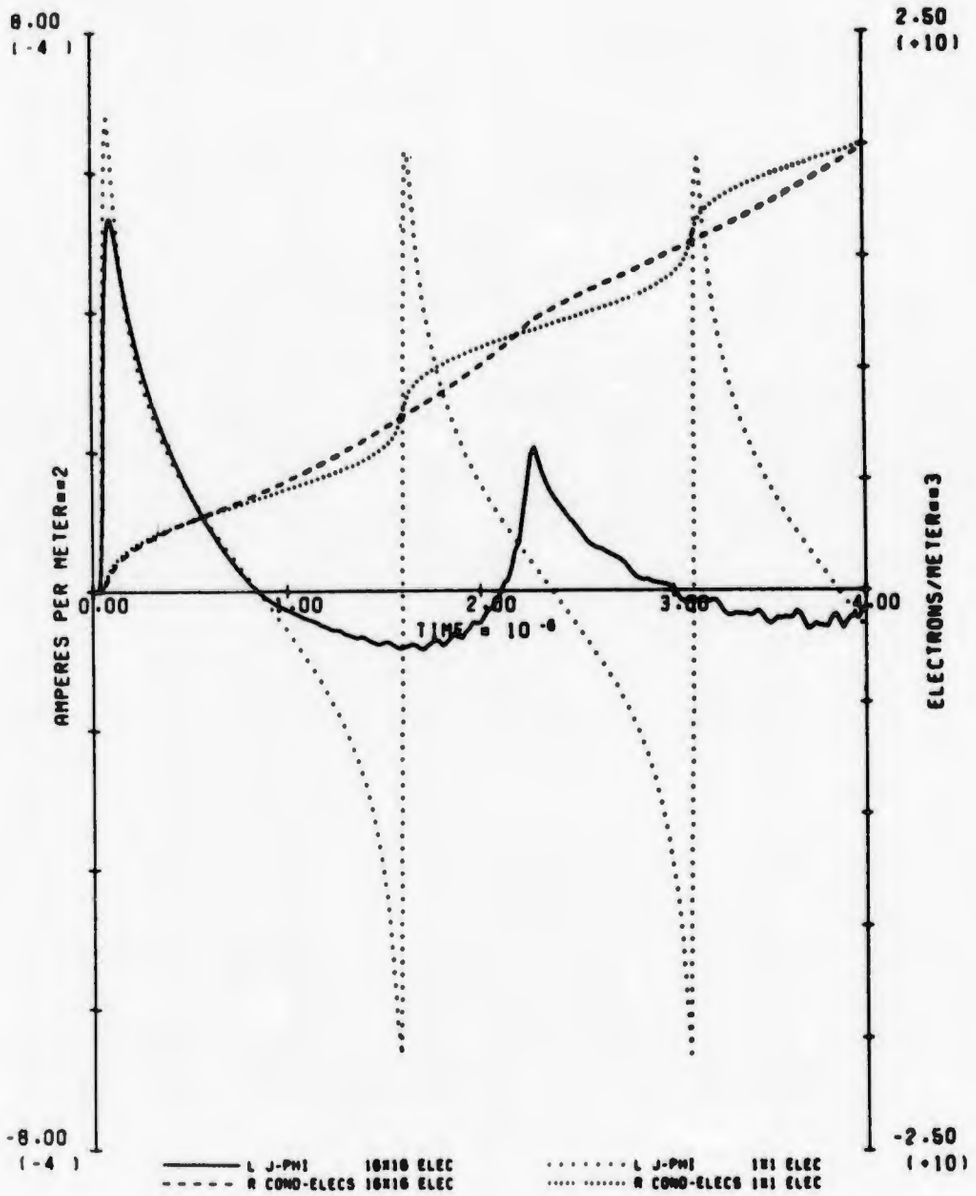

Fig. 69. Calculated Results for Parameter Set 69.

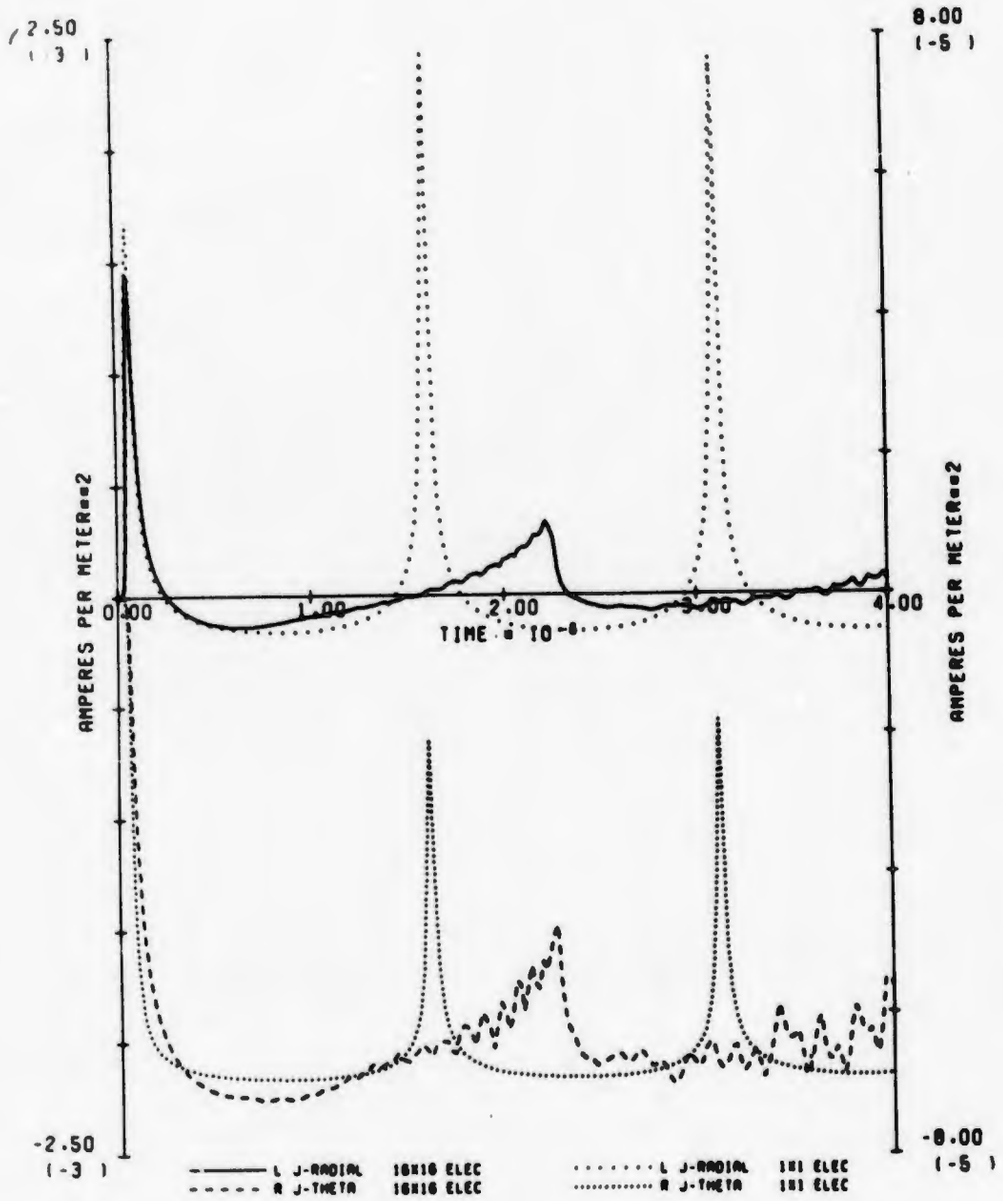

Fig. 70. Calculated Results for Parameter Set 70.

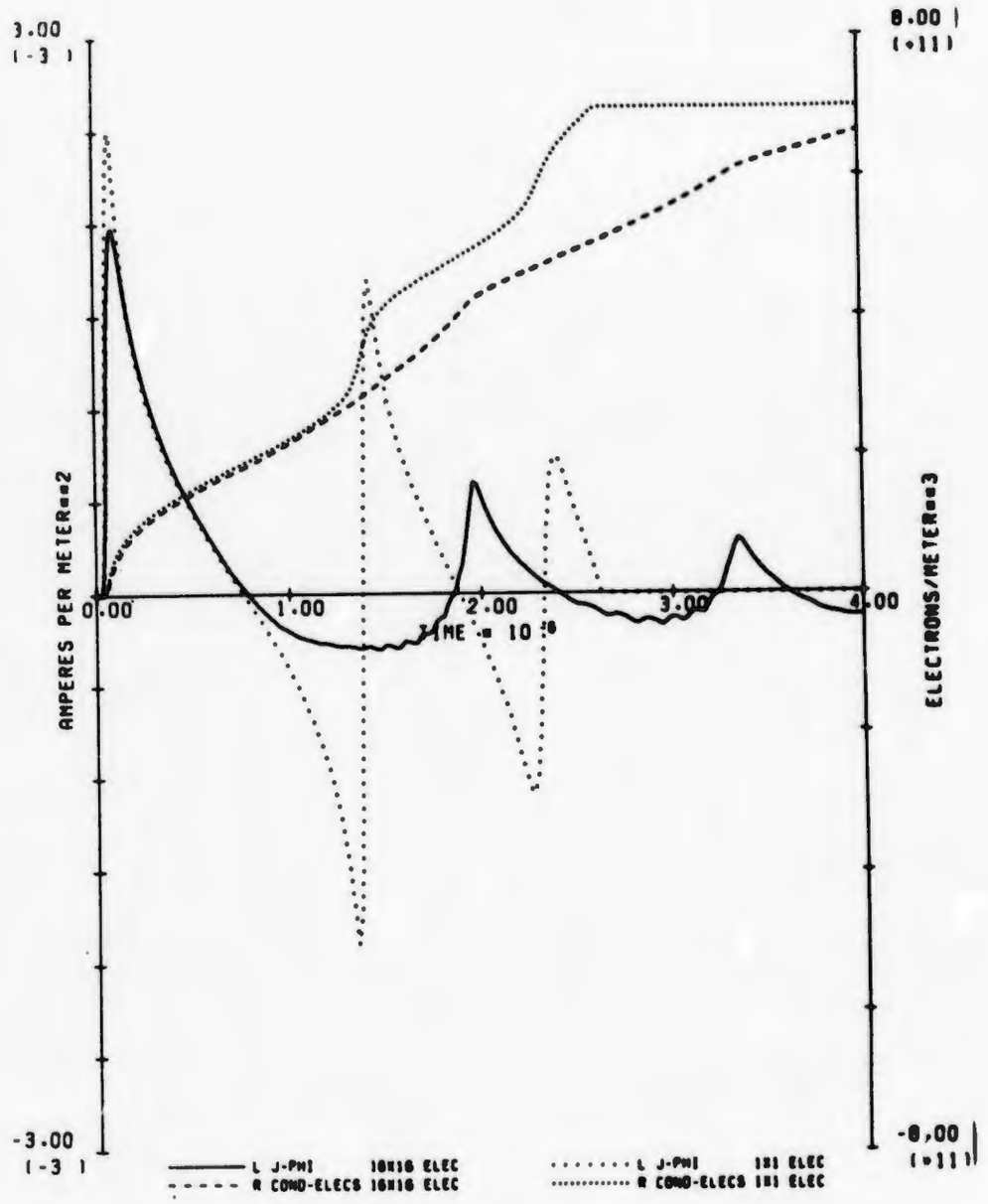

Fig. 71. Calculated Results for Parameter Set 71.

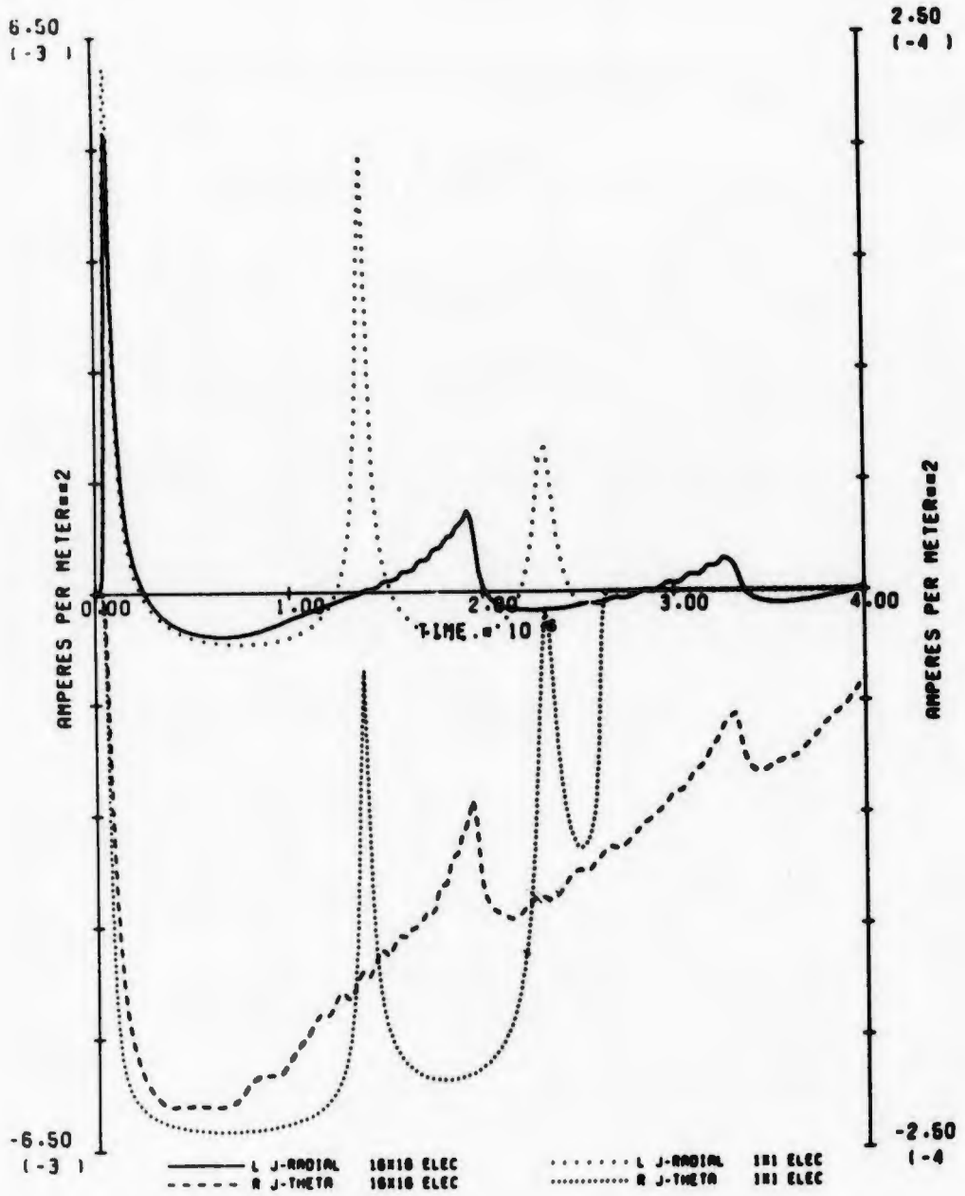

Fig. 72. Calculated Results for Parameter Set 72.

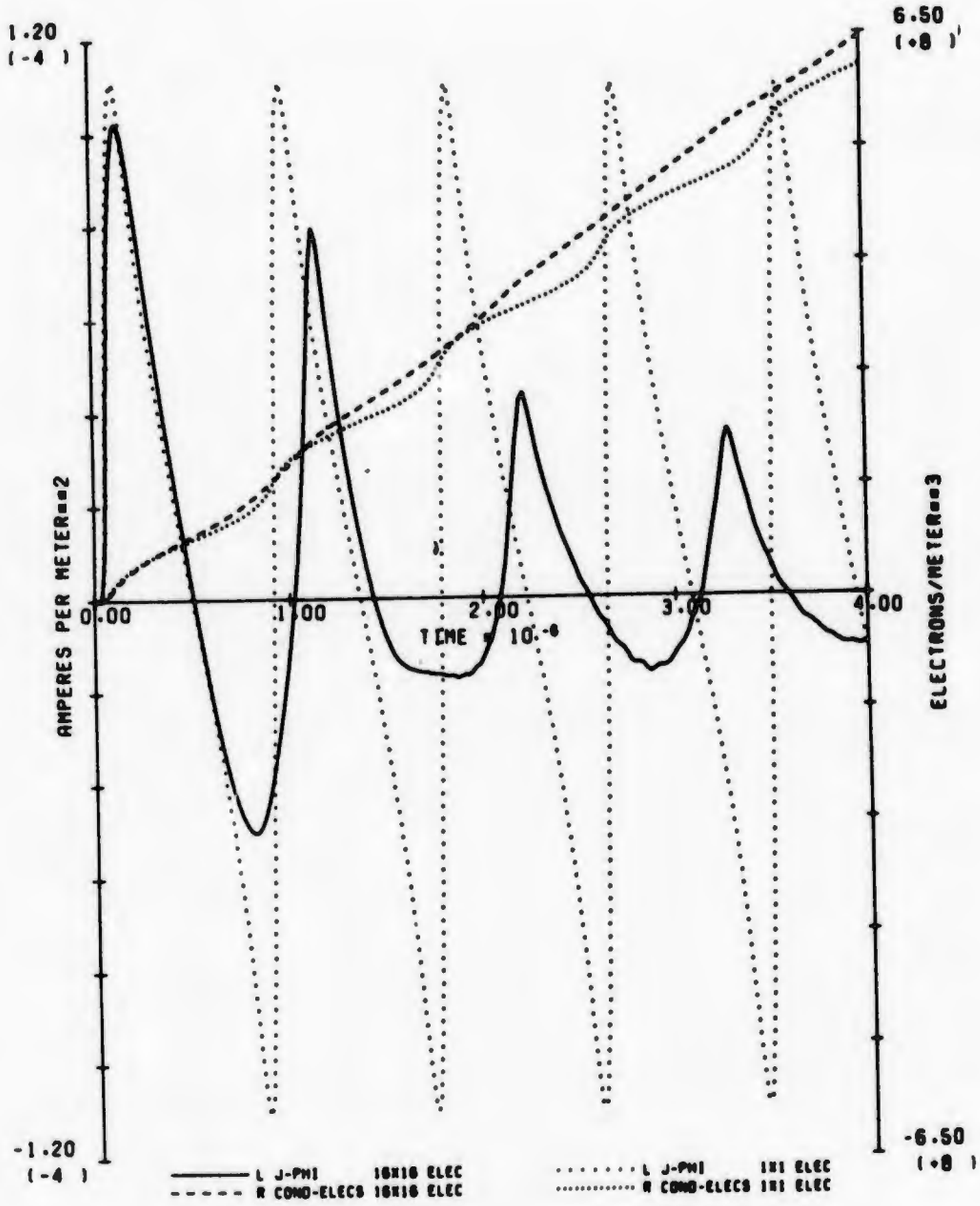

Fig. 73. Calculated Results for Parameter Set 73.

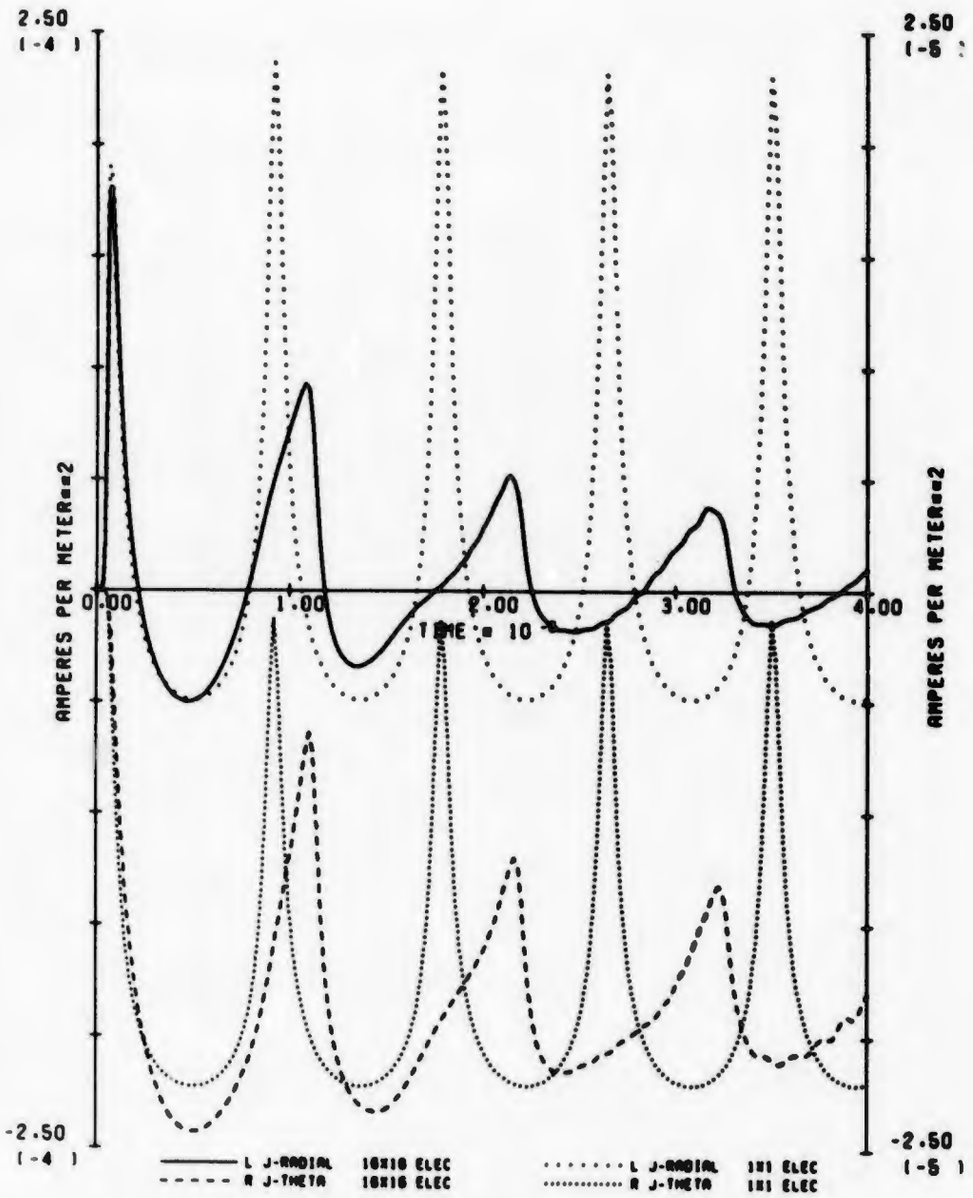

Fig. 74. Calculated Results for Parameter Set 74.

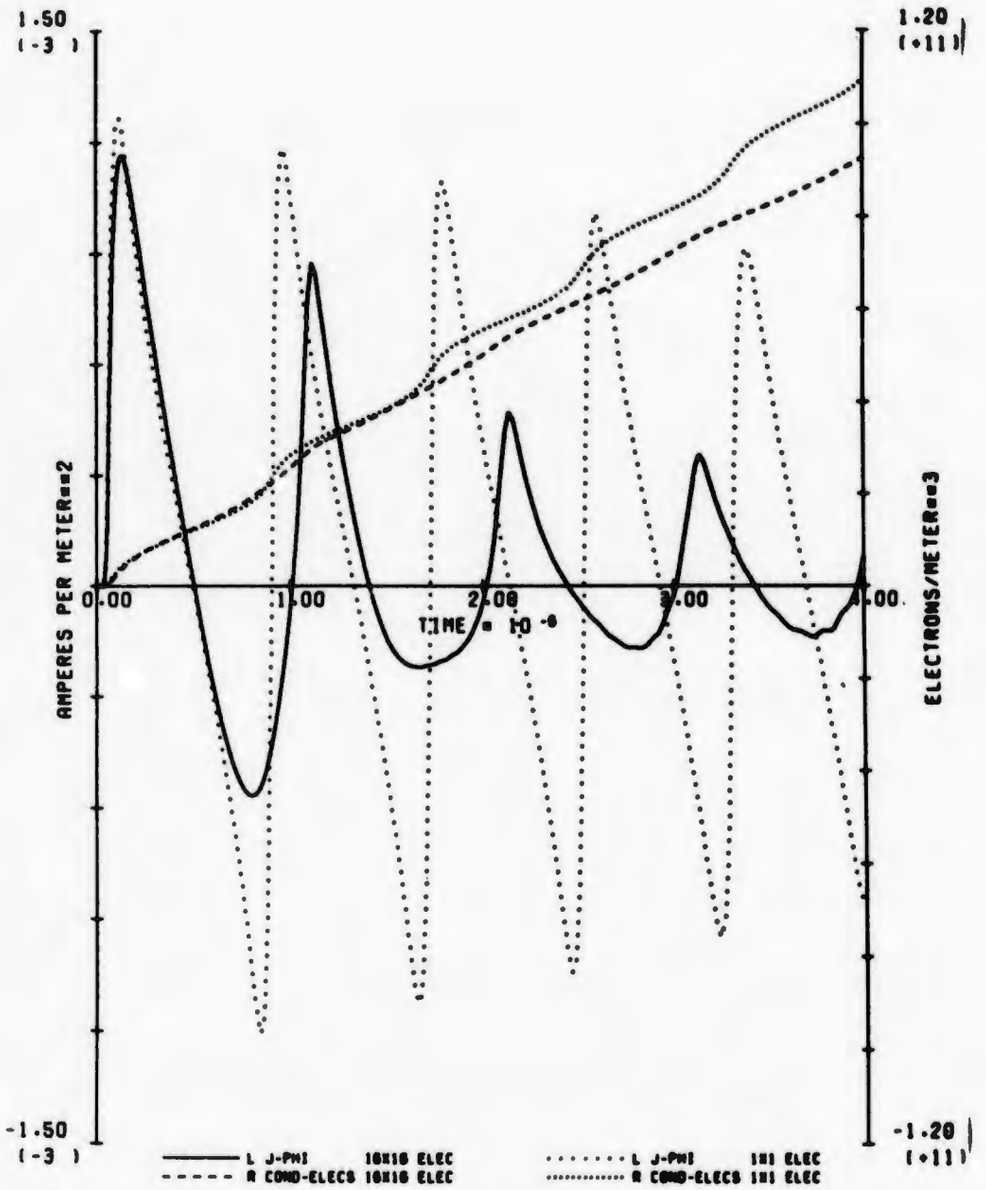

75. J-PHI AND ELEC DENS (60 KM. 0.6 MEV. 77.8 DEG)

Fig. 75. Calculated Results for Parameter Set 75.

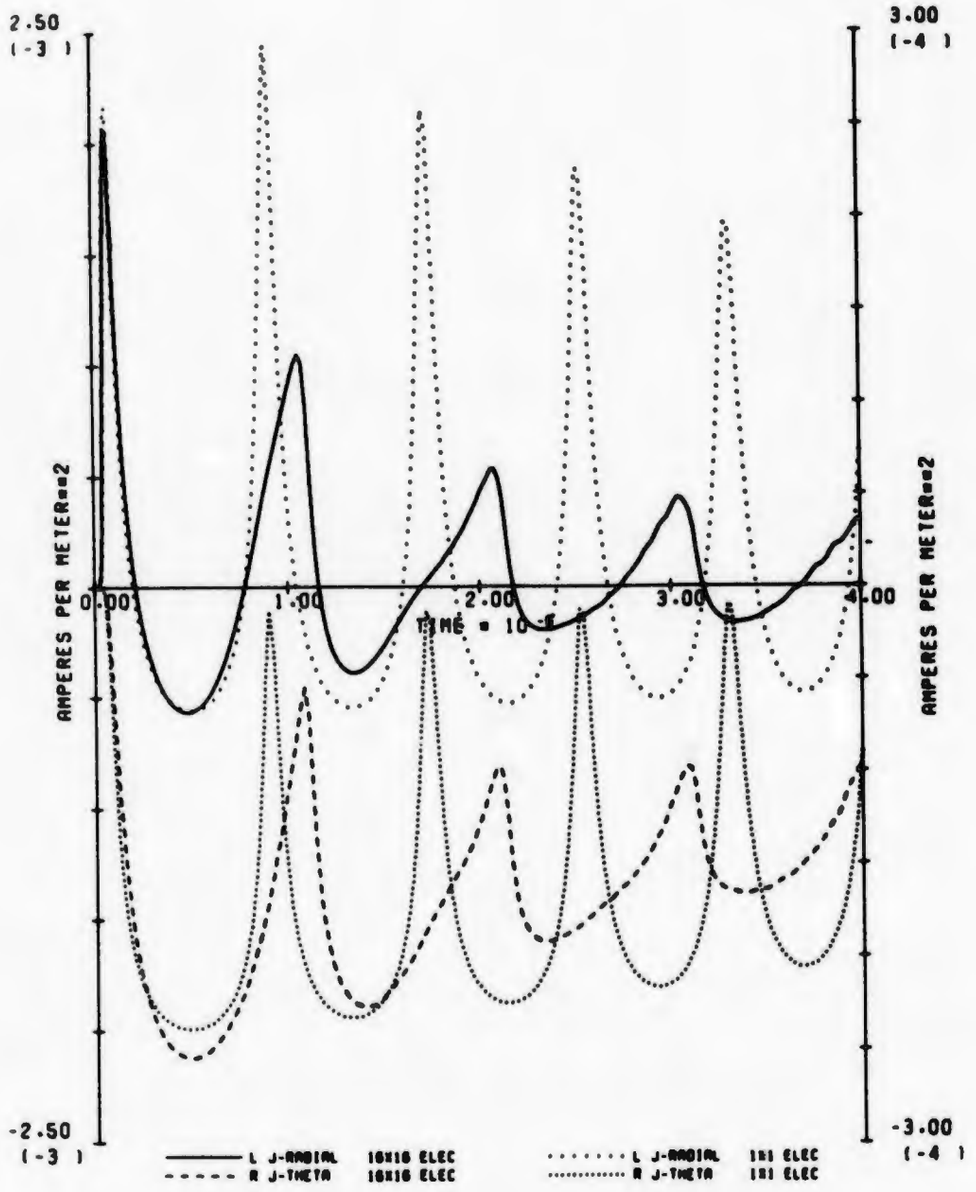

Fig. 76. Calculated Results for Parameter Set 76.

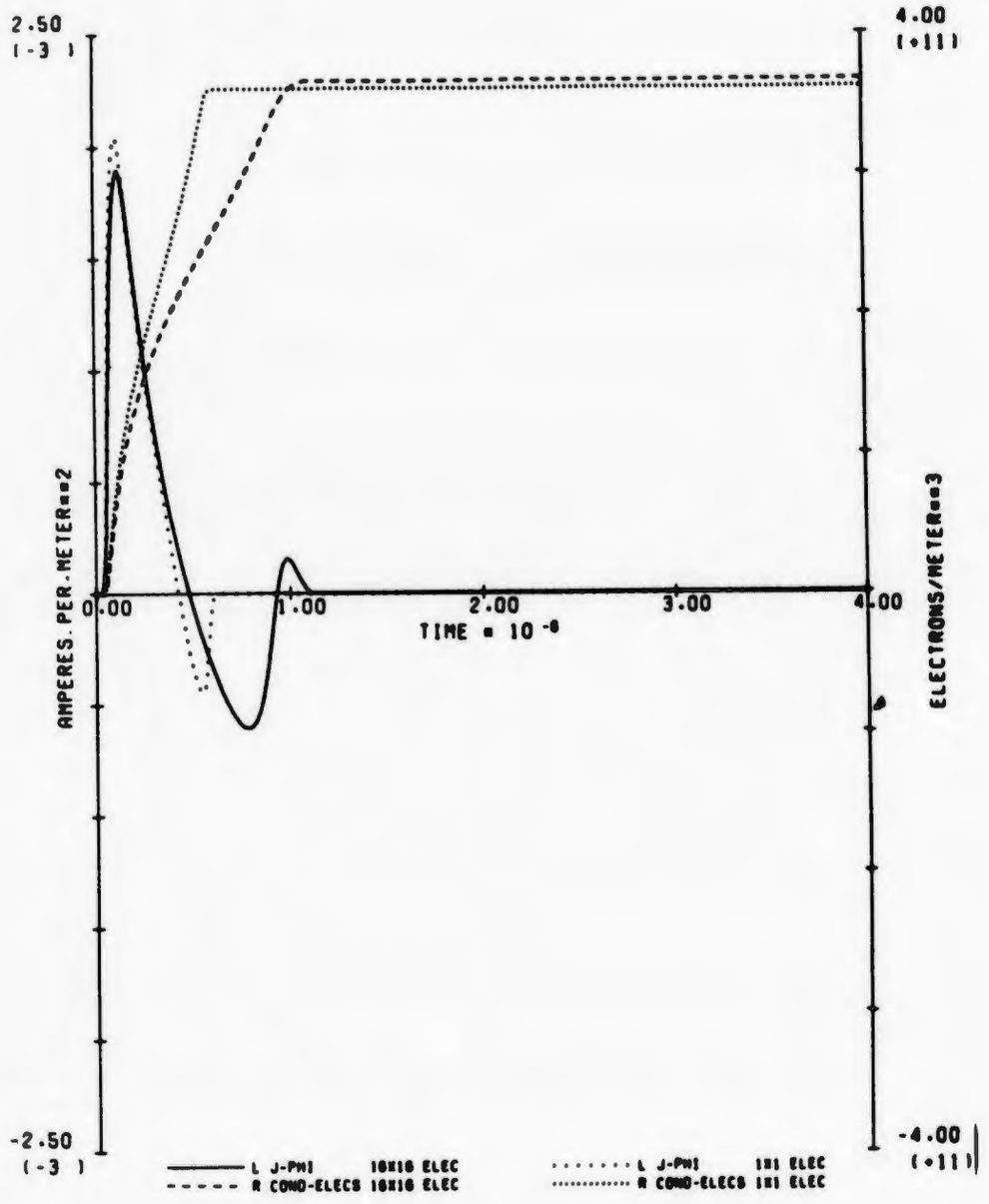

Fig. 77. Calculated Results for Parameter Set 77.

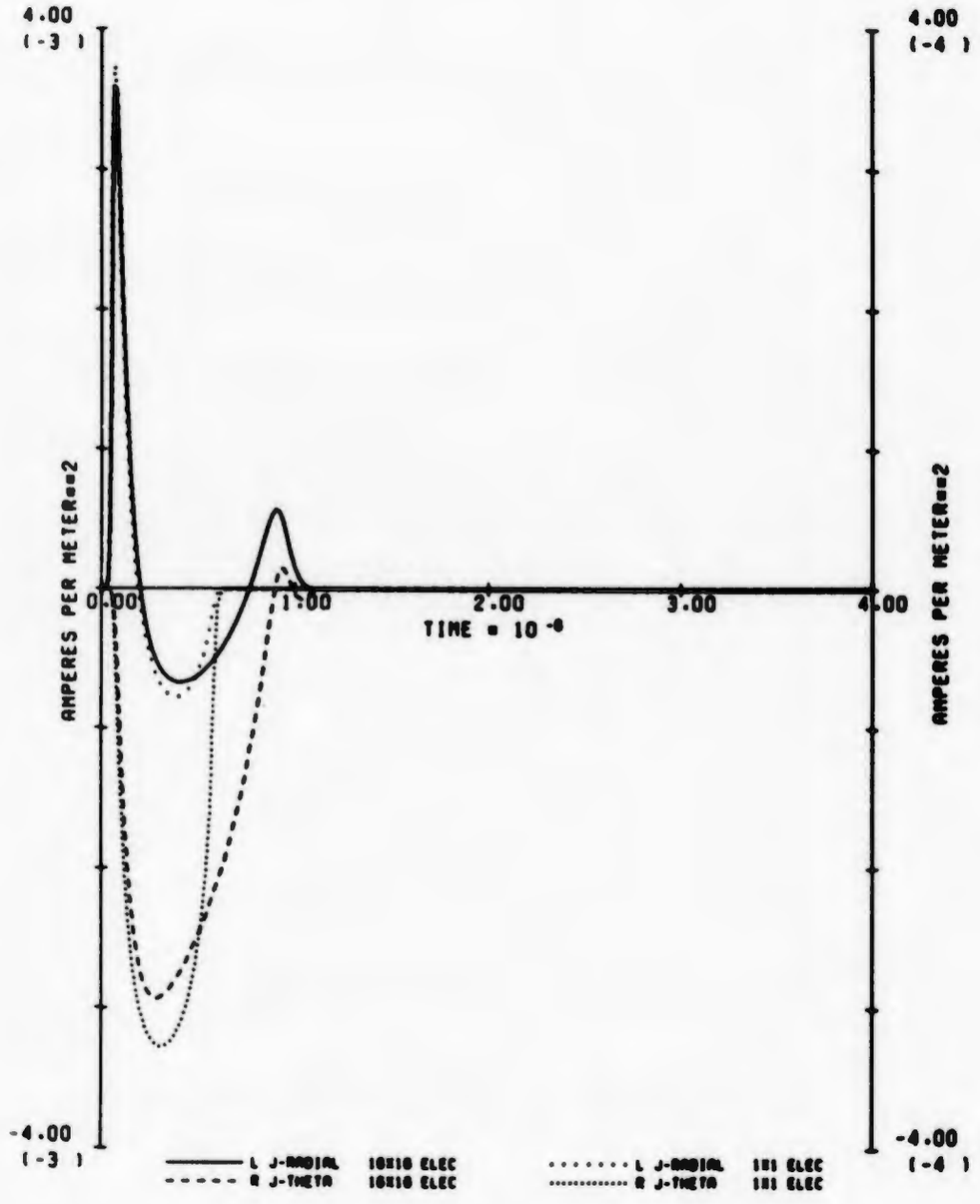

Fig. 78. Calculated Results for Parameter Set 78.

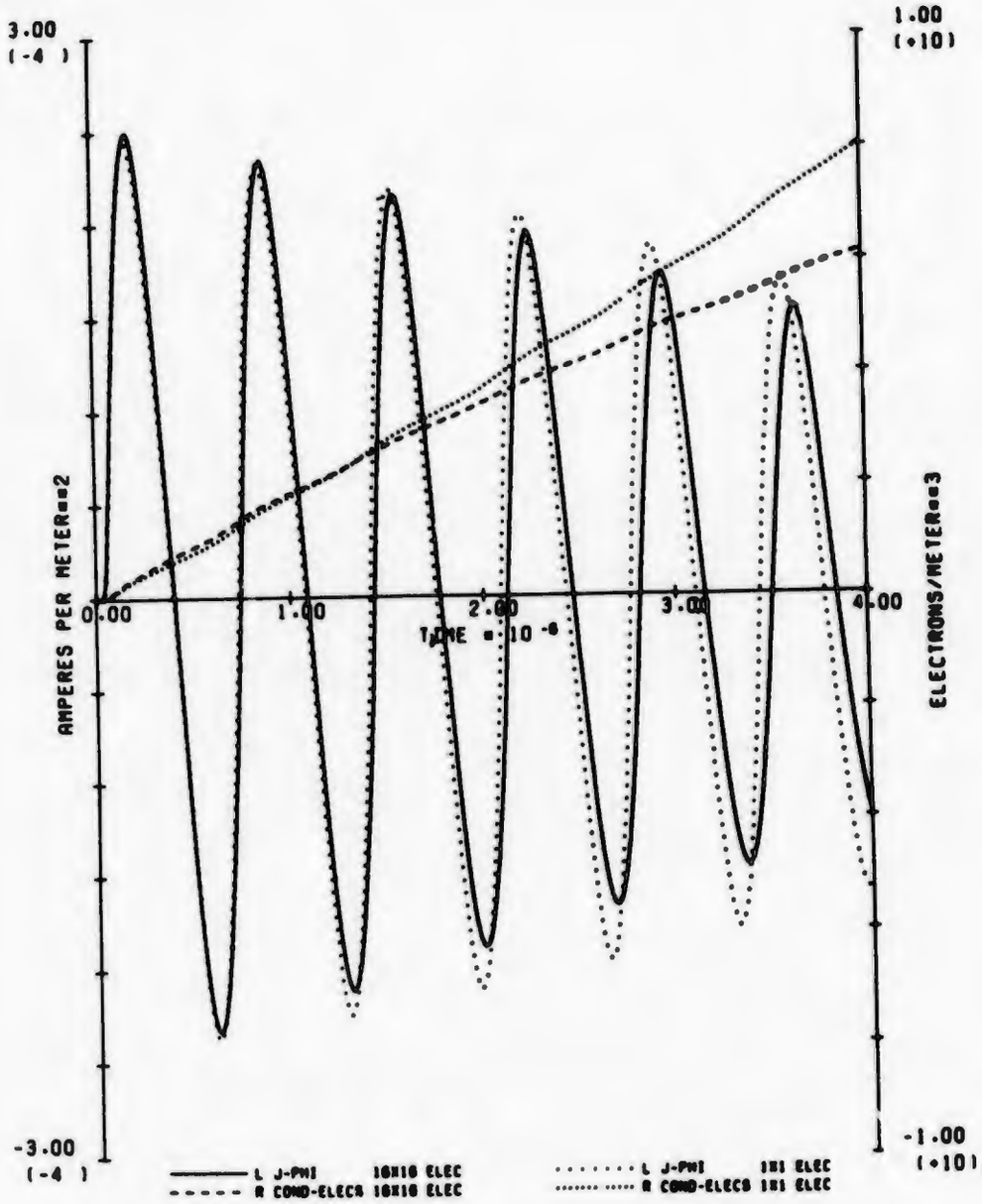

79. J-PHI AND ELEC DENS (80 KM, 0.1 MEV, 77.8 DEG)

Fig. 79. Calculated Results for Parameter Set 79.

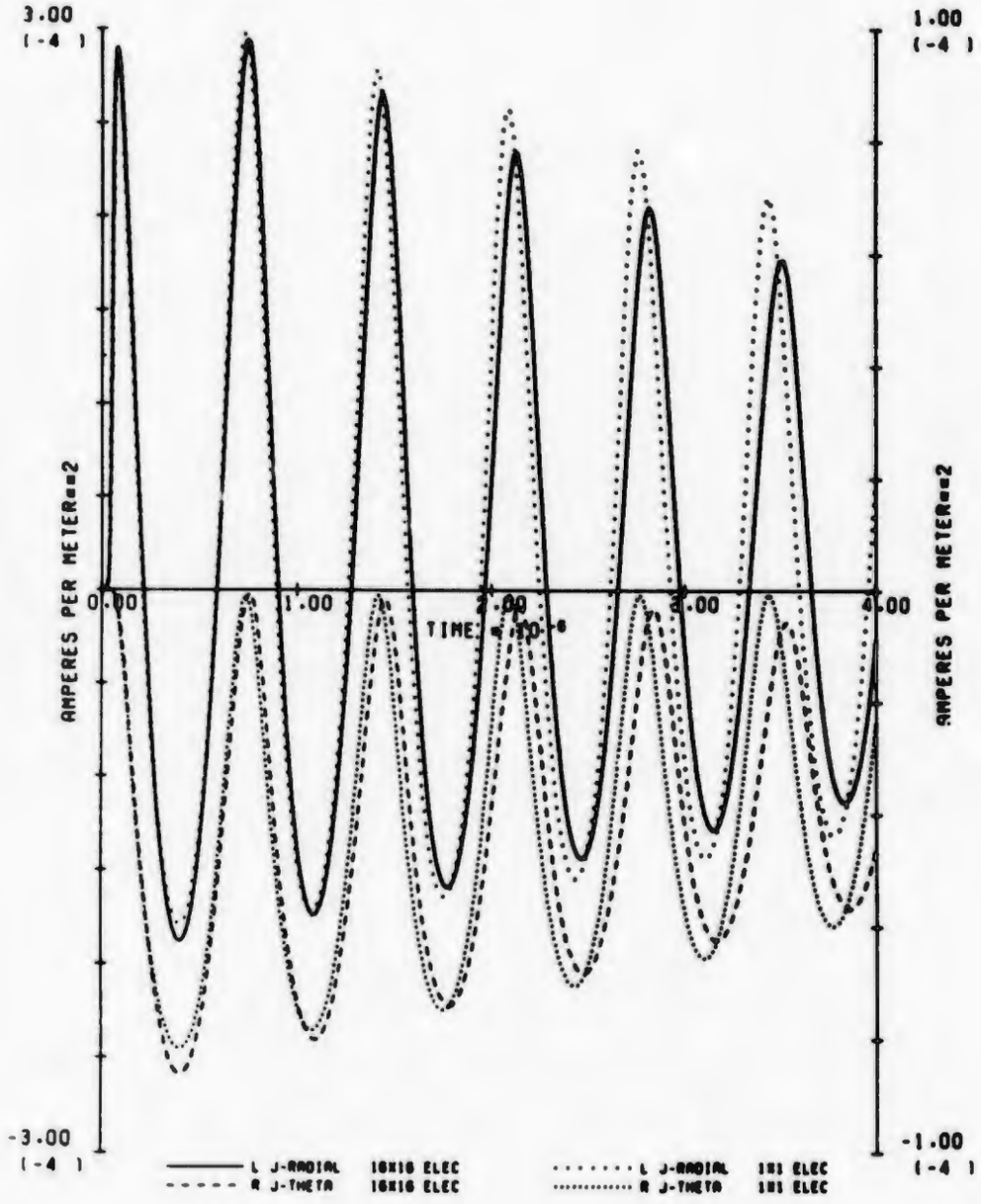

Fig. 80. Calculated Results for Parameter Set 80.

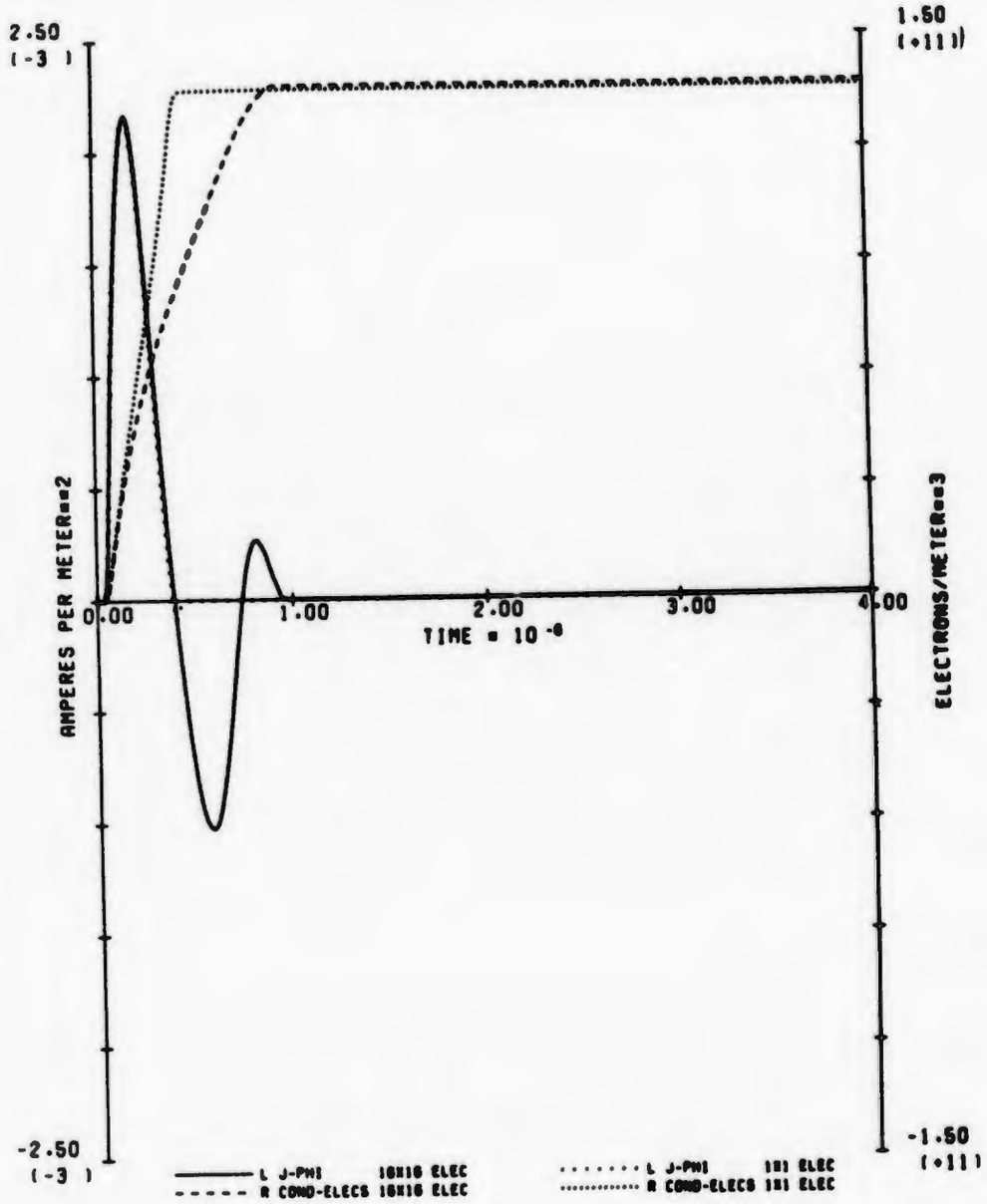

Fig. 81. Calculated Results for Parameter Set 81.

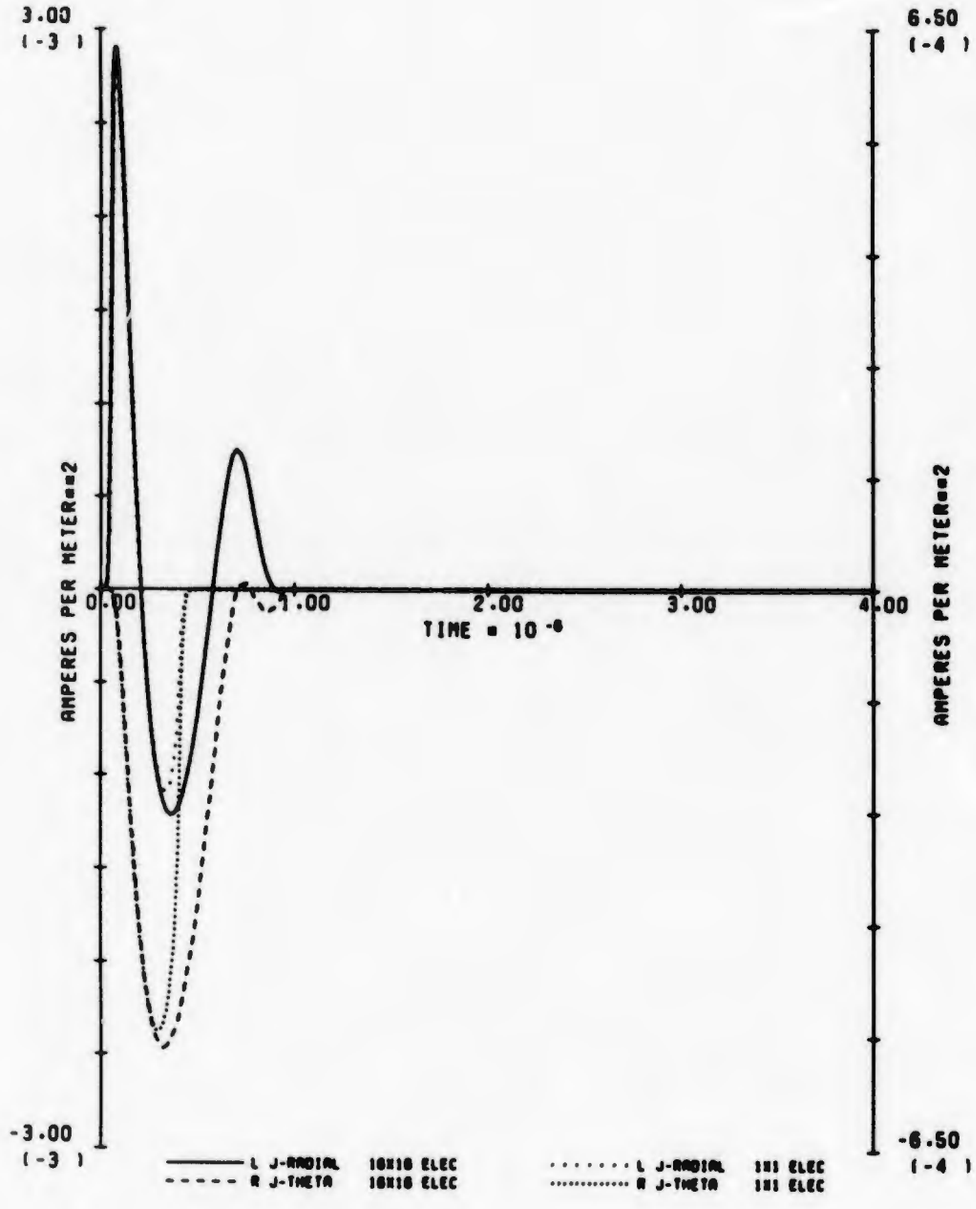

Fig. 82. Calculated Results for Parameter Set 82.

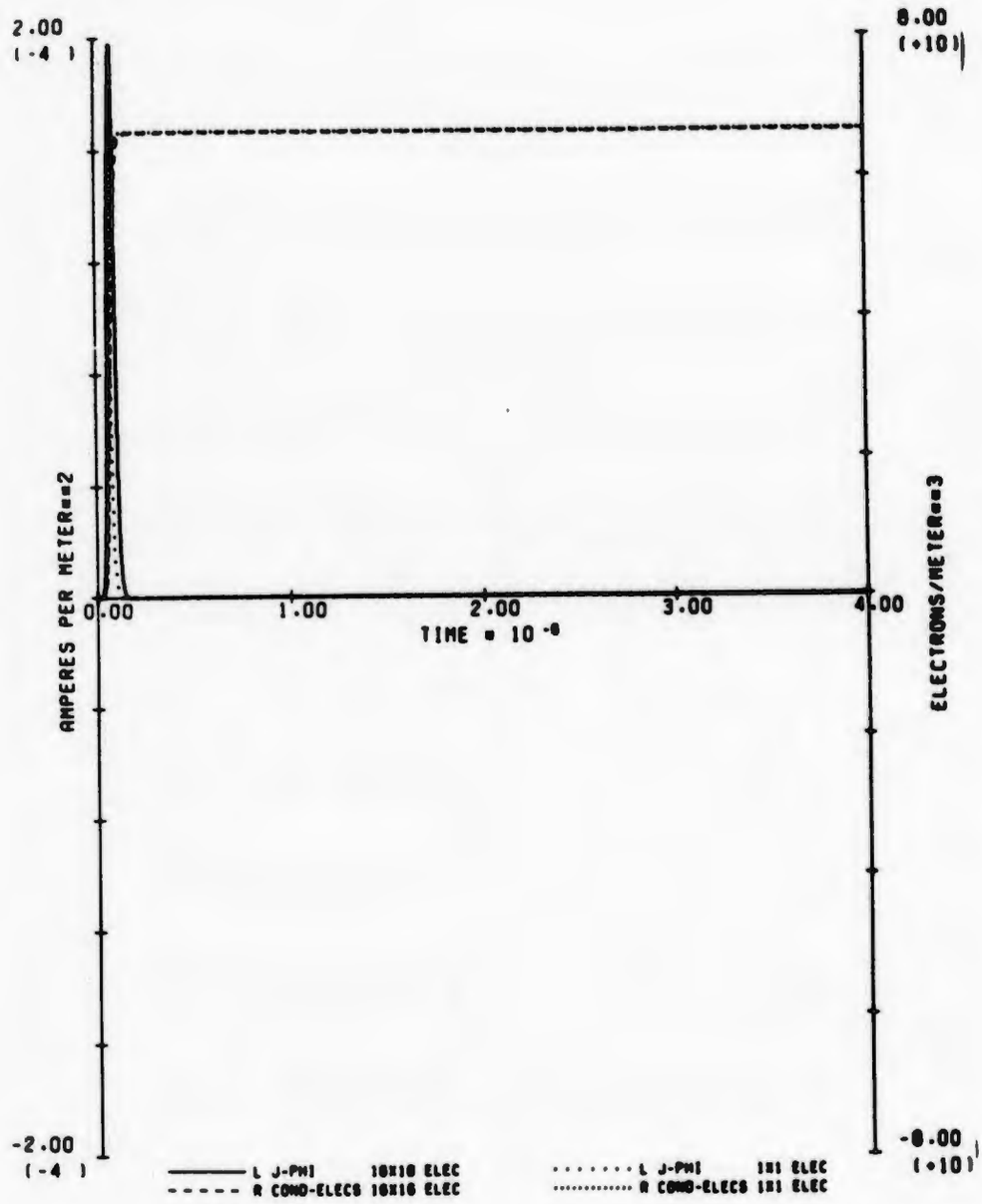

Fig. 83. Calculated Results for Parameter Set 83.

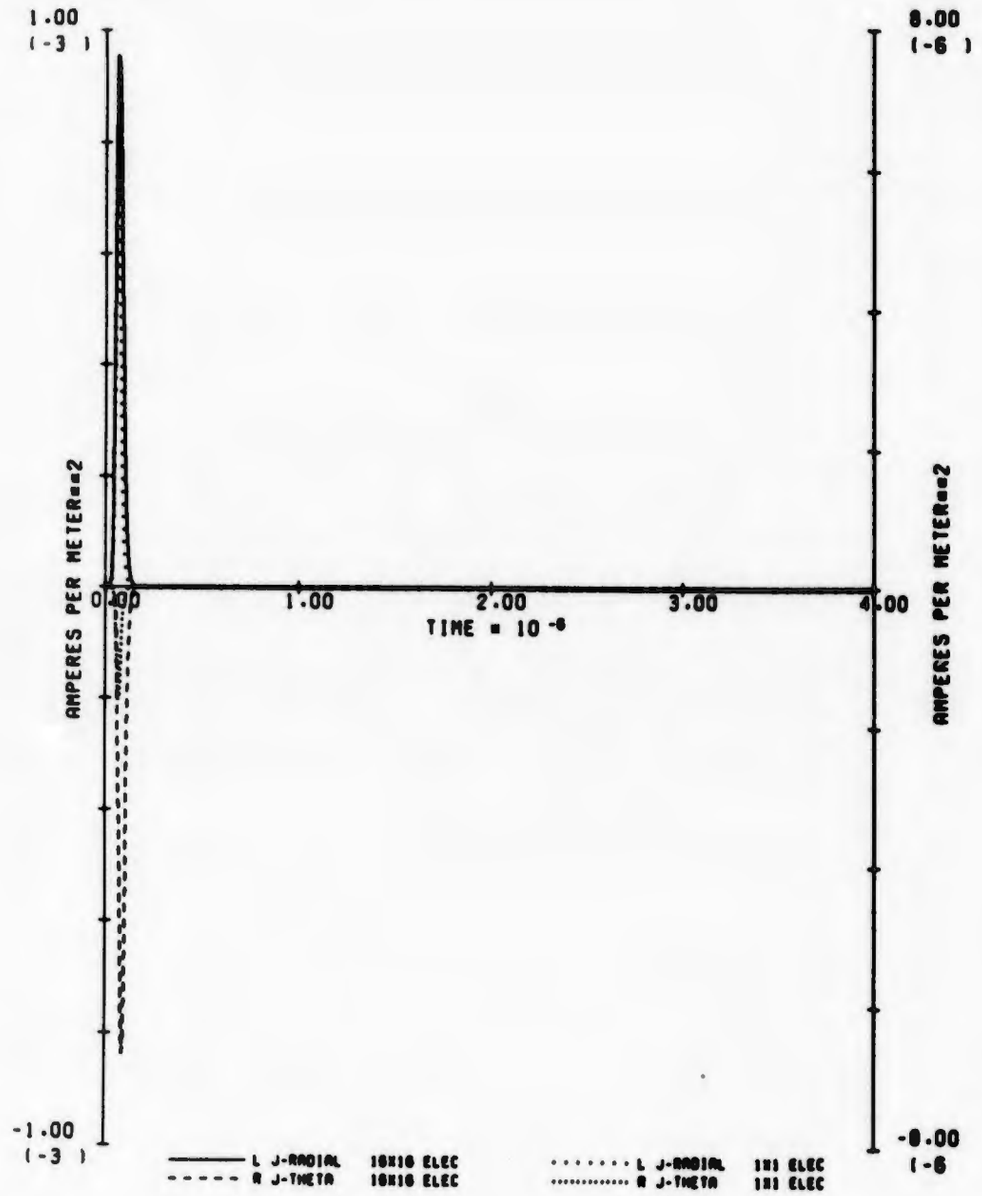

Fig. 84. Calculated Results for Parameter Set 84.

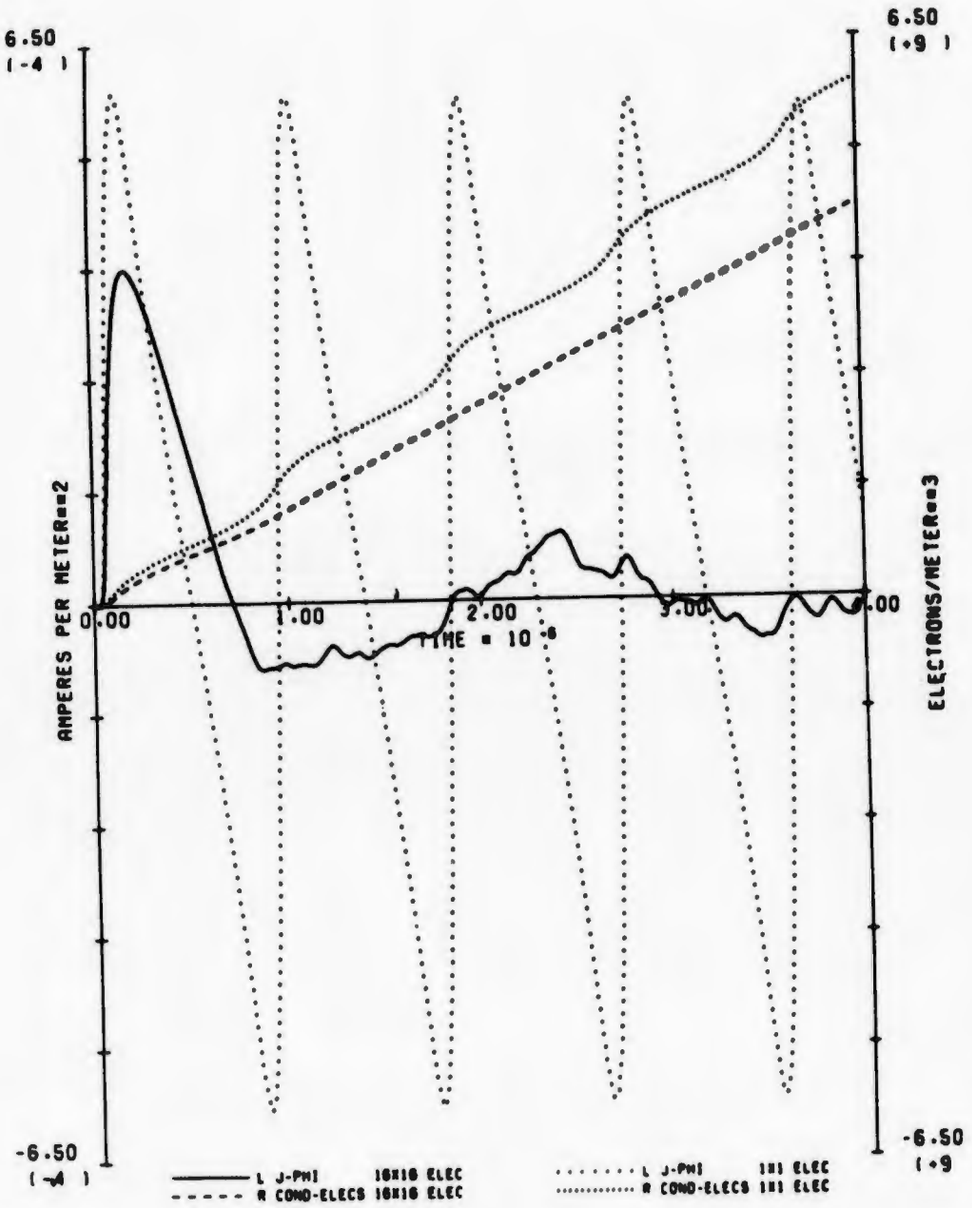

85. J-PHI AND ELEC DENS (80 KM. 1.5 MEV. 19.3 DEG)

Fig. 85. Calculated Results for Parameter Set 85.

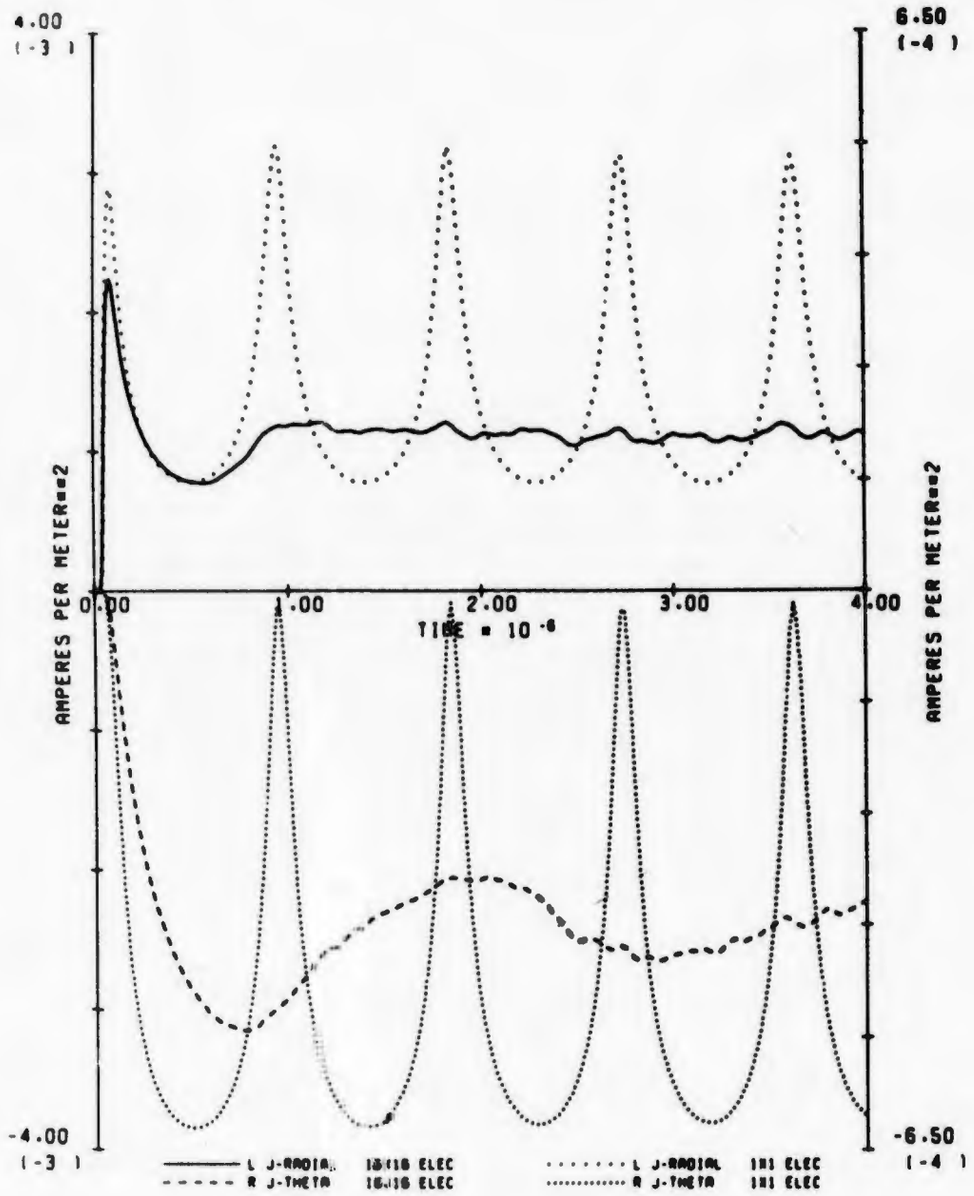

Fig. 86. Calculated Results for Parameter Set 86.

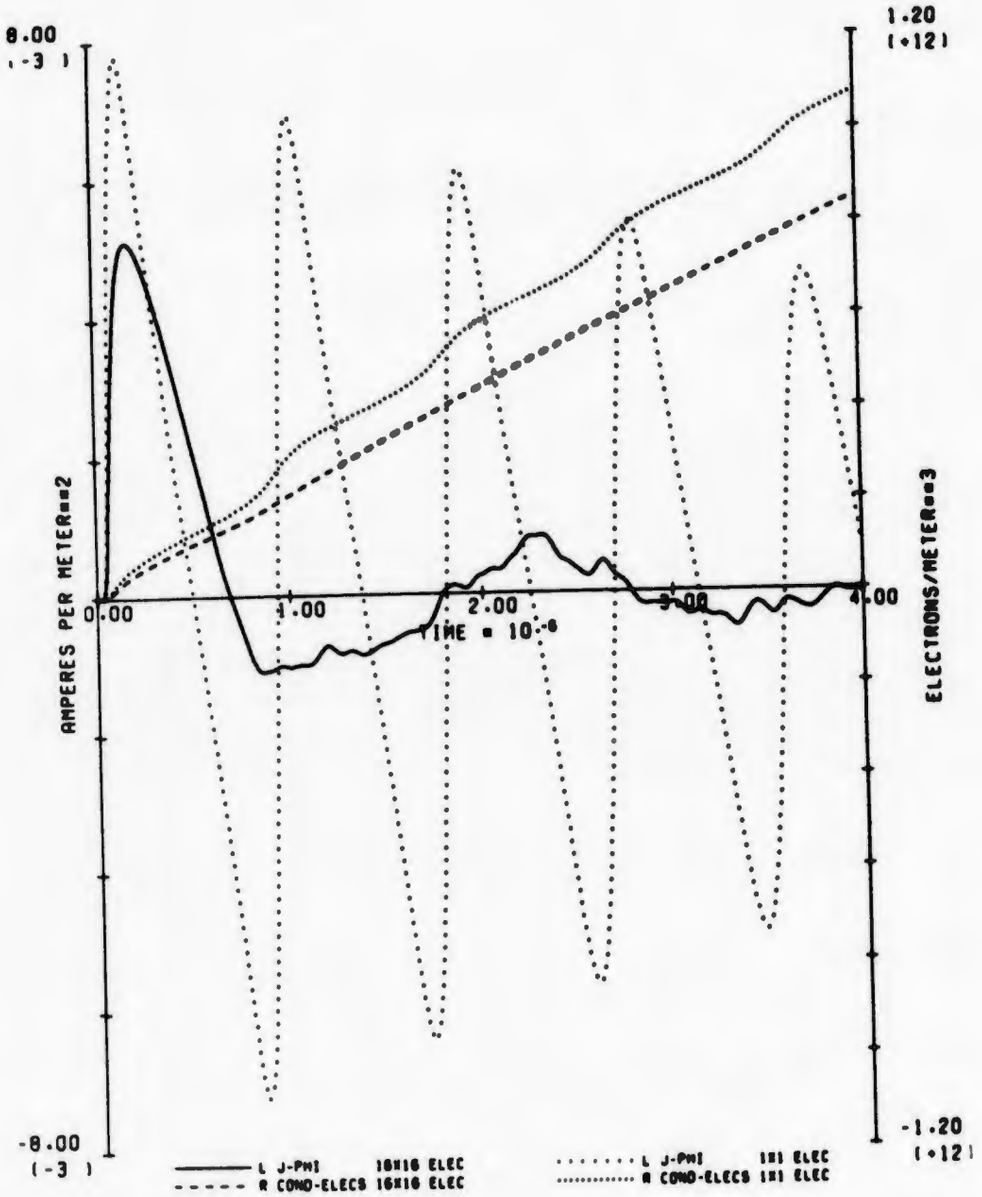

Fig. 87. Calculated Results for Parameter Set 87.

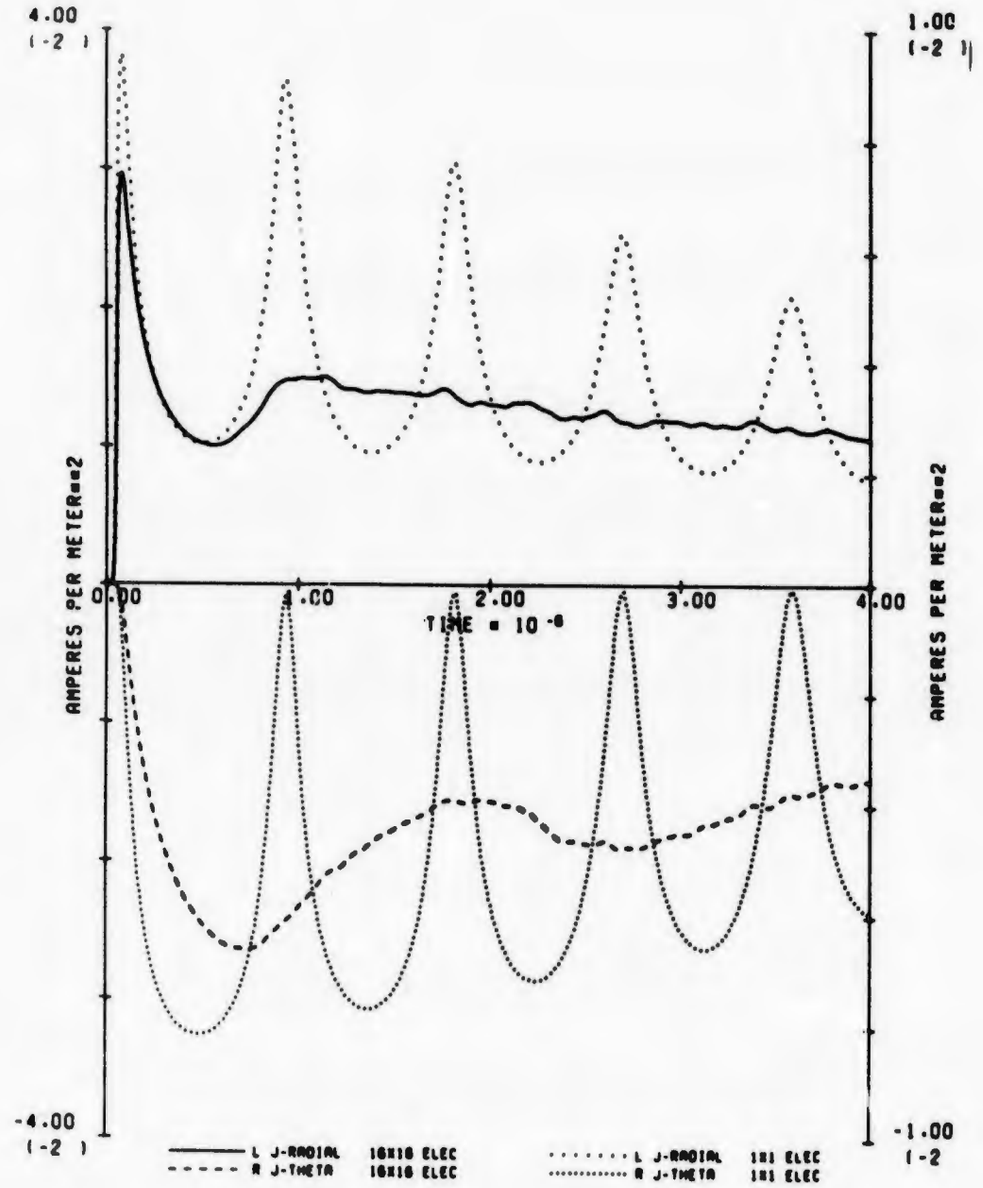

Fig. 88. Calculated Results for Parameter Set 88.

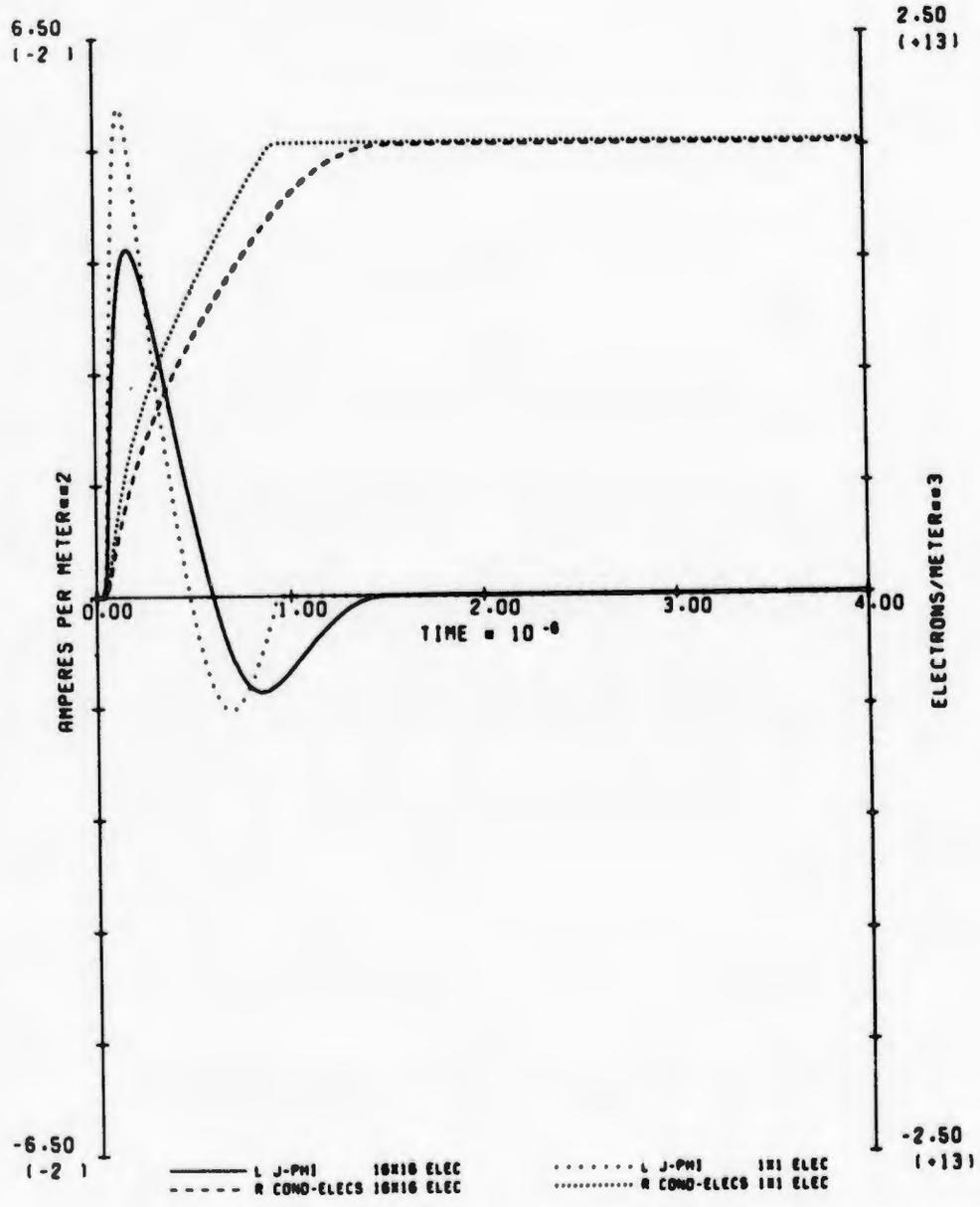

Fig. 89. Calculated Results for Parameter Set 89.

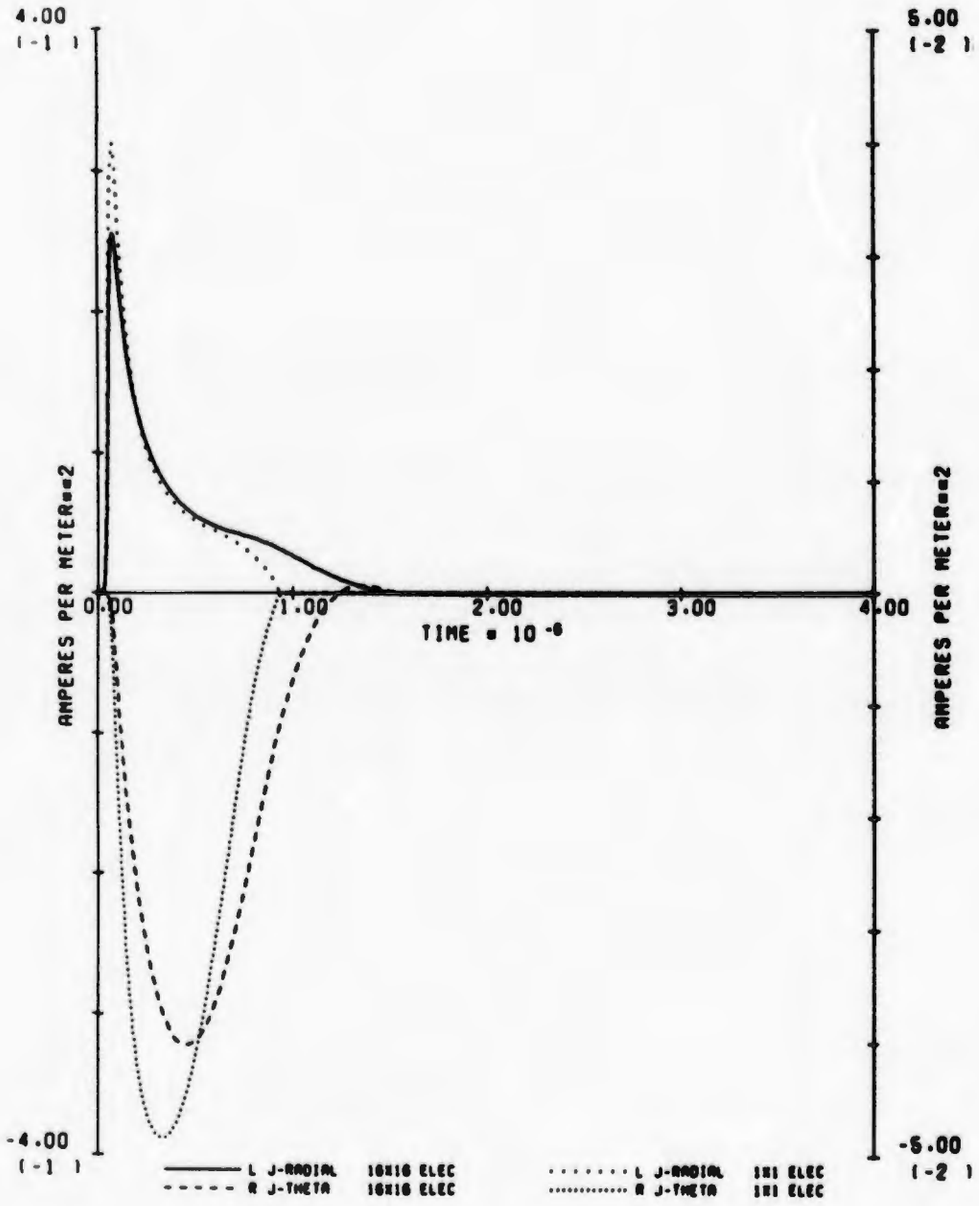

Fig. 90. Calculated Results for Parameter Set 90.

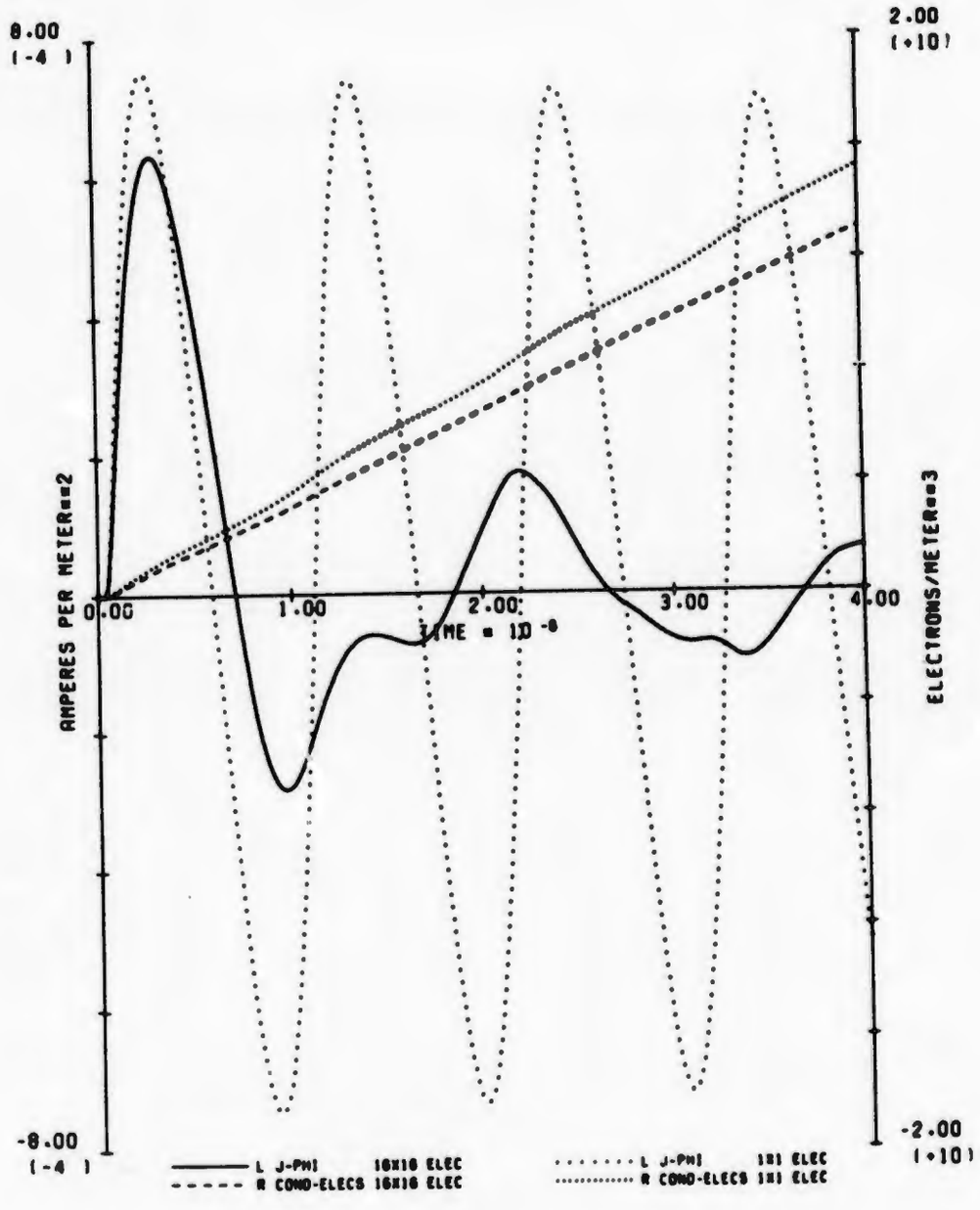

Fig. 91. Calculated Results for Parameter Set 91.

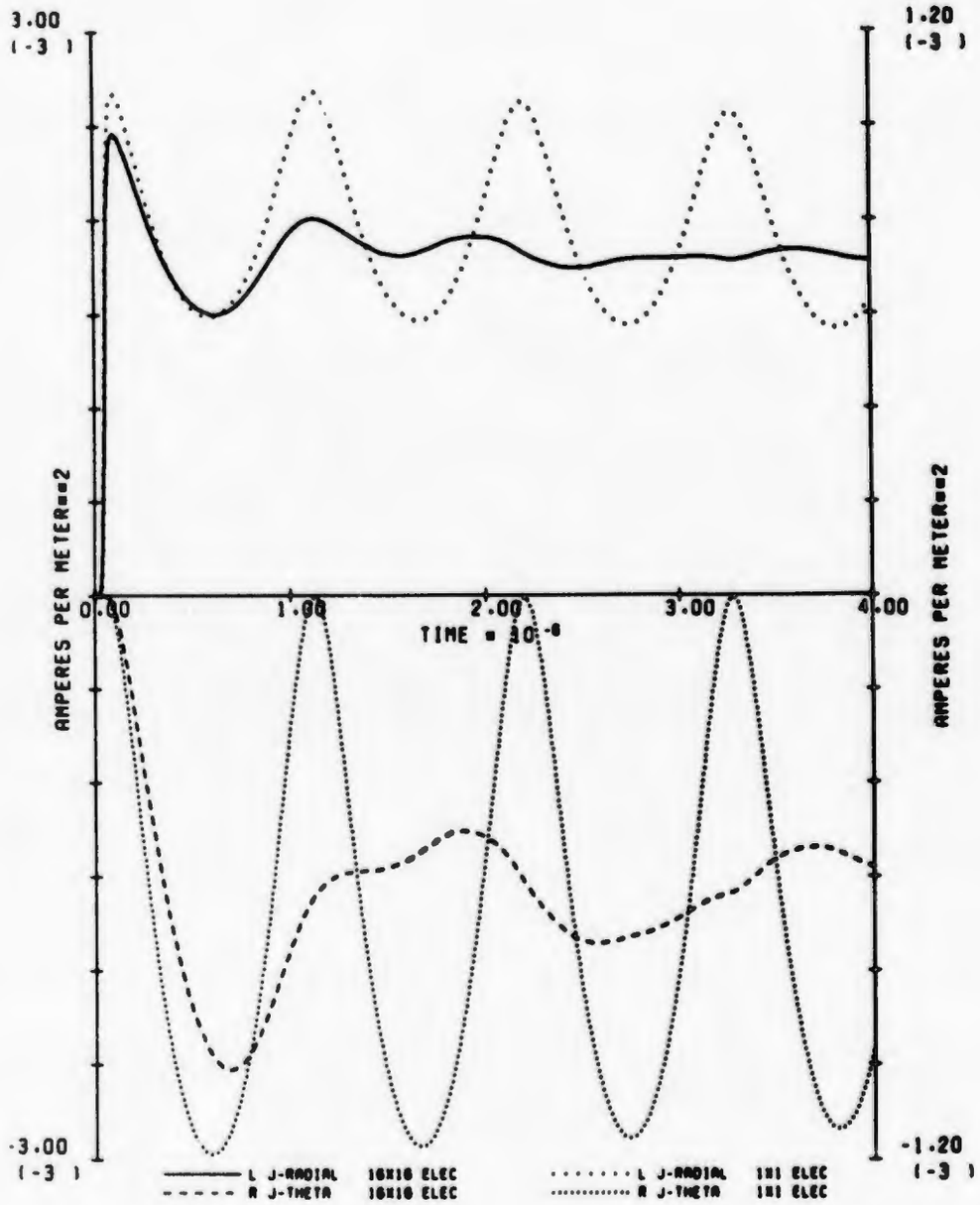

Fig. 92. Calculated Results for Parameter Set 92.

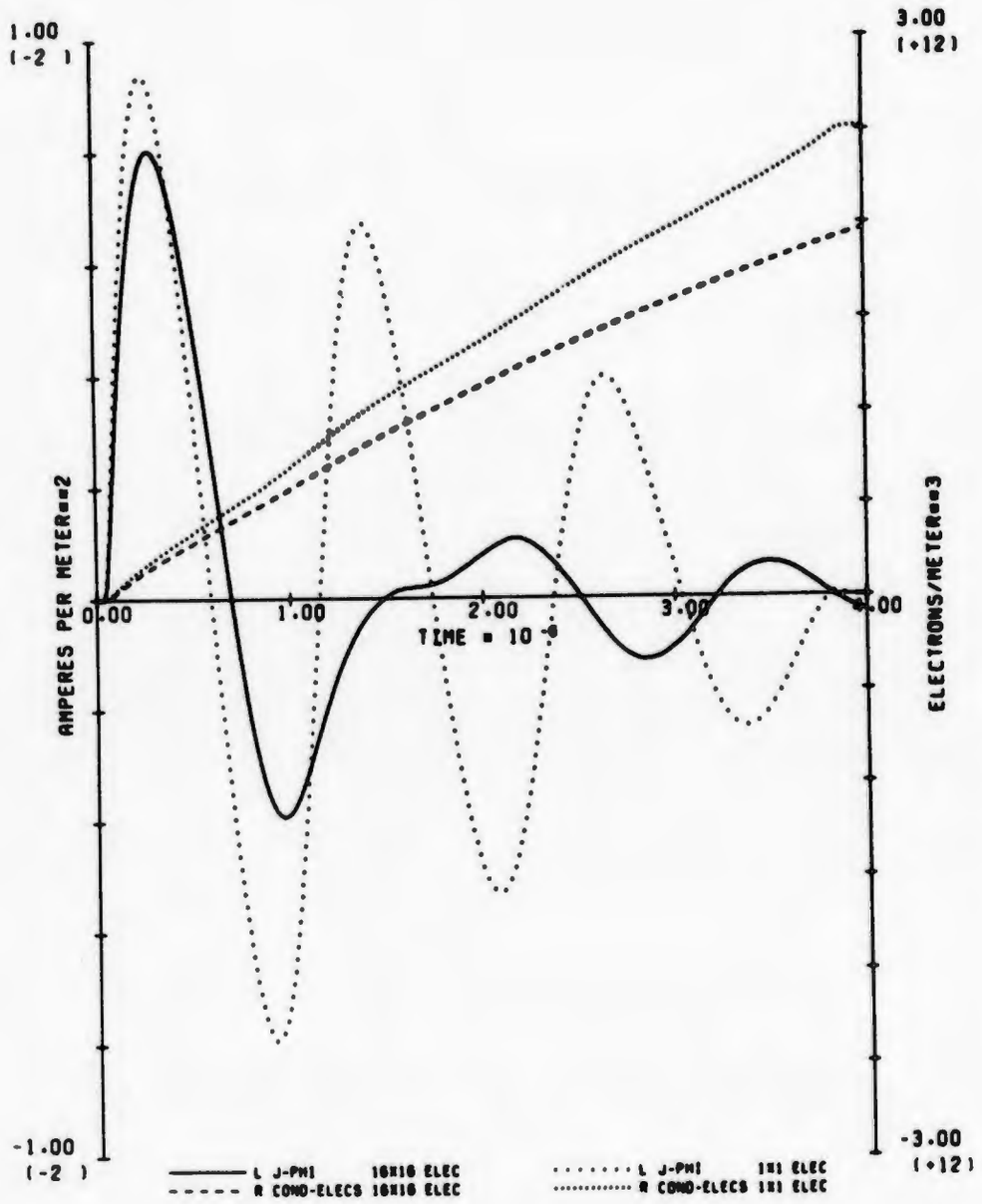

Fig. 93. Calculated Results for Parameter Set 93.

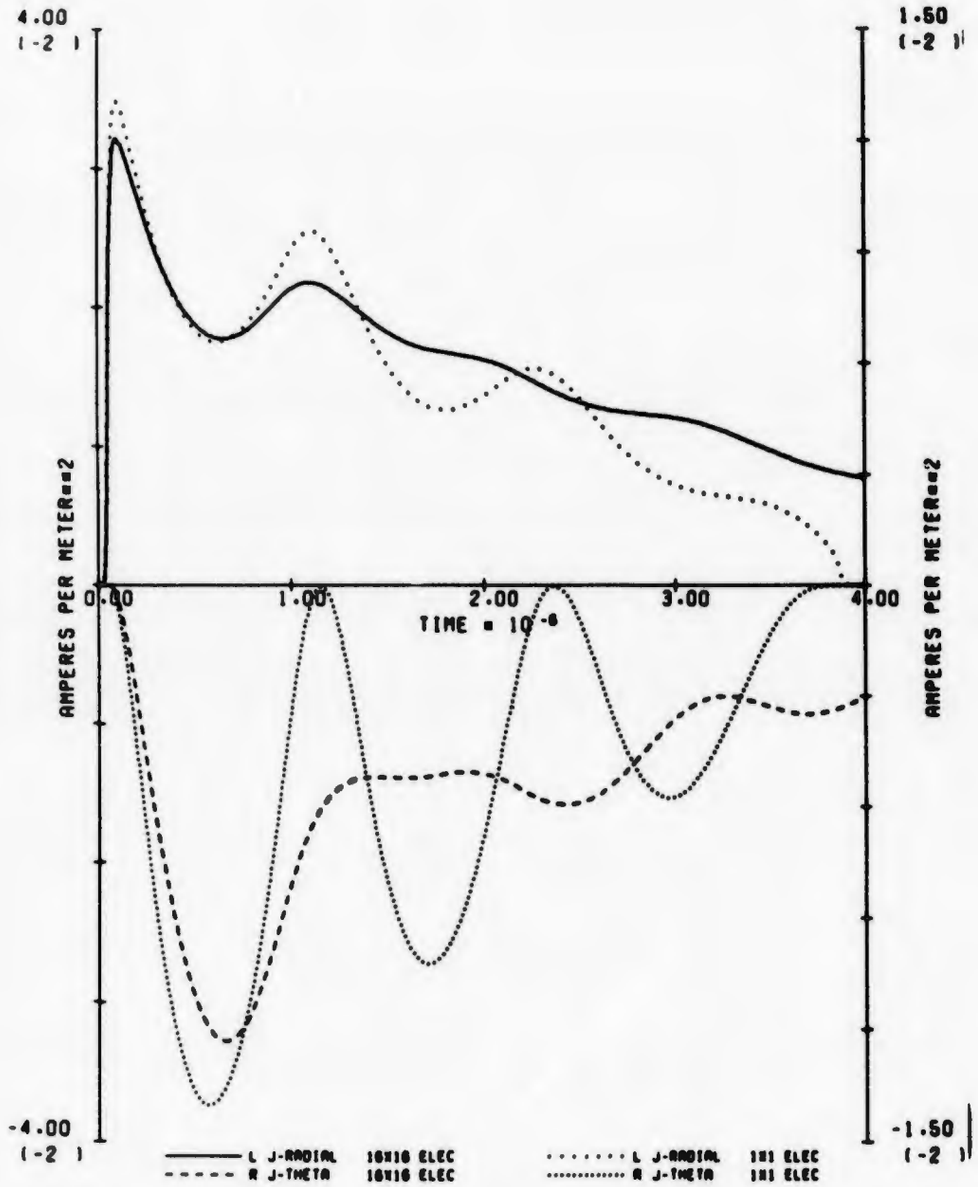

Fig. 94. Calculated Results for Parameter Set 94.

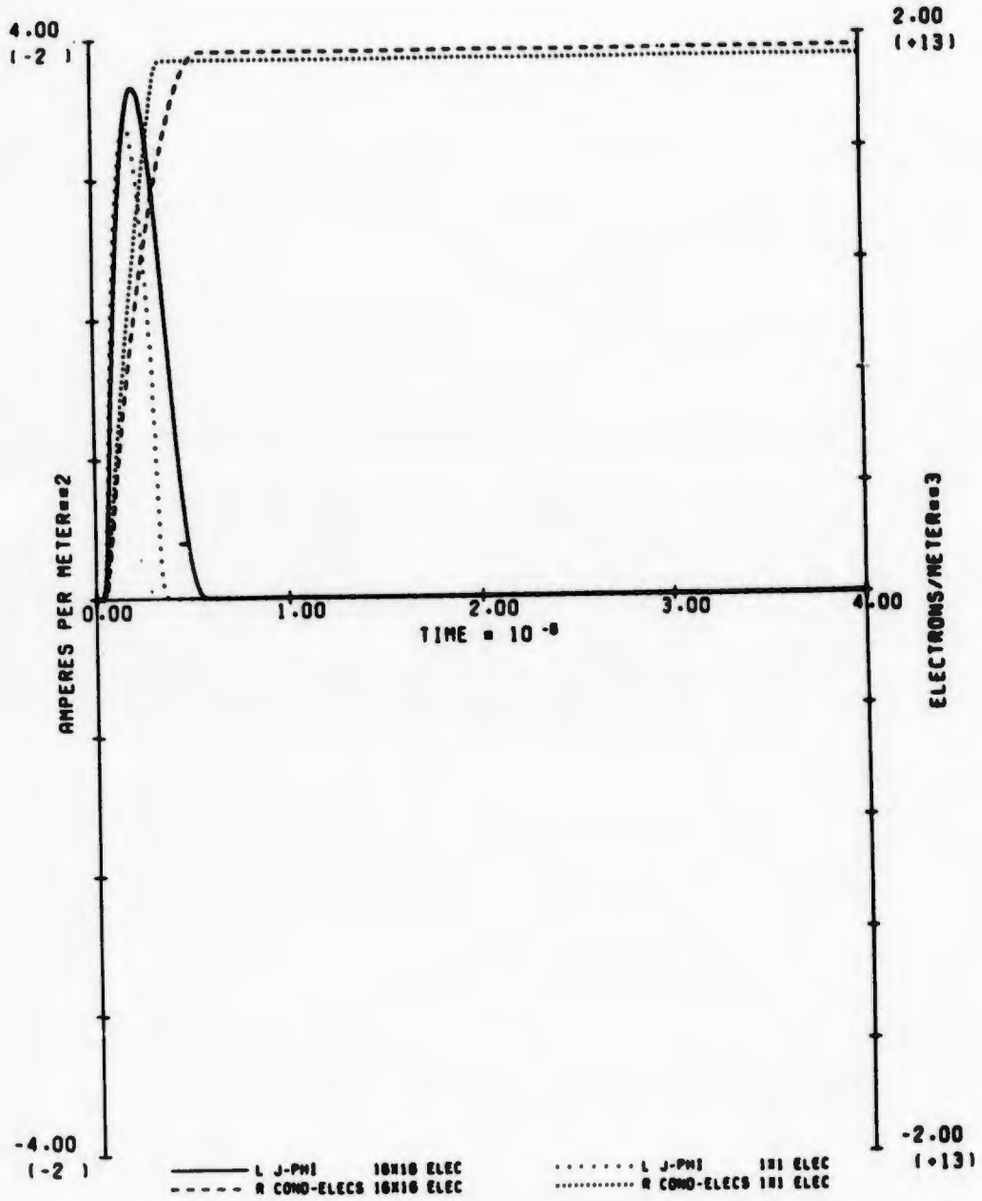

Fig. 95. Calculated Results for Parameter Set 95.

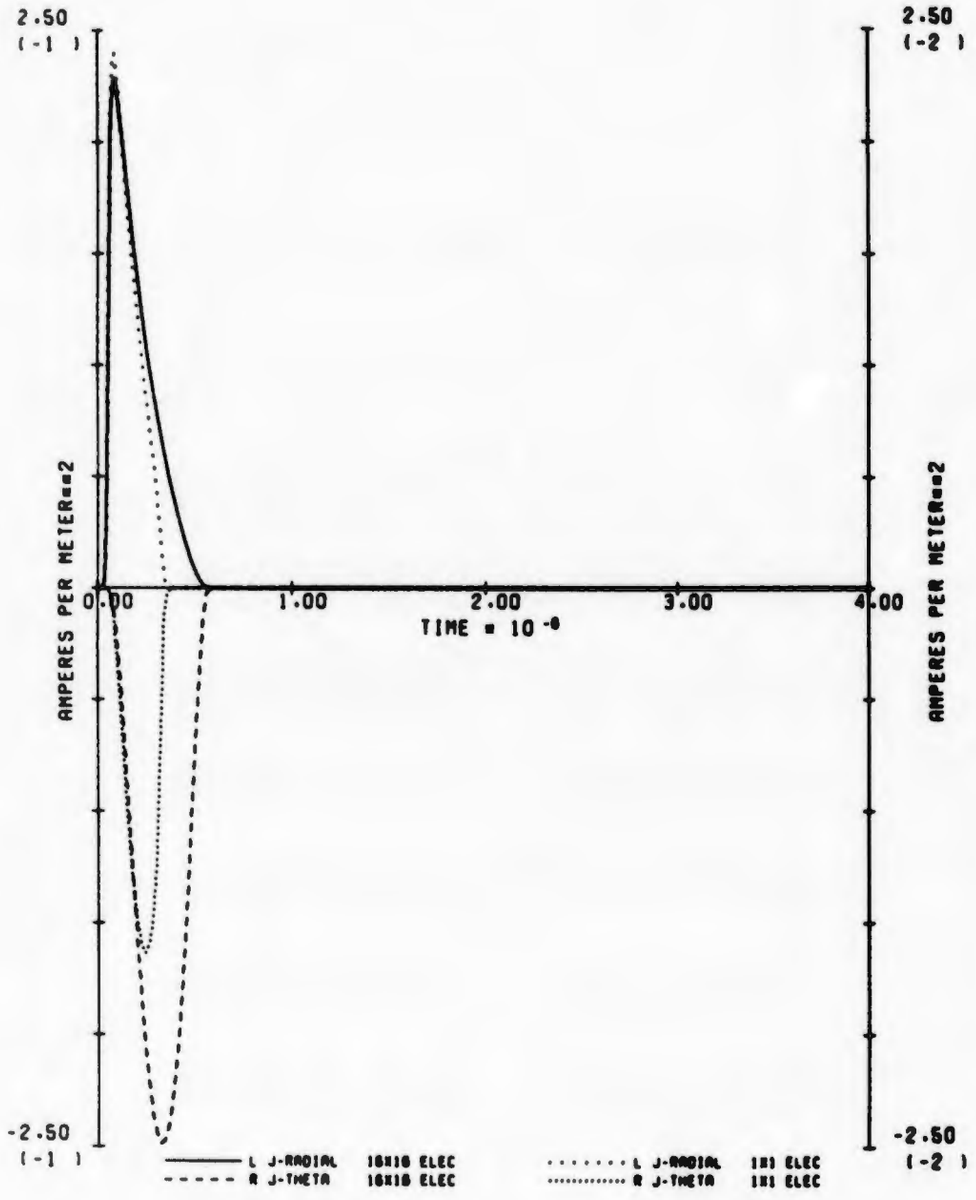

Fig. 96. Calculated Results for Parameter Set 96.

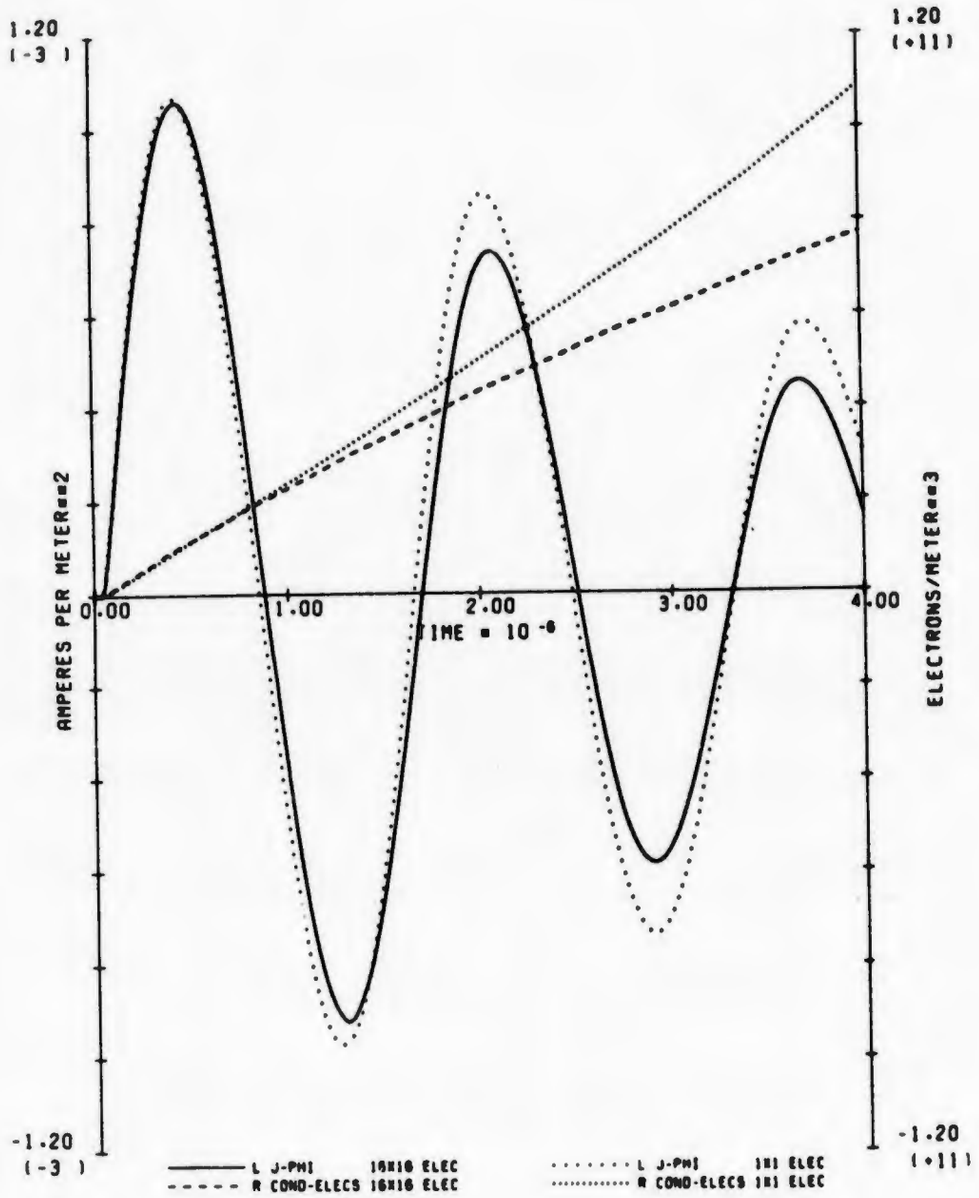

Fig. 97. Calculated Results for Parameter Set 97.

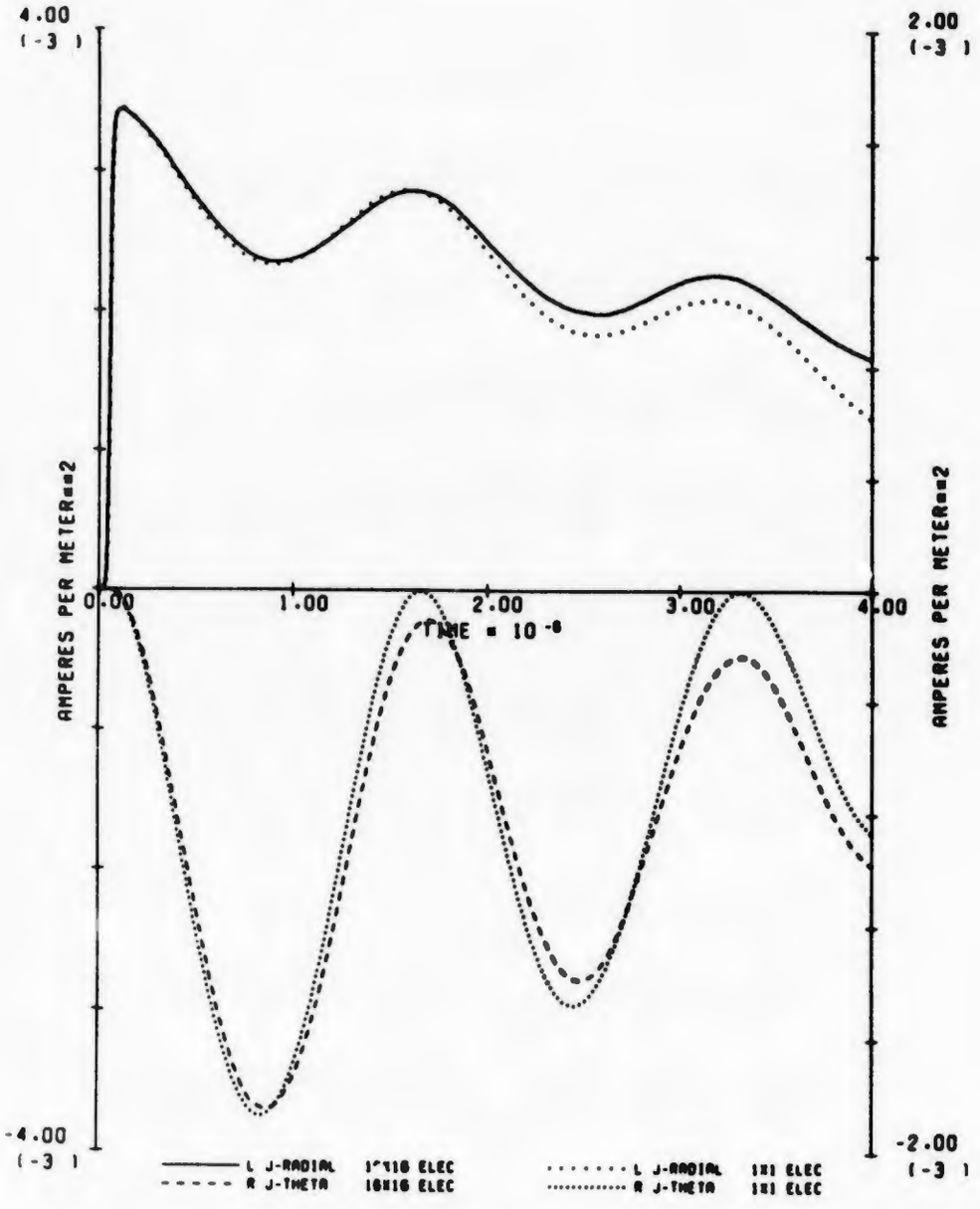

Fig. 98. Calculated Results for Parameter Set 98.

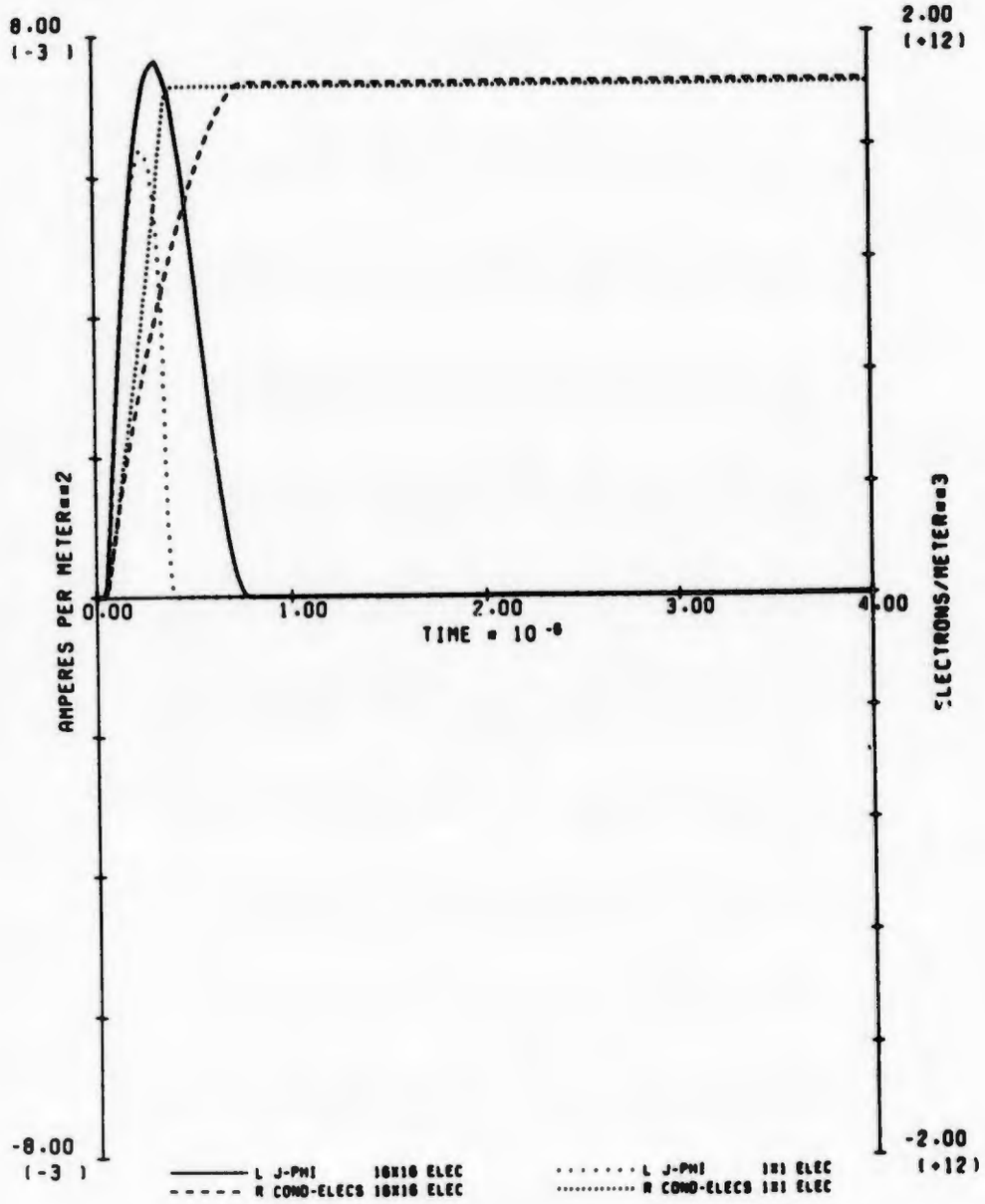

Fig. 99. Calculated Results for Parameter Set 99.

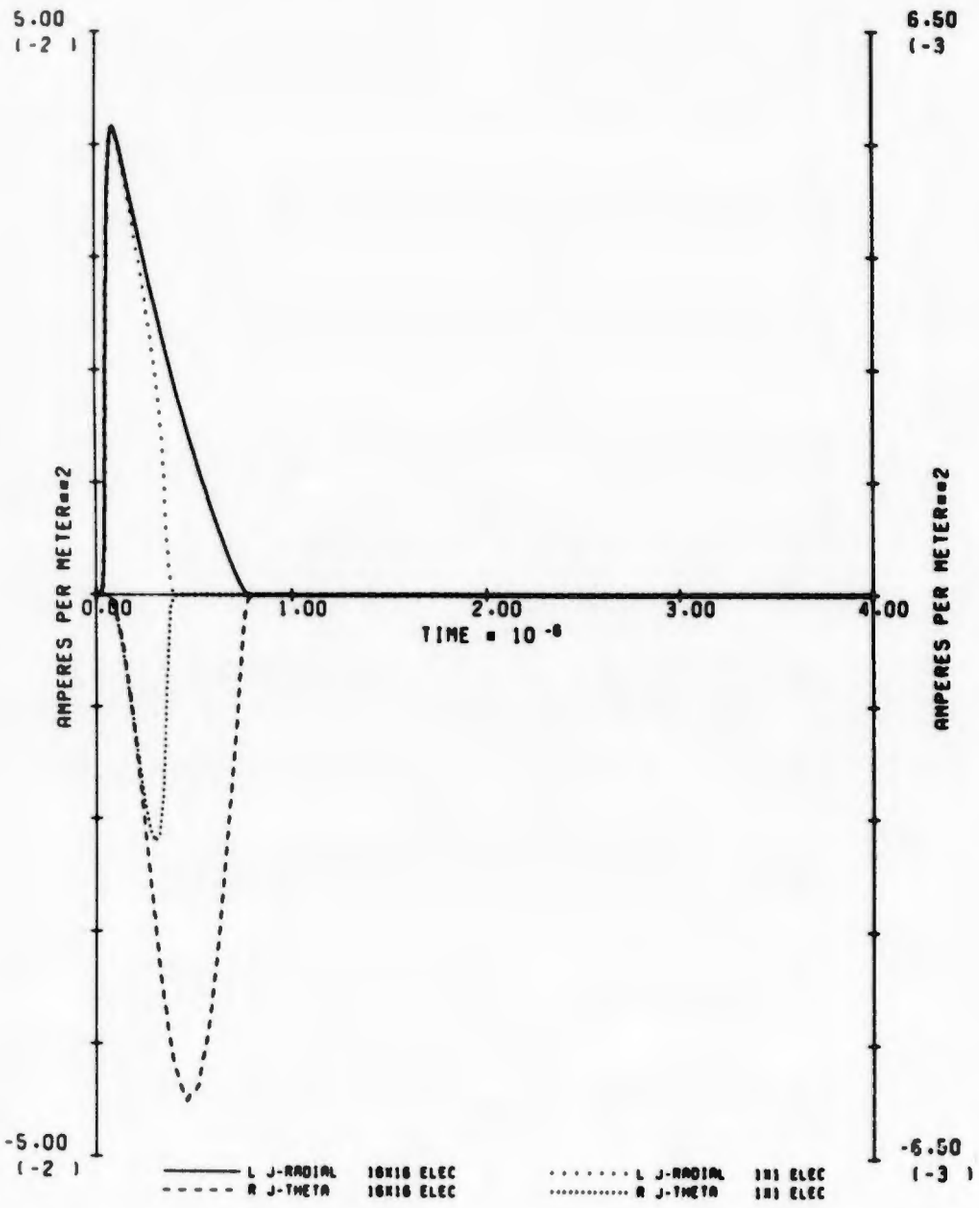

Fig. 100. Calculated Results for Parameter Set 100.

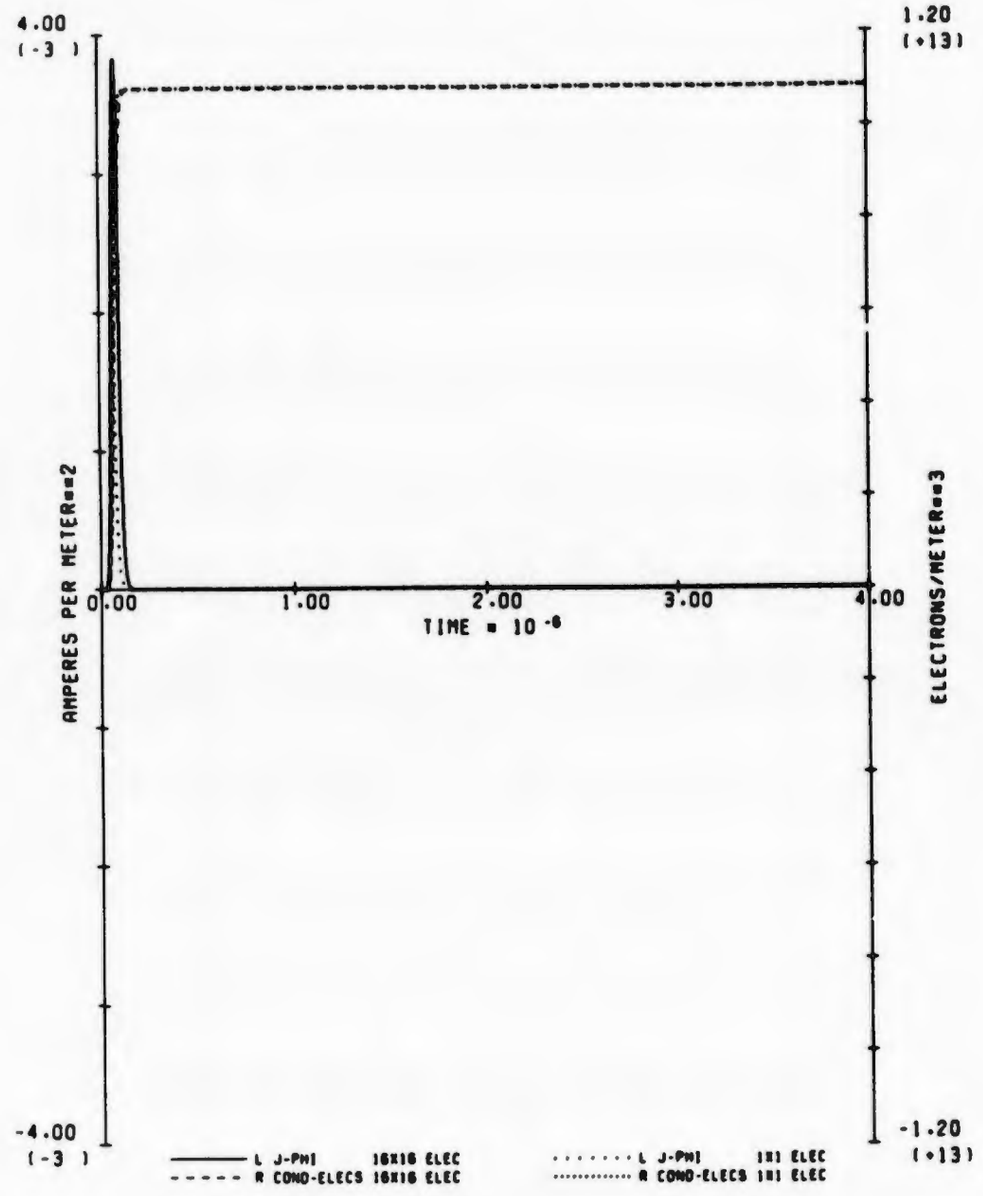

Fig. 101. Calculated Results for Parameter Set 101.

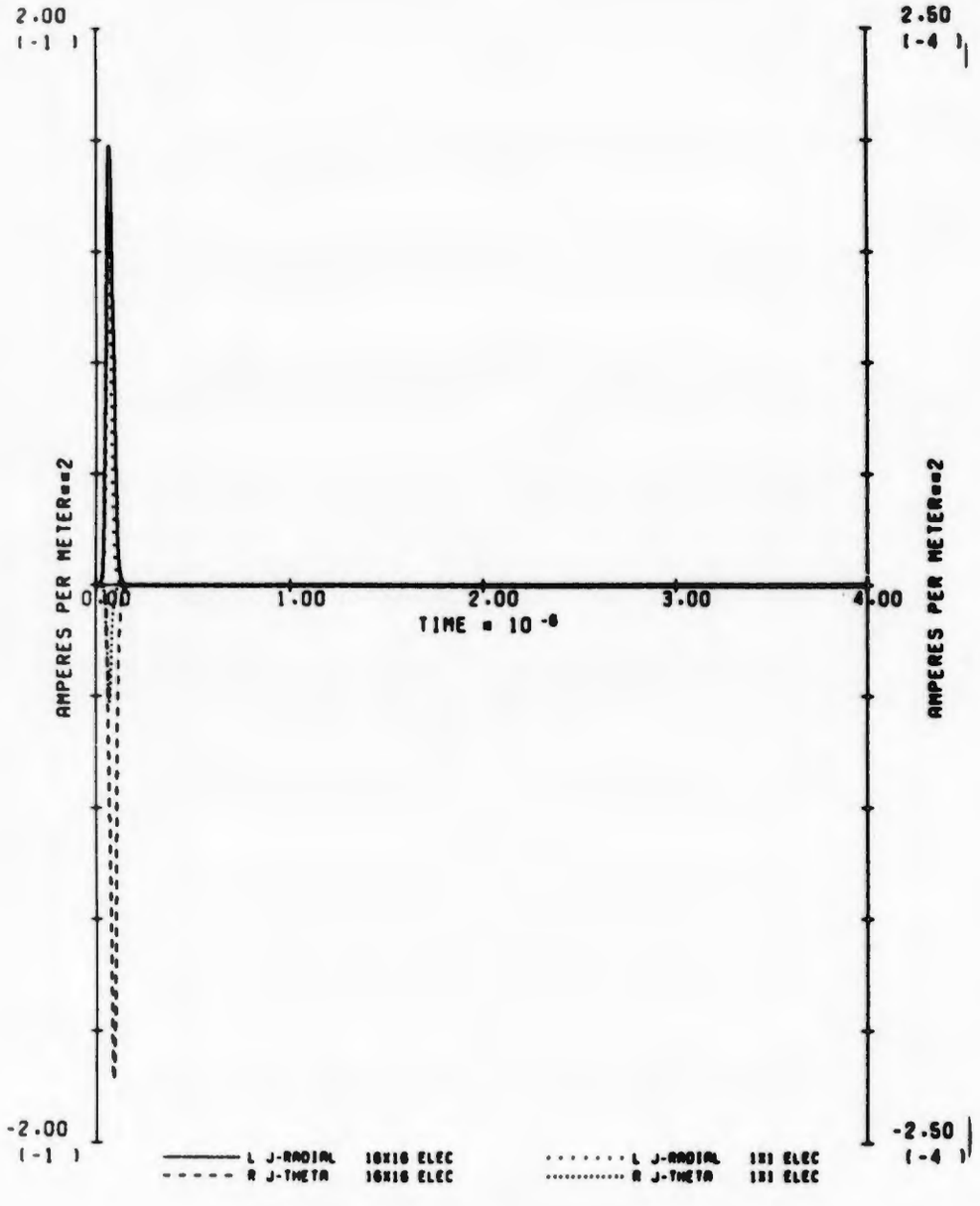

Fig. 102. Calculated Results for Parameter Set 102.

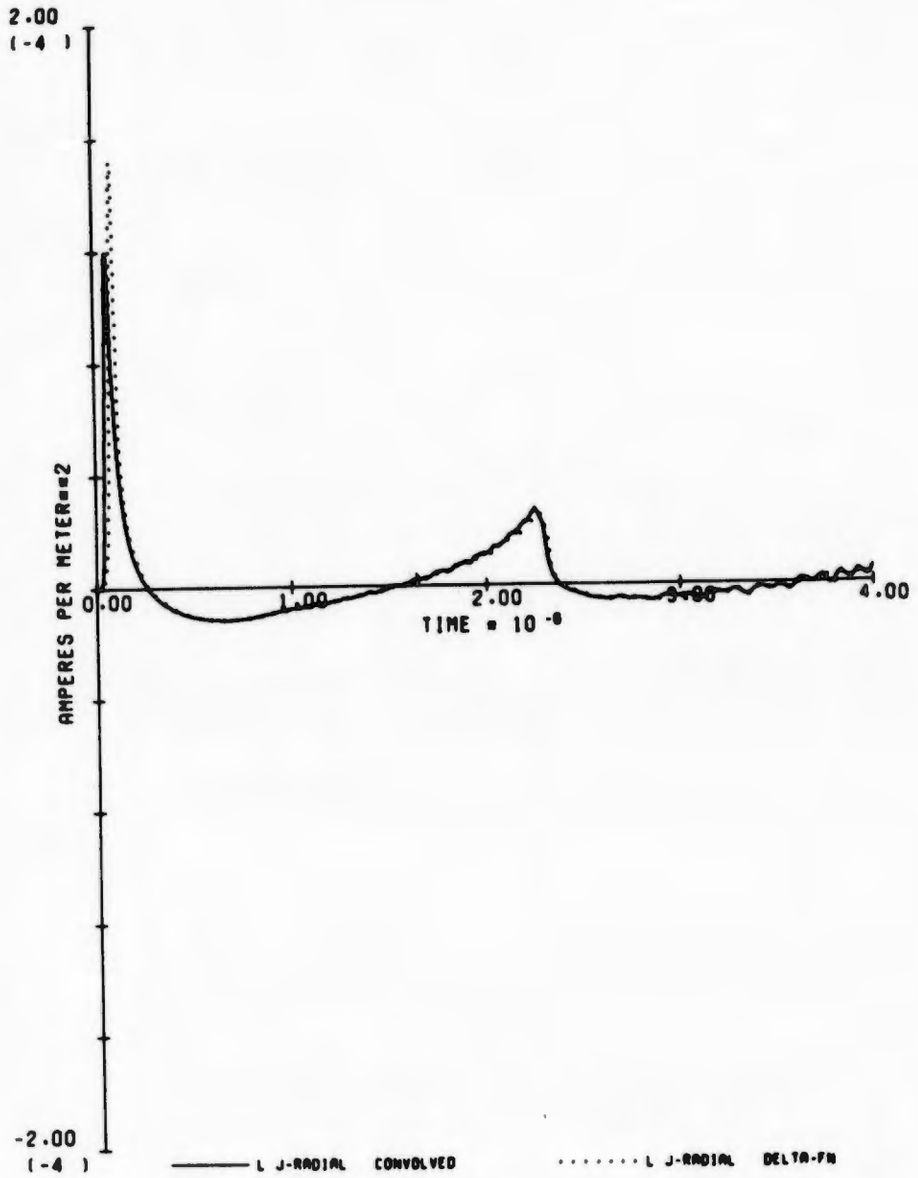

Fig. 103. Calculated Results for Parameter Set 103.

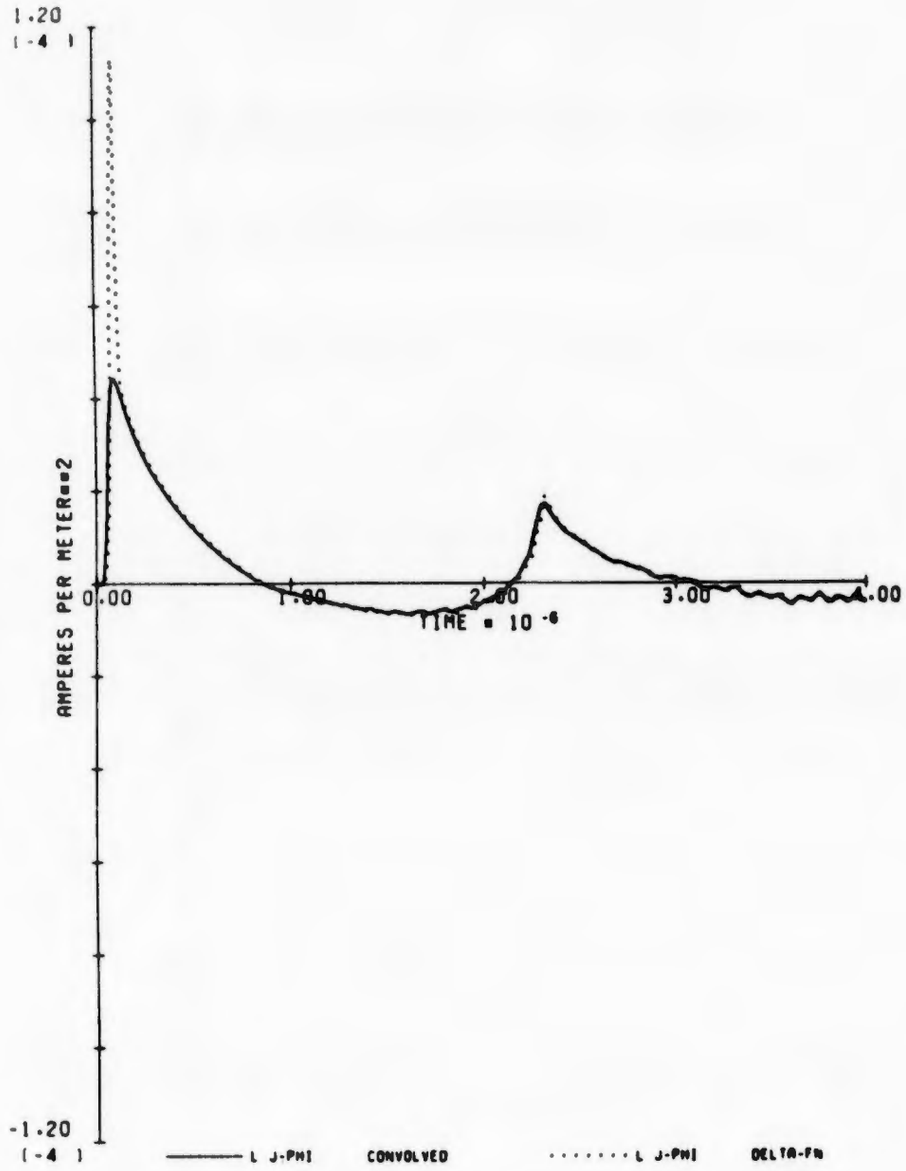

Fig. 104. Calculated Results for Parameter Set 104.

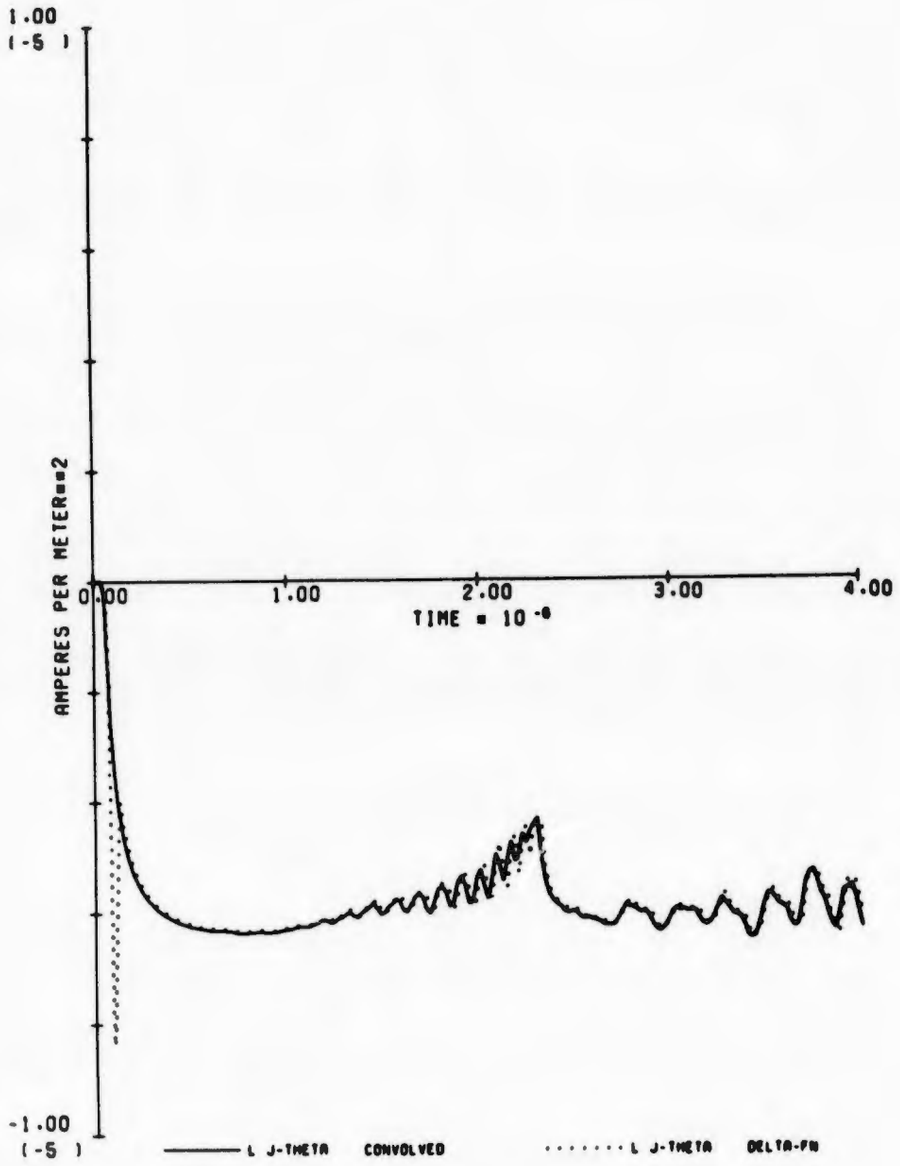

105. J-THETA (DELTA-FN) (80 KM. 1.5 MEV. 77.8 DEG)

Fig. 105. Calculated Results for Parameter Set 105.

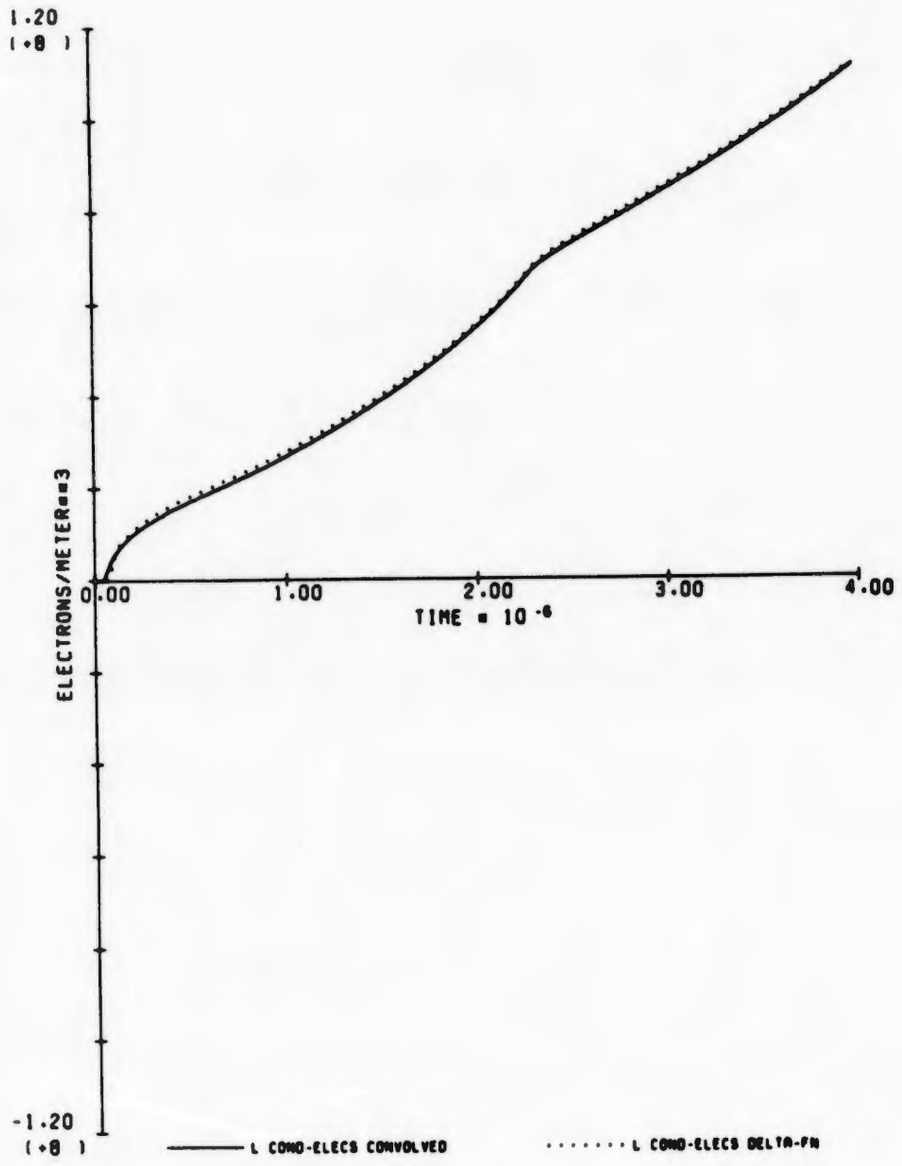

Fig. 106. Calculated Results for Parameter Set 106.

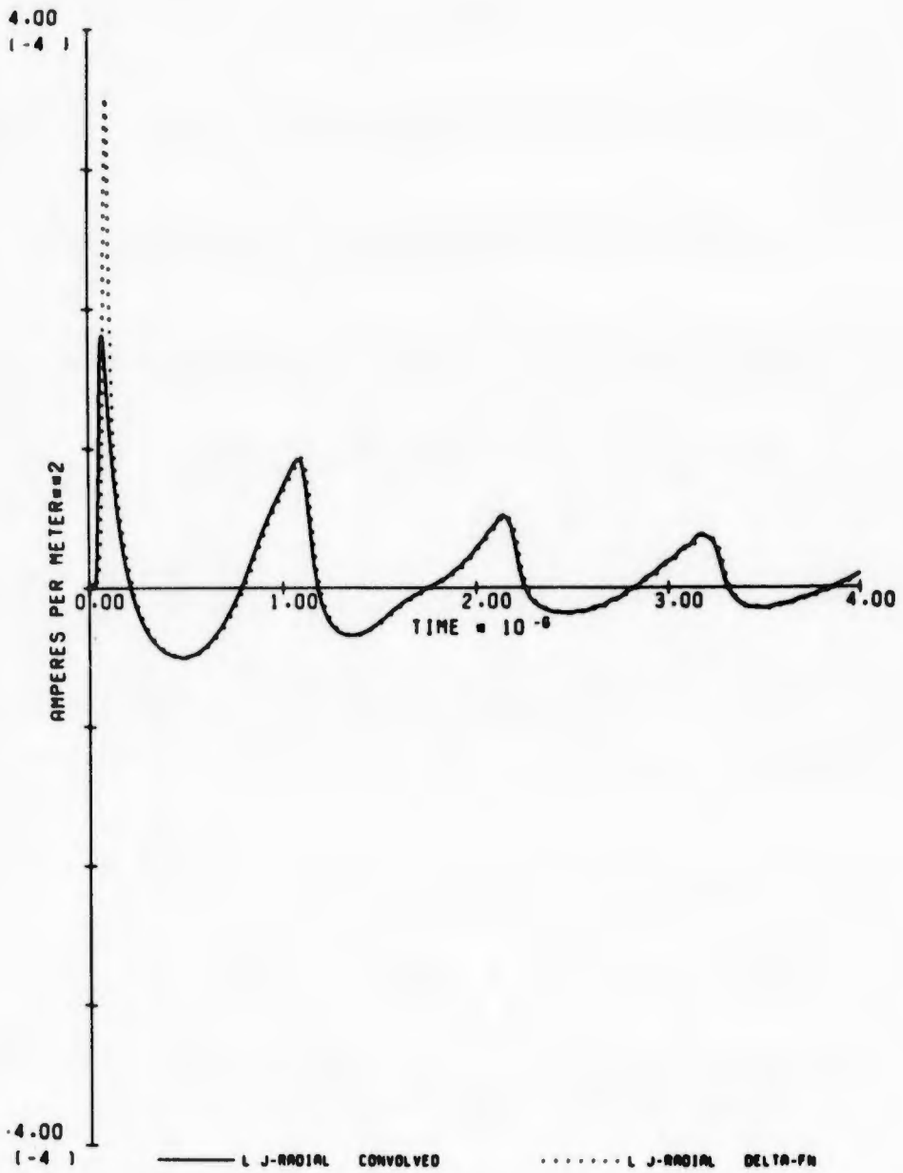

107.J-RADIAL (DELTA-FN) (80 KM. 0.5 MEV. 77.0 DEG)

Fig. 107. Calculated Results for Parameter Set 107.

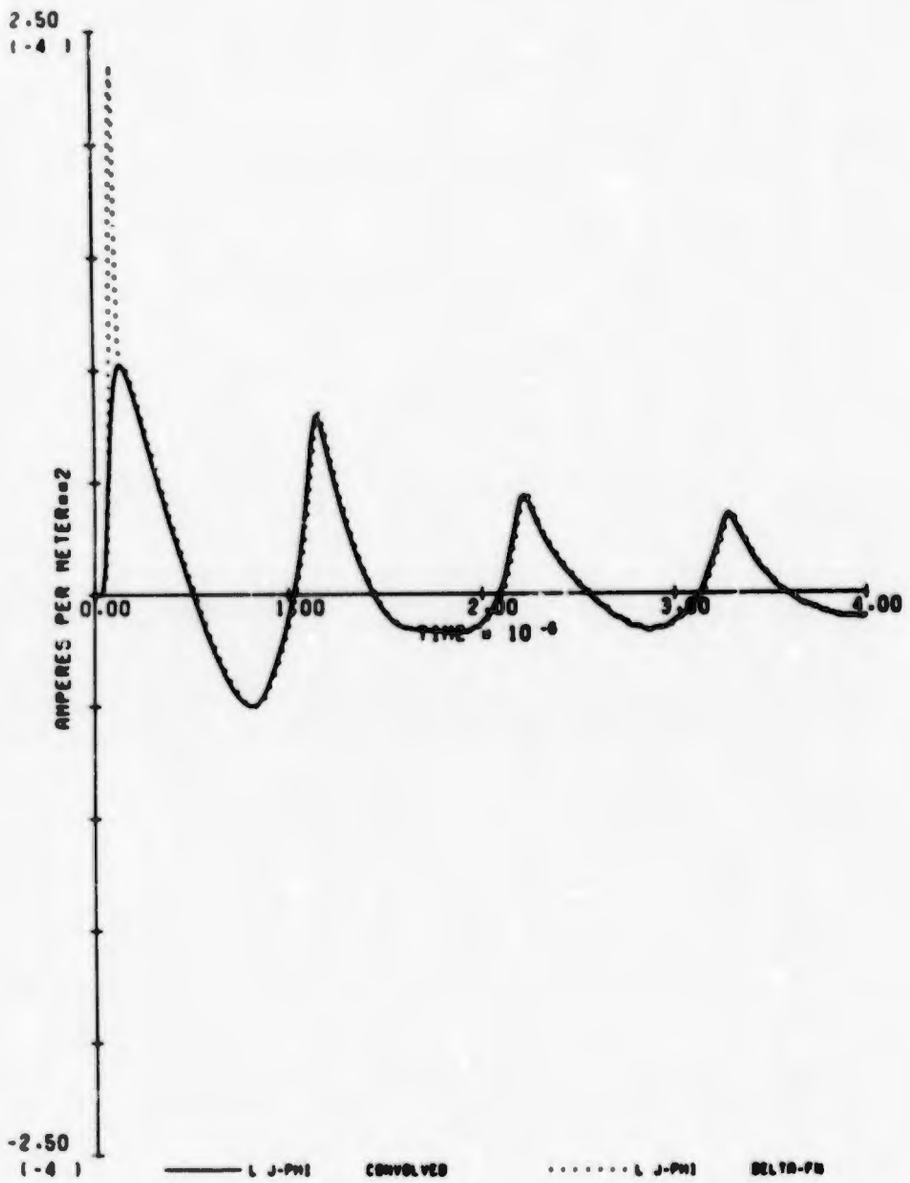

108. J-PHI (DELTA-FN) (80 KM, 0.5 MEV, 77.8 DEG)

Fig. 108. Calculated Results for Parameter Set 108.

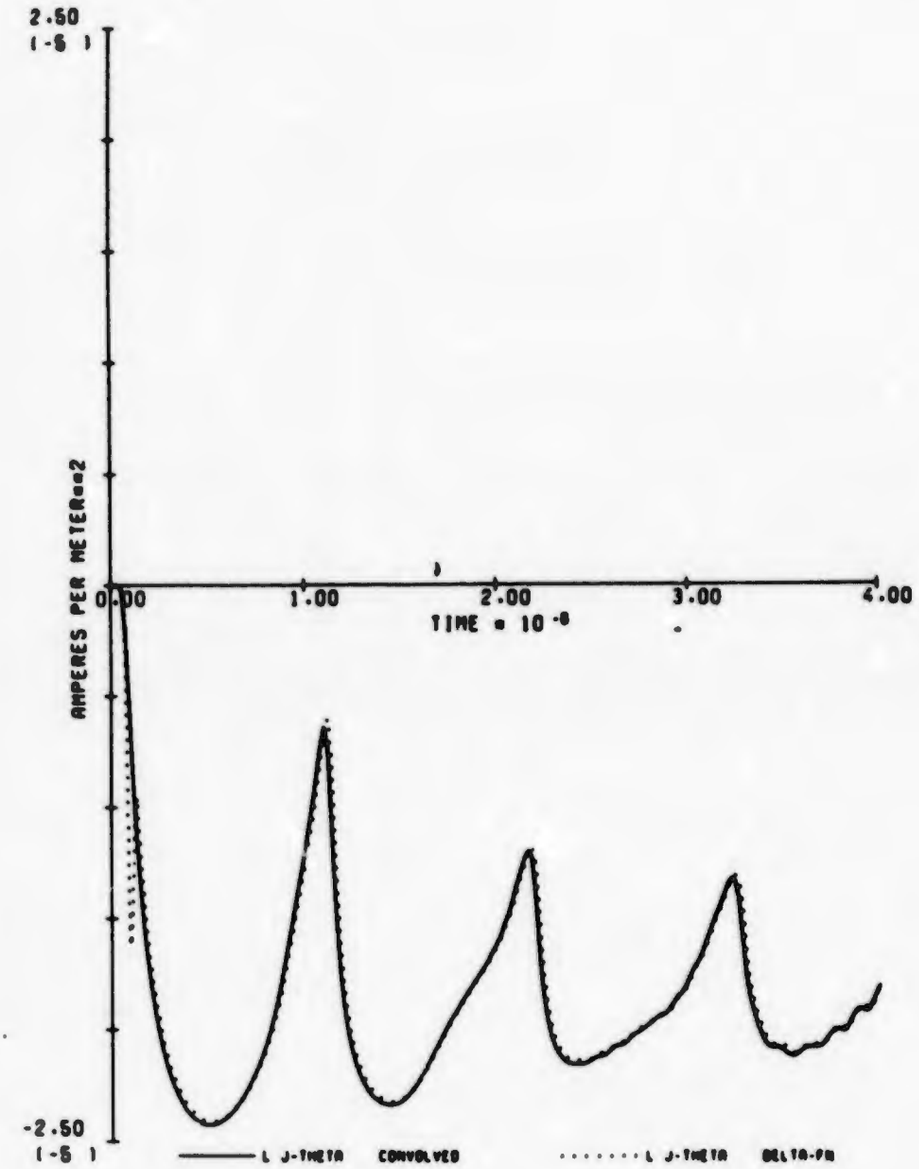

Fig. 109. Calculated Results for Parameter Set 109.

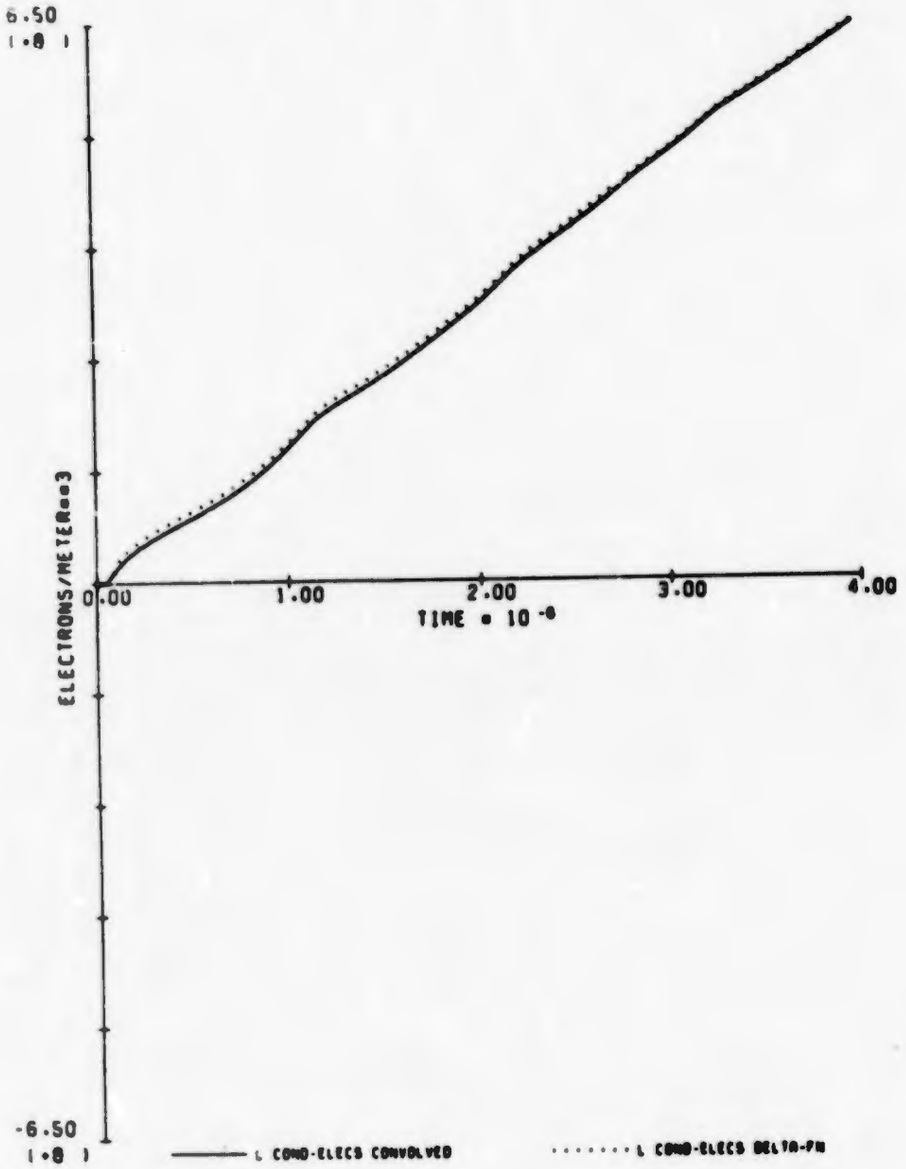

110.COND ELEC(DELTA-FN) (80 KM, 0.5 MEV, 77.0 DEG)

Fig. 110. Calculated Results for Parameter Set 110.

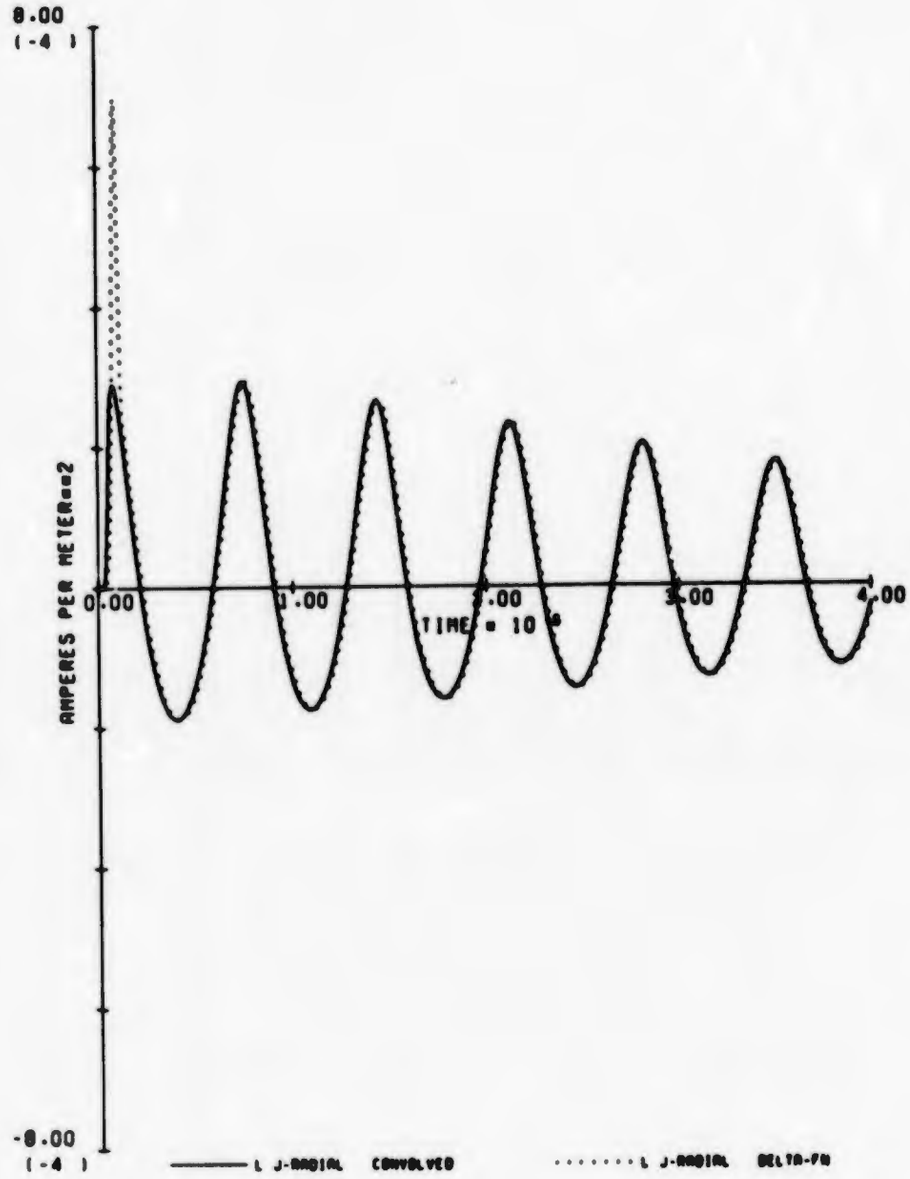

111.J-RADIAL (DELTA-FN) (80 KM, 0.1 MEV, 77.8 DEG)

Fig. 111. Calculated Results for Parameter Set 111.

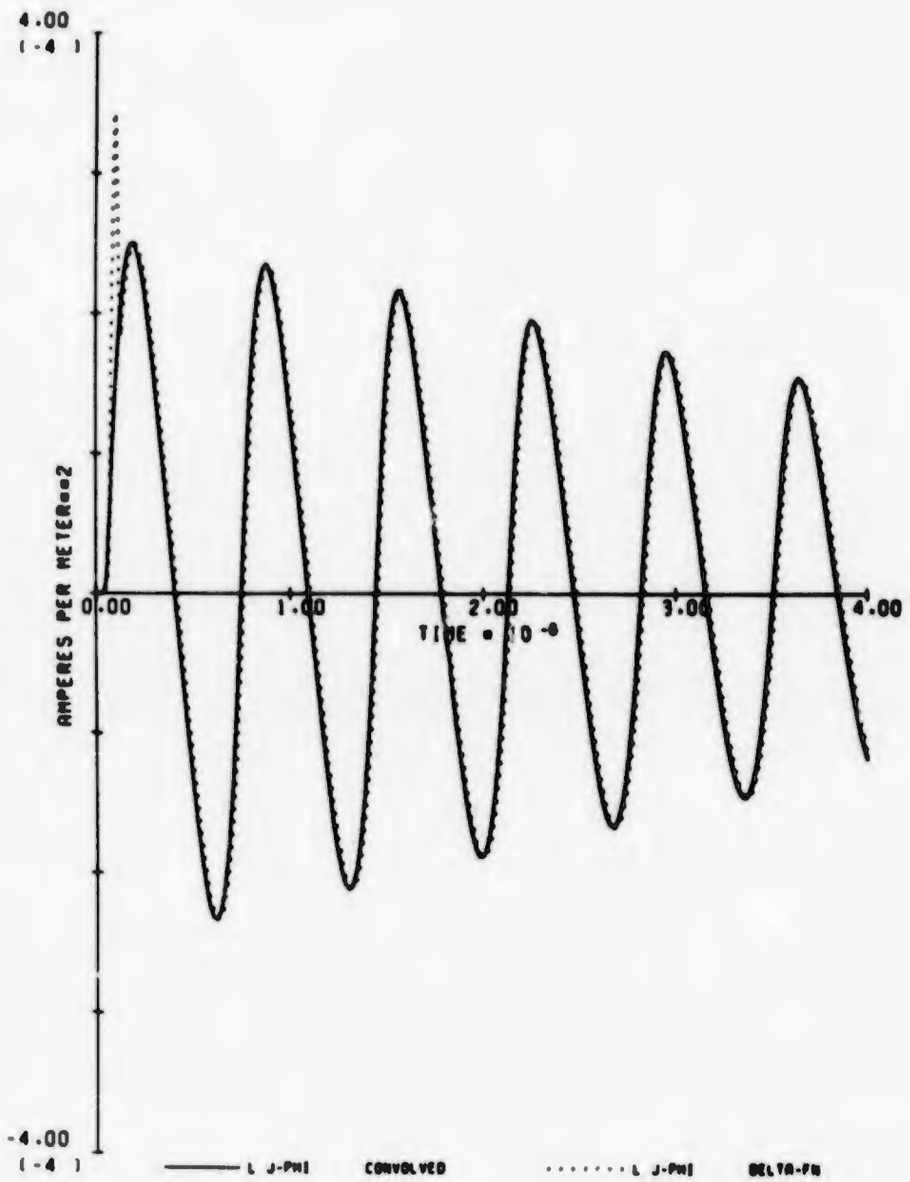

112. J-PHI (DELTA-FN) (80 KM, 0.1 MEV, 77.0 DEG)

Fig. 112. Calculated Results for Parameter Set 112.

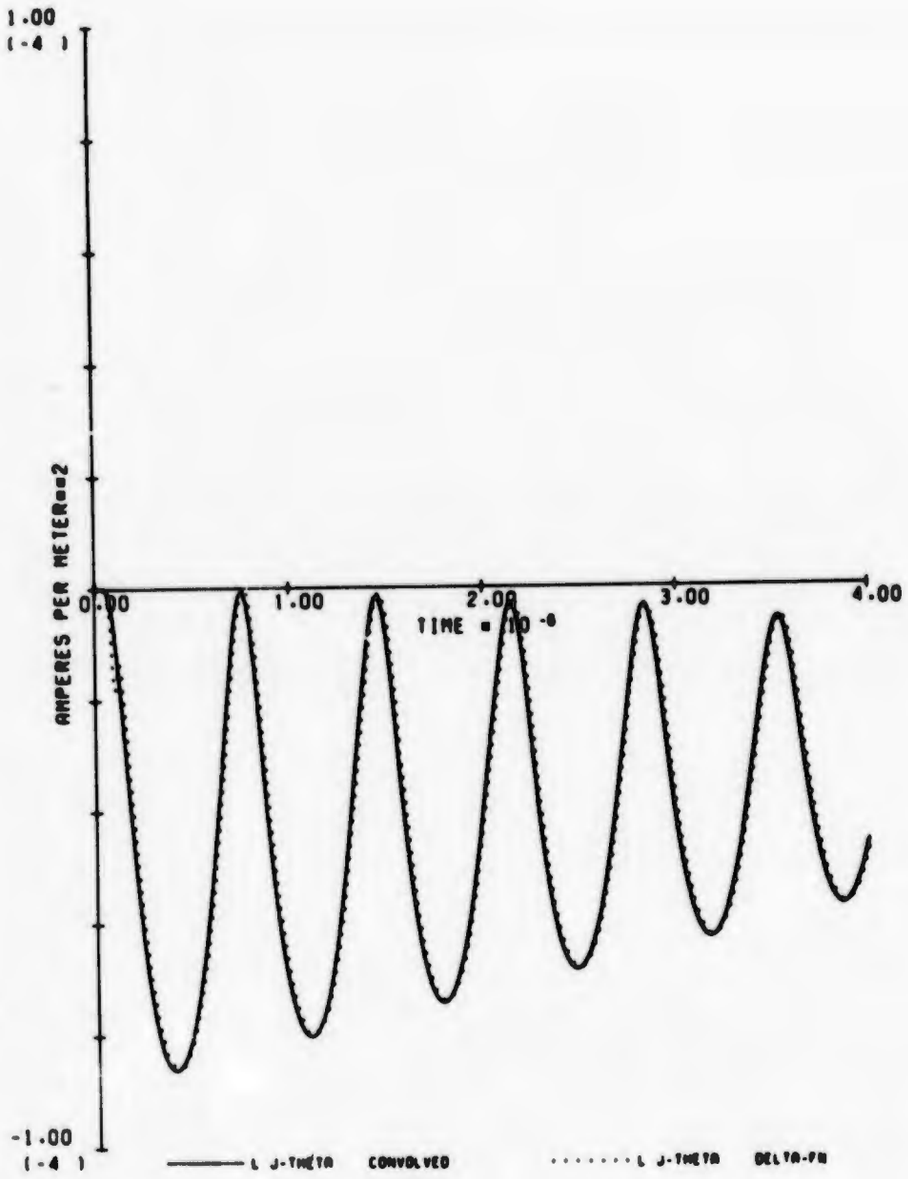

Fig. 113. Calculated Results for Parameter Set 113.

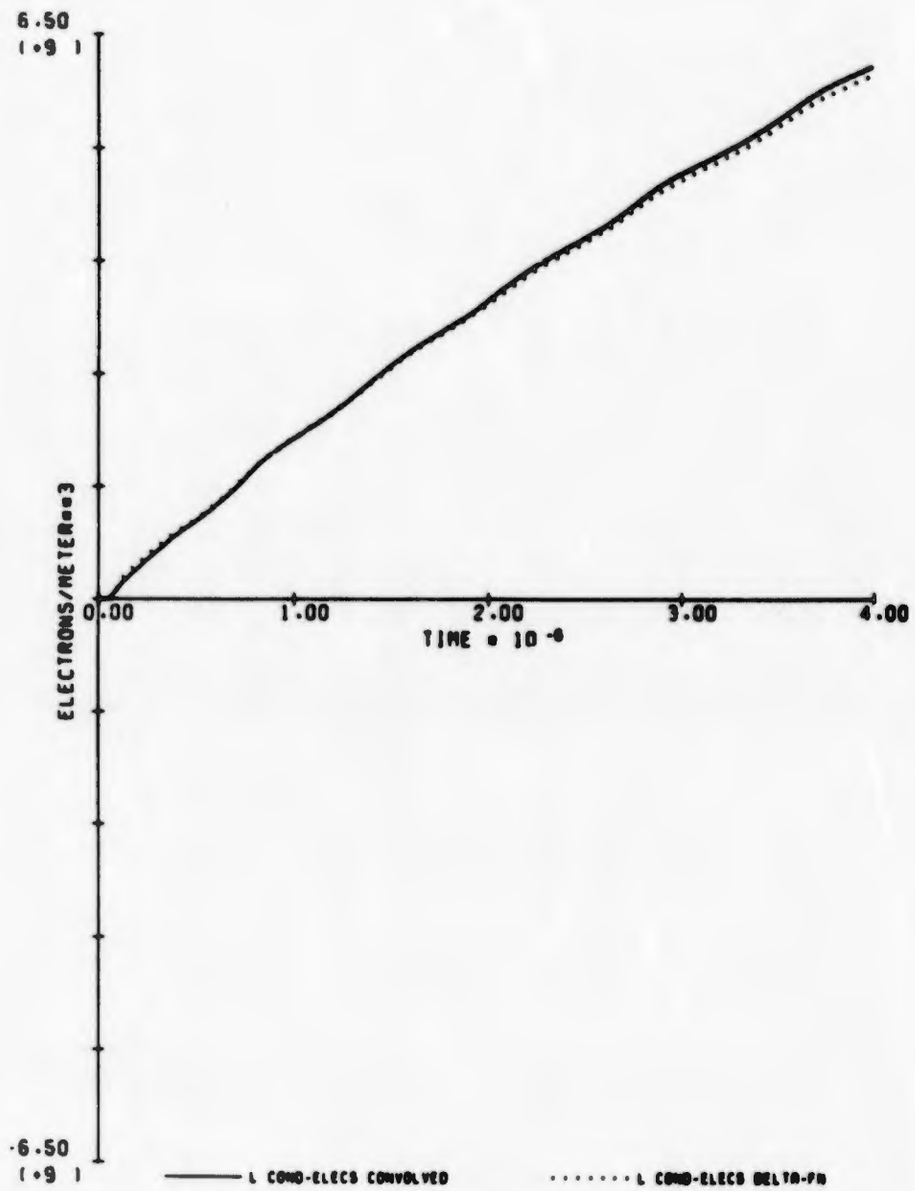

Fig. 114. Calculated Results for Parameter Set 114.

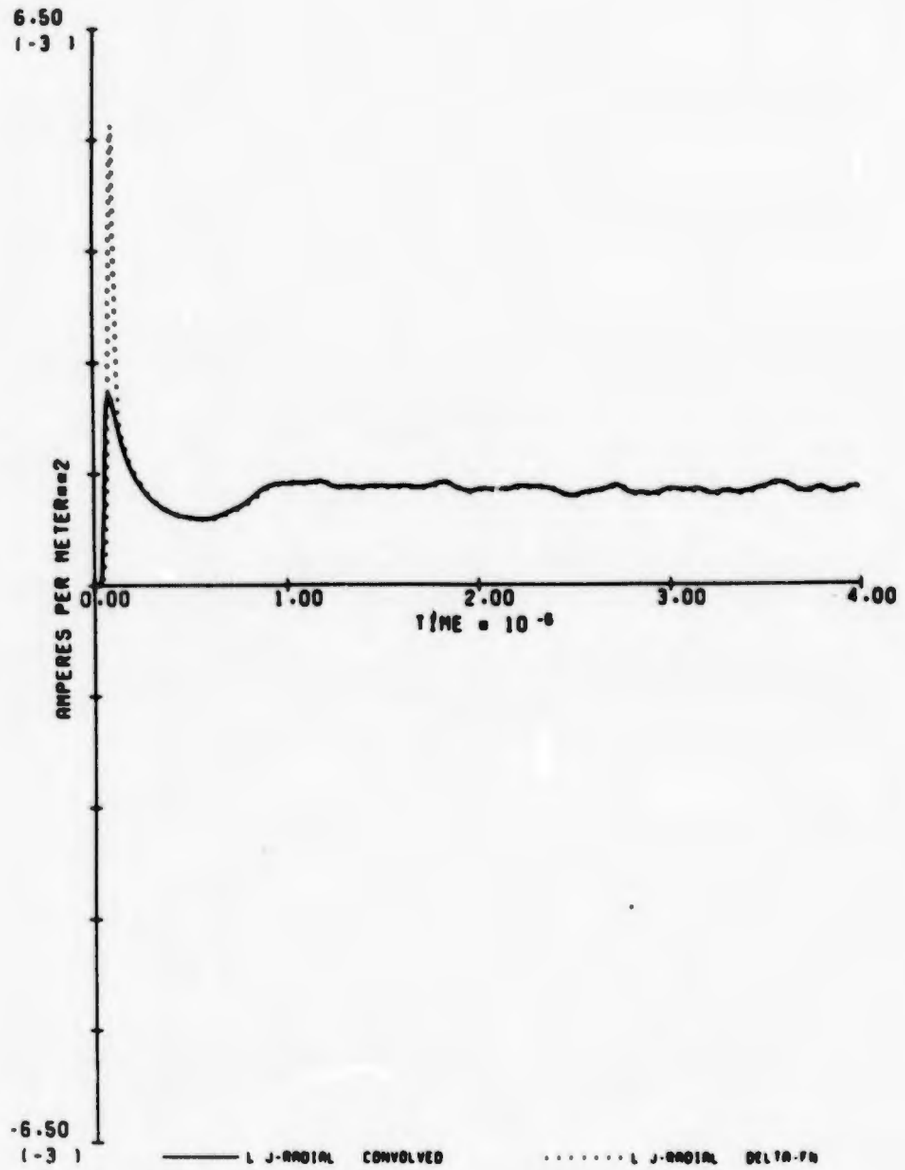

Fig. 115. Calculated Results for Parameter Set 115.

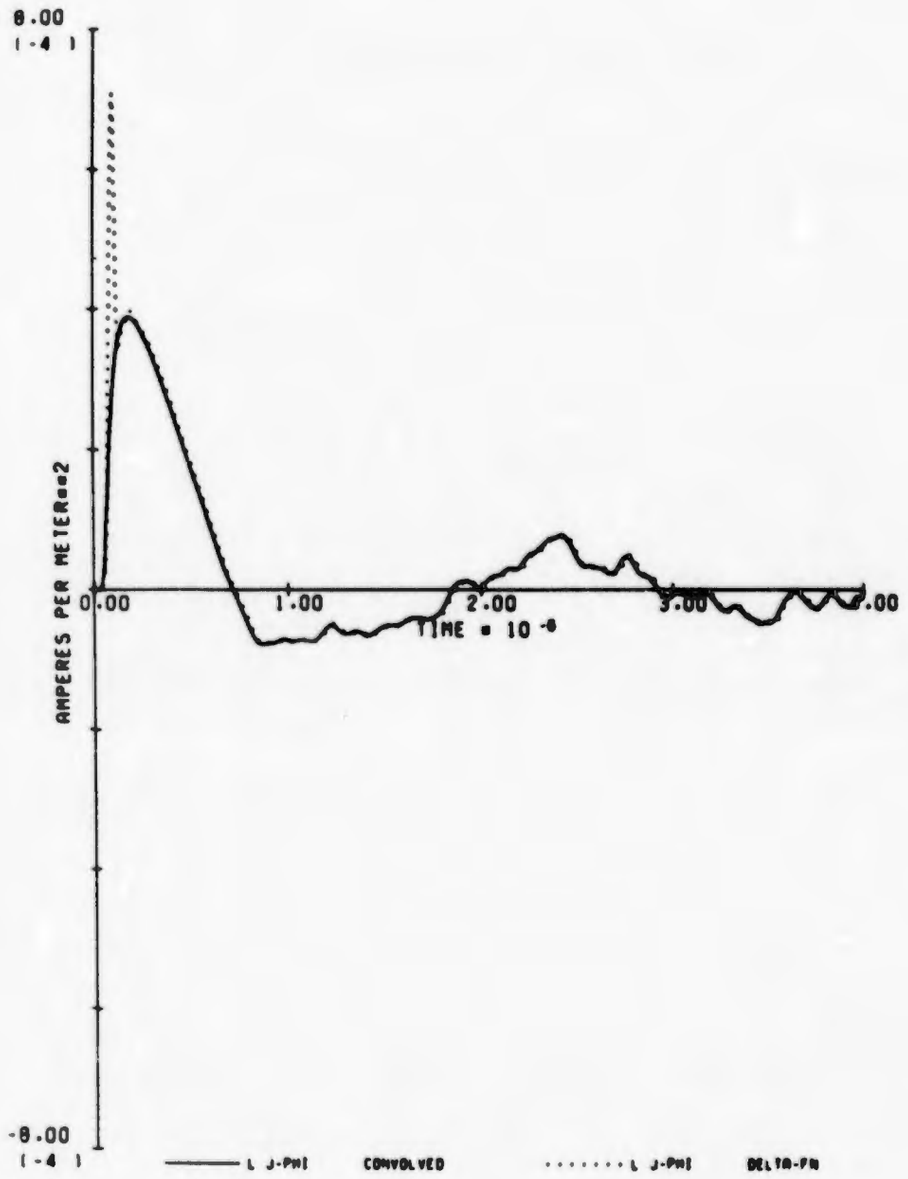

Fig. 116. Calculated Results for Parameter Set 116.

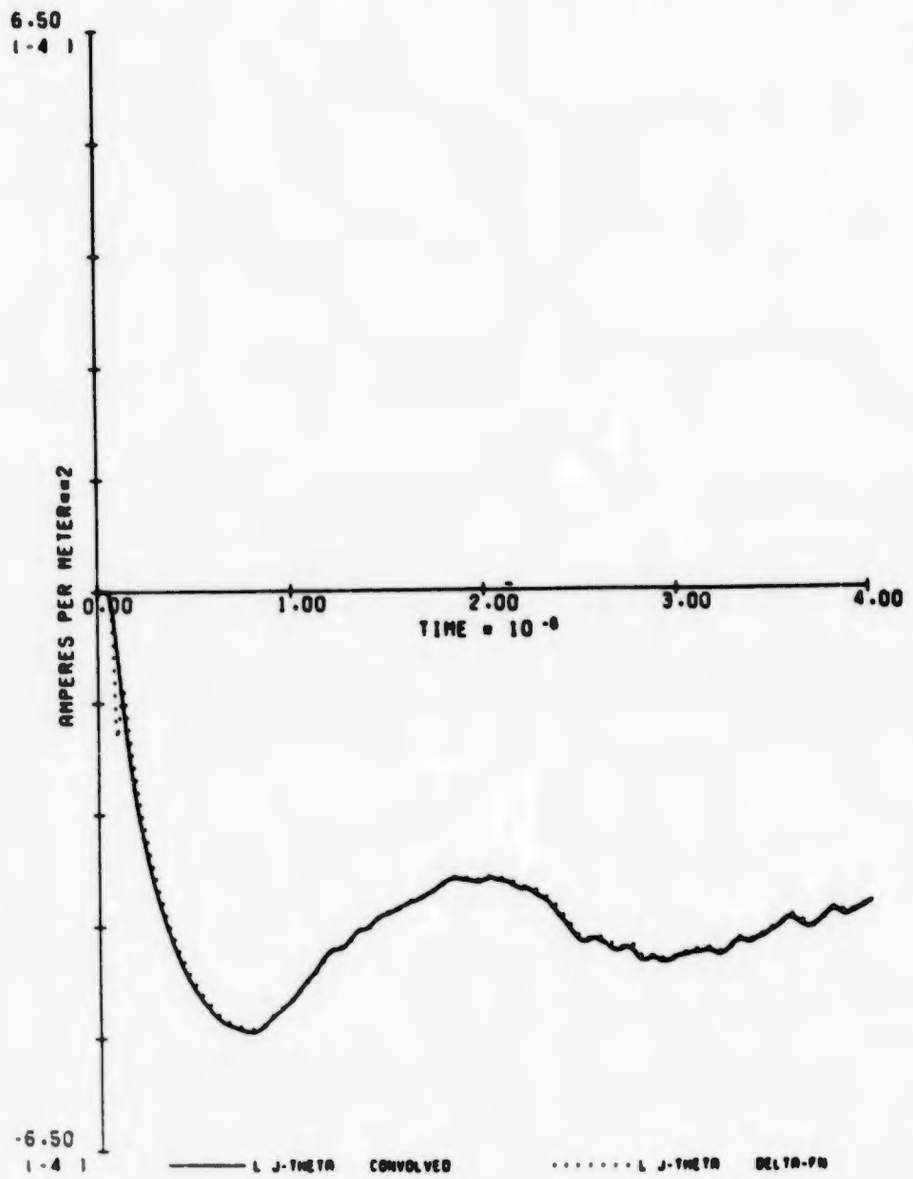

117. J-THETA (DELTA-FN) (80 KM. 1.5 MEV. 19.3 DEG)

Fig. 117. Calculated Results for Parameter Set 117.

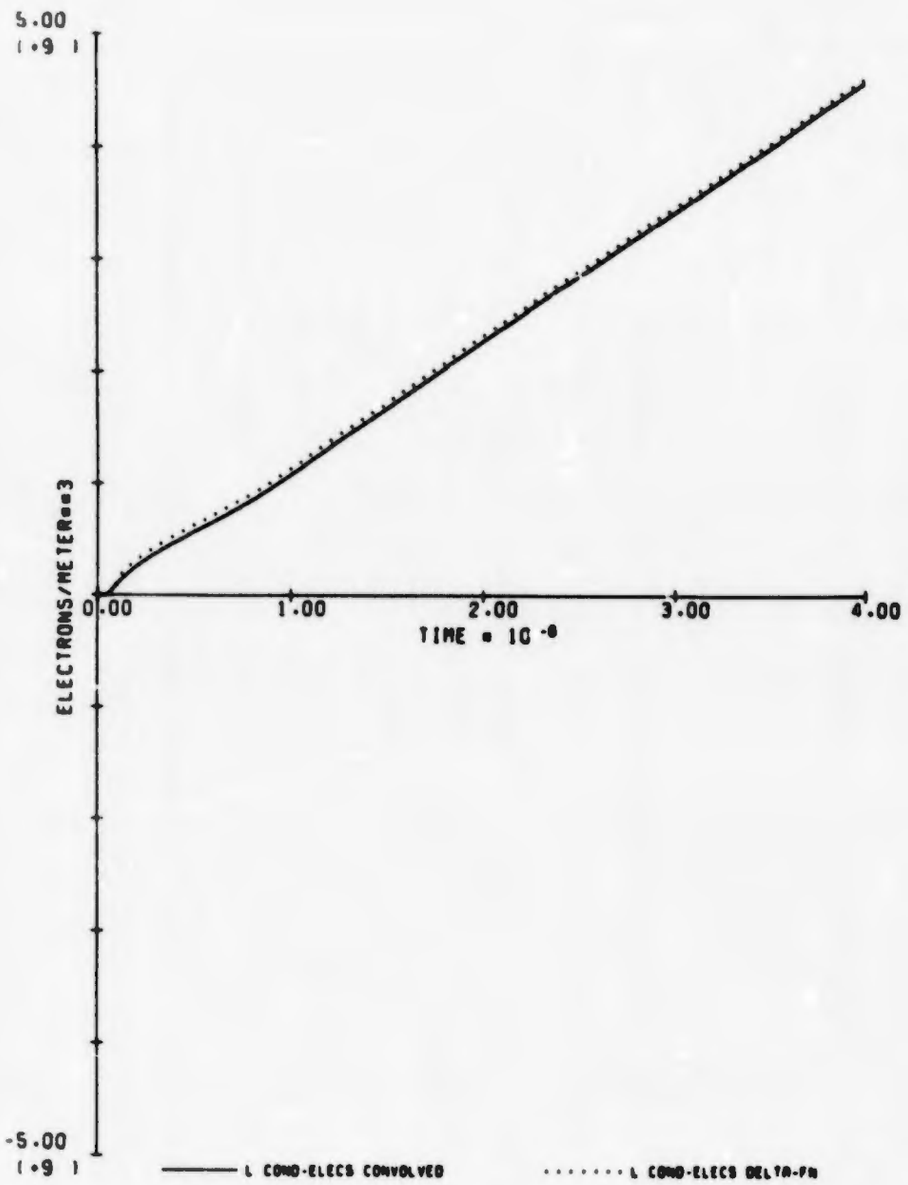

Fig. 118. Calculated Results for Parameter Set 118.

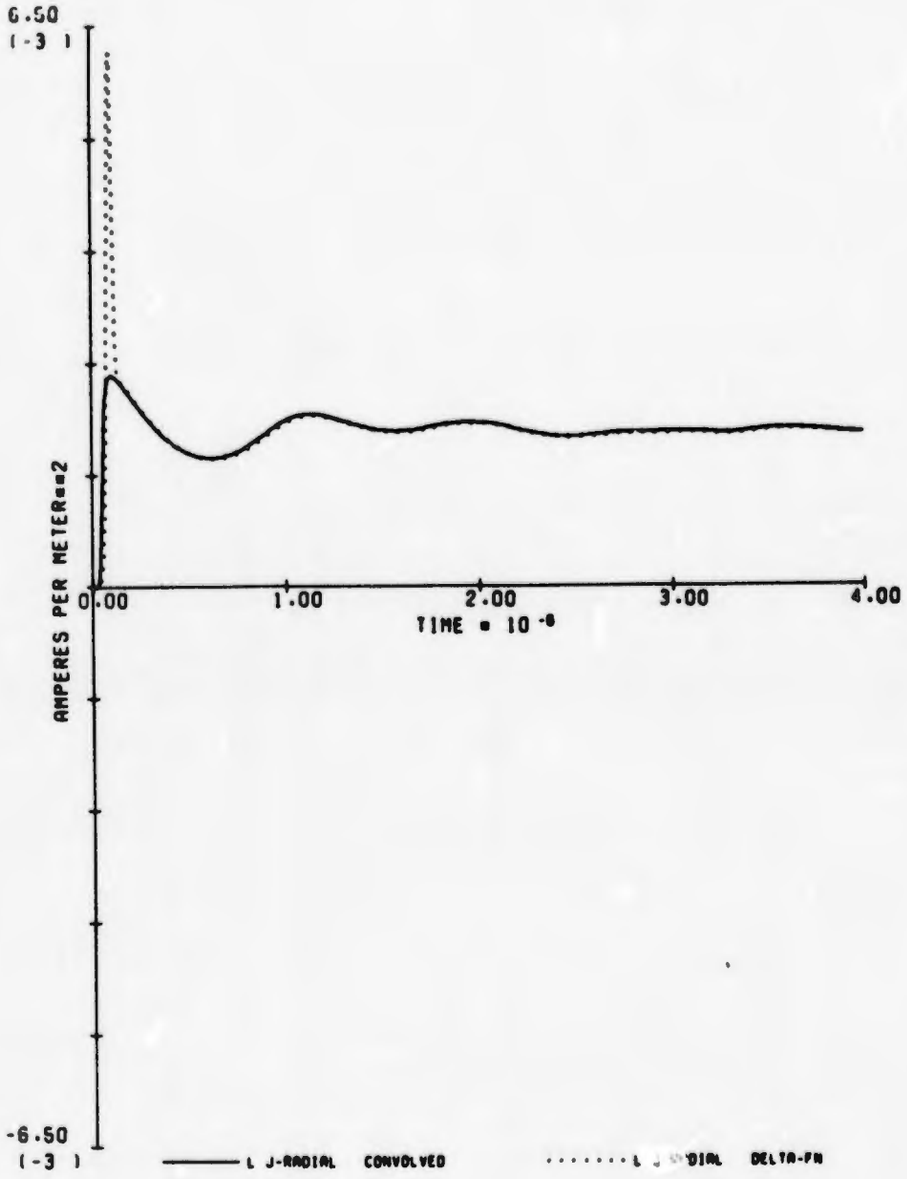

Fig. 119. Calculated Results for Parameter Set 119.

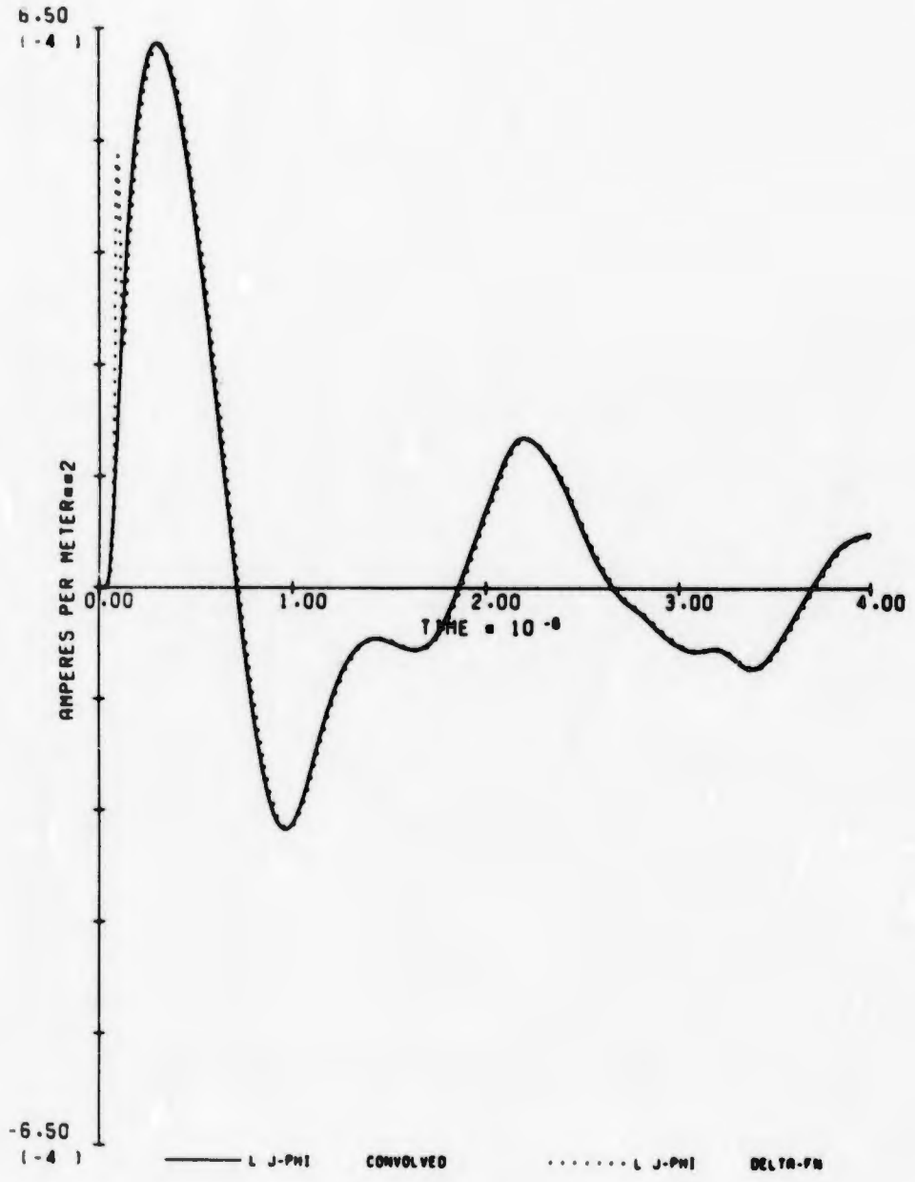

120. J-PHI (DELTA-FN) (80 KM, 0.5 MEV, 19.3 DEG)

Fig. 120. Calculated Results for Parameter Set 120.

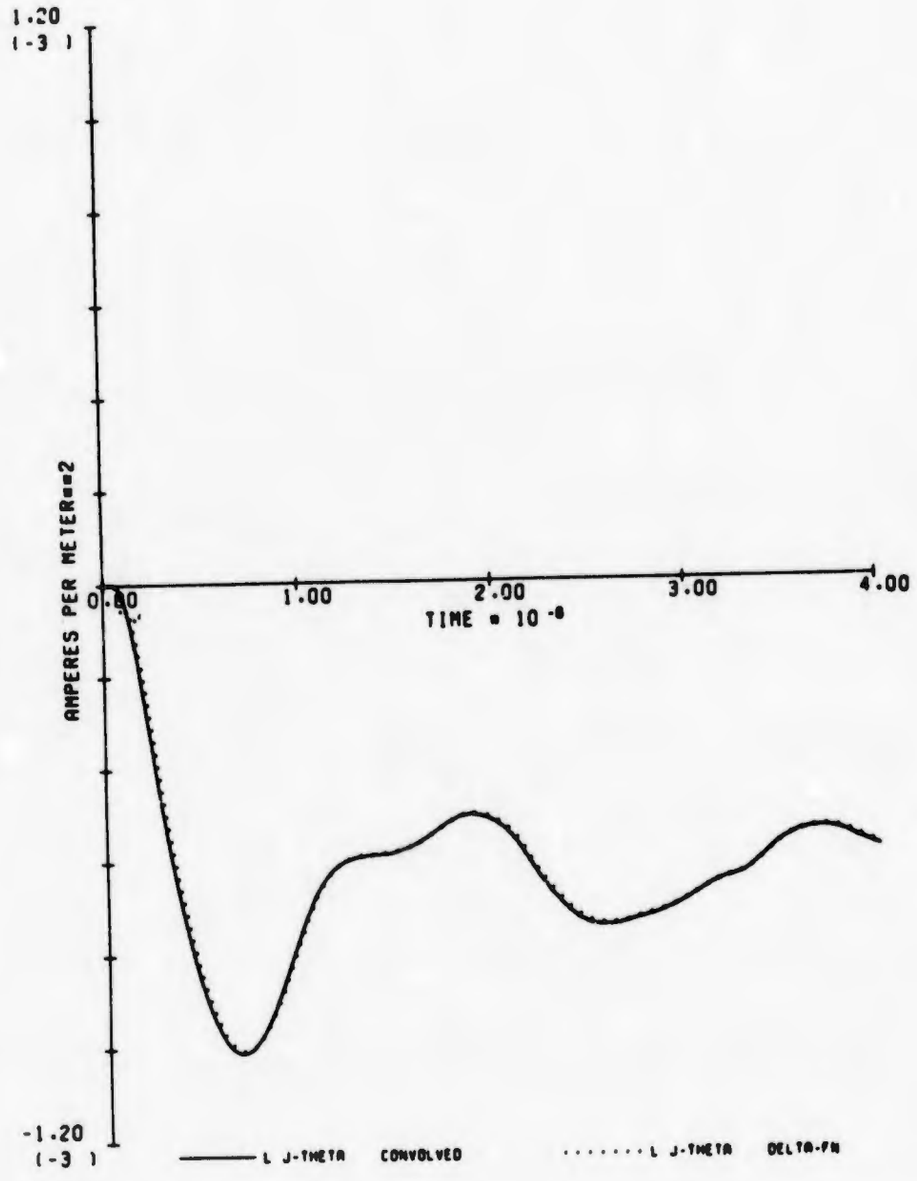

121. J-THETA (DELTA-FN) (80 KM, 0.5 MEV, 19.3 DEG)

Fig. 121. Calculated Results for Parameter Set 121.

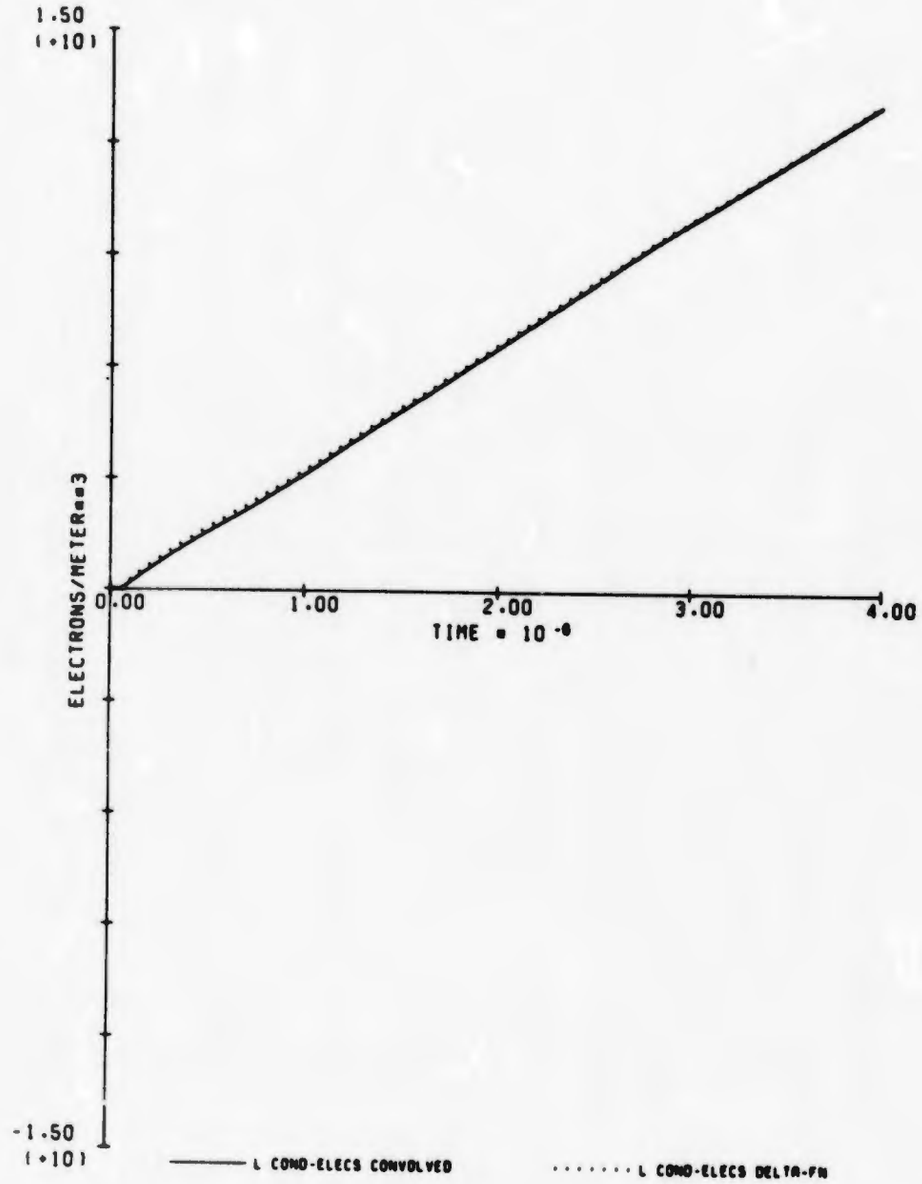

Fig. 122. Calculated Results for Parameter Set 122.

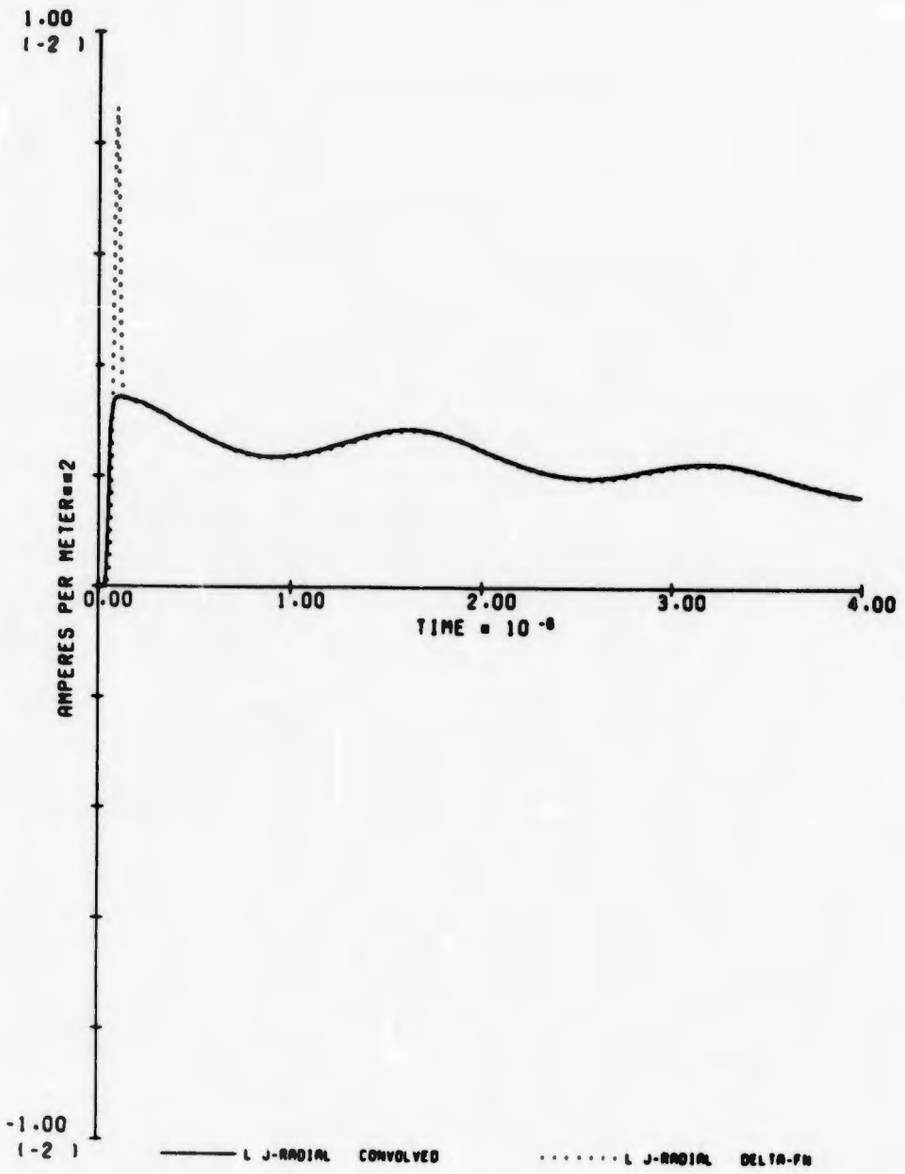

Fig. 123. Calculated Results for Parameter Set 123.

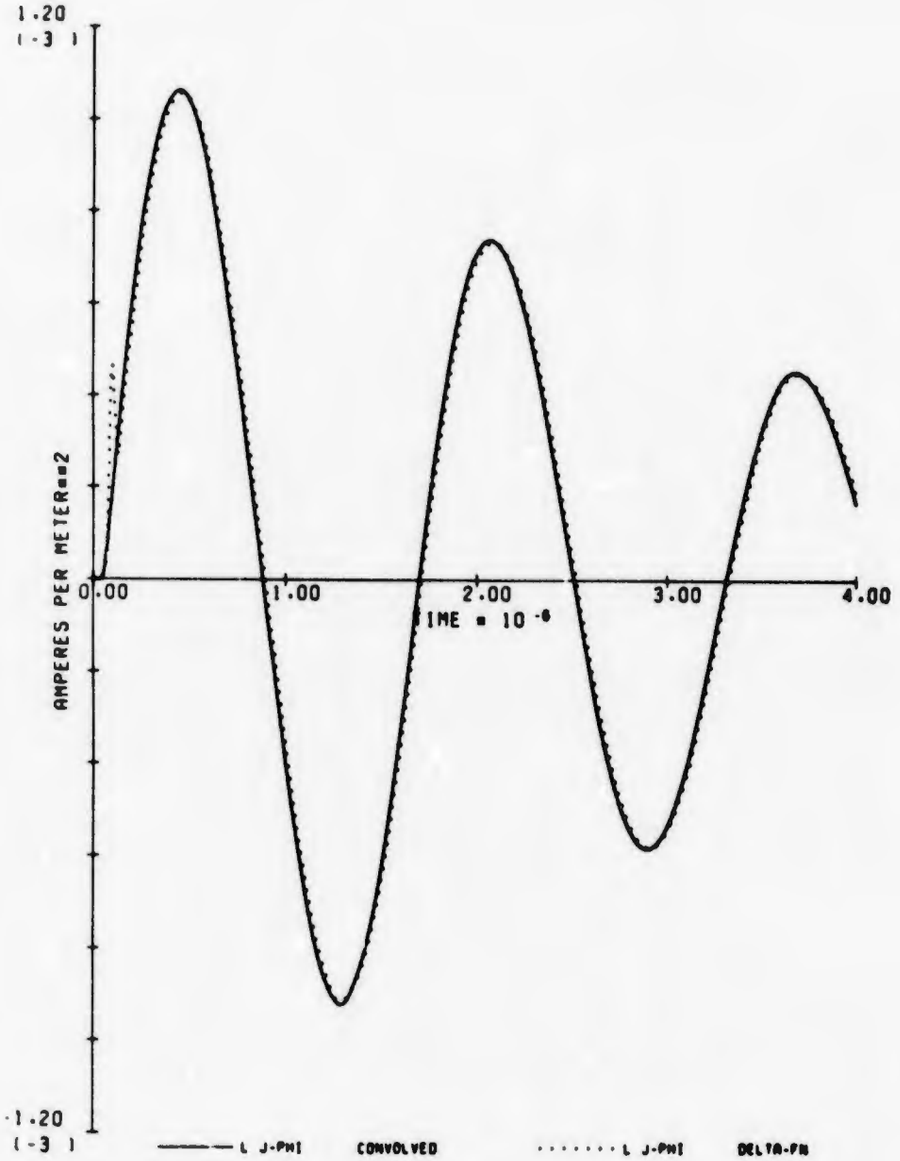

124. J-PHI (DELTA-FN) (80 KM, 0.1 MEV, 19.3 DEG)

Fig. 124. Calculated Results for Parameter Set 124.

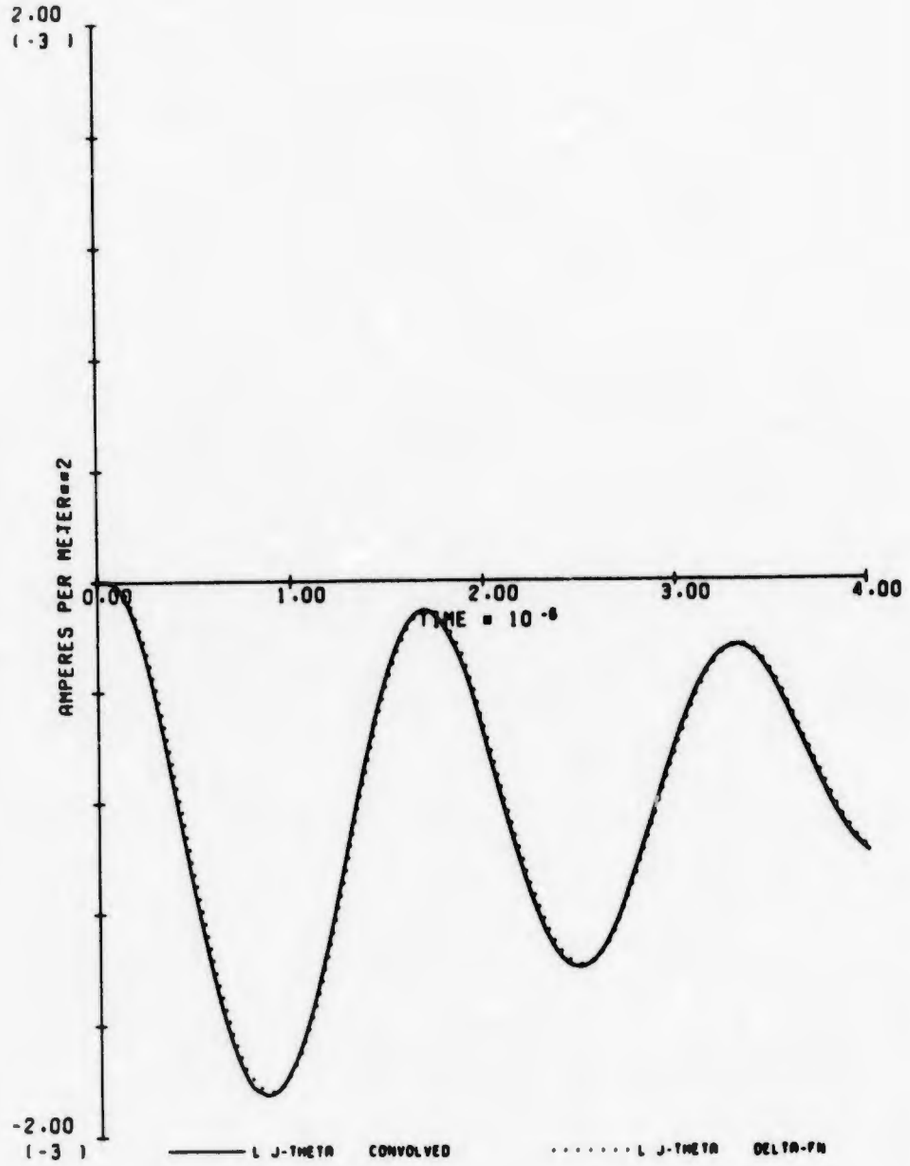

Fig. 125. Calculated Results for Parameter Set 125.

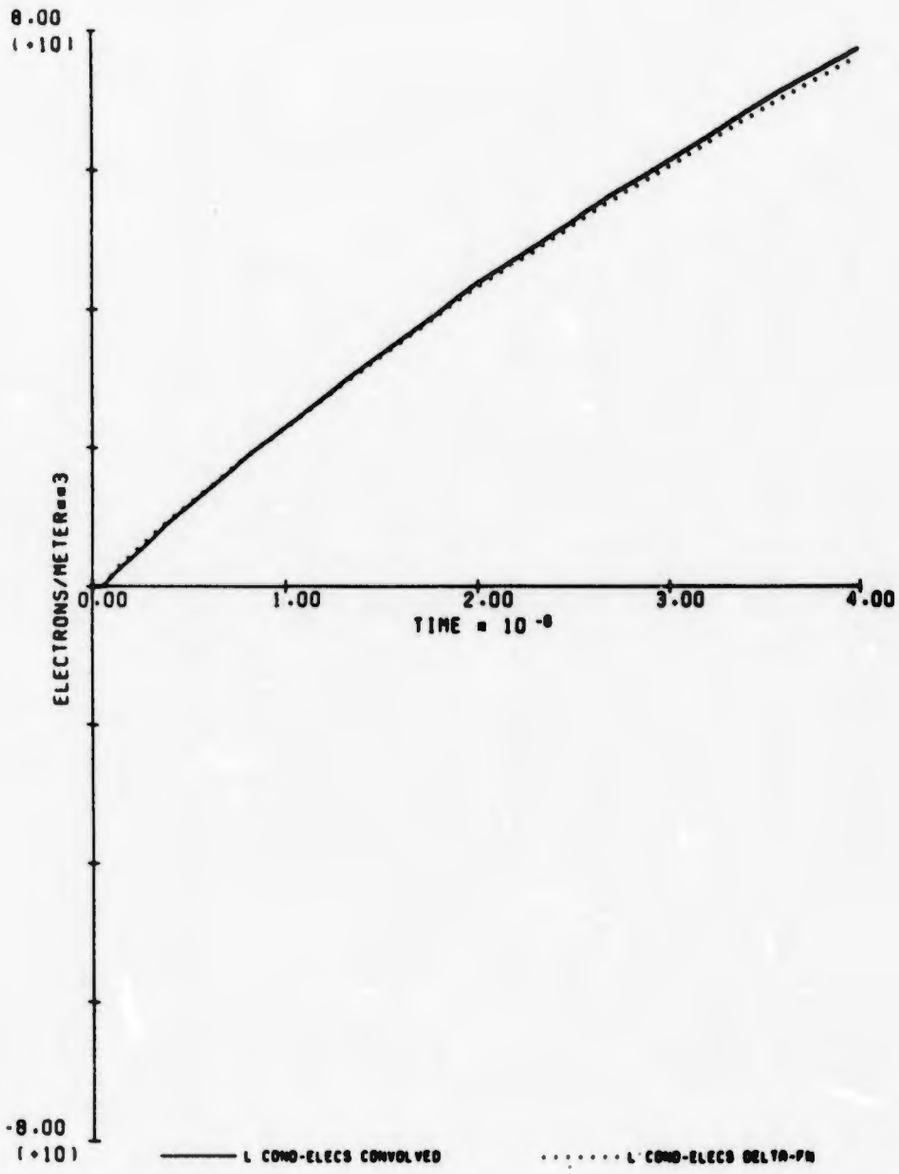

126.COND ELEC(DELTA-FN) (80 KM, 0.1 MEV, 19.3 DEG)

Fig. 126. Calculated Results for Parameter Set 126.